"Studies on Synthesis & Characterization of Thermoplastic Polyurethane-urea Copolymers"

A thesis submitted to the

UNIVERSITY OF PUNE

For the degree of

DOCTOR OF PHILOSOPHY

in

CHEMISTRY

by

Vipin P. Joshi

Complex Fluids & Polymer Engineering Group

Polymer Science & Engineering Division

National Chemical Laboratory

Pune - 411008

India

May 2009

Form 'A'

Certified that the work incorporated in the thesis entitled **'Studies on Synthesis & Characterization of Thermoplastic Polyurethane-urea Copolymers'** submitted by Vipin Joshi was carried out under my supervision. Such material as has been obtained from other sources has been duly acknowledged in the thesis.

May, 2009   A.K. Lele
NCL, Pune   (Research Guide)

ACKNOWLEDGEMENT

Abstract

A typical thermoplastic polyurethane (PU) and its analogue polyurethane-urea (PUU) are $(AB)_n$ type random block copolymers consisting of sequences of hard and soft segments. The soft segment is generally composed of polyether or polyester diols, while the hard segment is usually composed of the reaction products of diisocyanates with a chain extender. Thermodynamic incompatibility between hard and soft segments, and/or crystallinity in the hard segment drives them to phase separate. The extent of microphase separation and the phase morphology have a profound effect on the ultimate properties of the copolymer. Hence it is desirable to have a control on the microphase separation in polyurethanes.

In the present work we have tested a new hypothesis for achieving control on microphase separation namely, the use of defect structural moieties in hard segments. The inspiration for this idea is derived from semicrystalline polymers in which the role of defect moieties in controlling the size of crystalline structures is well known. Thus the overall objective of the present work was to achieve control on the phase morphology of PUUs via controlled introduction of defects in the hard segments. The defect moieties that we have studied are diamines having long aliphatic chains, which form short branches on the hard segments of Polyurethane.

Present study systematically investigates the role of the content and the length of aliphatic chain defect in hard segment on the morphology and microphase mixing in PUU copolymers. Morphology was characterized at molecular length scales (FTIR), mesoscopic length scales (SAXS) and macroscopic length scales (DMA, Rheology). Present study shows that aromatic chain extenders, when introduced in the hard segments, acted as defect sites and frustrated hard segment association as evidenced by FTIR, DSC, DMA, SAXS and rheological analysis. Phase mixing of soft segments in hard segment domains and the average domain spacing was found to be sensitive to both the content and the length of the chain defect in hard segment. Thus, we have successfully shown that morphology of polyurethanes can be controlled by introducing chain defects in the hard segments.

Table of Contents

Chapter 2 : Scope and Objectives

Chapter 3 : Synthesis of Chain Extenders and Polyurethane-ureas

Chapter 4 : Molecular Characterization of Polyurethane-ureas

Chapter 5 : Morphological Characterization of Polyurethane-ureas

Chapter 6 : Conclusions and Future Work

Glossary

AFM	Atomic Force Microscopy
BDO	1,4-butanediol
DBTDL	Dibutyltin dilaurate
DMA	Dynamic Mechanical Analysis
DMAc	N,N-dimethyl acetamide
DNBC	3,5-dinitrobenzoyl chloride
DSC	Differential Scanning Calorimetry
FTIR	Fourier Transform Infrared
IPDI	Isophorone Diisocyanate
MDI	Methylene Diisocyanate
MST	Microphase Separation Transition
NMR	Nuclear Magnetic Resonance
PDA	m-phenylene diamine
PTMO	Poly(tetramethylene oxide)
PU	Poly(urethane)
PUU	Poly(urethane-urea)
SAXS	Small Angle X-ray Scattering
TDI	Toluene Diisocyanate
T_g	Glass Transition Temperature
THF	Tetrahydrofuran
TPU	Thermoplastic Polyurethane
TTS	Time-temperature Superposition
WAXS	Wide Angle X-ray Diffraction

List of Schemes

List of Tables

List of Figures

Introduction and Literature Survey

Chapter - 1

1.1   History and Development of Polyurethanes

Polyurethanes, formed by a simple polyaddition reaction, prove to be very versatile, high-performance polymers having applications as diverse as coatings, adhesives, elastomers, fibers and foams. The first basic diisocyanate polyaddition reaction dates back to 1937 by Professor Otto Bayer in the I.G.Farben laboratories[1]. The polyurethane fiber formed using this reaction was trademarked by Bayer as Perlon U. Later, elastomeric properties were discovered by chemists at DuPont and ICI. Initial work on polyurethane was primarily focused on the production of fibers and elastomers with improved properties. During World War II Bayer developed elastomeric foams based on naphthalene 1,5-diisocyanate (NDI) and polyester resins. These foams were then used to reinforce the wings of military aircrafts to enhance their strength and performance.

In 1950's, polyurethane chemistry started to develop rapidly with toluene diisocyanate (TDI) and the first polyether polyols from Dow Chemical. In 1954, DuPont chemists successfully copolymerized polyethylene glycol and toluene 2,4-diisocyanate in the presence of water to form a polyurethane fiber spandex. The aim was to replace natural rubber threads. In 1959, DuPont commercialized a polyether urea fiber prepared using methylene bis (4-phenylene isocyanate) (MDI) and ethylene diamine under the trade name Lycra.

Earlier efforts on the synthesis of polyurethane elastomer resulted in the production of gummy materials, probably due to irregular elastomeric network from low hard segment concentration. These elastomers lacked adequate melt stability to function as practical thermoplastic elastomers. They were synthesized using bulky diisocyanates such as NDI, and had melting temperature higher than the decomposition temperature of urethane linkages. Properties of these elastomers were improved significantly when NDI was replaced by MDI and by the introduction of short chain extender diols and diamines.   In 1957, Schollenberger prepared a linear polyurethane elastomer from MDI, adipic acid and 1,4-butanediol.[2] The polymer had interesting properties such as high elasticity, extensibility, abrasion resistance and solubility. Schollenberger called this a "virtually crosslinked elastomer." A new family of thermoplastic polyurethane (TPU) elastomers, in a practical sense, thus became available. But structure-property relationship was still not very well

understood. A lot of research work had been carried out to understand the exact structure and its relationship with the properties. Cooper and Tobolsky[3] were the first to gain an understanding in this area in one of their study on "virtually crosslinked elastomer." They found out that phase separated hard and soft blocks were responsible for the excellent elastomeric properties of TPU.

During 1960's the polyurethane industry expanded dramatically with MDI becoming a key chemical to make elastomeric fibers. MDI became the raw material of choice for rapidly evolving applications of polyurethane (refrigeration, construction, spray foam etc.). Pure MDI applications went beyond Spandex to make thermoplastic polyurethanes, cast elastomers, adhesives and coatings. 1990's saw the start of major supplier consolidation and rapid globalization of the business. Today, the global business of polyurethanes is dominated by four major players BASF, Bayer, Dow and Huntsman. A dynamic development in the Chinese economy has influenced the polyurethane business considerably, with the major players concentrating on future strategies (primarily large scale manufacturing facilities) for the country.[4]

The range of polyurethane types, from flexible or rigid lightweight foams to tough, stiff elastomers allows them to be used in a wide diversity of consumer and industrial applications as illustrated below in **Table 1.1**.

Table 1.1 Polyurethane Applications[5]

Type	Applications
Rigid Foam	• Thermal insulation for buildings, refrigerators, deep freeze equipments, pipelines and storage tanks • Buoyancy aids in boats and flotation equipments • Packaging • Furniture • Equipment housings
Flexible Foam	• Household furniture including bedding • Automotive seating • Cushioning for diverse industrial applications • Textile laminates
Semi-rigid and Low Density Structural Foam	• Steering wheels, head rests and other automotive interior trim components • Furniture elements • Sport goods such as skis and surf boards
Elastomers	• Shoe soles • Vehicle body panels • Rollers and gear wheels • Conveyors • Sealants for construction and automotive industries • Fibers
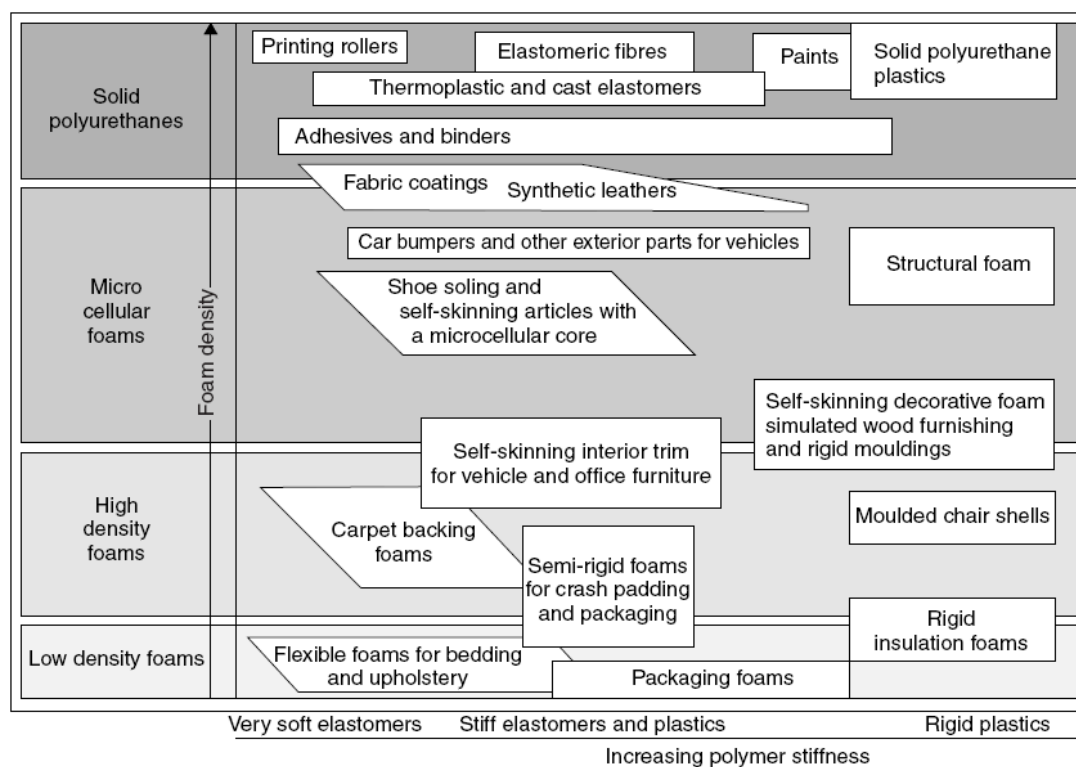
Figure 1.1 Property matrix for polyurethanes.[6]

1.2   Raw Materials

Polyurethanes are linear polymers that have a molecular backbone containing carbamate groups ($-NHCO_2$). These groups, called urethane, are produced through an addition reaction between a diisocyanate and a polyol. The reaction rapidly yields high molecular weight materials. Polyurethanes typically also contain other functional groups in the molecule including esters, ethers or urea groups. A variety of raw materials are used to produce polyurethanes. These include monomers, prepolymers, stabilizers which protect the integrity of the polymer, and colorants.

1.2.1   Isocyanates

Isocyanates are highly reactive compounds and readily react with groups containing active hydrogen. These reactions are most important in the formation of polyurethane elastomers. The chemistry of polyurethanes is therefore called as chemistry of isocyanates. Several aromatic and aliphatic isocyanates are available, but most of the commercial polyurethanes are based on two of them: toluene diisocyanate (TDI) and methylene bis 4-phenylene isocyanate (diphenylmethane diisocyanate or

MDI), and its derivatives. Most of the TDI used is a mixture of two isomers: the 2,4- and 2,6- isomers in 80:20 mixture. A 65:35 mixture is also available. The pure 2,4 isomer is used in some elastomer applications. The two isomers of TDI are shown below.

2,4-toluene diisocyanate   2,6-toluene diisocyanate
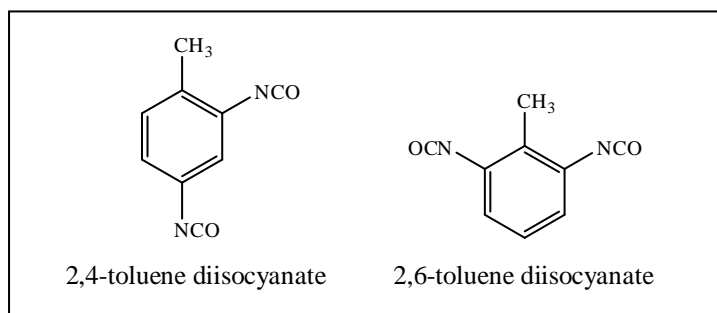
MDI is available in several forms based on two types of products, purified monomeric MDI and polymeric MDI. Pure MDI is substantially 4,4'-MDI. It usually contains a small amount of 2,4'-isomer. The two isomers of MDI are shown below. Polyisocyanate mixtures are formulated by the producers of isocyanate to offer a range of differing functionalities.

4,4'-diphenylmethane diisocyanate   2,4'-diphenylmethane diisocyanate
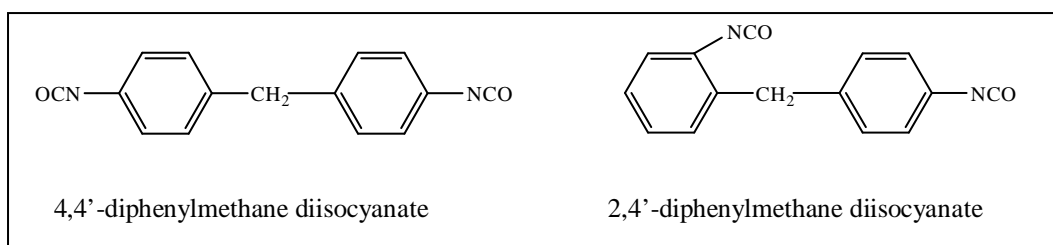
Diisocyanates are required for making elastomers, while high functionality MDI polyisocyanates are desirable for the manufacture of rigid foams and binding materials. Polymeric MDI compositions are characterized by their viscosity and their content of reactive isocyanate groups. In addition to TDI and MDI, other aromatic isocyanates used for specialty applications include 1,5-diisocyanato naphthalene (naphthalene diisocyanate or NDI) and 1,4-diisocyanato-benzene (*p*-phenylene diisocyanate or PPDI).

Polyurethanes obtained from aromatic diisocyanates undergo slow oxidation in the presence of air and light causing discoloration, which is unacceptable in some applications. In contrast, polyurethanes obtained from aliphatic diisocyanates are colour stable, although it is necessary to add antioxidants and UV stabilizers to the formulations to maintain physical properties of the polymers with time. Some

commonly used aliphatic isocyanates are 1-isocyanato-3-isocyanatomethyl-3,5,5-trimethylcyclohexane (isophorone diisocyanate or IPDI), 1,6-diisocyanato-hexane (hexamethylene diisocyanate or HDI) and 4,4-diisocyanato-dicyclohexylmethane (hydrogenated MDI or HMDI). **Table 1.2** lists some commonly used isocyanates for polyurethane synthesis.

Table 1.2 Isocyanates used for making polyurethanes

Name	Structure
2,4-, 2,6-toluene diisocyanate (TDI)	
4,4'-methylenediphenyl diisocyanate (MDI)	
1,5-naphthalene diisocyanate (NDI)	
p-phenylene diisocyanate (PPDI)	
1,6-hexamethylene diisocyanate (HDI)	
Cyclohexyl diisocyanate (CHDI)	
Isophorone diisocyanate (IPDI)	
4,4'-dicyclohexylmethane diisocyante (HMDI)	

The first isocyanates were produced by Wurtz[7] in 1849 by reacting organic sulphates with cyanic acid salts.

$$R_2SO_4 \ + \ 2KCNO \ \longrightarrow \ 2RNCO \ + \ K_2SO_4$$
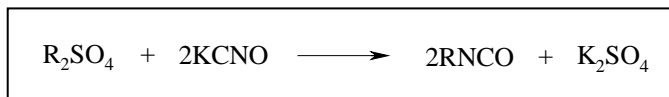
Scheme 1.1 Wurtz synthesis of isocyanate

The standard method for synthesis of isocyanates pioneered by Hentschel[8] in 1884 is phosgenation of amines or amine salts (**Scheme 1.2**). Using this method, a solution of diamine in chlorobenzene is added to excess phosgene in the same solvent below 20°C. The resultant slurry consisting of dicarbamoyl chloride (1) and diamine dihydrochloride (2) is treated with excess phosgene at temperatures up to 130°C. Upon heating above 65°C the dicarbamoyl chloride dissociates to generate diisocyanate. The conversion of (2) is very slow, and use of polar solvents or higher pressures increases the rate of reaction.
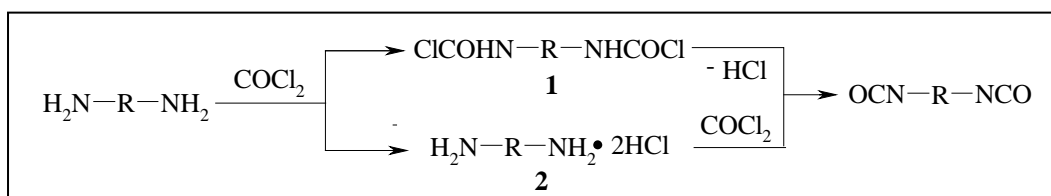
Scheme 1.2 Isocyanate synthesis by phosgenation route

The synthetic route for TDI starts with toluene and proceeds via nitration, hydrogenation and phosgenation. MDI is synthesized from aniline and formaldehyde using hydrochloric acid as a catalyst, followed by phosgenation of the corresponding diamine (**Scheme 1.3**). Aliphatic isocyanates can also be made from the corresponding aliphatic diamines via phosgenation process.
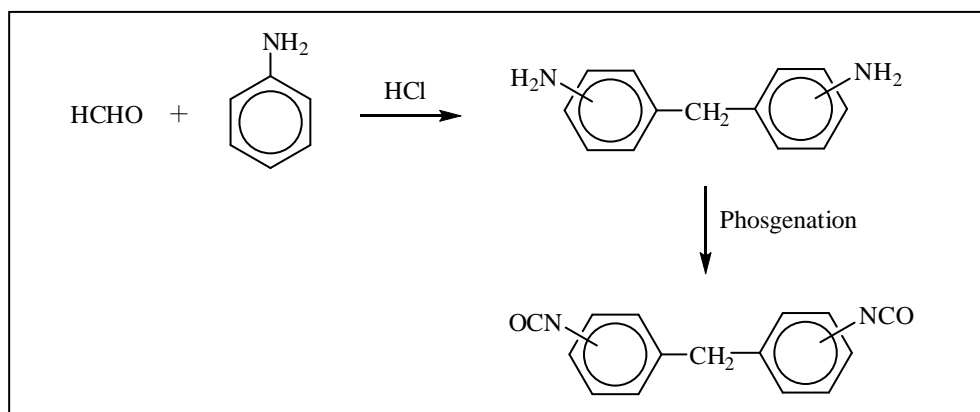
Scheme 1.3 Synthesis of MDI

The other important aliphatic diisocyanate, IPDI is based on isophorone chemistry. Trimerization of acetone gives isophorone **I**, which on reaction with HCN

yields β-cyanoketone **II**. Reductive amination of **II** to the diamine **III**, followed by phosgenation, gives IPDI **IV** as shown below.
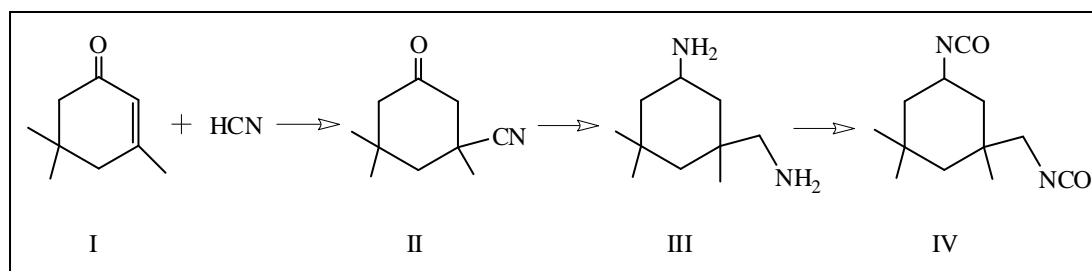
Scheme 1.4 Synthesis of IPDI

1.2.2 Reactions of Isocyanates

The high reactivity of isocyanate toward nucleophilic reagents is mainly due to pronounced electropositive character of the carbon atom caused by the delocalization of electrons onto oxygen, nitrogen and aromatic group. Aromatic isocyanates are therefore more reactive than aliphatic isocyanates, due to negative charge delocalization. Substitution on the aromatic ring can affect delocalization of negative charge in case of aromatic isocyanates. Electron withdrawing groups on the ortho or para position can increase the reactivity of the NCO group, while an electron donating group will have the opposite effect on the reactivity of isocyanate. The electronic structure of isocyanate group can be represented by resonance structures as shown in the following **Figure 1.2**.
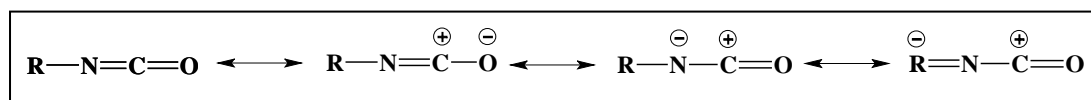
Figure 1.2 Resonance structures of isocyanate group

(I) Primary reactions of isocyanates:

Polyols: The addition reaction of isocyanate with a polyol is an exothermic reaction, influenced by the structure of both reactants. Aliphatic polyols with primary hydroxyl end groups are the most reactive. They react with isocyanates about ten times faster than similar polyols with secondary hydroxyl groups. Phenols react more slowly with the isocyanates, and the resulting urethane groups are easily broken on heating to yield the original isocyanate and phenol. The reaction is strongly influenced by catalysts; e.g. acid compounds (mineral acid, acid halide etc.) slow the reaction,

whereas basic compounds (tertiary amines) and metal compounds (Sn, Zn, Fe salts) accelerate the reaction.

$$R-OH \ + \ OCN-R' \ \underset{K_b}{\overset{K_a}{\rightleftharpoons}} \ R-O-\overset{\overset{\textstyle O}{\|}}{C}-\underset{\underset{\textstyle H}{|}}{N}-R'$$

Hydroxyl   Isocyanate   Urethane
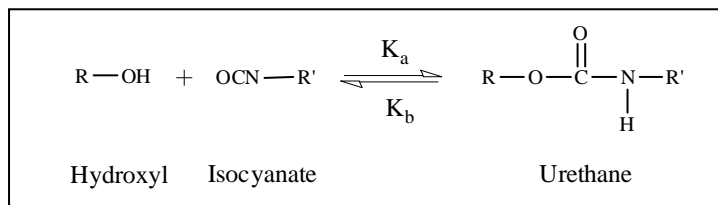
Scheme 1.5 Reaction of isocyanate with polyol

Water: The reaction of isocyanate with water yields a substituted urea and carbon dioxide, which is the source of gas for the manufacture of low density flexible foams. The primary product of the reaction with water is a substituted carbamic acid, which breaks down into an amine and carbon dioxide. The amine then reacts with further isocyanate to yield the substituted urea. This reaction underscores the importance of complete exclusion of water from the reaction system.

$$R-NCO \ + \ H_2O \ \longrightarrow \ R-\underset{\underset{\textstyle H}{|}}{N}-\overset{\overset{\textstyle O}{\|}}{C}-O-H \ \overset{CO_2}{\longrightarrow} \ R-NH_2$$

Carbamic Acid

$$\downarrow OCN-R'$$

$$R-\underset{\underset{\textstyle H}{|}}{N}-\overset{\overset{\textstyle O}{\|}}{C}-\underset{\underset{\textstyle H}{|}}{N}-R'$$

Urea
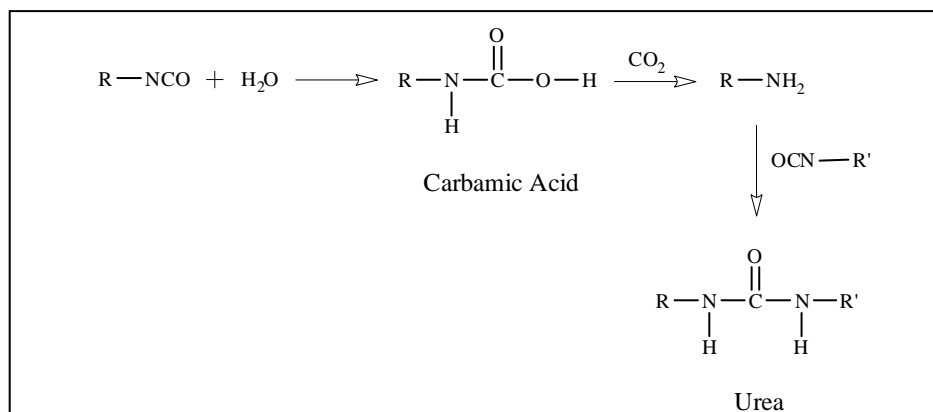
Scheme 1.6 Reaction of isocyanate with water

Amines: Reaction of diisocyanates with diamines is the third most important reaction in polyurethane chemistry. The reaction of isocyanates with primary amines, at room temperature in the absence of catalyst, is about 100 to 1000 times faster than the reaction with primary alcohols. The reactivity of amines increases with the basicity of the amine, and aliphatic amines react much faster than aromatic amines. In case of aromatic amines, steric hindrance and electron withdrawing substituents reduces the reactivity towards isocyanate. Tertiary amines, due to the absence of active hydrogen atoms, do not react with isocyanates.
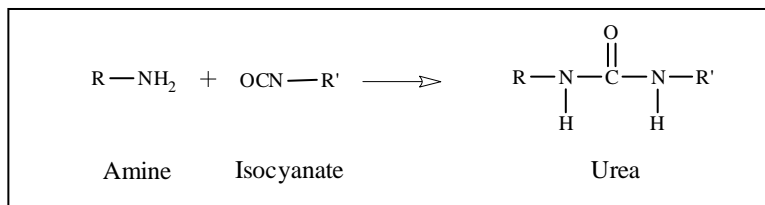
Scheme 1.7 Reaction of isocyanate with amine

(II) Secondary reactions of isocyanates:

Isocyanates, under certain conditions may react with the active hydrogen atoms of the urethane and urea linkages to form allophanate and biuret linkages, respectively. Both reactions are cross-linking reactions, and occur at an appreciable rate over the temperature intervals of 100-150°C and 120-150°C, respectively. The reaction of isocyanates with urea groups is significantly faster than that with urethane groups. However, these linkages are thermally reversible, and dissociates at higher temperatures into starting components.
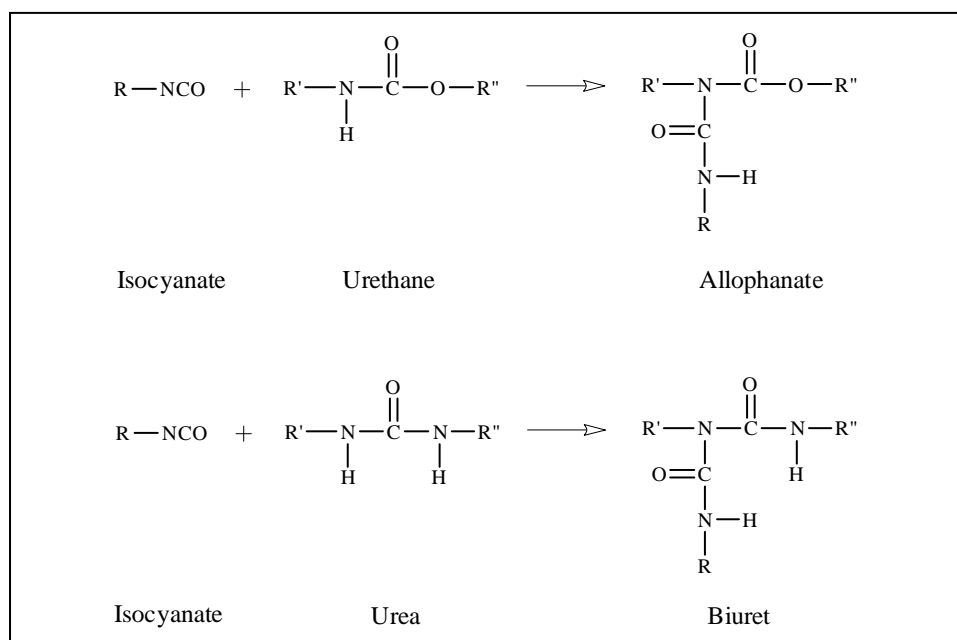
Scheme 1.8 Secondary reactions of isocyanate

(III) Isocyanate polymerization reactions:

Isocyanates form oligomers, especially in the presence of basic catalysts, giving uretidinediones (dimers), and isocyanurates (trimers). Dimer formation arises only from aromatic isocyanates and it is inhibited by ortho substituents. Thus, 2,4- and 2,6-TDI do not form dimers at normal temperatures but 4,4'-diphenylmethane

diisocyanate (MDI) dimerises slowly at room temperature. At higher temperatures insoluble polymeric materials are formed.
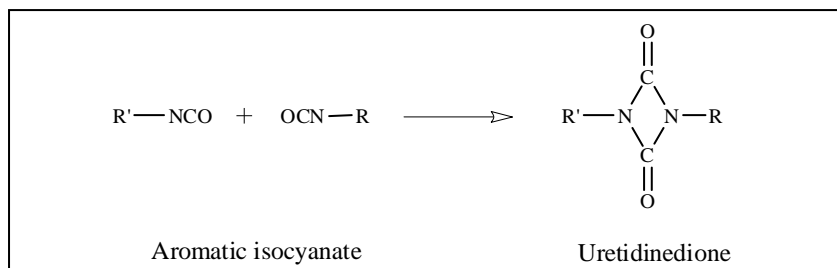
Scheme 1.9 Isocyanate dimer formation

In presence of basic catalysts, isocyanurates are formed on heating both aliphatic and aromatic isocyanates. Isocyanurates are more stable and the reaction is not easily reversed compared to the urethane, uretidinedione, biuret and allophanate linkages.
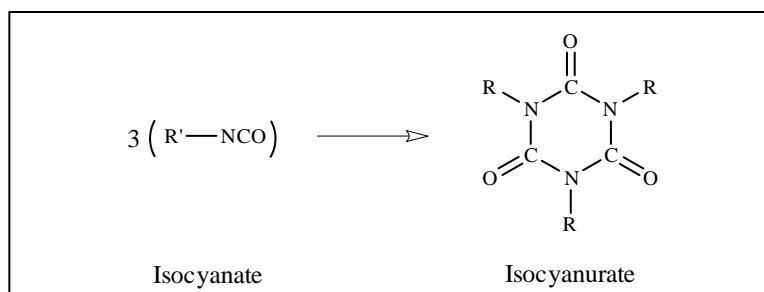
Scheme 1.10 Isocyanate trimer formation

In presence of special catalysts isocyanates can condense, with the elimination of carbon dioxide, to form carbodiimides which then react reversibly with further isocyanate to give uretonimine.
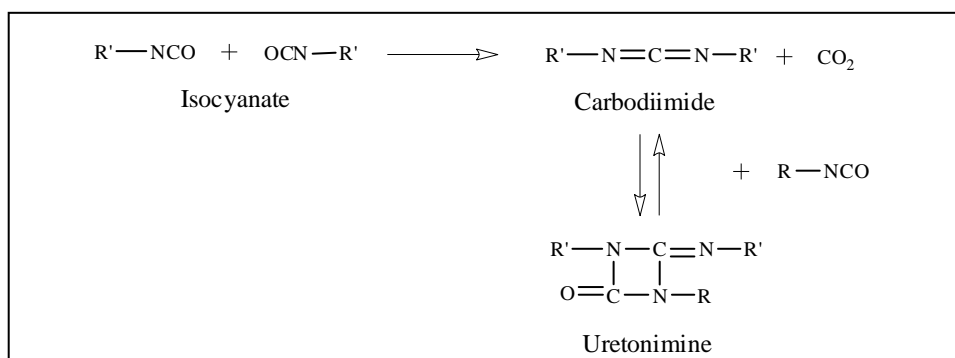
Scheme 1.11 Isocyanate reactions

1.2.3 Polyols

Polyols are hydroxyl terminated macromolecules, with molecular weights ranging from 250 to 8000. The structure of polyol is an important factor in determining the properties of polyurethane. A wide range of polyols are used for the manufacture of polyurethanes. However, most of them fall under two classes: hydroxyl terminated polyethers and hydroxyl terminated polyesters. Polyols are characterized by their hydroxyl value, which is related to its molecular weight and functionality as follows.

$$\text{Hydroxyl value (mg KOH/g)} = \frac{56.1 \times \text{functionality}}{\text{molecular weight}} \times 1000 \qquad (1.1)$$

Polyether Polyols: The backbone of polyether polyols are either propylene oxide homopolymers or random or block copolymers with ethylene oxide. These are made by the addition of alkylene oxides on to alcohols or amines, which are usually called starters or initiators. The addition polymerization of propylene oxide occurs with either anionic (basic) or cationic (acidic) catalysis. A special class of polyether polyols, poly (tetramethylene glycol) is synthesized by cationic ring opening polymerization of tetrahydrofuran. The economically attractive polyether polyols based on alkylene oxides are listed in **Table 1.3.**

Important characteristics of polyols are their hydroxyl functionality, hydroxyl equivalent weight, and their reactivity and compatibility with the other components used in the polyurethane formulation. Blending of polyols of different functionality, molecular weight, and reactivity can be used to tailor a polyol for a specific application. Since primary hydroxyl groups are more reactive than secondary groups, it is advantageous to produce block copolymers with terminal primary hydroxyl groups. Some of the characteristic features imparted by the use of polyether polyols are following:

- High hydrolysis resistance
- Excellent low temperature flexibility
- Resistance to microbial degradation
- Excellent clarity

Table 1.3 Commercial polyether polyols

Polyol	Structure
Polyethylene oxide (PEO)	$HO\left(\!\!\begin{array}{c} O \end{array}\!\!\right)_n H$
Polypropylene oxide (PPO)	$HO\left(\!\!\begin{array}{c} O \\ CH_3 \end{array}\!\!\right)_n H$
Polytetramethylene oxide (PTMO)	$HO\left(\!\!\begin{array}{c} O \end{array}\!\!\right)_n H$

Polyester Polyols: Initially polyester polyols were commonly used for making polyurethanes, but today cost effective polyether polyols dominate the polyurethane market. Polyester polyols are based on saturated aliphatic or aromatic carboxylic acids and diols or mixtures of diols. The carboxylic acid of choice is adipic acid because of its favorable cost/performance ratio. The typical hydroxyl terminated polyester is made from adipic acid and an excess of diol such as ethylene glycol, 1,4-butanediol, 1,6-hexanediol, neopentyl glycol, or mixtures of these diols. Polyols resulting from adipic acid and straight chain diols are crystalline with melting points up to ca $60^{\circ}C$. The properties of the elastomer are governed mainly by the overall molecular weight of the polyester and only to a minor degree by the molecular weight distribution.

There are two special classes of polyesters of commercial interest, polycaprolactones and aliphatic polycarbonates. Polycaprolactones are made from ε-caprolactone and a bifunctional initiator, such as 1,6-hexanediol. Polycarbonates offer excellent hydrolytic stability. They are made from diols, for example, 1,6-hexanediol, and phosgene or by transesterification with low molecular weight carbonates such as diethyl or diphenyl carbonate.

For elastomers, linear polyester polyols of molecular weight of ca 2000 are preferred. Branched polyester polyols are used for foam and coating applications. Compared to polyether polyols, polyester polyols have lower hydrolytic stability, but they have better oxidation and thermal stabilities. Characteristic features obtained by using polyester polyols are as follows.

- Excellent mechanical properties
- Heat resistance
- High resistance to oils and chemicals
- Outstanding tear strength
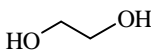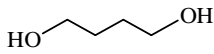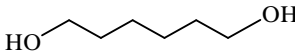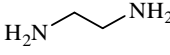
Table 1.4 Commercial polyester polyols

Polyol	Structure
Polyethylene adipate (PEA)	$HO\text{-}(CH_2)_2\text{-}[O\text{-}\overset{O}{\overset{\|}{C}}\text{-}(CH_2)_4\text{-}\overset{O}{\overset{\|}{C}}\text{-}O\text{-}(CH_2)_2\text{-}]_n\text{-}OH$
Polytetramethylene adipate (PTMA)	$HO\text{-}(CH_2)_4\text{-}[O\text{-}\overset{O}{\overset{\|}{C}}\text{-}(CH_2)_4\text{-}\overset{O}{\overset{\|}{C}}\text{-}O\text{-}(CH_2)_4\text{-}]_n\text{-}OH$
Polycaprolactone (PCL)	$HO\text{-}[(CH_2)_5\text{-}\overset{O}{\overset{\|}{C}}\text{-}O]_n\text{-}(CH_2)_5\text{-}OH$

1.2.4 Chain Extenders

Chain extenders are low molecular weight hydroxyl or amine terminated compounds that play an important role in polymer morphology. The choice of chain extender and diisocyanate determines the characteristics of the hard segment and to a large extent the physical properties of polyurethane. The most important chain extenders are linear diols such as ethylene glycol, 1,4-butanediol, 1,6-hexanediol, and hydroquinone bis(2-hydroxyethyl) ether. These diols form well crystallized hard segments with isocyanates. Diamines react faster with isocyanates and results in the formation of the hard segment with a higher density of secondary bonding, high hard segment T_g, and high thermal stability of the polymer. **Table 1.5** lists some common chain extenders.

Table 1.5 Chain extenders

Polyol	Structure
Ethylene glycol	HO⌒OH
1,4-butanediol	HO⌒⌒OH
1,6-hexanediol	HO⌒⌒⌒OH
Ethylene diamine	H_2N⌒NH_2

1.3 Synthesis of Segmented Polyurethane Elastomer

The 'one-shot method' and the 'prepolymer method' are the two principle routes used for synthesis of segmented polyurethanes (**Figure 1.3**). The exothermic polyaddition reactions are generally carried out at temperatures in the range 70-80°C. In order to obtain a polymer with desirable properties, the molar ratio of isocyanate to hydroxyl and/ amine should be maintained at one. Stoichiometry of the reacting groups is very essential as even a slight deviation limits the polymer molecular weight.
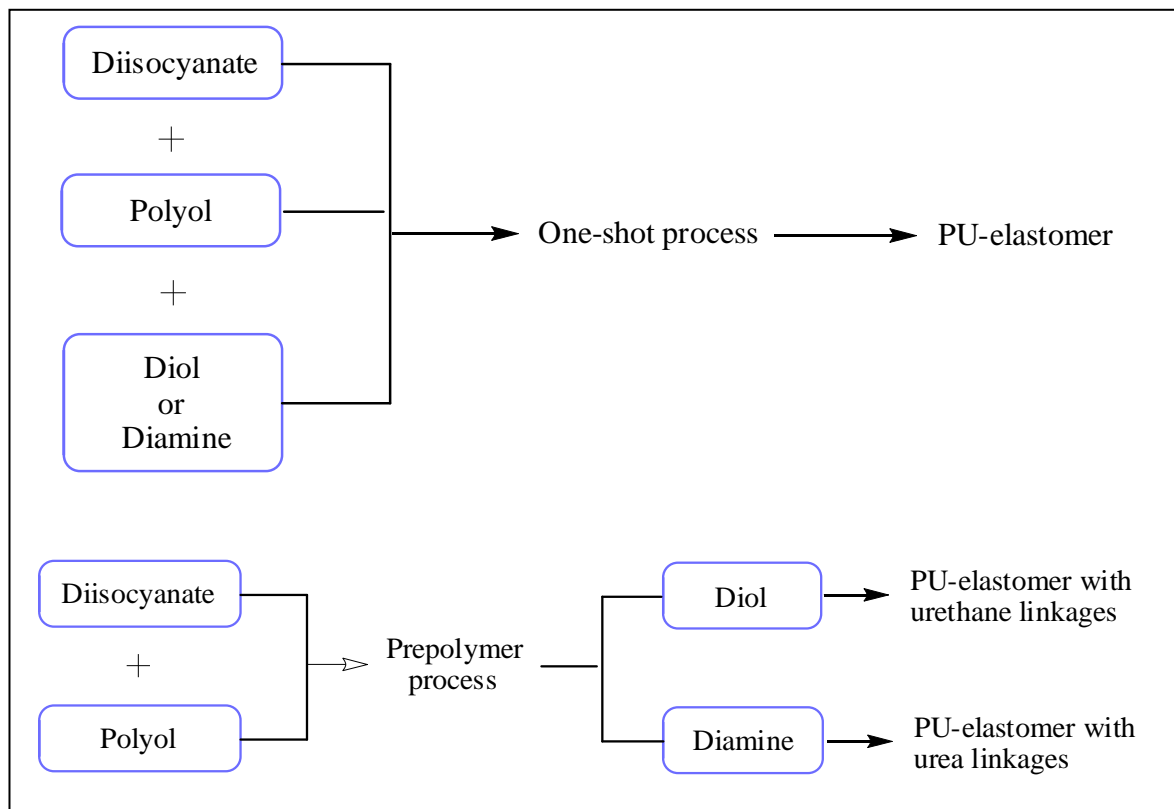
Figure 1.3 One-shot and Prepolymer method of polymerization

In the one-shot method of synthesis, all reaction components namely polyol, isocyanate and chain extender are mixed simultaneously, and allowed to polymerize. The reaction is highly exothermic and vigorous. In the prepolymer method, a NCO – terminated prepolymer is synthesized in the first step by reacting diisocyanate with polyol in a high NCO/OH ratio. High molecular weight polymer is obtained in the second step by reacting –NCO terminated prepolymer with the chain extender (diol or diamine). Polar aprotic solvents such as N,N-Dimethylacetamide (DMAc) and dimethylformamide (DMF) are commonly used for solution polymerization reactions. There is also a literature report on the use of isopropanol as a reaction solvent for the preparation of polyether-urea copolymers.[9]

The method used for synthesis has a marked influence on the morphology as well as properties of the resulting polymer. Generally solution reaction results in a product with far less side reactions (allophanate and biuret), which causes chain branching and an increase of molecular weight.[10] Reaction conditions also influence structural heterogeneity and molecular weight of the product. When the one-shot

method is used in bulk polymerization, the reactivity difference between the –OH groups of the polyol and the chain extender with different isocyanate groups affect the sequence of hard segments in the polymer chain. In case of prepolymer method, sequences are found to be more regular compared to the one shot method. Prepolymer method produces polyurethanes with superior properties since structural regularity leads to the better packing of hard segments, which crystallize to form physical crosslink points.

1.4 Morphology

1.4.1 Heterophase Morphology

Segmented thermoplastic polyurethane and its closest analogue polyurethane-urea (PUU), containing randomly alternating hard and soft blocks, constitute an industrially important class of block copolymers. Thermodynamic incompatibility between the polar hard and the less polar soft segments makes the free energy of mixing positive, and thus forces them to phase separate. However, the length scale of phase separation is limited by the connectivity of the blocks. Further, the shorter hard and soft segment chain lengths (compared to the diblock and triblock copolymers), the high level of polydispersity and the presence of weak secondary interactions (dipole-dipole or hydrogen bonding) between the hard and soft segments, results in an ill-defined microphase separated morphology in polyurethanes. The degree to which hard and soft segments microphase separate and the resulting morphology have a profound effect on the ultimate properties of the copolymer.

The tendency to microphase separate into periodic morphologies depends on composition (volume fraction of hard/soft blocks, ϕ), the overall degree of polymerization (N), and the segment-segment (Flory-Huggins) interaction parameter (χ). The interaction parameter χ has inverse temperature dependence, and consequently a first order phase transition, called as order-disorder transition (ODT) takes place as the temperature is raised. At high temperatures, the entropy dominates and segments mix randomly to form a homogeneous (disordered) phase. At low temperatures, the drive to lower the energy of the system dominates, and the blocks locally segregate to minimize contacts between unlike monomers. This process,

referred to as microphase separation, results in the formation of periodic morphology.[11] Such a transition is associated with a significant change in the viscoelastic properties of the material. ODTs of this kind have been commonly observed in block copolymers,[12-19] and have been the subject of extensive investigations using techniques such as scattering,[20-23] rheology[12,24] and calorimetry.[25] Polyurethanes, on the other hand typically show a weak ODT or a continuous microphase mixing because of their ill defined microphase morphology.[26]

For block copolymers comprising of A and B blocks the interaction parameter χ can be defined as the product of lattice coordination number (Z) and change in interaction energy (ε) reduced by the thermal energy ($k_B T$)

$$\chi = Z\left[\varepsilon_{AB} - \left(\varepsilon_{AA} + \varepsilon_{BB}\right)/2\right]/K_B T \qquad (1.2)$$

where ε_{AA}, ε_{BB} and ε_{AB} denote interactions for a A-A contact, a B-B contact and a A-B contact, respectively. The value of χN is an estimate of the extent of phase separation. If the value of χ or N is very small, the entropic factors will dominate, leading to a compositionally disordered phase. As χN is increased, a delicate balance between energetic and entropic factors produces a disorder-to-order phase transition.

In case of PUs, the two parameters ϕ and N can be regulated through polymerization stoichiometry, whereas, χ depends on the choice of the hard and the soft segments. In general, phase separation is more pronounced in PUs containing polyether soft segments than polyester soft segments. Highly non-polar soft segments such as polydimethylsiloxane, polybutadine and polytetramethylene oxide (PTMO) show greater levels of microphase separation. Apart from the parameters mentioned above, segmental crystallinity is another factor which increases phase separation in PU block copolymers.

The morphology of a multiphase system, such as polyurethanes, plays an important role in determining the final properties of product. Therefore, in order to obtain desired product properties, a control over the morphology is essential. A profound knowledge of morphology is thus vital to understanding structure-property relationships. In general, heterophase morphology in polyurethane block copolymers is complicated by the presence of hydrogen bonding, hard segment crystallization, segmental mixing due to secondary association, and temperature sensitivity.

1.4.2 Structure-Property Relationship

The physical properties of polyurethanes can vary considerably depending upon the nature and amount of the three main components namely, polyol, diisocyanate and chain extender. The mechanical properties of polyurethane are strongly dependent on the extent of microphase separation and the details of domain structure of phase separated morphology. At a primary level the morphology is controlled by the chemical nature of monomers, molecular weight and distribution of hard and soft segments, crosslinking, and degree of branching. At a secondary level, the morphology is controlled by the three dimensional chain orientations and crystallinity.

Soft Segment (SS):

The long flexible soft segment largely controls the low temperature properties, weather resistance, solvent resistance and mechanical properties. The structure and the molecular weight of soft segments also influence the morphology of polyurethanes. Typically, soft segments with average molecular weights of 1000 – 5000 are used for synthesis of thermoplastic polyurethanes. Polyether urethanes show a higher degree of phase separation than polyester urethanes due to greater incompatibility of polyether soft segments with the polar hard segments.

Increasing the molecular weight of soft segments affects the properties of both polyether and polyester urethanes. Velankar and Cooper[27] studied the effect of increasing soft segment molecular weight on microphase separation and viscoelastic properties of polyester polyurethanes. A series of polyesterurethanes with differing block length (soft segment MW = 830, 1250, 2000 & 3000) and constant composition (soft segment$\approx 5\,0$ wt %) were synthesized and characterized by DSC, SAXS and rheology. DSC and SAXS data showed that PUs synthesized with SS MW 830 and 1250 were single phase materials. The rheological behaviour of these two PUs was akin to that of homopolymer melts and followed predictions of Rouse theory reasonably well. DSC, SAXS and rheological analysis (Time Temperature Superposition) for PUs having SS MW 2000 and 3000 showed progressive increase in the extent of microphase separation with SS MW. In addition, the relaxation time and Newtonian viscosity also showed strong dependence on soft segment length.

Although soft segments in polyurethanes are normally in the amorphous state, tendency towards crystallization and cold-hardening increases with increase in soft segment molecular weight. Soft segments were also observed to crystallize during tensile deformation at low and medium elongations.[28] Strain induced crystallization leads to a self reinforcing effect, which enhances the modulus of the polymer. Yeh et al.[28] studied structure development during deformation of a segmented polyurethane-urea elastomer. Stress induced crystallization of isotropically oriented PTMO soft segments was observed with increasing strain. Also, both orientation and stress induced crystallization relaxed after releasing the applied stress. WAXD results showed that the initially isotropically oriented soft segments increase in orientation with the increasing strain. At strains approaching 300-500%, strain induced crystallization of soft segments was detected. Based on x-ray and vibrational spectroscopic data, the authors proposed a morphological model of hard and soft segment microphase separation, orientation and strain induced crystallization in the soft segment.

In a recent work Korley et al.[29] studied the effects of crystallinity in soft segment phase comprising of polyether soft blocks with varying tendencies to crystallize. In this study, the authors examined the morphology and mechanical behavior of a series of polyurethanes containing PEO (1000 and 4600 g/mol) and PEO-PPO-PEO (1900 g/mol) soft segments with varying hard segment content. It was found that soft segment crystallinity in PEO (1000 g/mol) improved the storage modulus of polyurethane below the T_m of the soft block and enhanced toughness compared to the polyurethanes containing PEO-PPO-PEO soft segments. The study showed that soft segments not only impart extensibility, but ordered soft segment regions also reinforce the polyurethane matrix during deformation process in a similar manner to the hard domains, dissipating energy and contributing to the overall toughness.

Hard Segment (HS):

The elastomeric properties of polyurethane segmented block copolymers result from the microphase separation between soft segment and hard segment sequences which are respectively above and below their T_g at ambient conditions. HS sequences, which are formed by the isocyanate and the chain extender molecules, can be

crystalline, semicrystalline or glassy. They form a nonresilient phase dispersed in the continuous phase of the soft elastomeric segments. The HS microdomains act as thermally labile physical cross-link sites as well as fillers for the rubbery SS matrix. Considerable efforts have been made to elucidate the nature of hard segments in polyurethanes.[30-34]

Typically, the morphology of polyurethanes consists of many HS rich domains with sizes ranging from tens to hundreds of angstroms, dispersed in the matrix of soft segments. The primary driving force for domain formation is the strong intermolecular interaction between the urethane units, which are capable of forming interurethane hydrogen bonds. The HS structure plays an important role in phase separation. The incorporation of urea linkages in the HS has a profound effect on the phase separation and domain structure of polyether polyurethane-ureas. This is due to the increased polarity difference between hard and soft segments, and a likely development of three dimensional hydrogen bonding network.[35-37]

Chain extender components and their properties also determine the intermolecular interactions as well as the morphology of polyurethanes. Blackwell et al.[38] extensively studied the structure of hard segments in MDI-diol-polytertamethylene adipate polyurethanes. They used butanediol (BDO), propanediol (PDO), and ethylene glycol (EDO) as chain extenders. Poly MDI-BDO was found to be the most crystalline hard segment. This was due to the extended chain conformation of the HS resulting in strong hydrogen bonded network.

Urea groups, formed by the reaction of diisocyanate with diamine chain extender, are excellent functionalities for use in hard segments of thermoplastic elastomers because they are known to associate via bifurcated hydrogen bonds. Their hydrogen bond strength exceeds that of amides and urethanes. But these elastomers suffer from disadvantages such as poor melt processibility and incomplete solubility in organic solvents. Due to very strong bifurcate hydrogen bonding between urea groups, the melting or softening temperatures of urea segments are much higher than their thermal decomposition temperatures.

In general, there are two different types of dispersed HS morphologies present in segmented polyurethanes, when the concentration of HS is low: I) fibrillar domains in which the domain axes coincide with the polymer chain axes, and II) the lamellar domains in which the domain axes are perpendicular to the polymer chain axes. These

hard segment domains connect the linear polymer chains in both the lateral direction and the chain direction, producing an effective crosslink network that is responsible for the elastic properties of the polymer. Each microphase domain behaves as a cross-link junction that is thermally reversible.

Generally, the HS content is a major factor influencing the mechanical properties. It was observed using thermal, X-ray and AFM techniques that increasing the HS content resulted in enhancement of hard domain crystallinity. Initial moduli and tensile strength were also found to increase with concomitant decrease in the ultimate elongation.[29] This was attributed to the formation of more interconnected HS domain morphology from randomly dispersed hard domains. Cooper et al.[39] studied the orientation of elastomeric polyurethane block copolymers using differential infrared dichroism. Hard segment length and crystallinity were found to be primarily responsible for the orientation. A drastic change in the orientation behaviour was observed with the onset of interlocking hard segment morphology when the hard segment content was increased from 24 to 28 wt%. Once the interlocked, semicrystalline hard segments are formed, only minor changes in the orientation behaviour due to change in volume fraction of hard segments were observed. Van Bogart et al.,[40] on the basis of X-ray scattering and DSC studies, concluded that MDI/BD hard segments exist in semicrystalline domains whose crystallinity increased as the hard segment length increased. The length of the hard segment blocks forms the upper limit to the size of the hard segment crystals in the chain direction, which, in turn determines the melting point. Increasing hard segment content was also found to be accompanied with the broadening of the melting transition resulting from a distribution of the hard segment crystal thickness.

Versteegen et al.[41] studied the effect of uniform hard segments on the morphology and properties of polyether ureas. Their study demonstrated that block copoly(ether urea) with exactly two urea groups in the hard blocks showed mechanical properties superior to less defined analogue possessing polydisperse hard blocks. The strain at break (1000 – 2100%) and toughness of these materials were claimed to be higher than commercially available thermoplastic elastomers. The morphology of these materials consisted of long stacks of associated hard blocks embedded in soft phase.

Yilgor et al.[42] studied the influence of hydrogen bonding and diisocyanate symmetry on microphase morphology. Their study on non-chain extended, segmented polyether urethanes and polyether ureas showed some interesting results regarding the microphase separation in these polymers. In their work, polyurethanes that were prepared by using symmetrical diisocyanates, such as 1,4-phenylene diisocyanate (PPDI), 1,6-hexamethylene diisocyanate (HDI) and 1,4-cyclohexyl diisocyanate (CHDI) all showed microphase morphology, where ribbon-like hard segments percolated through the soft segment matrix. On the other hand polyurethanes based on unsymmetrical diisocyanates such as bis(4-isocyanatocyclohexyl)methane (HMDI), 2,6- and 2,4-toluene diisocyanate (TDI), MDI and 1,3-phenylene diisocyanate (MPDI) did not display microphase morphology at room temperature. In contrast to their urethane counterparts all polyether ureas, regardless of the structure or symmetry of the diisocyanate displayed microphase morphology at room temperature. Their study shows the important role of hard segment symmetry on the microphase morphology of polyurethanes.

Over the past few years, there have been reports on the preparation of segmented polyurethanes and polyureas without chain extenders and investigation of their structure-property relationships.[41-45] These polymers, not only display microphase morphologies, but also show very attractive thermal and mechanical properties comparable to the chain extended copolymers. These results disproved the widely held belief that it is necessary to employ chain extension to produce segmented polyurethanes and polyurea copolymers with useful structural properties.

Hydrogen Bonding:

Hydrogen bond, the strongest secondary chemical bond, is formed between a proton donor and a proton acceptor. The urethane and urea linkages in polyurethanes can serve both as proton donor and acceptor. Typical polyurethane is extensively hydrogen bonded, the donor being N-H group of urethane or urea linkage in the hard segment. At room temperature, approximately 90% of the N-H groups are found to be hydrogen bonded.[46] The proton acceptor may be either C=O in the urethane or urea hard segment, or the ester C=O or ether –O- in the soft segment. **Figure 1.4** shows hydrogen bonds between various donors and acceptors in polyurethane and

polyurethane-ureas. Polyether polyurethane has fewer hydrogen bonds than polyester urethane with same hard segment content.
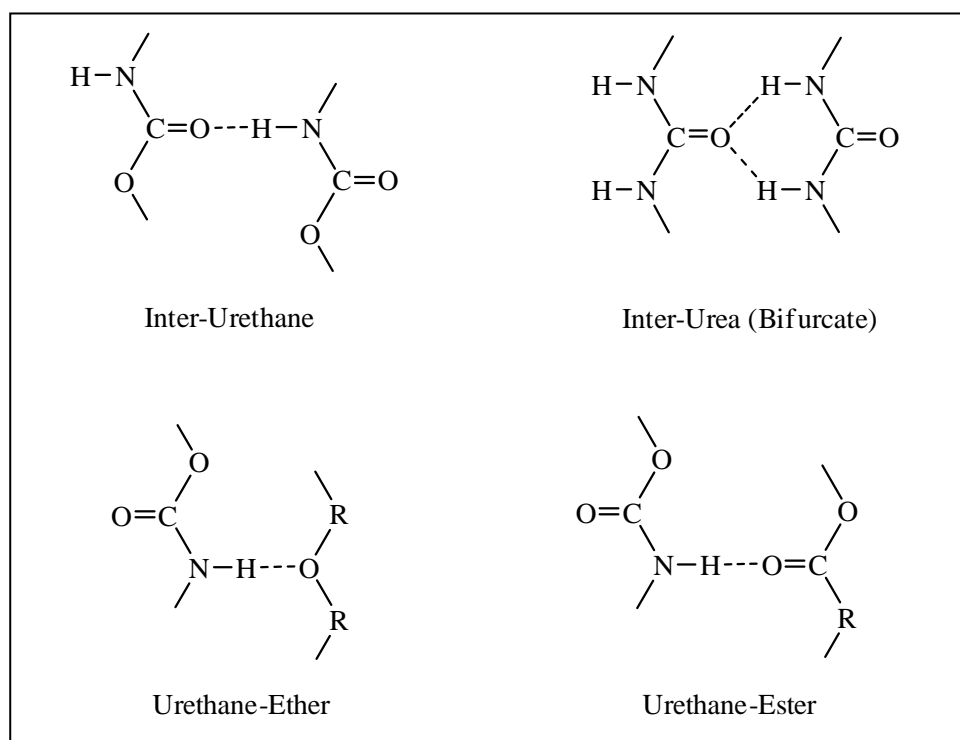
Figure 1.4 Hydrogen bonding in polyurethanes (A) between hard-hard segments and (B) between hard-soft segments.

The extent of hydrogen bonding can be affected by the structure and composition of polyurethane as well as by temperature. Hydrogen bonding starts disrupting with increase in temperature above the hard segment T_g. High temperature infrared studies carried on aliphatic polyurethanes by McKiernan et al.[47] showed the existence and high concentration (≈75%) of hydrogen bonding in these polyurethanes even in the melt. Their study also shows that hydrogen bonding controls the crystallization, packing, and morphology of polyurethanes, resulting in a crystal structure analogous to that of aliphatic polyamides.

The primary force for microphase separation is believed to be the strong intermolecular interaction (hydrogen bonding) between urethane units. Thus, qualitative information of phase separation can be extracted from hydrogen bonding between the two phases. If hydrogen bonds exist only within the hard segment domains, phase separation occurs to a greater extent. On the other hand, if they can be

formed between the soft and hard segments, the interphase hydrogen bonding enhances the degree of phase mixing. The higher strength of hydrogen bonding in polyureas[48-50] and the three dimensional configuration of hydrogen bonded urea groups have been studied.[35,36]

Wang and Cooper[51] studied the effect of urea linkage, hard segment content, and block length on the extent of phase separation, domain structure and physical properties. It was observed that the presence of three dimensional hydrogen bonding between the urea groups leads to unusually strong hard domain cohesion. That is, single urea N-H group is bonded to two urea C=O in a nonplanar three dimensional configuration.

FTIR spectroscopy has been used as a sensitive tool for the characterization of hydrogen bonding.[36,47,52-59] Although a number of vibrational modes are present in the system, valuable information can be obtained from the N-H and C=O stretching vibrations near 3200-3400 and 1600-1700 cm^{-1}, respectively.

1.5   Morphological Characterization

Morphology of polyurethane block copolymers can be studied at three different length scales. The smallest length scales correspond to molecular sizes such as the block sequence, sequence distribution, hard segment crystallinity (up to few nanometers), and these can be studied by NMR, FTIR spectroscopy and wide angle X-ray diffraction (WAXD). The next length scale corresponds to mesoscopic size, and this typically refers to the microphase separated domain structure (tens of nanometers). The same can be investigated by direct methods such as TEM, AFM or qualitatively by SAXS. The third level of microstructure is the spherulitic texture (in micrometers) and can be characterized by using small angle light scattering, electron microscopy and polarized light microscopy. However, complete characterization of the morphology needs other supplementary thermal analytical methods such as DSC, dynamic mechanical analysis (DMA), and rheology. Depending on the chemical composition and the hard segment content, microphase morphologies such as spherical, cylindrical and lamellar have been reported. Several characterization techniques are used in combination to study microphase separation and the resulting morphologies in polyurethanes.

Several studies have reported the application of FTIR technique for characterization of hydrogen bonding in polyurethanes. Hydrogen bonding is evidenced by a frequency shift to values lower than those observed when these groups are free. Such shifts in the peak positions of N-H and C=O groups, depending on their strength and the environment (ordered or disordered) of hydrogen bonding, yield important information about the phase separated or phase mixed states.[46,51,54,60-62] Based on their FTIR study, Wang and Cooper[51] proposed the formation of three-dimensional urea hydrogen bonds in segmented polyether polyurethane-urea copolymers. Stress-strain studies carried out on these copolymers using IR dichroism measurements showed, that the hard segments within the domains initially orient transverse to the stretch direction, whereas soft segments orient parallel to the stretch direction.

Painter and coworkers have done extensive studies on the characterization of morphology in polyurethane and polyurethane-urea block copolymers. In a recent study, Mattia and Painter used FTIR to examine the role of hydrogen bonding on the morphology of polyurethane and polyurethane-urea and their blends with polyethylene glycol.[60] Their results indicate that polymer mixtures with polyethylene glycol, form small ordered structures (imperfect crystals) with largely two-dimensional packing of chain segments.

Yilgor et al.[63] have also reported FTIR study of the time-dependent morphology development in polyurethanes and polyureas to obtain valuable quantitative information on the extent of microphase separation. IR dichroism has the ability to provide a quantitative picture of average spatial orientation of several IR absorbing species simultaneously. This technique has been used as a sensitive tool for the analysis of orientation and relaxation responses of both amorphous as well as crystalline regions of polyurethanes undergoing mechanical deformation.[30,39,64,65] Dynamic IR spectroscopy has also been used successfully in the study of molecular and submolecular origins of macroscopic rheological properties of polymeric materials.[66]

Nuclear magnetic resonance (NMR) spectroscopy has also been used as a tool for studying morphology of PU. Pulsed NMR technique is sensitive to the molecular dynamics of polymers and was used for the investigation of phase interfaces as well as the extent of microphase separation.[67-70]

Microscopy is the most direct way of the observation of morphology. Higher magnification imaging is possible with electron microscopy, given sufficient electron density contrast. However, poor natural contrast between hard and soft segments in PU becomes a limiting factor in the extensive use of this technique. Heavy elemental staining of domains is therefore required to generate sufficient contrast for TEM.[71-78]

More recently, atomic force microscopy (AFM) has proved to be an important tool for the morphological investigation.[79-84] For soft materials such as PU, the tapping mode is more popular since it involves lower forces and only intermittent contact between tip and the sample surface. This technique allows for simultaneous detection of height and phase information which respectively provides insight into the variations in topography and local stiffness.

In a comparative study of the morphology of highly branched polyurethane urea copolymers, with their linear analogs, J.P. Sheth et al.[85] have used AFM phase imaging for the microstructure characterization. AFM imaging revealed differences in the morphology of hard segment domains such as disorded, particulate, short rod like and percolating. In another study, Sheth et al.[86] have used AFM as a primary tool for probing the hard segment phase connectivity and percolation in segmented polyurethane-urea copolymers. The tapping mode phase images of the PUU sample without hard segment branching showed the presence of long ribbon like hard domains that percolated through the soft matrix. This long range connectivity was found to be increasingly disrupted with higher levels of hard segment branching.

Korley et al.[29] have used AFM imaging to study the effect of hard and soft segment ordering on the development of morphology. At lower hard segment contents, hard domains are observed to be randomly dispersed in a continuous soft matrix. It was observed that interlocking hard domain morphology was developed on increasing the hard block length. S. Das et al.[45] recently carried out morphological analysis of non-chain extended polyether polyureas which showed phase separated morphologies with hard segments forming thread-like crystalline structures that were dispersed in the continuous soft segment matrix.

Small angle X-ray scattering (SAXS), is another technique which is very popular in the morphological study of PU.[27,33,34,64,87-93] SAXS is advantageous in some aspects such as ease of sample preparation. Advent of synchrotron X-ray sources has opened up the possibility of real time measurements of morphological changes,

including those caused by mechanical deformation and microphase separation kinetics. Scattering in the Porod region is related to morphological fine detail. Generally this can be attributed to the nature of interfaces between micordomains. SAXS has been successfully utilized to study the width and the nature of interphases[94] (Porod scaling). The ratio of SAXS invariants has been used as an indicator of the extent of phase separation in TPU. But, interpretation of morphology from SAXS data alone is not unambiguous, and requires help from other techniques.

The majority of information about polyurethane microstructure has been obtained through X-ray scattering experiments which have resulted in different schematic models of hard segment structure. Laity et al.[90] have provided an excellent review on small angle scattering models for segmented polyether urethane copolymers. The authors have reviewed various models proposed as a basis for interpreting scattering data from polyurethanes. SAXS data from several experimental and commercial polyether formulations was used to test scattering models based on different morphologies. In one of the early X-ray scattering experiments on polyurethanes, Bonart et al.[30,95,96] proposed a hard segment packing model in which hard segments are ordered laterally in order to maximize the hard-hard segment hydrogen bonding. Hard segment sequences were assumed to exist in extended configurations within lamellar or sheetlike microdomains. Koberstein and Stein[97] carried out a detailed SAXS study and proposed that hard segment sequences must be present in either coiled or folded configurations and have developed a lamellar model based on their study. Support to such lamellar model allowing partially coiled hard segment sequence came due to a detailed work by Leung and Koberstein from SAXS and neutron scattering analysis.[33] The thickness of the hard segment microdomain obtained from the model was approximately four hard segment repeat units. Their results also provided evidence for a transition from discrete to continuous hard domain morphology with increase in hard segment content above ca. 50%. X-ray scattering data was also analyzed to estimate details of microphase separated domains such as their diffuse boundary thickness, surface-to-volume ratio, microdomain purity and specific interfacial area.

Ryan et al. have used small angle X-ray scattering as a tool for studying the temperature dependent morphological properties of polyurethane.[87] Time resolved

SAXS data showed a strong Bragg reflection at low temperatures, and the same disappeared at high temperatures due to order-disorder transition.

Differential scanning calorimetry (DSC) has been used as a common tool to determine thermal changes, for example, enthalpy changes associated with glass transitions (T_g), and enthalpy changes associated with phase separation,[98] crystallization,[89] and ordering in the hard segments.[46] DSC data has also been used to estimate the phase composition of a microphase separated sample from the measured T_g values of the two phases.[27,99]

The presence of multiple α-transitions in PU block copolymers have been studied by many research groups using dynamic mechanical analysis (DMA). The detection of hard segment T_g in PUs often becomes difficult due to very small changes in the heat capacity associated with the transition.[100] DMA proves to be a more sensitive tool in such cases. Extensive studies on the use of dynamic mechanical analysis for the characterization of PU have been carried out by Cooper,[101,102] Wilkes,[103] Schneider and co-workers[104] to name a few.

The effects of viscoelasticity on the kinetics and morphology of phase separation in block copolymers have been studied since past two decades following the first observation by DeGennes et al.[105-108] Rheological techniques have been in use as an alternative method for the characterization of microstructural changes taking place in the sample, especially during phase transition stages.[109-111] In case of block copolymers, the order-to-disorder transition (ODT) is known to take place with concurrent changes in the viscoelastic parameters. Viscoelastic behavior of a block copolymer in the ordered and disordered state is quite different. Ordering causes the copolymer to resist flow leading to higher shear modulus.[111,112] In isochronal dynamic temperature sweep experiment, elastic modulus, would therefore, be expected to drop discontinuously with the onset of phase mixing. This is expected to be more pronounced in case of molecules with well defined architectures, such as diblock copolymers having long range microstructure ordering. A homogeneous, molten polymer on the other hand, displays a gradual decrease of elastic modulus with increasing temperature in isochronal temperature sweep test.

The principle of time temperature superposition (TTS) has also been used as a test for heterogeneous morphology. TTS works when all measured relaxation times have the same temperature dependence. Heterogeneity in the sample is associated

with the differences in temperature dependence of relaxation times, leading to violation of TTS. Velankar and Cooper[27] carried out an extensive rheological study on polyester urethanes to investigate the effect of soft segment block length on microphase separation using TTS as one of the characterization tools. Yoon and Han[113] studied the effect of thermal history on the rheological behaviour of commercial PUs. Time evolution of the dynamic storage and loss moduli (G' and G'') during isothermal annealing was found to be sensitive to the thermal history of the samples.

Dario Nichetti and Nano Grizzuti have used rheological measurements for studying microstructure modifications in TPU that occur during phase transitions.[109] It was observed that microstructural aging during isothermal annealing, which was not detected by DSC, was clearly observed as an increase in elastic modulus. Their work showed that rheology can be successfully used for the qualitative as well as quantitative characterization of kinetics of phase transition.

1.6   Morphologies Reported in the Literature

Estes and co-workers[65] were the first to propose a two phase model for polyurethane morphology with semicontinuous and interpenetrating domains. Lamellar morphologies have been reported in PUs based on the TEM observations.[73,74,76,78] This morphology is observed in block copolymers with a volume fraction of one of the component (ϕ_A) around 0.5, and characterized by extensive parallel sheets of alternating composition. Chi Li and co-workers[114] studied the morphology of polybutadine-polyurethanes containing a wide range of hard segment content (MDI-BDO). It was observed that polyurethanes containing low hard segment content showed dispersed, short, hard segment cylinders embedded in a matrix of polybutadine soft segments. Polyurethanes having higher hard segment content showed alternating rod like or lamellar microdomain structure. Whereas, at high hard segment contents, dispersed soft segment phase morphology was observed.

Versteegen et al.[41] have observed long stacks of hard blocks embedded in soft phase for the segmented copoly(ether urea)s having uniform hard segments. Das et al.[45] studied structure-property relationship of segmented, non-chain extended polyureas. AFM imaging on these polyureas showed the presence of a microphase

separated structure, with thread like hard segments randomly dispersed throughout the soft segment matrix. Revenko et al.[115] studied heterophase morphology of polyurethanes containing aliphatic soft segments (HS content 30 wt %) using tapping mode AFM. Authors have observed rod like hard domains of about 50 nm length dispersed in the soft segment matrix. Later Christenson et al.[116] have also reported a similar morphology in polycarbonate polyurethanes. Hard segment domains were found to be cylindrical having 5-10 nm in width and 40-100 nm in length for this polyurethane.

Hernandez et al.[117] recently studied phase organization in a series of segmented polyurethanes having different soft segment chemistries by AFM, SAXS, FTIR and DSC. Three series of polyurethanes synthesized in this study had soft segments composed of either an aliphatic polycarbonate, polytetramethyleneoxide, or a mixed macrodiol of polyhexamethyleneoxide (PHMO) and hydroxyl terminated PDMS and the same hard segment chemistry (MDI and 1,4-butanediol). Their morphological analysis demonstrates the presence of three phase core-shell morphology in PHMO/PDMS based copolymers, while the other two copolymers demonstrated two phase microstructure. Hard domain dimensions were approximately 50-75 nm^2.

1.7   Summary

A typical thermoplastic polyurethane (TPU) and its analogue polyurethane-urea (PUU) are $(AB)_n$ type block copolymers consisting of random sequences of hard and soft segments. As a result of the pioneering efforts of Otto Bayer and co-workers (1930), polyurethane chemistry opened the way to a new class of high performance materials. Since then TPUs have become the materials of choice in a steadily increasing number of very different applications in the form of fibers, elastomers, rigid and soft foams. TPUs today play an important role within the rapidly growing family of thermoplastic elastomers. The versatility of chemistry allows the production of polyurethanes using a wide range of monomers which consists of three basic components: an aromatic or aliphatic diisocyanate, a polyether or polyester polyol (soft segment), and a short chain extender diol, or a diamine. Tailoring the molecular weight, chemistry, topology, and composition of the different blocks can result in materials ranging from soft elastomers to rigid, hard thermoplastics.

The exothermic polyaddition reaction between diols and diisocyanates can be carried out in bulk or in solution. In 'one-shot method' method of synthesis, all reaction components are mixed simultaneously and allowed to polymerize. The 'prepolymer method' of synthesis involves formation of isocyanate terminated prepolymer in the first step by reacting excess of diisocyanate with polyol, which is then reacted with the chain extender to produce high molecular weight polymer. Reaction conditions as well as the method used for the synthesis has a marked influence on the morphology and hence on the properties of resulting polymer. Prepolymer method produces polyurethanes having superior properties due to regular structural arrangements of blocks leading to better packing and crystallization of hard segment sequences.

Polyurethane macromolecules are composed of flexible polyether or polyester segments of low T_g (typically below ambient temperature) and rigid urea or urethane blocks having high T_g (typically above ambient temp.). The incompatibility between hard and soft segments lead to mircophase separation forming hard urea or urethane domains segregated from soft matrix. The degree to which hard and soft segments microphase separate and the resulting morphology have a profound effect on the mechanical properties of these polymers. Their tendency to microphase separate into periodic morphologies depends upon the composition, molecular weight, and monomer-monomer interaction parameter (χ). The driving force for phase separation is believed to be the strong hydrogen bonding between urethane and urea groups. Phase separation is thus stronger in the case of polyurea as a result of strong bifurcate hydrogen bonding.

Many techniques have been used to investigate microphase separation in polyurethanes and the resulting morphology. The multiple bands observed by infrared spectroscopy have been used for studying hard segment hydrogen bonding in phase mixed or phase separated environments. DMA and DSC have been used extensively to study multiple glass transitions and enthalpy peaks related to the microphase separation. The data obtained from DSC has also been used successfully for determining phase compositions. Low natural contrast between microdomains has prohibited the widespread use of transmission electron microscopy in studying polyurethane morphology. More recently, atomic force microscopy (AFM) has become an essential tool for studying polyurethane morphology. Small angle X-ray

scattering (SAXS) is one of the most popular technique for morphological study of polyurethanes. SAXS has been used to obtain valuable information about the extent of phase separation, type of microphase morphology, average size of the microdomains, nature of interfaces etc. Rheological techniques have also been used as alternative method for the characterization of microstructural changes taking place in the sample, especially during phase transition stages.

References :

(1)   Otto Bayer *German patent* **1937**.

(2)   Schollenberger, C. S.; Scott, H.; Moore, G. R. *Paper presented at the ACS Rubber Div. Mtg.* **2008**.

(3)   Cooper, S. L.; Tobolsky, A. V. *J. Appl. Polym. Sci.* **1966**, 10, 1837.

(4)   Grieve, R. L. *Internet Communication* **2008**.

(5)   Huntsman Polyurethanes *Internet Communication* **2008**.

(6)   Woods, G. *The ICI Polyurethanes Book*; John Wiley and Sons, New York: 1990.

(7)   Wurtz.A *Ann.* **1849**, 71, 326.

(8)   Hentschel.W. *Ber.* **1884**, 17, 1284.

(9)   Yilgor, I.; Mather, B. D.; Unal, S.; Yilgor, E.; Long, T. E. *Polymer* **2004**, 45, 5829.

(10)   G.Woods *The ICI Polyurethanes Book*; John Wiley and Sons, New York: 1990.

(11)   Leibler, L. *Macromolecules* **1980**, 13, 1602.

(12)   Sakamoto, N.; Hashimoto, T.; Han, C. D.; Kim, D.; Vaidya, N. Y. *Macromolecules* **1997**, 30, 1621.

(13)   Khandpur, A. K.; Fo¨rster, S.; Bates, F. S.; Hamley, I. W.; Ryan, A. J.; Bras, W.; Almdal, K.; Mortensen, K. *Macromolecules* **1995**, 28, 8796.

(14)   Fo¨rster, S.; Khandpur, A. K.; Zhao, J.; Bates, F. S.; Hamley, I. W.; Ryan, A. J.; Bras, W. *Macromolecules* **1994**, 27, 6922.

(15)   Hamley, I. W.; Koppi, K. A.; Rosedale, J. H.; Bates, F. S.; Almadal, K.; Mortensen, K. *Macromolecules* **1993**, 26, 5659.

(16) Almdal, K.; Koppi, K. A.; Bates, F. S.; Mortensen, K. *Macromolecules* **1992**, 25, 1743.

(17) Hajduk, D. A.; Gruner, S. M.; Rangarajan, P.; Register, R. S.; Fetters, L. J.; Honeker, C.; Albalak, R. J.; Thomas, E. L. *Macromolecules* **1994**, 27, 490.

(18) Sakurai, S.; Momii, T.; Taie, K.; Shibayama, M.; Nomura, S.; Hashimoto, T. *Macromolecules* **1993**, 26, 458.

(19) Sakurai, S.; Kawada, H.; Hashimoto, T.; Fetters, L. *Macromolecules* **1993**, 26, 5796.

(20) Korbestein, J. T.; Russell, T. P.; Walsh, D. J.; Pottick, L. *Macromolecules* **1990**, 23, 877.

(21) Yang, Y.; Tanodekaew, S.; Mai, S.; Booth, C.; Ryan, A. J.; Bras, W.; Viras, K. *Macromolecules* **1995**, 28, 6029.

(22) Adams, J. L.; Quiram, D. J.; Graessley, W. W.; Register, R. A.; Marchand, G. R. *Macromolecules* **1996**, 29, 2929.

(23) Sakamoto, N.; Hashimoto, T. *Macromolecules* **1995**, 28, 6825.

(24) Lee, K. M.; Han, C. D. *Macromolecules* **2002**, 35, 760.

(25) Bates, F. S.; Bair, H. E.; Hartney, M. A. *Macromolecules* **1984**, 17, 1987.

(26) Eitouni, H. B.; Rappl, T. J.; Gomez, E. D.; Balsara, N. P.; Qi, S.; Chakraborty, A. K.; Fre´chet, J. M. J.; Pople, J. A. *Macromolecules* **2004**, 37, 8487.

(27) Velankar, S.; Cooper, S. L. *Macromolecules* **1998**, 31, 9181.

(28) Yeh, F.; Hsiao, B. S.; Sauer, B. B.; Michel, S.; Siesler, H. W. *Macromolecules* **2003**, 36, 1940.

(29) Korley, L. T. J.; Pate, B. D.; Thomas, E. L.; Hammond, P. T. *Polymer* **2006**, 47, 3073.

(30) Bonart, R.; Morbitzer, L.; Hentze, G. *J. Macromol. Sci. -Phys.* **1969**, 3[2], 337.

(31) Cooper, S. L.; Tobolsky, A. V. *J. Appl. Polym. Sci.* **1966**, 10, 1837.

(32) Wilkes, C. W.; Yusek, C. *J. Macromol. Sci.* **1973**, B7, 157.

(33) Leung, L. M.; Koberstein, J. T. *J. Polym. Sci. -Phys.* **1985**, 23, 1883.

(34) Musselman, S. G.; Santosusso, T. M.; Barnes, J. D.; Sperling, L. H. *J. Polym. Sci. -Phys.* **1999**, 37, 2586.

(35) Bonart, R.; Morbitzer, L.; Muller, E. H. *J. Macromol. Sci. Phys.* **1974**, B9, 447.

(36) Sung, C. S. P.; Smith, T. W.; Sung, N. H. *Macromolecules* **1980**, 13, 117.

(37) Knutson, K.; Lvman, D. *J. Adv. Chem. Ser.* **1982**, 199.

(38) Blackwell, J.; Nagarajan, M. R. *Polymer* **1981**, 22, 202.

(39) Seymour, R. W.; Allegrezza, A. E.; Cooper, S. L. *Macromolecules* **1973**, 6[6], 896.

(40) Van Bogart, J. W. C.; Gibson, P. E.; Cooper, S. L. *J. Polym. Sci. -Phys.* **1983**, 21, 65.

(41) Versteegen, R. M.; Kleppinger, R.; Sijbesma, R. P.; Meijer, E. W. *Macromolecules* **2006**, 39, 772.

(42) Yilgor, I.; Yilgor, E. *Polym. Rev.* **2007**, 47, 487.

(43) Sheth, J. P.; Klinedinst, D. B.; Wilkes, G. L.; Yilgor, I.; Yilgor, E. *Polymer* **2005**, 46, 7317.

(44) Versteegen, R. M.; Sijbesma, R. P.; Meijer, E. W. *Macromolecules* **2005**, 38, 3176.

(45) Das, S.; Yilgor, I.; Yilgor, E.; Inci, B.; Tezgel, O.; Beyer, F. L.; Wilkes, G. L. *Polymer* **2007**, 48, 290.

(46) Seymour, R. W.; Cooper, S. L. *Macromolecules* **1973**, 6, 48.

(47) McKiernan, R. L.; Heintz, A. M.; Hsu, S. L.; Atkins, E. D. T.; Penelle, J.; Gido, S. P. *Macromolecules* **2002**, 35, 6970.

(48) Coleman, M. M.; Lee, K. L.; Skrovanek, D. J.; Painter, P. C. *Macromolecules* **1986**, 19, 2149.

(49) Coleman, M. M.; Skrovanek, D. J.; Hu, J.; Painter, P. C. *Macromolecules* **1988**, 21, 59.

(50) Coleman, M. M.; Sobkowiak, M.; Pehlert, G. J.; Painter, P. C. *Macromol. Chem. Phys.* **1997**[198], 117.

(51) Wang, C. B.; Cooper, S. L. *Macromolecules* **1983**, 16, 775.

(52) Lee, H. S.; Wang, Y. K.; Hsu, S. L. *Macromolecules* **1987**, 20, 2089.

(53) Lee, H. S.; Hsu, S. L. *Macromolecules* **1989**, 22, 1100.

(54) Senich, G. A.; MacKnight, W. J. *Macromolecules* **1980**, 13, 106.

(55) Sung, C. S. P.; Hu, C. B. *Macromolecules* **1981**, 14, 212.

(56) Tang, W.; MacKnight, W. J.; Hsu, S. L.; Wang, Q.; Stidham, H. D. *Macromolecules* **1995**, 28, 4284.

(57) Teo, L. S.; Chen, C. Y.; Kuo, J. F. *Macromolecules* **1997**, 30, 1793.

(58) Irusta, L.; Iruin, J. J.; Fernandez-Berridi, M. J.; Sobkowiak, M.; Painter, P. C.; Coleman, M. M. *Vib. Spectrosc.* **2000**, 23, 187.

(59) Painter, P. C.; Shenoy, S. L.; Bhagwager, D. E.; Fishburn, J.; Coleman, M. M. *Macromolecules* **1991**, 24, 5623.

(60) Mattia, J.; Painter, P. C. *Macromolecules* **2007**, 40, 1546.

(61) Seymour, R. W.; Estes, G. M.; Cooper, S. L. *Macromolecules* **1970**, 3, 579.

(62) Yilgor, E.; Burgaz, E.; Yurtsever, E.; Yilgor, I. *Polymer* **2000**, 41, 849.

(63) Yilgor, I.; Yilgor, E.; Guler, G. I.; Ward, T. C.; Wilkes, G. L. *Polymer* **2006**, 47, 4105.

(64) Bonart, R. J. *J. Macromol. Sci-Phys.* **1968**, B2[1], 115.

(65) Estes, G. M.; Seymour, R. W.; Cooper, S. L. *Macromolecules* **1971**, 4, 452.

(66) Gregoriou, V. G.; Rodman, S. E.; Nair, B. R.; Hammond, P. T. *J. Phys. Chem. B* **2002**, 106, 11108.

(67) Assink, R. A.; Wilkes, G. L. *Polym. Eng. Sci.* **1977**, 17[8], 606.

(68) Voda, M. A.; Demco, D. E.; Voda, A.; Schauber, T.; Adler, M.; Dabisch, T.; Adams, A.; Baias, M.; Blu1mich, B. *Macromolecules* **2006**, 39, 4802.

(69) Clayden, N. J.; Nijs, C.; Eeckhaut, G. *Macromolecules* **1998**, 31, 7820.

(70) Nierzwicki, W. *J. Appl. Polym. Sci.* **1984**, 29, 1203.

(71) Koutsky, J. A.; Hien, N. V.; Cooper, S. L. *Polymer Letters* **1970**, 8, 353.

(72) Hamley, I. W.; Stanford, J. L.; Wilkinson, A. N.; Elwell, M. J.; Ryan, M. J. *Polymer* **2000**, 41, 2569.

(73) Eisenbach, C. D.; Stadler, E. *Macromol. Chem. Phys.* **1995**, 196, 1981.

(74) Eisenbach, C. D.; Heinemann, T.; Ribbe, E.; Stadler, E. *Macromol. Symp.* **1994**, 77, 125.

(75) Eisenbach, C. D.; Heinemann, T.; Ribbe, E.; Stadler, E. *Angew. Makromol. Chem.* **1992**, 202, 221.

(76) Serrano, M.; MacKnight, W. J.; Thomas, E. L.; Ottino, J. M. *Polymer* **1987**, 27, 1667.

(77) Wang, G.; Fang, B.; Zhang, Z. *Polymer* **1994**, 35, 3178.

(78) Ryan, A. J.; Stanford, J. L.; Tao, X. Q. *Polymer* **1993**, 34, 4020.

(79) O'Sickey, M. J.; Lawrey, B. D.; Wilkes, G. L. *J. Appl. Polym. Sci.* **2003**, 89, 3520.

(80) O'Sickey, M. J.; Lawrey, B. D.; Wilkes, G. L. *J. Appl. Polym. Sci.* **2002**, 84, 229.

(81) Garrett, J. T.; Siedlecki, C. A.; Runt, J. *Macromolecules* **2001**, 34, 7066.

(82) Garrett, J. T.; Runt, J.; Lin, J. S. *Macromolecules* **2000**, 33, 6353.

(83) Kaushiva, B. D.; Wilkes, G. L. *Polymer* **2000**, 41, 6981.

(84) McLean, R. S.; Sauer, B. B. *Macromolecules* **1997**, 30, 8314.

(85) Sheth, J. P.; Unal, S.; Yilgor, E.; Yilgor, I.; Beyer, F. L.; Long, T. E.; Wilkes, G. L. *Polymer* **2005**, 46, 10180.

(86) Sheth, J. P.; Wilkes, G. L.; Fornof, A. R.; Long, T. E.; Yilgor, I. *Macromolecules* **2005**, 38, 5681.

(87) Ryan, A. J.; Macosko, C. W.; Bras, W. *Macromolecules* **1992**, 25, 6277.

(88) Chu, B.; Gao, T.; Li, Y.; Wane, J.; Deeper, C. R.; Byrne, C. A. *Macromolecules* **1992**, 25, 5724.

(89) Koberstein, J. T.; Russell, T. P. *Macromolecules* **1986**, 19, 714.

(90) Laity, P. R.; Taylor, J. E.; Wong, S. S.; Khunkamchoo, P.; Norris, K.; Cable, M.; Andrews, G. T.; Johnson, A. F.; Cameron, R. E. *Polymer* **2004**, 45, 7273.

(91) Velankar, S.; Cooper, S. L. *Macromolecules* **2000**, 33, 382.

(92) Tyagi, D.; McGrath, J. E.; Wilkes, G. L. *Polym. Eng. Sci.* **1986**, 26, 1371.

(93) Wilkes, C. E.; Yusek, C. S. *J. Macromol. Sci-Phys.* **1973**, B7[1], 157.

(94) Koberstein, J. T. *J. Polym. Sci. -Phys.* **1983**, 21, 2181.

(95) Bonart, R.; Morbitzer, L.; Muller, E. H. *J. Macromol. Sci. Phys.* **1974**, B9, 447.

(96) Bonart, R.; Muller, E. H. *J. Macromol. Sci. Phys.* **1974**, B10, 177.

(97) Koberstein, J. T.; Stein, R. S. *J. Polym. Sci. -Phys.* **1983**, 21, 1439.

(98) Leung, L. M.; Koberstein, J. T. *Macromolecules* **1986**, 19, 706.

(99) Saiani, A.; Daunch, W. A.; Verbeke, H.; Leenslag, J. W.; Higgins, H. S. *Macromolecules* **2001**, 34, 9059.

(100) Camberlin, Y.; Pascault, J. P. *J. Polym. Sci. -Phys.* **1984**, 22, 1835.

(101) Huh, D. S.; Cooper, S. L. *Polym. Eng. Sci.* **1971**, 11, 369.

(102) Ng, H. N.; Allegrezza, A. E.; Seymour, R. W.; Cooper, S. L. *Polymer* **1973**, 14, 255.

(103) Samuels, S. L.; Wilkes, G. L. *J. Polym. Sci. Pt. C* **1973**, 43, 149.

(104) Illinger, J. L.; Schneider, N. S.; Karasz, F. E. *Polym. Eng. Sci.* **1972**, 12, 25.

(105) De Gennes, P. G. *Macromolecules* **1976**, *9*, 594.

(106) De Gennes, P. G. *Macromolecules* **1976**, 9, 587.

(107) Brochard, F.; De Gennes, P. G. *Macromolecules* **1977**, 10, 1157.

(108) De Gennes, P. G. *J. Chem. Phys.* **1980**, 72, 4756.

(109) Nichetti, D.; Grizzuti, N. *Polym. Eng. Sci.* **2004**, 44[8], 1514.

(110) Ryu, D. Y.; Jeong, U.; Kim, J. K.; Russell, T. P. *Nature Materials* **2002**, 1[October], 114.

(111) Rosedale, J. H.; Bates, F. S. *Macromolecules* **1990**, 23, 2329.

(112) Bates, F. S.; Rosedale, J. H.; Bair, H. E.; Russell, T. P. *Macromolecules* **1989**, 22, 2257.

(113) Yoon, P. J.; Han, C. D. *Macromolecules* **2000**, 33, 2171.

(114) Li, C.; Goodman, S. L.; Albercht, R. M.; Cooper, S. L. *Macromolecules* **1988**, 21, 2367.

(115) Revenko, I.; Tang, Y.; Santerre, J. P. *Surf. Sci.* **2001**, 491, 346.

(116) Christenson, E. M.; Dadesetan, M.; Wiggins, M.; Anderson, J. M.; Hiltner, A. J. *Biomed. Mat. Res.* **2004**, 69, 407.

(117) Hernandez, R.; Weksler, J.; Padsalgikar, A.; Choi, T.; Angelo, E.; Lin, J. S.; Xu, L.; Siedlecki, C. A.; Runt, J. *Macromolecules* **2008**, 41, 9767.

Objectives and Scope

Chapter - 2

Polyurethane elastomers are industrially important polymeric materials because of their wide range of applications, and their properties, which can be controlled by changes in the starting materials, preparation conditions and so on.[1] As described in Chapter 1, thermoplastic polyurethanes (PU) and their analogue polyurethane-ureas (PUU) are $(AB)_n$ type random block copolymers consisting of sequences of hard and soft segments. Thermodynamic incompatibility between hard and soft segments, and/or crystallinity in the hard segment drives them to phase separate.[2] However, phase separation is limited at the segmental level due to connectivity of the blocks.[3,4] The primary driving force for domain formation is the intermolecular interactions between urethane / urea units which are capable of forming hydrogen bonds. The incorporation of urea linkages in PU hard segment has a profound effect on the phase separation and microphase morphology.[5-7]

The extent of microphase separation and the phase morphology have a profound effect on the ultimate properties of the copolymer. Hence it is desirable to have a control on the microphase separation in polyurethanes. Factors that are known to control the degree of microphase separation include copolymer composition, block length and crystallizability of either segment.[8] In the present work we have tested a new hypothesis for achieving control on microphase separation namely, the use of structural moieties that produce 'defects' in the packing of hard segments. The inspiration for this idea is derived from semicrystalline polymers in which the role of defect moieties in controlling the size of crystalline structures is well known. For example, alpha olefins when copolymerized with ethylene in linear low density polyethylene chains act as defects since they cannot be incorporated into the unit cell of a polyethylene crystal and thereby inhibit the formation of long range crystalline order. As a result, thinner lamellae and smaller spherulites are formed. This microstructure is used to make polyethylene films of improved transparency and toughness. In a similar manner, we hypothesize that defect moieties when incorporated into hard segments of a PU or PUU might inhibit the effective organization of hard domains. Thus the primary objective of the present work was to test this hypothesis, and consequently to study the effect of controlled introduction of defects in the hard segments on the phase morphology and the ultimate properties of PUUs. The defect moieties that we have studied in this work are diamines having long

aliphatic side chains, which form short branches on the hard segments of a PU molecule.

Present study systematically investigates the role of the content and the length of aliphatic chains on the microphase mixing in PUU copolymers. Our study demonstrates that morphology of polyurethanes can indeed be controlled by introducing chain defects in the hard segments.

The scope of the present study is as follows:

- Synthesis of a linear aliphatic polyurethane containing poly(tetramethylene oxide) as the soft segment and isophorone diisocyanate in combination with butanediol chain extender as the hard segment. The ratio of hard segment to soft segment was 50:50. This is the control sample.

- Design and synthesis of two different aromatic diamine monomers having pendent aliphatic chains of different lengths which can be used as chain extender molecules. Specifically, these molecules were *n-dodecyl 3,5-diaminobenzoate* and *n-docosyl 3,5-diaminobenzoate*.

- Synthesis of two different series of branched polyurethane-ureas using the two aromatic diamine chain extenders indicated above; each series contained varying amounts of the aromatic diamines. The adjective 'branched' used here refers to the presence of alkyl side chains on the polymer.

- Synthesis of a series of linear polyurethane-ureas with varying content of a chain extender that had no pendent alkyl chain (*m-phenylenediamine*).

- Synthesis of model hard segments using *n-dodecyl 3,5-diaminobenzoate* and *m-phenylenediamine* in combination with *1,4-butanediol*.

- Molecular characterization of the polymers synthesized using ^{1}H-NMR and gel permeation chromatography (GPC).

- Morphological characterization of synthesized polymers by using differential scanning calorimetry (DSC), dynamic mechanical analysis (DMA), and small angle x-ray scattering (SAXS) and rheology.

- Measurement of tensile properties of the polymers.

Here, we briefly take a look at the forthcoming chapters in the thesis. The next chapter, Chapter 3: Synthesis of Chain Extenders and Polyurethane-ureas, is divided into four parts: Part I discusses about the two-step synthesis of branching agents (*n-alkyl 3,5-diaminobenzoates*) and their structural characterization by ^{1}H NMR, FTIR and Elemental Analysis. Part II describes the synthesis of linear polyurethane L-PU, as a control sample. This part also discusses the synthesis of a series of linear polyurethane-ureas L-PUUs using *m-phenylenediamine*. Part III describes the two-step solution polymerization of polyurethane-ureas containing *n-alkyl 3,5-diaminobenzoate* (*n* = 10, 20) branching agents (B12-PUU and B22-PUU series). Lastly, part IV of this chapter explains the synthesis of model hard segments using diisocyante (IPDI), in combination with of *1,4-butanediol* and *n-alkyl 3,5-diaminobenzoates*. This follows their characterization using proton NMR, FTIR, and DSC.

Chapter 4 discusses the molecular characterization of synthesized polymers described in chapter 3, by ^{1}H-NMR, FTIR and molecular weight analysis by GPC. This leads to chapter 5, which details the systematic investigation of heterophase morphology of synthesized polymers at various length scales. This involves probing hydrogen bonding as a function of temperature by using FTIR, thermal analysis by DSC and DMTA, SAXS, viscoelastic behaviour by rheology, and finally, mechanical properties by tensile measurements. This is followed by chapter 6 which draws some important conclusions on morphology of PUUs. This chapter finally, provides some suggestions for future work based on interesting observations of this study.

References:

(1) Meckel, W.; Goyert, W.; Wieder, W.; Wussow, H.-G. *Thermoplastic Elastomers.* 2005, 3rd[2], 15.

(2) Cooper, S. L.; Tobolsky, A. V. *J. Appl. Polym. Sci.* **1966**, 10, 1837.

(3) Fredrickson, G. H.; Helfand, E. *J. Chem. Phys.* **1987**, 87, 697.

(4) Leibler, L. *Macromolecules* **1980**, 13, 1602.

(5) Wilkes, G. L.; Abouzahr, S. *Macromolecules* **1981**, 14, 458.

(6) Bonart, R.; Morbitzer, L.; Muller, E. H. *J. Macromol. Sci. Phys.* **1974**, B9, 447.

(7) Sung, C. S. P.; Smith, T. W.; Sung, N. H. *Macromolecules* **1980**, 13, 117.

(8) Wang, C. B.; Cooper, S. L. *Macromolecules* **1983**, 16, 775.

Synthesis of Chain Extenders and Polyurethane-ureas

Chapter - 3

3.1   Chemicals and Methods Used

3.1.1 Solvents -

N,N-Dimethylacetamide
Acronym: DMAc
Supplier: Aldrich Chemical Company
Molecular Formula: C_4H_9NO
Molecular Weight: 87.12 g/mol
Boiling Point: 165°C/760 torr
Chemical Structure:
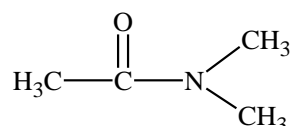
Anhydrous DMAc (99.8% purity) from Aldrich was received in a sealed bottle with septum and was used without any purification. Fresh DMAc was taken from the bottle each time maintaining anhydrous conditions.

Chloroform
Supplier: Ranchem Chemical Company
Molecular Formula: $CHCl_3$
Molecular Weight: 119.38 g/mol
Density: 1.48 g/cm^3
Boiling Point: 61.2°C

Methanol
Supplier: Ranchem Chemical Company
Molecular Formula: CH_3OH
Molecular Weight: 32.04 g/mol
Density: 0.791 g/cm^3
Boiling Point: 64.7°C

Petroleum Ether
Acronym: Pet ether
Supplier: Ranchem Chemical Company
Molecular Formula: Mixture of hydrocarbons
Molecular Weight: 87-90 g/mol
Boiling Point Range: 60-80°C

Ethyl Acetate
Supplier: Ranchem Chemical Company
Molecular Formula: $C_4H_8O_2$
Molecular Weight: 88.105 g/mol
Density: 0.897 g/cm^3
Boiling Point: 77.1°C
Chemical Structure:

$$\underset{H_3C}{\,}\overset{\displaystyle O}{\underset{\displaystyle \|}{C}}\!\!-\!\!O\!\!-\!\!CH_2\!\!-\!\!CH_3$$
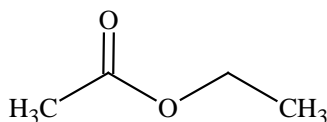
3.1.2 Monomers and Oligomers –

3.1.2.1 1-Isocyanato-3-Isocyanatomethyl-3,5,5-Trimethylcyclohexane
Acronym: IPDI
Supplier: Aldrich Chemical Company
Molecular Formula: $C_{12}H_{18}N_2O_2$
Molecular Weight: 222.29 g/mol
Density: 1.062 g/cc^3 @ 20°C
Boiling Point: -60°C
Chemical Structure:

PTMO oligomer with a number average molecular weight 2900 was stored under nitrogen blanket and was vacuum dried at 60°C before use.
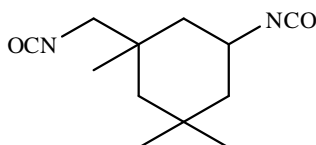
IPDI was kindly supplied by Bayer AG and was used as such. Isocyanate was stored under nitrogen.

3.1.2.2 Polytetramethylene Oxide
Acronym: PTMO
Supplier: Aldrich Chemical Company
Molecular Formula: $(C_4H_8O)_n$
Molecular Weight: M_n 2900 g/mol
Melting Point: 27°C
Chemical Structure:
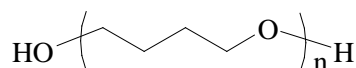
$$HO\!\!-\!\!\left(\!CH_2CH_2CH_2CH_2\!\!-\!\!O\right)_{\!n}\!\!H$$

PTMO oligomer with a number average molecular weight 2900 was stored under nitrogen blanket and was vacuum dried at 60°C before use.

3.1.2.3 1,4-Butanediol
Acronym: BDO
Supplier: Merk Chemical Company
Molecular Formula: $C_4H_{10}O_2$
Molecular Weight: 90.12 g/mol
Melting Point: 16°C
Boiling Point: 230°C/760 torr

Chemical Structure:
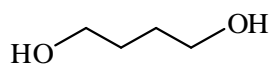
1,4-Butanediol > 99 % purity was distilled under vacuum and was stored under nitrogen atmosphere. BDO was vacuum dried at 55°C each time before use.

3.1.2.4 N-Dodecyl 3,5-Diaminobenzoate

Acronym: B12 Amine
Supplier: Lab Synthesized
Molecular Formula: $C_{19}H_{32}N_2O_2$
Molecular Weight: 320 g/mol
Melting Point: 64°C
Chemical Structure:
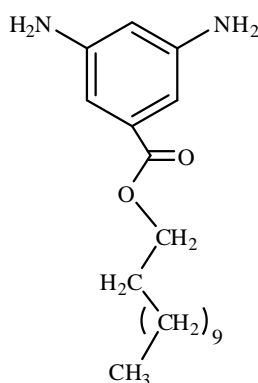
After column chromatography compound was crystallized in methanol and stored in desiccator before use.

3.1.2.5 N-Docosyl 3,5-Diaminobenzoate

Acronym: B22 Amine
Supplier: Lab Synthesized
Molecular Formula: $C_{29}H_{52}N_2O_2$
Molecular Weight: 460 g/mol
Melting Point: 91°C
Chemical Structure:
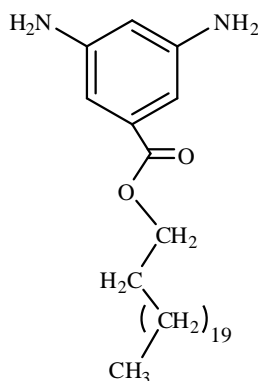
Column purified compound was crystallized and stored in desiccator before use.

3.1.2.6 Dibutyltin Dilaurate

Acronym: DBTDL
Supplier: Merk Chemical Company
Molecular Formula: $C_{32}H_{64}O_4Sn$
Molecular Weight: 631.6 g/mol
Chemical Structure:

$$(C_4H_9)_2Sn(OOC(CH_2)_{10}CH_3)_2$$

DBTDL > 97 % purity was stored under nitrogen and was used without further purification.

3.1.3 Analytical Methods

3.1.3.1 Proton Nuclear Magnetic Resonance (^{1}H-NMR)

Samples were analyzed for ^{1}H-NMR using a Bruker AV200 spectrometer at operating frequency 200 MHz. $CDCl_3$ was used as a solvent, with 1 % (v/v) TMS as internal standard. Peaks were referenced to the TMS peak ($\delta = 0$ ppm).

3.1.3.2 Fourier Transform Infrared Spectroscopy (FTIR)

FTIR experiments were conducted on a Perkin Elmer Spectrum GX spectrometer.
Samples were scanned by forming KBr pellets. Fifteen scans were signal averaged at a resolution of 4 cm^{-1} for each sample.

3.1.3.3 Elemental Analysis

Elemental analysis was carried out by CHNS-O, EA 1108- Elemental Analyzer of Carlo-Erba Instruments, Italy.

3.2 Synthesis and Characterization of Diamine Chain Extenders Containing Alkyl Branches

Diamines were synthesized from an A_2B type tri-functional compound wherein the B functionality was used to couple a monofunctional molecule, which acted as the side chain, leaving the difunctional A_2 molecule, which was used for further polymerization. Using this strategy aromatic diamines with alkyl side chains were synthesized by a two step method as shown in the scheme below.

Two aromatic diamines with different side chain lengths were synthesized in two steps, starting from 3,5-Dinitrobenzoyl chloride (DNBC). In the first step, an alkanol was attached to DNBC by esterification; the dinitroester was then catalytically reduced to the corresponding diamine in the second step. n-Dodecanol and n-Docosanol were selected to vary the length of the aliphatic chain. Esterification of n-Docosanol with DNBC was done at room temperature, whereas esterification of n-Dodecanol was carried out at 0°C as shown in **Scheme 3.1** and **Scheme 3.2**.

3.2.1   Esterification of 3,5-Dinitrobenzoyl chloride

Reactants alkanol, triethylamine (TEA) and DNBC were separately dissolved in freshly dried chloroform (90 % by volume) in a molar ratio of 1:1:1.2. The DNBC solution was introduced in a three neck, round bottom flask with a magnetic stirring bar. The temperature of the round bottom flask was maintained at 0°C by surrounding it with ice-salt mixture. Alkanol and TEA solutions were taken in two addition funnels, fitted on the side necks of the round bottom flask. The system was purged with nitrogen gas and sealed. The alkanol and TEA solutions were added drop wise and simultaneously to the acid chloride solution for about 40 min under constant stirring. About 15 min after addition the reaction mixture turned into a clear, yellow coloured solution. The reaction was continued further at the same temperature for 2.5 hrs after which it was stopped by pouring cold distilled water in the flask. Workup of the reaction was done as follows.

The reaction mixture was transferred to a separating funnel for the separation of aqueous and organic layers. The aqueous layer was washed with fresh chloroform and was mixed with the organic layer. Two sodium bicarbonate washes were given to the organic layer to neutralize the traces of acid formed during the reaction. This was then followed by a sodium chloride solution wash and a few washes of plain, distilled water to neutralize the pH of the solution. The chloroform solution was transferred to a clean round bottom flask and was stirred over sodium sulphate for about 8 hrs to

remove water. The solution was then filtered thorough ordinary filter paper and chloroform was stripped off by using rotavapor to get a yellow powder. The yield of the isolated compound was 85 %. A TLC of the compound, in petroleum ether and ethyl acetate (9:1 v/v) showed three spots under UV light. A distinct, dark spot at the top, for the desired compound, was followed by two faint spots of impurity.

Further purification of the dinitroester was carried out by column chromatography. The compound was loaded on a silica gel column and eluted by a binary solvent petroleum ether and ethyl acetate. Elution was monitored by doing TLC of the eluted solution. The compound so obtained was then dried and scanned for ^{1}H-NMR, FTIR and elemental analysis.
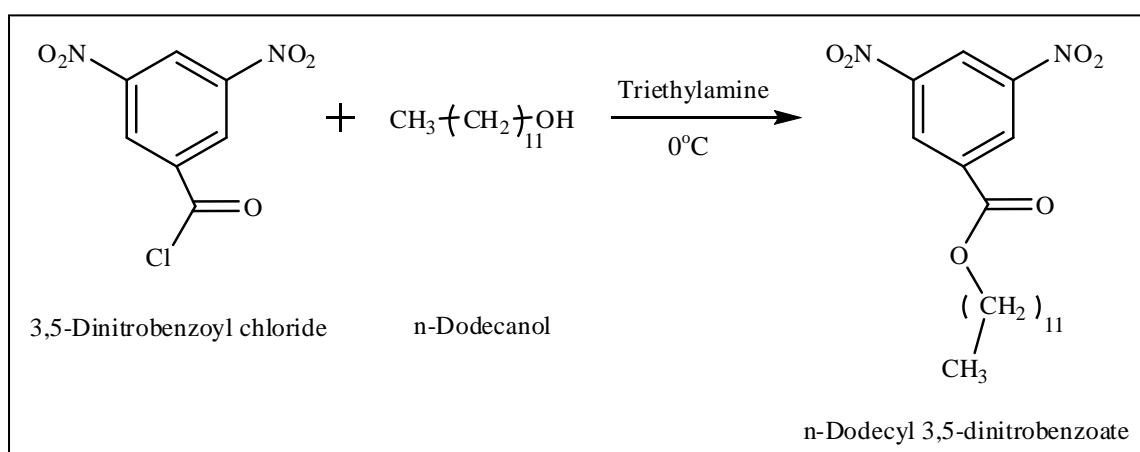
Scheme 3.1 Synthesis of n-Dodecyl 3,5-dinitrobenzoate.
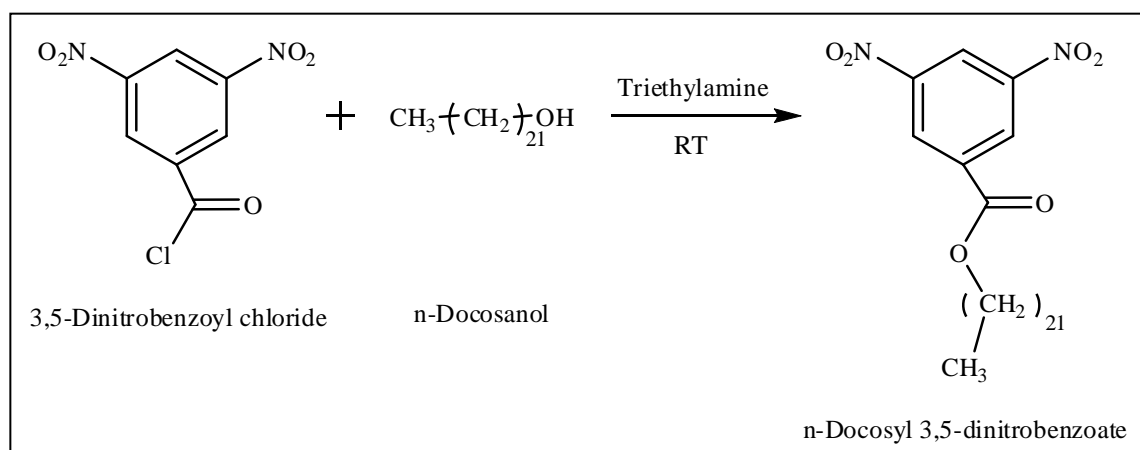
Scheme 3.2 Synthesis of n-Docosyl 3,5-dinitrobenzoate.

3.2.2 Characterization of n-alkyl 3,5-dinitro benzoates

n-Dodecyl 3,5-Dinitrobenzoate – Yield: 85 %. Mp: 64°C.

^{1}H-NMR (CDCl3, 200 MHz): δ 9.23 (1H), 9.16 (2H), 4.45 (t, 2H), 1.84 (m, 2H), 1.26 (m, 18H), 0.88 (m, 3H) ppm.

FTIR (KBr): 3098 (aromatic C-H stretch), 2920 and 2852 (aliphatic C-H stretch), 1727 (C=O), 1543 (N-O asymmetric stretch) and 1346 (N-O symmetric stretch) cm^{-1}.

Elemental Analysis:	C%	H%	N%
Calculated:	60	7.36	7.36
Observed:	60.04	7.43	7.30

^{1}H-NMR spectrum of n-dodecyl 3,5-dinitrobenzoate in **Figure 3.1** shows a multiplet at 0.88 δ ppm due to terminal methyl protons, a multiplet at 1.26 δ ppm corresponding to the methylenes of aliphatic chain. Methylenes β- and α- to ester oxygen gives rise to a multiplet around 1.84 δ ppm, and a triplet centered at 4.45 δ ppm. The presence of these peaks demonstrates the formation of ester. Solvent CDCl$_3$ displayed a peak at 7.27 δ ppm. Aromatic protons *ortho* and *para* to ester group are observed downfield as a doublet around 9.16 δ ppm, and a triplet centered at 9.23 δ ppm respectively, due to electron withdrawing nitro groups.
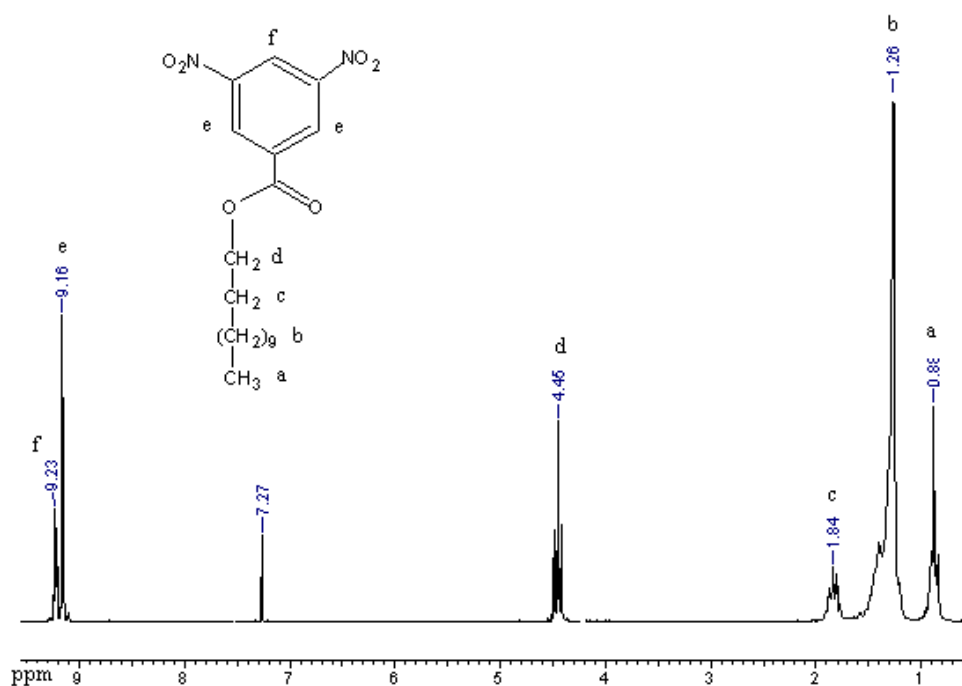
Figure 3.1 ^{1}H-NMR spectrum of n-Dodecyl 3,5-dinitrobenzoate.

FTIR spectrum of n-dodecyl 3,5-dinitroester in **Figure 3.2** serves as another proof for the formation of ester. A strong absorption band, characteristic of ester carbonyl, is observed at 1727 cm^{-1}. Apart from this, other important absorption bands at 1543 cm^{-1} and 1346 cm^{-1} corresponding respectively to N-O asymmetric and N-O symmetric stretching are observed. A high frequency stretching absorption of aromatic C-H group (3098 cm^{-1}), aliphatic C-H stretching (2920 and 2852 cm^{-1}) are also seen in the spectrum.
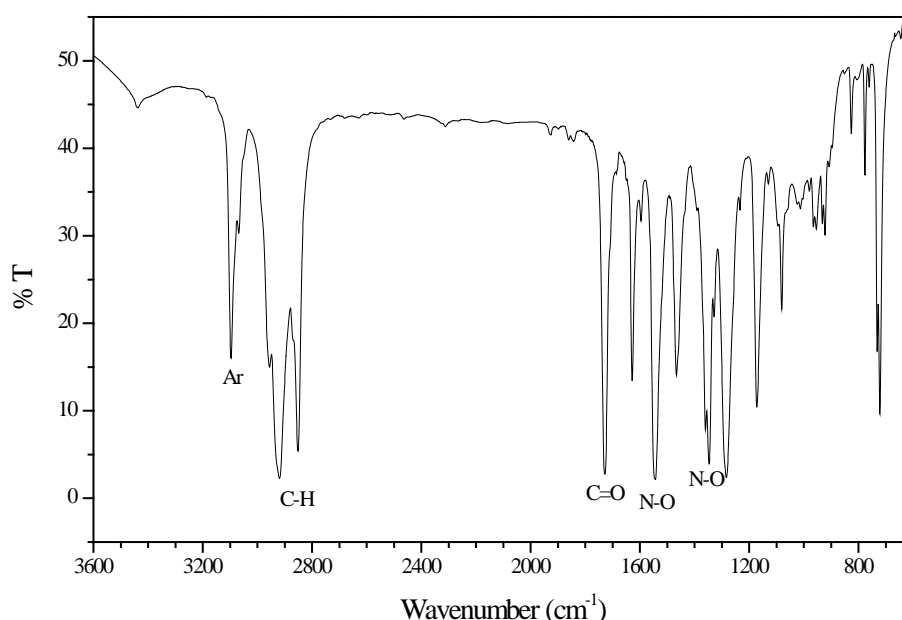
Figure 3.2 FTIR spectrum of n-Dodecyl 3,5-dinitrobenzoate in KBr pellet.

1-Docosyl 3,5-Dinitrobenzoate – Yield: 70 %. Mp: 85°C

^{1}H-NMR (CDCl3, 200 MHz): δ 9.23 (1H), 9.16 (2H), 4.45 (t, 2H), 1.84 (m, 2H), 1.25 (m, 38H), 0.88 (m, 3H) ppm

FTIR (KBr): 3101 (aromatic C-H stretch), 2918 and 2850 (aliphatic C-H stretch), 1729 (C=O), 1543 (N-O asymmetric stretch) and 1349 (N-O symmetric stretch) cm^{-1}.

Elemental Analysis:	C%	H%	N%
Calculated:	66.92	9.23	5.38
Observed:	66.90	9.21	5.40

Figure 3.3 shows ^{1}H-NMR spectrum of n-docosyl 3,5-dinitrobenzoate. Terminal methyl protons of the pendent aliphatic chain displays a multiplet at 0.88 δ ppm. Methylene protons α- and β- to the ester oxygen exhibits a triplet and a doublet respectively at 4.45 and 1.84 δ ppm. Other methylene protons give rise to a multiplet at 1.25 δ ppm. A triplet (9.23 δ ppm), and a doublet (9.16 δ ppm) from aromatic protons *ortho* and *para* to ester group are also observed.

Figure 3.3 ^{1}H-NMR spectrum of n-Docosyl 3,5-dinitrobenzoate.

FTIR spectrum of n-docosyl 3,5-dinitrobenzoate in KBr disc is shown in **Figure 3.4**. Strong absorption band at 3101 cm^{-1} from aromatic C-H stretch, 2918 cm^{-1} from asymmetric C-H stretching, 2850 cm^{-1} due to symmetric C-H stretching are seen. A strong absorption at 1729 cm^{-1}, corresponding to ester C=O, confirms the ester formation. Characteristic bands of NO_2 group are observed in the spectrum at 1543 and 1349 cm^{-1} from asymmetric and symmetric stretching respectively.
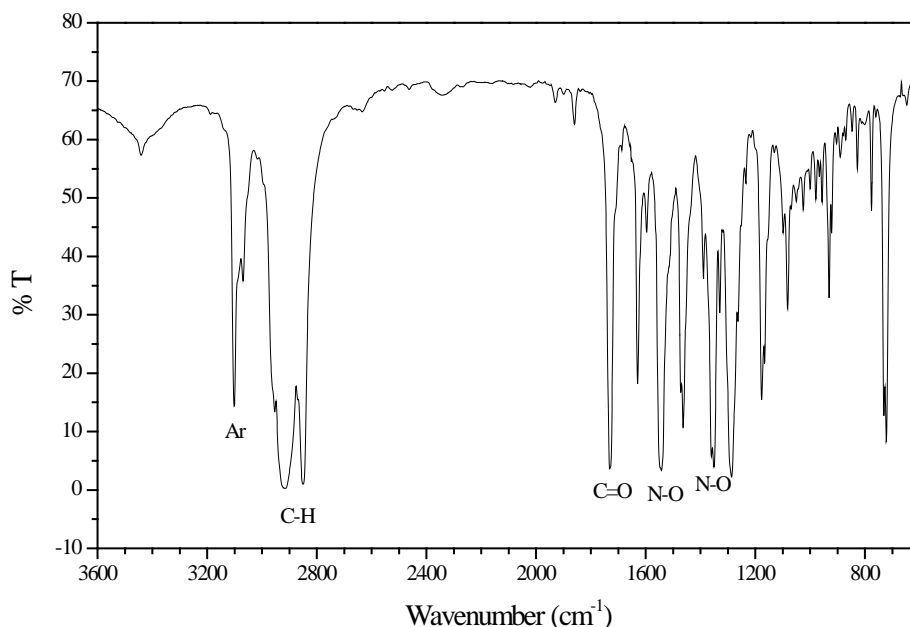
Figure 3.4 FTIR spectrum of n-Docosyl 3,5-dinitrobenzoate in KBr pellet.

3.2.3   Catalytic Reduction of n-alkyl 3,5-dinitrobenzoates

Dinitroester was reduced catalytically in a PARR high pressure reactor. The compound was dissolved in methanol and 3 % Palladium on charcoal was used as a catalyst. Reduction was carried out at 70°C for four hours with hydrogen gas pressure maintained at about 800 psi. **Scheme 3.3** and **Scheme 3.4** shows catalytic reduction of n-dodecyl 3,5-dinitrobenzoate and n-docosyl 3,5-dinitrobenzoate respectively. After reduction the solution was filtered to remove catalyst, and solvent was stripped using rotavapor to obtain a faint pink coloured amine. After crystallization the compound was stored under nitrogen blanket in a closed container. The compound was characterized by NMR, FTIR and elemental analysis.
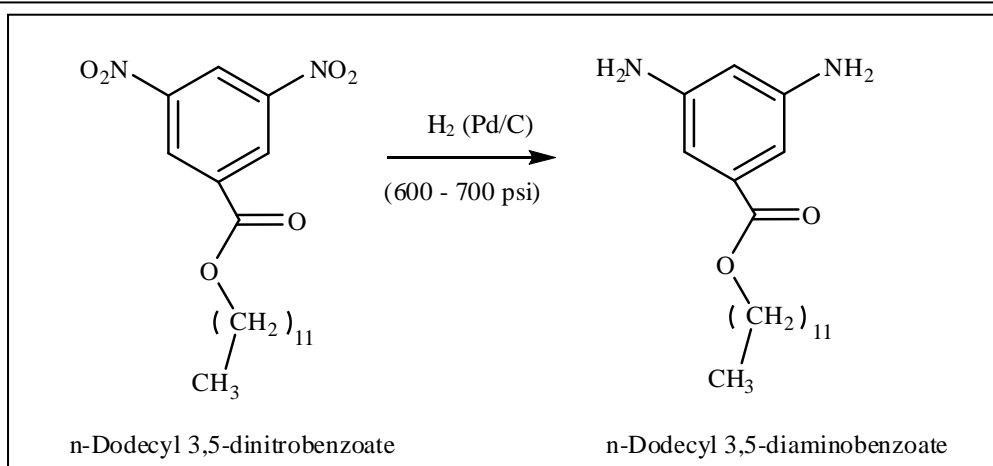
Scheme 3.3 Catalytic reduction of n-dodecyl 3,5-dinitrobenzoate.
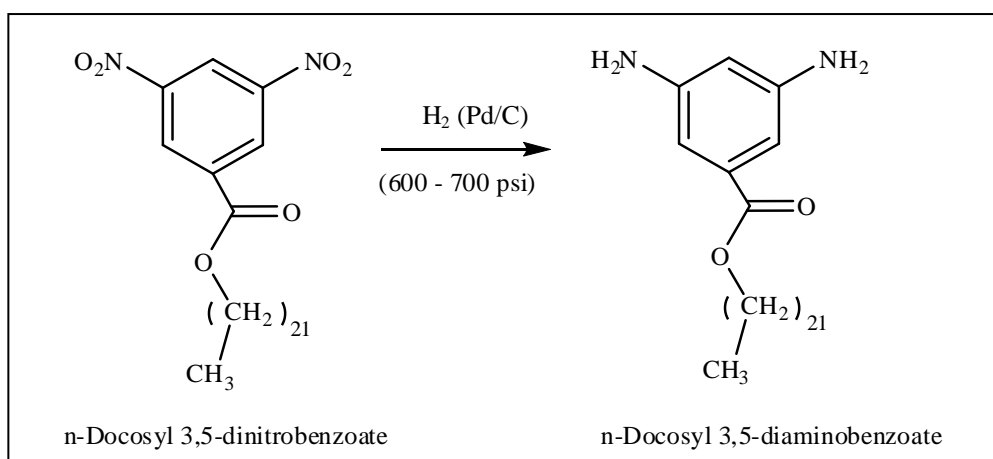
Scheme 3.4 Catalytic reduction of n-docosyl 3,5-dinitrobenzoate.

3.2.4   Characterization of n-alkyl 3,5-diaminobenzoates

***n-Dodecyl 3,5-Diaminobenzoate* -** Yield: 95 %. Mp: 64°C.

^{1}H-NMR (CDCl3, 200 MHz): δ 6.78 (2H), 6.18 (1H), 4.25 (t, 2H), 3.67 (s, 4H), 1.73 (m, 2H), 1.25 (m, 18H), 0.88 (t, 3H) ppm

FTIR (KBr): 3412, 3321 and 3221 (N-H stretch 1° amine), 2918 and 2850 (aliphatic C-H stretch), 1708 (C=O), 1617(N-H bend 1° amine).

Elemental Analysis:	C%	H%	N%
Calculated:	71.25	10	8.75
Observed:	71.15	9.96	8.69

Figure 3.4 shows ^{1}H-NMR spectrum of n-dodecyl 3,5-diaminobenzoate. The spectrum shows a multiplet at 0.88 δ ppm from methyl protons and a multiplet at 1.25 δ ppm due to methylene protons. Another multiplet observed in the spectrum at 1.73 δ ppm is due to methylene protons β- to ester oxygen, while protons α- to oxygen displays a triplet centered at 4.25 δ ppm. A broad singlet located at 3.67 δ ppm in the spectrum is a characteristic signature of amine protons. NMR spectrum thus confirms the formation of amine. Peaks from aromatic protons *para* and *ortho* to the ester group are located at 6.18 and 6.78 δ ppm in the form of a triplet and a doublet.
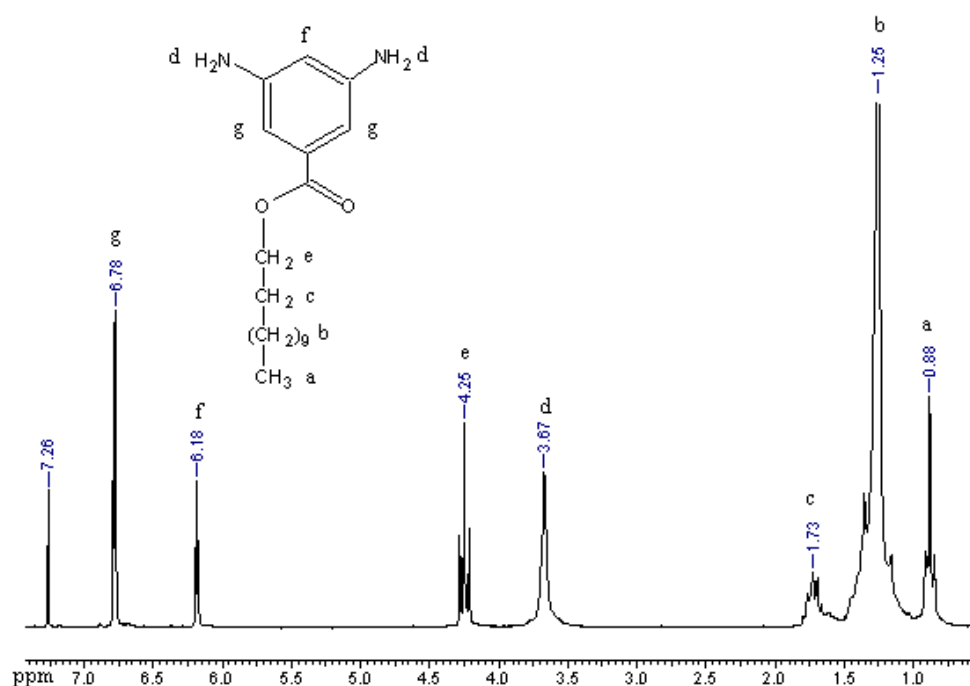
Figure 3.5 ^{1}H-NMR spectra of n-Dodecyl 3,5-diaminobenzoate.

FTIR spectrum of n-dodecyl 3,5-diaminobenzoate displayed in **Figure 3.6** further supports the formation of diamine. Spectrum shows characteristic N-H stretching bands of primary amine group at 3412, 3321 and 3221 cm^{-1}. Two more absorptions from N-H are seen in the spectrum. A strong band at 1617 cm^{-1} and a broad absorption around 760 cm^{-1} from N-H bending in primary amine and N-H wagging respectively. A band at 1708 cm^{-1} due to ester C=O, C-H stretching absorptions at 2918 and 2850 cm^{-1}, are among the other important bands that are observed in the spectrum.
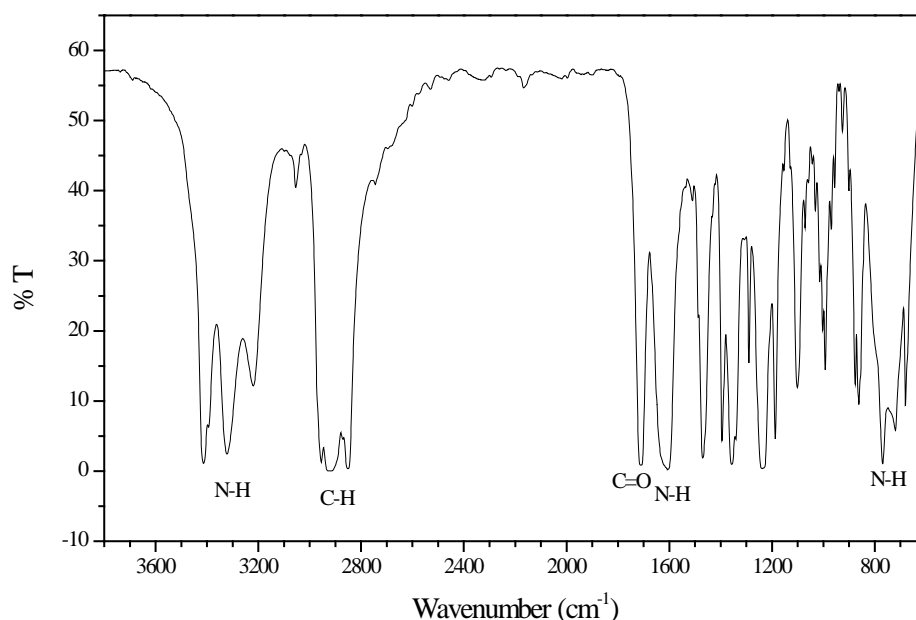
Figure 3.6 FTIR spectrum of n-Dodecyl 3,5-diaminobenzoate.

n-Docosyl 3,5-Diaminobenzoate - Yield: 95 %. Mp: 91°C.

^{1}H-NMR (CDCl3, 200 MHz): δ 6.79 (2H), 6.18 (1H), 4.25 (t, 2H), 3.66 (s, 4H), 1.73 (m, 2H), 1.25 (m, 38H), 0.88 (t, 3H) ppm

FTIR (KBr): 3413, 3322 and 3220 (N-H stretch 1° amine), 2917 and 2850 (aliphatic C-H stretch), 1710 (C=O), 1605 (N-H bend 1° amine).

Elemental Analysis:	C%	H%	N%
Calculated:	75.65	11.30	6.08
Observed:	75.89	11.12	6.00

^{1}H-NMR spectrum of n-docosyl 3,5-diaminobenzoate is shown in **Figure 3.7**. Multiplets seen in the spectrum at 0.88 and 1.25 δ ppm corresponds to the methyl and methylene protons of pendent aliphatic chain. A multiplet at 1.73 is displayed by the methylene protons β- to ester oxygen, while methylene protons α- to oxygen shows a triplet centered at 4.25 δ ppm. A broad singlet at 3.66 δ ppm is a characteristic of NH$_2$ protons. Aromatic protons *para* and *ortho* to ester group display a triplet at 6.18 δ ppm and a doublet at 6.79 δ ppm.
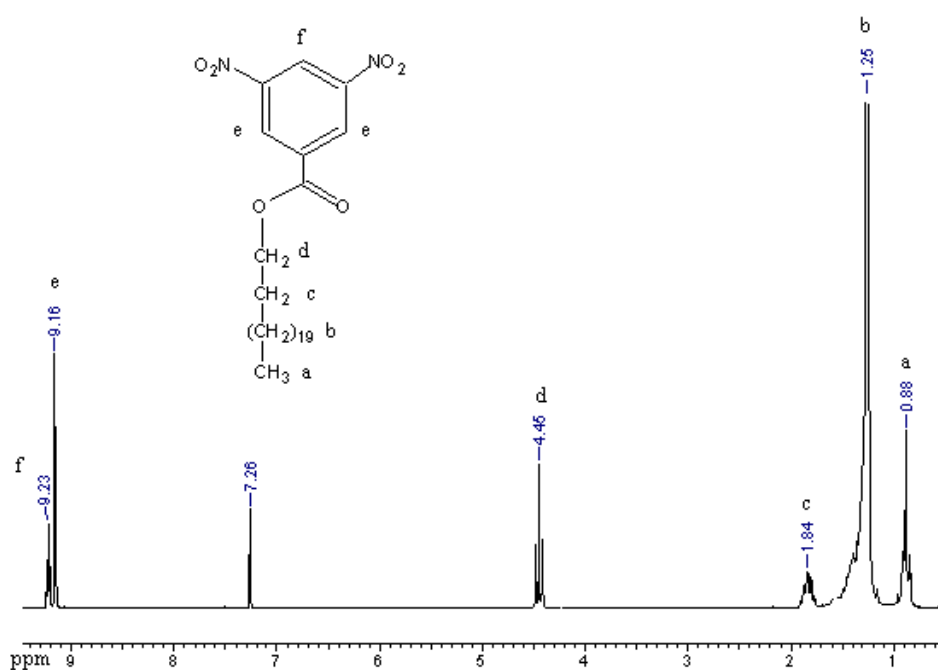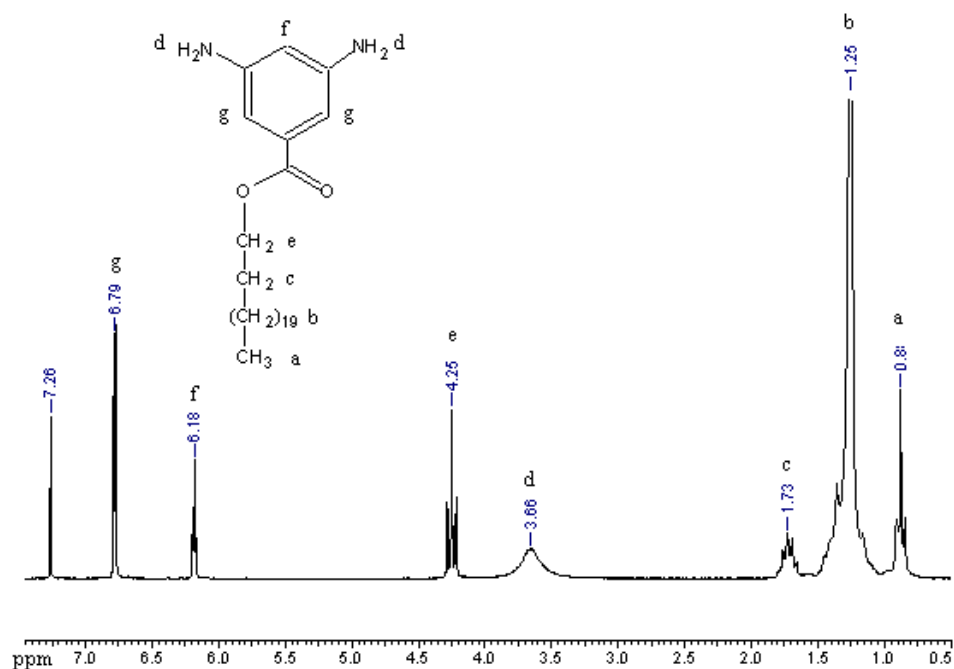
Figure 3.7 ^{1}H-NMR spectra of n-Docosyl 3,5-diaminobenzoate.

FTIR spectrum of n-docosyl 3,5-diaminobenzoate in KBr pellet is shown in **Figure 3.8**. The presence of primary amine group is confirmed in the spectrum by three characteristic absorption bands at 3413, 3322, 3220 cm^{-1}. Strong bands observed at 2917, 2850 cm^{-1} assigned to aliphatic C-H stretching vibration. Characteristic absorption due to ester carbonyl is seen as a strong band at 1710 cm^{-1}. Two other bands due to amine group are seen in the spectrum at 1605 cm^{-1} due to N-H bending and around 760 cm^{-1} due to N-H wagging respectively.
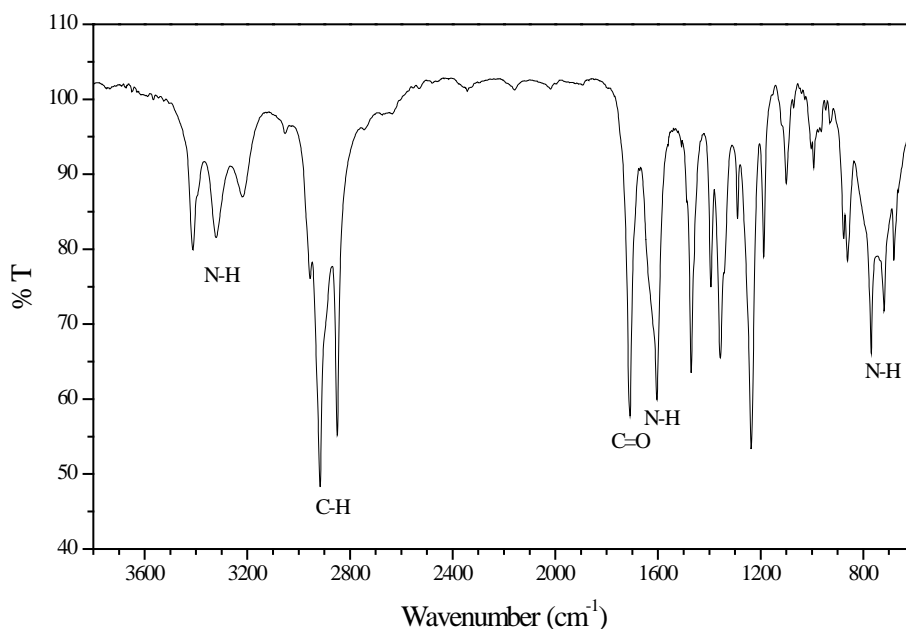
Figure 3.8 FTIR spectra of n-Docosyl 3,5-diaminobenzoate in KBr pellet.

3.3   Synthesis of Linear Polyurethane and Polyurethane-ureas

A two-step or prepolymer method was adopted for the synthesis of polyurethane and polyurethane-urea copolymers. Dibutyltin dilaurate (DBTDL) was used as a catalyst and N,N-dimethylacetamide (DMAc) was used as a solvent for the polymerization. We have used a slightly higher –OH: -NCO ratio for the synthesis of polymers. A molar ratio of -OH: -NCO (for L-PU) and (–OH + -NH2) : -NCO (for all PUUs) was kept at 1:1.05. This ratio was optimized after several polymerizations. In the first step of the reaction, an isocyanate end-capped prepolymer was produced by reaction of PTMO oligomer with an excess Isophorone diisocyanate (IPDI). The second step involved chain extension of the prepolymer with a diol and/or diamine, to increase the overall molecular weight of the polymer. In addition to the 'branched' polyurethane-ureas prepared using the alkyl side chain containing diamine chain extenders, a 'linear' polyurethane and a series of 'linear' polyurethane-ureas having aromatic diamine without any pendent aliphatic chain were synthesized as control samples. We reiterate that the adjectives 'branched' and 'linear', mentioned above and hereafter in thesis refer respectively to the presence and absence of the alkyl side chains in the polymers.

3.3.1 Synthesis of Linear Polyurethane Control

The first control sample, a linear polyurethane, was synthesized using 1,4-butanediol (BDO) as the chain extender, and is henceforth referred to as L-PU. The hard segment content was maintained at 50 % by weight. Hard segment content was calculated using following formula.

$$\% \text{ Hard Segment Content} = \frac{\text{wt. of IPDI} + \text{wt. of BDO}}{\text{wt. of IPDI} + \text{wt. of BDO} + \text{wt. of PTMO}} \qquad (3.1)$$

Polymerization was conducted in a 500 ml, three-neck, round bottom flask equipped with a magnetic stirring bar, a nitrogen gas inlet and outlet fitted to the two necks of the flask, and an addition funnel fitted to the third neck. Reactants, IPDI, PTMO and BDO were dissolved separately in dry DMAc to prepare 20 % by weight solutions. Calculated amount of the PTMO solution was taken in the round bottom flask to which 0.5 mol % of catalyst, DBTDL was added. Under vigorous stirring, the isocyanate solution was added by dropping funnel over 25-30 min. Temperature was then slowly raised to 70°C and the reaction was carried out for 3 hrs. After this prepolymerization step, the temperature was lowered to ambient, and the chain extender 1,4-butanediol solution was added to the vigorously stirred prepolymer. The temperature was raised again to 70°C and reaction was continued for 4 hrs under constant stirring and nitrogen atmosphere. The polymer solution thus formed, was precipitated in cold distilled water and dried at 60°C under vacuum for four days.

3.3.2 Synthesis of Linear Polyurethane-ureas

The second set of control samples namely, a series of linear polyurethane-ureas (PUUs), were synthesized by replacing 1,4-butanediol with different amounts of m-phenylenediamine (PDA). Three such control polymers were synthesized in this series and were labeled as L-PUU10, L-PUU50, and L-PUU100 where, L refers to linear and the number after PUU refers to the mole percent of 1,4-butanediol replaced using PDA. The hard segment content in all polymers was maintained at 50 % by weight.

All PUUs in this series were synthesized by following a similar prepolymer synthesis protocol. Briefly, polymerizations were carried out in 500 ml, three-neck, round bottom flask fitted with a nitrogen gas inlet, outlet and an addition funnel.

Reactants were dissolved separately in dry DMAc to prepare 20 % by weight solutions. 0.5 mol% of DBTDL was added to the PTMO solution in the round bottom flask. The solution of IPDI was added dropwise into the PTMO solution for about 30 min under constant stirring and at room temperature. Reaction was carried out for three hours at 70°C. After this prepolymer step, the temperature was lowered to ambient, and solutions of the chain extenders BDO and PDA were simultaneously added to the reaction vessel under vigorous agitation. The temperature was raised to 70°C and reaction was continued for a further 3.5 hrs under constant stirring and nitrogen atmosphere. The polymer solution thus formed, was precipitated in cold distilled water and dried at 60°C under vacuum for four days.

An important point relating to the chemistry of polyurethane-urea synthesis needs a comment here. As discussed in the chapter no. 1, section 1.2.2, reactivity of isocyanate with primary amines is substantially higher as compared to primary alcohol groups (even in the absence of catalyst). Accordingly, a small excess of diisocyanate (–OH + -NH2 : -NCO = 1:1.05 mol), and combination of a diol and diamine chain extenders, as used in this study, can influence the resulting hard and soft segment sequence in the polymer chain. Thus, for all polyurethane-ureas synthesized in the present work (by simultaneous addition of chain extenders to the prepolymer solution), there is a propensity of formation of urea linkages in preference to the urethane linkages. Therefore, we do not rule out the possibility of formation of a few longer urea hard segment sequences. This is particularly more likely in copolymer compositions having high diamine content.

3.4 Synthesis of Branched Polyurethane-ureas Containing Diamine Chain Extenders

The same two step solution polymerization method was used for the preparation of branched polyurethane-urea copolymers containing equivalent hard and soft segments (approximately 50 wt. % each). The prepolymer method followed is illustrated in **Figure 3.9.**

3.4.1 Synthesis of Polyurethane-ureas Containing C12 Branches

Polymers synthesized in this series will be referred to as B12-PUU10, B12-PUU50, B12-PUU70 and B12-PUU100, where B12 denotes B –for branch and 12 – for the number carbon atoms in the alkyl side chain, and last number refers to the mole percentage of chain extender BDO replaced with n-Dodecyl 3,5-diaminobenzoate. A representative procedure for the synthesis of B12 series PUUs is described below.

All reactants were separately dissolved in anhydrous DMAc (80% by vol.). PTMO (12.00 g / 0.004 mol) solution was added to a 250 ml three neck round bottom flask equipped with an addition funnel, a nitrogen gas inlet and outlet, and a magnetic stirring bar. A few drops of catalyst DBTDL were added to the PTMO solution and solution was stirred. IPDI (9.336 g / 0.042 mol) solution was added dropwise from the addition funnel into the PTMO solution for 35-40 min under constant stirring. Temperature was then increased slowly to 70°C and the prepolymerization reaction was carried out for ca. four hours under nitrogen atmosphere. The reaction mixture was allowed to cool down to room temperature.

Chain extension or polymerization step was then carried out by simultaneous addition of BDO (2.808 g / 0.0312 mol) and n-Dodecyl 3,5-diaminobenzoate (1.504 g / 0.0047 mol) solutions to the prepolymer under vigorous stirring. Temperature was again raised to 70°C and was maintained for four hours before the polymer was precipitated in cold, distilled water. The polymer was dried at 60°C under vacuum for four days.
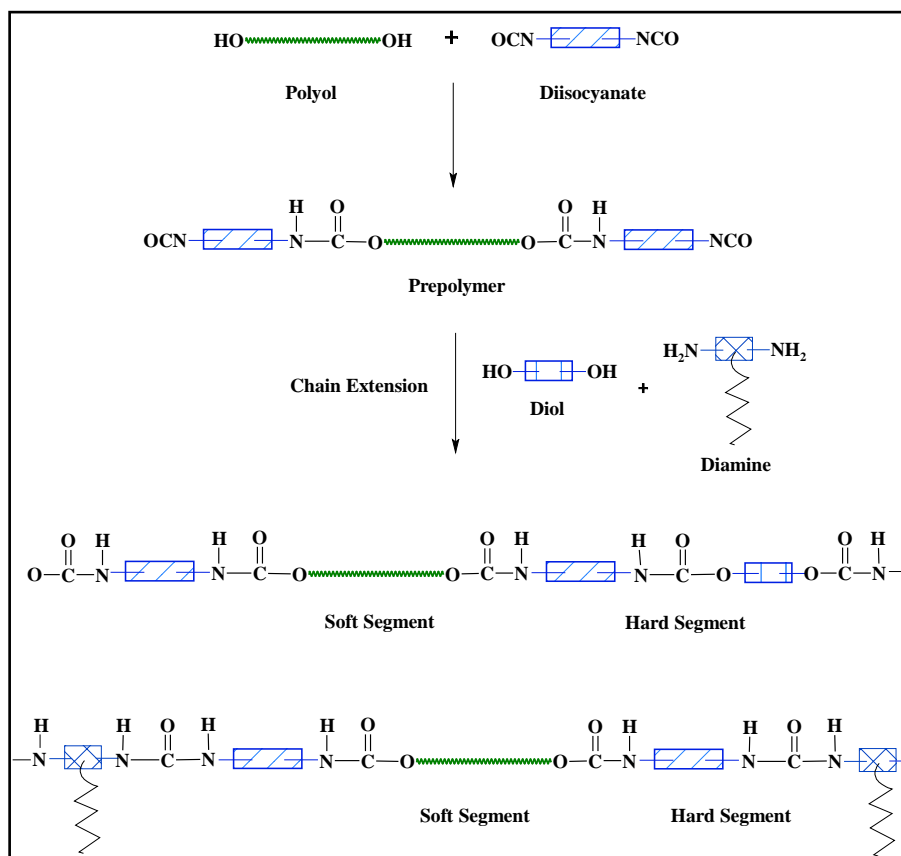
Figure 3.9 Branched PUU Synthesis Method.

3.4.2 Synthesis of Polyurethane-ureas Containing C22 Branches

Branched polyurethane-ureas of this series are labeled as B22-PUU10, B22-PUU30, B22-PUU50. The labels have the usual meanings viz., B- for branch, 22 –for the number of carbon atoms in the alkyl side chain, and the last number indicating the mole percentage of 1,4-butanediol chain extender replaced with n-Docosyl 3,5-diaminobenzoate.

B22-PUUs were synthesized by following a similar prepolymer synthesis protocol as described for B12-PUUs.

3.5 Synthesis and Characterization of Model Hard Segment Polymers

Model hard segment polymers were synthesized in order to analyze the thermal and SAXS data of PUUs, which are described in the next chapter. Synthesis was carried out by reacting diisocyanate and chain extender (20 wt % solutions) in DMAc solvent under anhydrous conditions. The diisocyanate and chain extender were separately dissolved and charged at once in the round bottom flask. The solution was then stirred at room temperature for about 30 min. Reactions were carried out for four hours at 70°C, Polymers were obtained in the form of films by solvent casting from DMAc at 80°C. This was followed by vacuum drying of the samples at 60°C for five days. Samples were stored in air tight container before the analysis was done.

An example of a model hard segment polymer synthesized using isophorone diisocyanate and 1,4-butanediol as shown in the following **Scheme 3.5.**
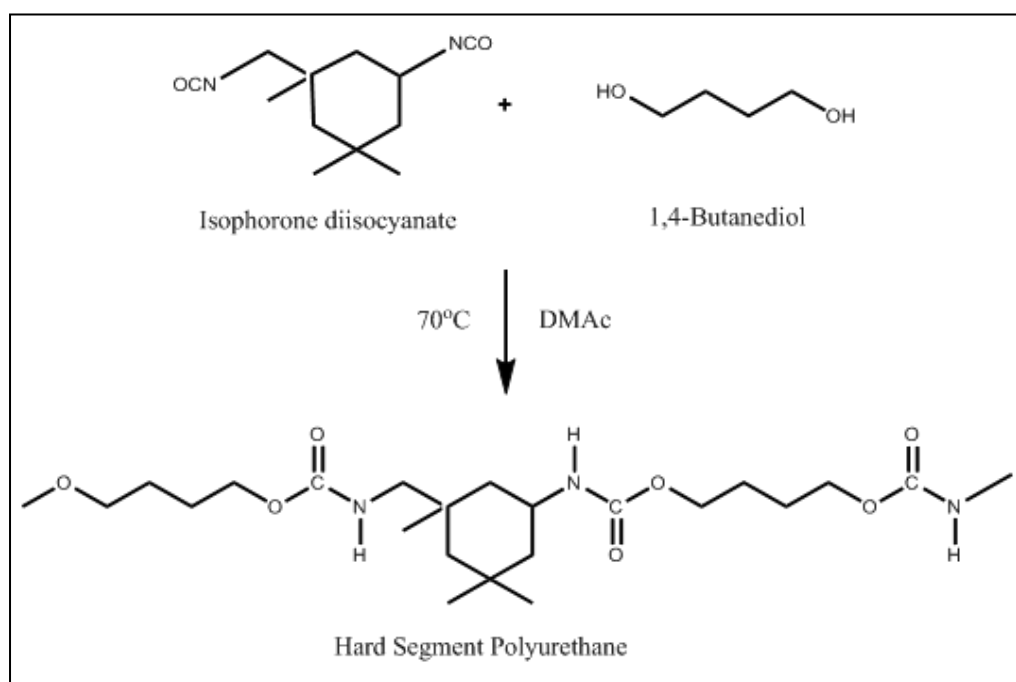
Scheme 3.5 Synthesis of model hard segment polyurethane.

Also, a series of hard segment polymers were synthesized using isophorone diisocyanate and a combination of 1,4-butanediol and n-dodecyl 3,5-diaminobenzoate as given in the **Scheme 3.6.** The mole ratio of (-OH + -NH$_2$) : -NCO was kept at 1 : 1.05. **Table 3.1** lists five hard segment PUUs synthesized in the present work.
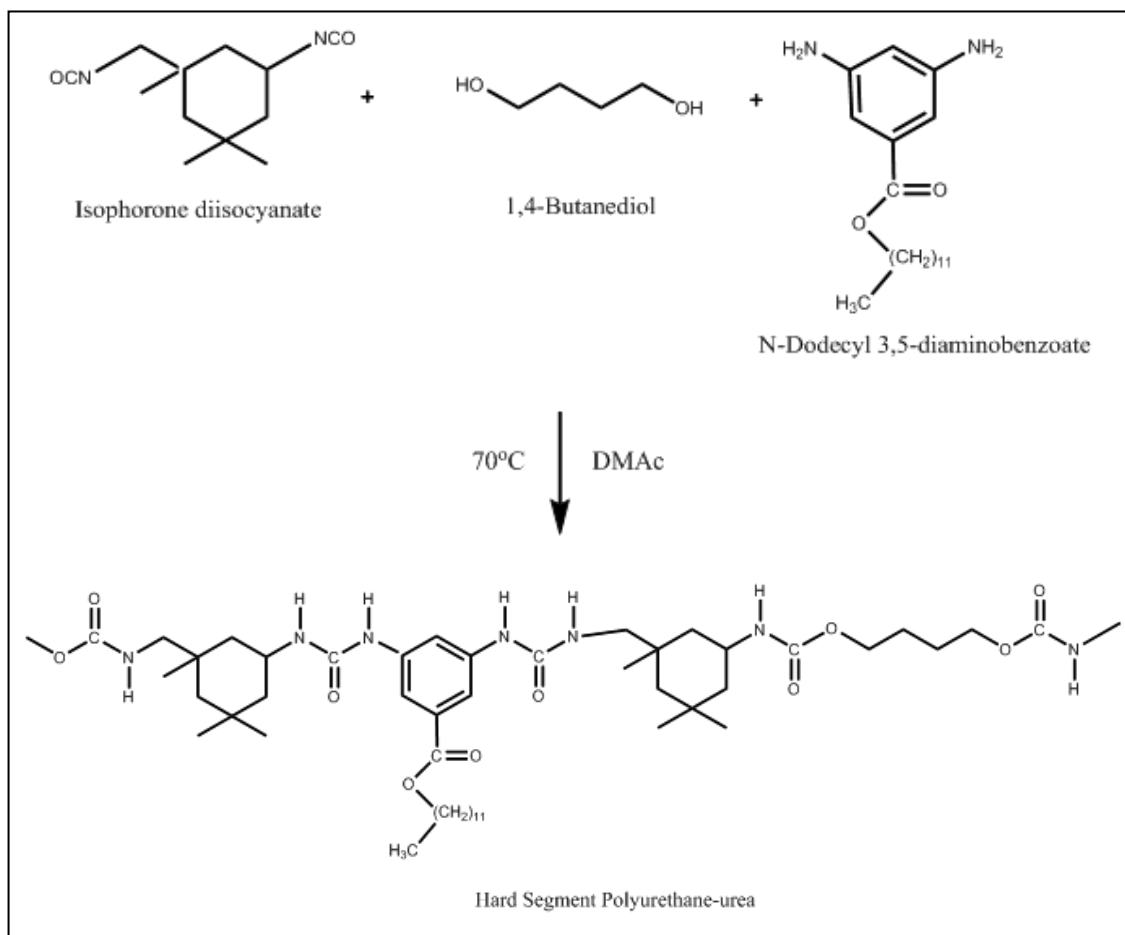
Scheme 3.6 Synthesis of model hard segment PUUs containing B12 diamine.

Table 3.1 Model Hard Segment Polymers.

Sr. No.	Model Polymers	
	Isocyanate	Chain Extender
1	IPDI	BDO
2	IPDI	BDO (90 mol%) + DAB (10 mol%)
3	IPDI	BDO (50 mol%) + DAB (50 mol%)
4	IPDI	BDO (30 mol%) + DAB (70 mol%)
5	IPDI	DAB

* IPDI – Isophorone diisocyanate
* BDO – 1,4-Butanediol
* DAB – N-Dodecyl 3,5-diaminobenzoate

3.8 Summary

In summary, this chapter has described

- Two step synthesis of diamine chain extenders *n-dodecyl 3,5-diaminobenzoate* and *n-docosyl 3,5-diaminobenzoate* starting from *3,5-dinitrobenzoylchloride*.

- Characterization of diamine chain extenders by spectral methods and elemental analysis.

- Synthesis of 'linear' polyurethane and a series of linear polyurethane-ureas (chain extender *m-phenylenediamine*) via a two-step solution polymerization scheme.

- Synthesis of two series of 'branched' polyurethane-ureas with varying amounts of chain extenders *n-dodecyl 3,5-diaminobenzoate* and *n-docosyl 3,5-diaminobenzoate* by a two-step solution polymerization scheme.

- Synthesis of a series of model hard segment polymers (chain extender *1,4-butanediol* and *n-dodecyl 3,5-diaminobenzoate*).

Molecular Characterization of Polyurethane-ureas

Chapter - 4

All polymers synthesized in this work (as described in Chapter No. 3) were characterized for their molecular structure by ^{1}H-NMR, FTIR, and Gel Permeation Chromatography. The experimental methods used in this work for molecular characterization and the results obtained thereof are presented in this chapter.

4.1 Proton Nuclear Magnetic Resonance (^{1}H-NMR)

Polymers were analyzed for ^{1}H-NMR using a Bruker AV200 spectrometer at an operating frequency of 200 MHz and using $CDCl_3$ as a solvent. Peaks were referenced to TMS peak at $\delta = 0$ ppm. These spectra will be referred to as the ^{1}H-NMR(200) spectra.

4.1.1 L-PU and L-PUU Series

^{1}H-NMR(200) spectrum of L-PU is shown in **Figure 4.1**. Methyl protons of cyclohexane ring displayed a doublet at 0.94 δ ppm while the cyclohexane methylenes appeared as a singlet at 1.07 δ ppm. The methylene protons of poly(tetramethylene oxide) (PTMO) that are α- and β- to ether oxygen atom appeared respectively as multiplets at 3.41 and 1.62 δ ppm. The methylene protons of PTMO α- to urethane linkage displayed a slightly broad singlet at 4.08 δ ppm. Urethane N-H protons did not show any peak in the spectrum, possibly due to proton exchange with the solvent.
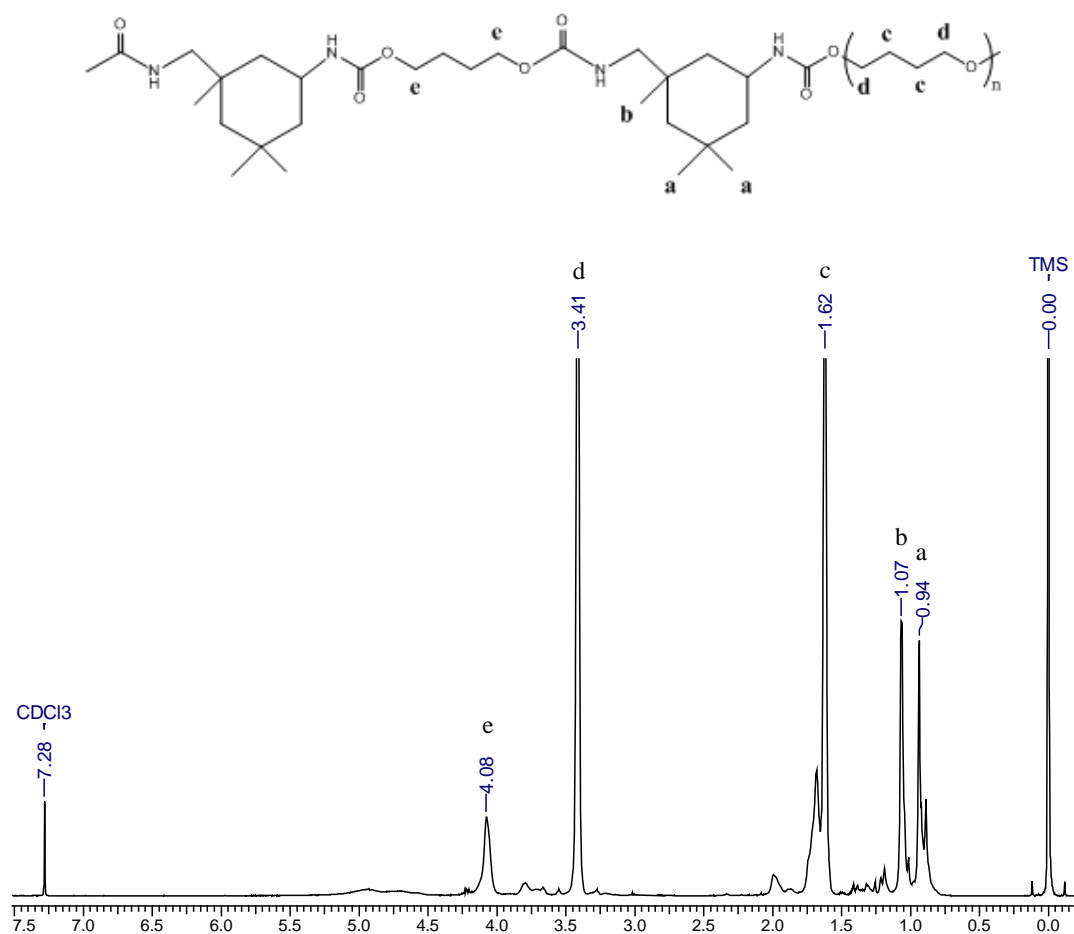
Figure 4.1 ^{1}H-NMR spectrum of L-PU.

Figure 4.2 shows ^{1}H-NMR(200) spectrum of L-PUU10. The major peaks seen in the spectrum are identical to those described in **Figure 4.1** and have the same assignment. No distinct peaks corresponding to the presence of m-phenylenediamine were observed in this spectrum.
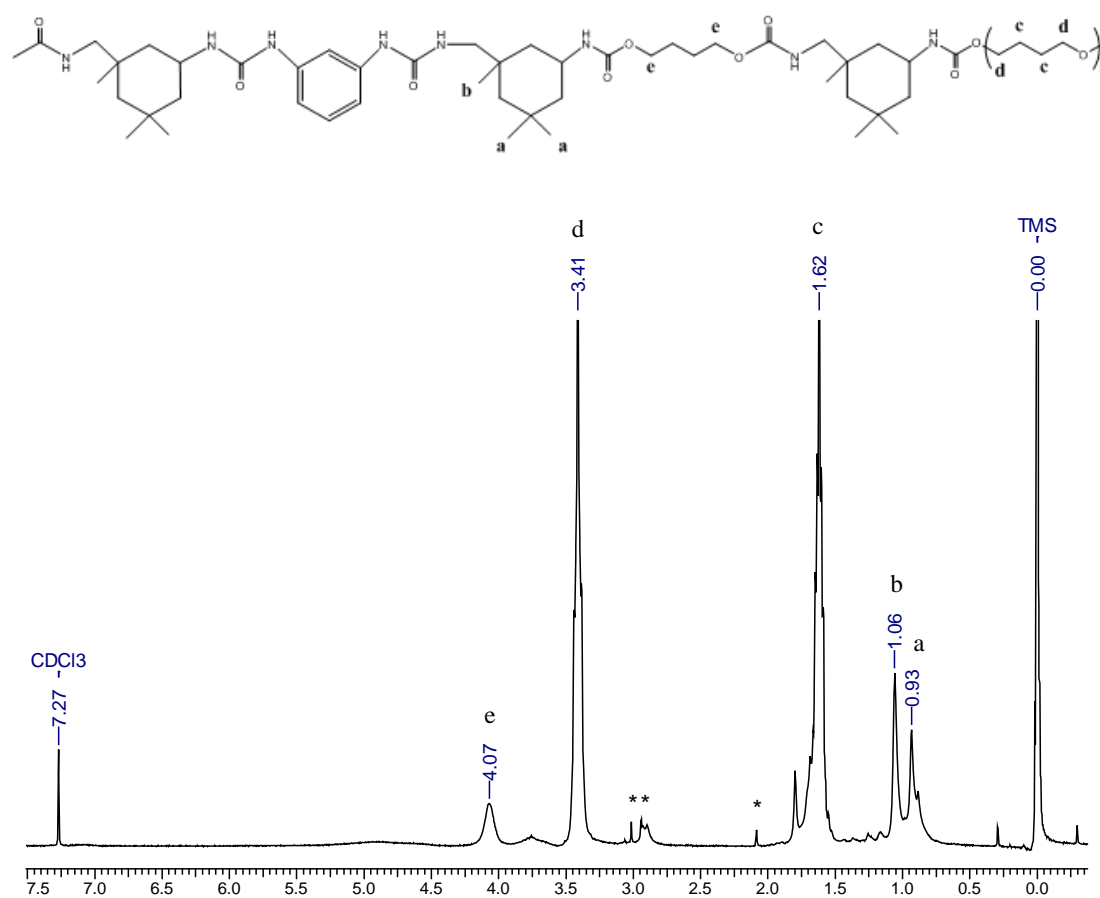
Figure 4.2 ^{1}H-NMR spectrum of L-PUU10. Peaks marked as * are of DMAc.

Figure 4.3 shows ^{1}H-NMR(200) spectrum of L-PUU50. The major peaks seen in the spectrum are identical to those described in **Figure 4.1** and have the same assignment. Again, no distinct peaks corresponding to the presence of m-phenylene diamine were observed in this spectrum.
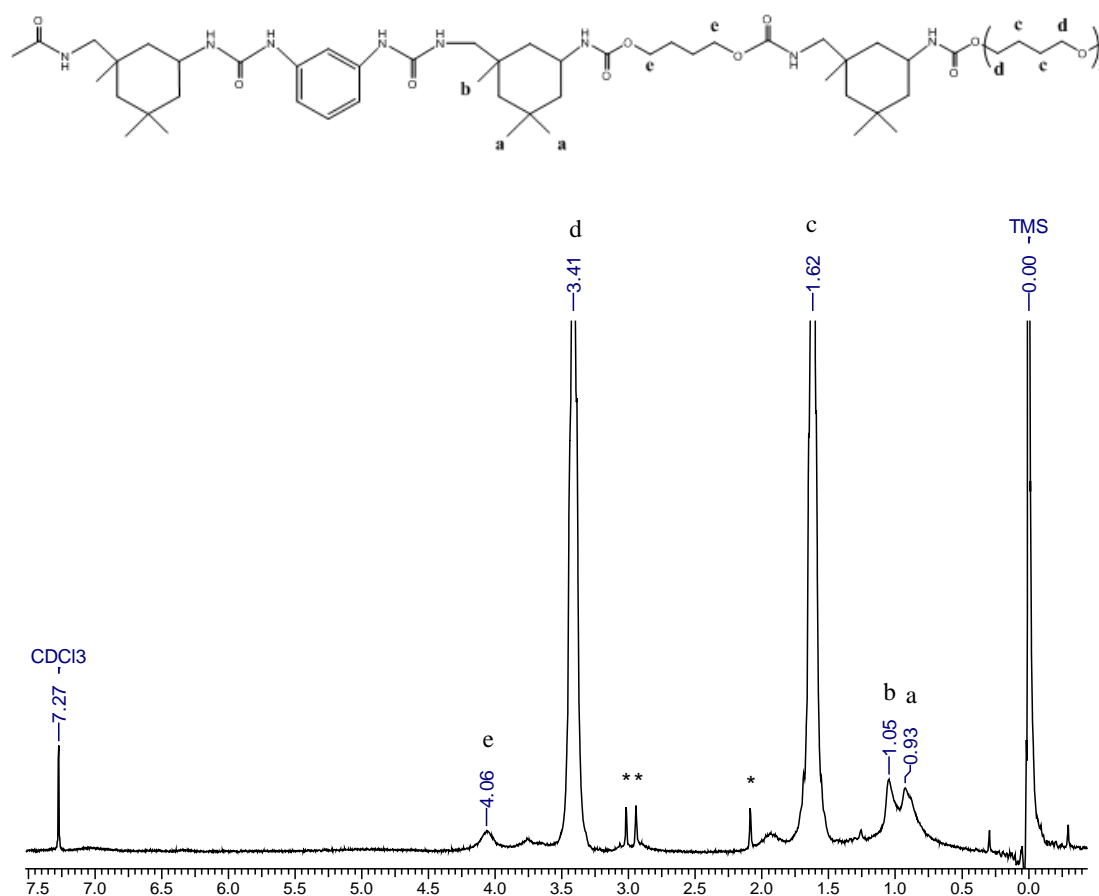
Figure 4.3 ^{1}H-NMR spectrum of L-PUU50. Peaks marked as * are of DMAc.

Polymer L-PUU100, due to high urea content, was insoluble in common solvents, and thus could not be characterized by NMR.

4.1.2 B12-PUU Series

^{1}H-NMR(200) spectrum of B12-PUU10 is shown in **Figure 4.4**. The major peaks seen in the spectrum are identical to those described in **Figure 4.1** and have the same assignment. Additionally, methylene protons from the pendent aliphatic chain of n-dodecyl 3,5-diaminobenzoate were observed as a multiplet at 1.26 δ ppm. While this indicated the presence of n-dodecyl 3,5-diaminobenzoate in the polymer, it does not suggest whether the diamine chain extender has actually reacted to form the urea linkage or merely physically present. Evidence for the reaction was indeed provided by the ^{1}H-NMR(500) spectrum as shown later.
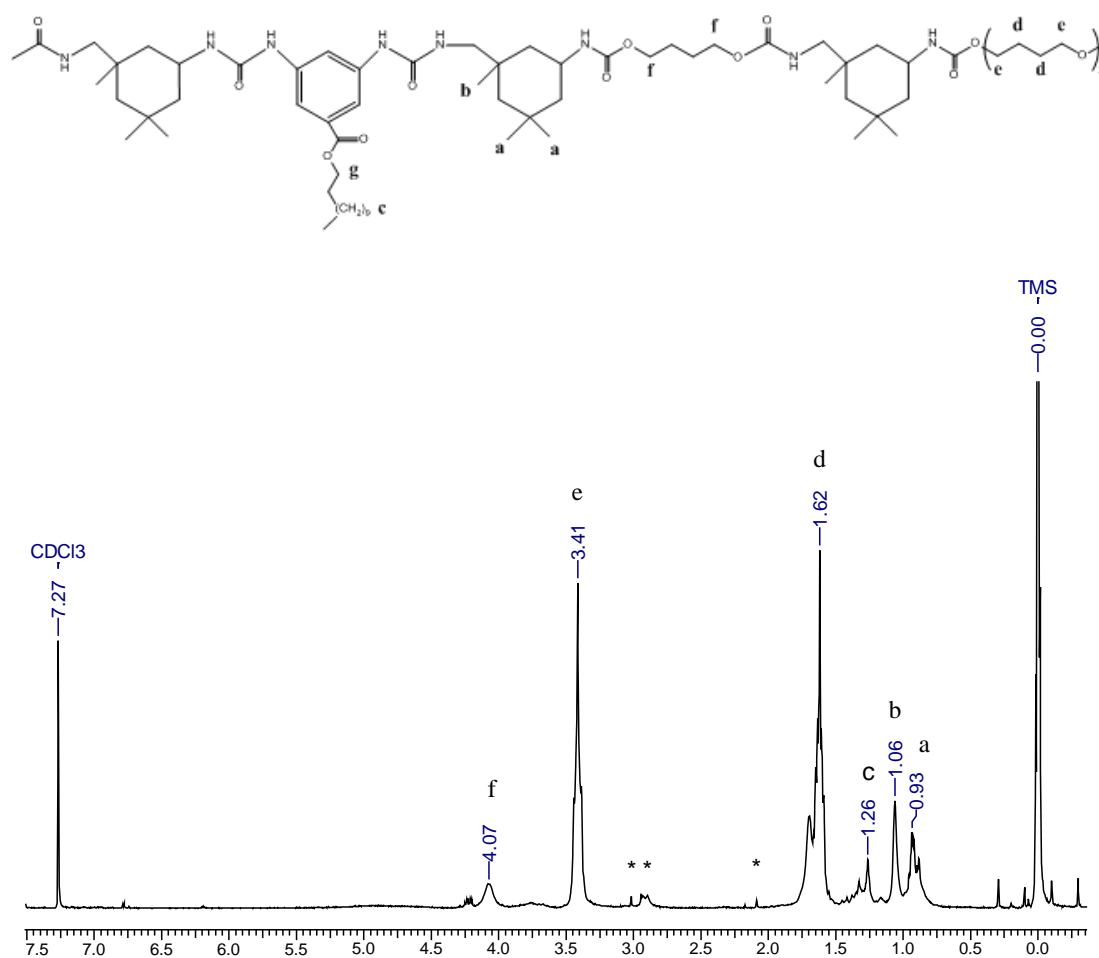
Figure 4.4 ^{1}H-NMR spectrum of B12-PUU10. Peaks marked as * are of DMAc.

^{1}H-NMR(200) spectrum of B12-PUU50 is shown in **Figure 4.5** The major peaks seen in the spectrum are identical to those described in **Figure 4.1** and have the same assignment. The methylene protons of diamine pendent chain, which are α- to ester oxygen atom, display a triplet at 4.23 δ ppm while the remaining methylene protons of the aliphatic chain appear as a multiplet at 1.26 δ ppm. Once again, the evidence for a reaction between the diamine chain extender and isocyanate is not obvious from this spectrum.
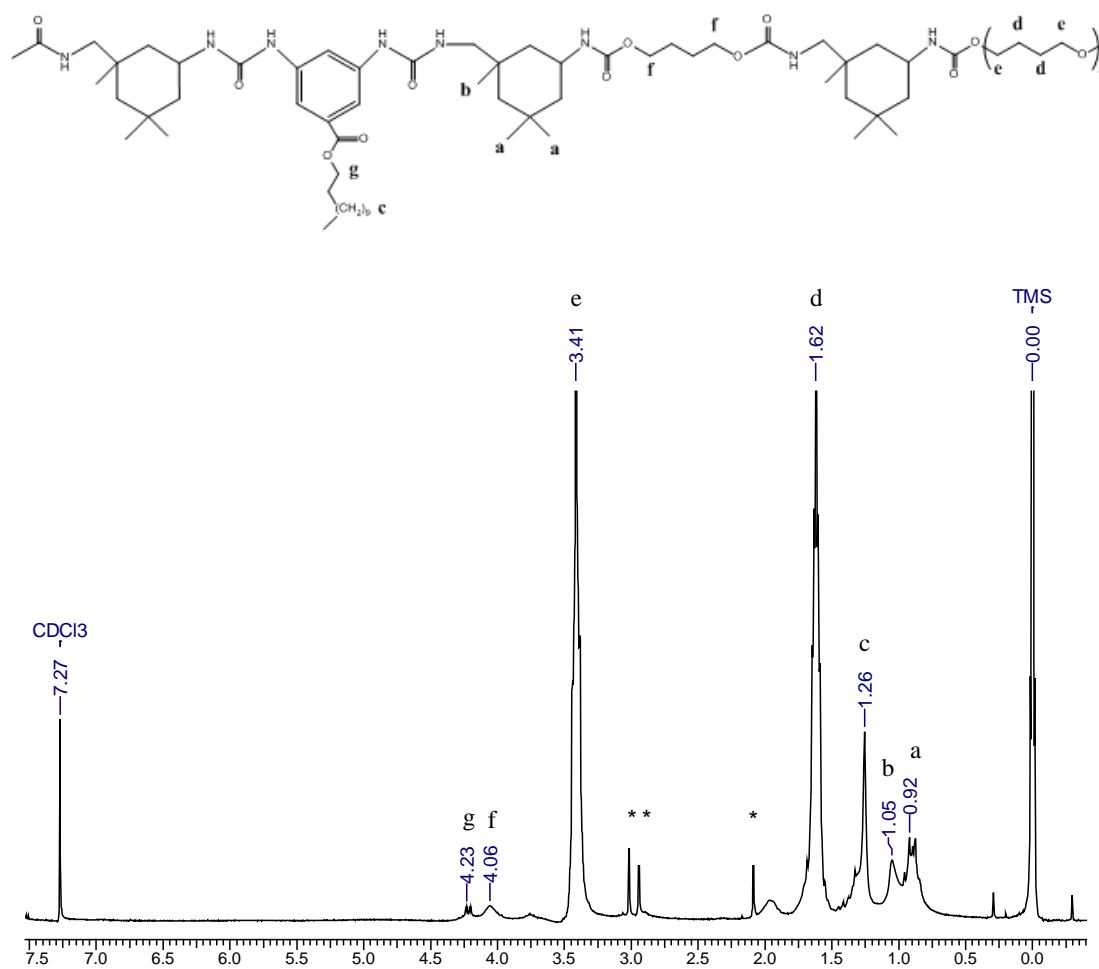
Figure 4.5 ^{1}H-NMR spectrum of B12-PUU50. Peaks marked as * are of DMAc.

Figure 4.6 shows ^{1}H-NMR spectrum of B12-PUU70. The major peaks seen in the spectrum are identical to those described in **Figure 4.5** and have the same assignment.
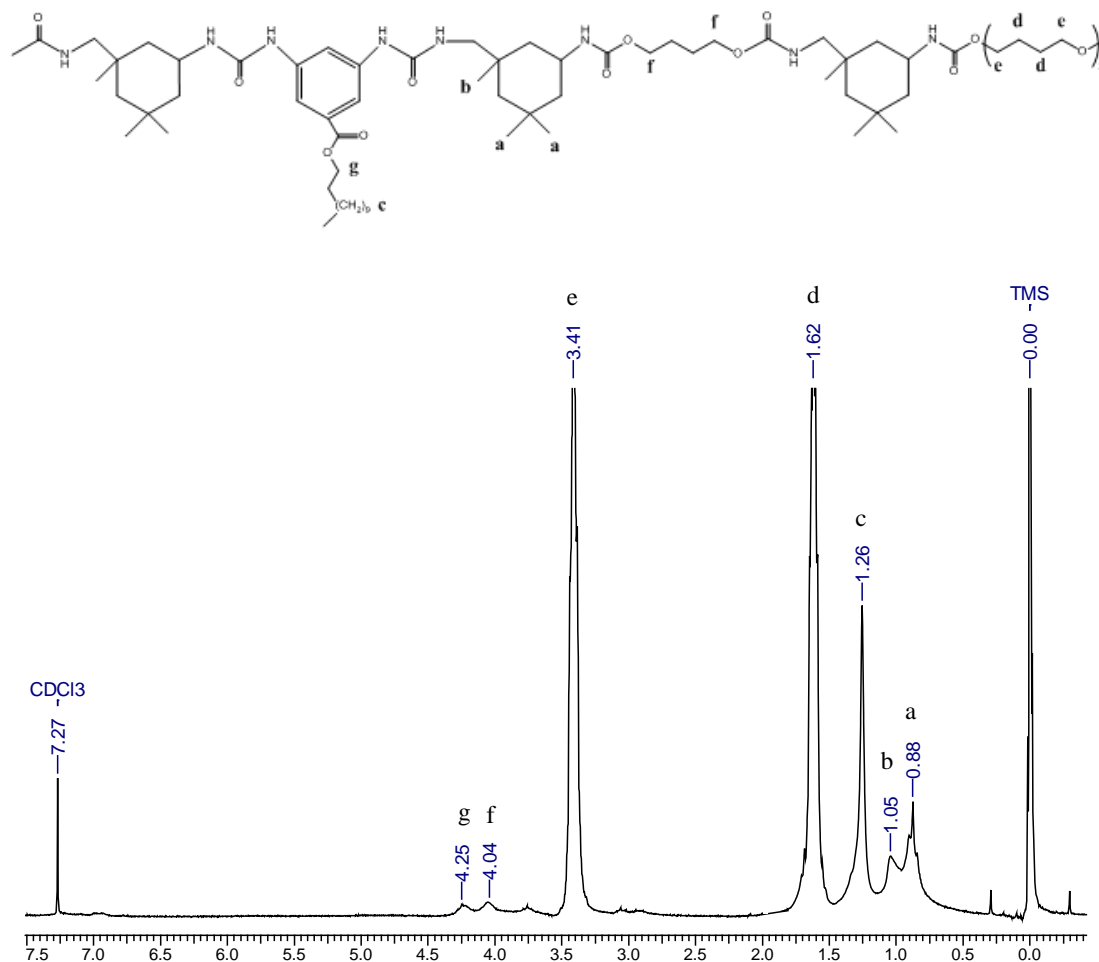
Figure 4.6 ^{1}H-NMR spectrum of B12-PUU70.

^{1}H-NMR(200) spectrum of B12-PUU100 is shown in **Figure 4.7** The methyl and methylene protons of the pendant aliphatic chain have the same assignments as discussed for **Figure 4.5**. Additionally, aromatic protons of diamine *ortho* to ester linkage exhibited a doublet at 6.79 δ ppm, while the aromatic proton *para* to ester linkage displayed a triplet at 6.20 δ ppm. The other major peaks seen in the spectrum are identical to those described in **Figure 4.1** and have the same assignment. It may be noted that the B12-PUU100 sample was soluble in *d*-chloroform whereas the L-PUU100 was insoluble.
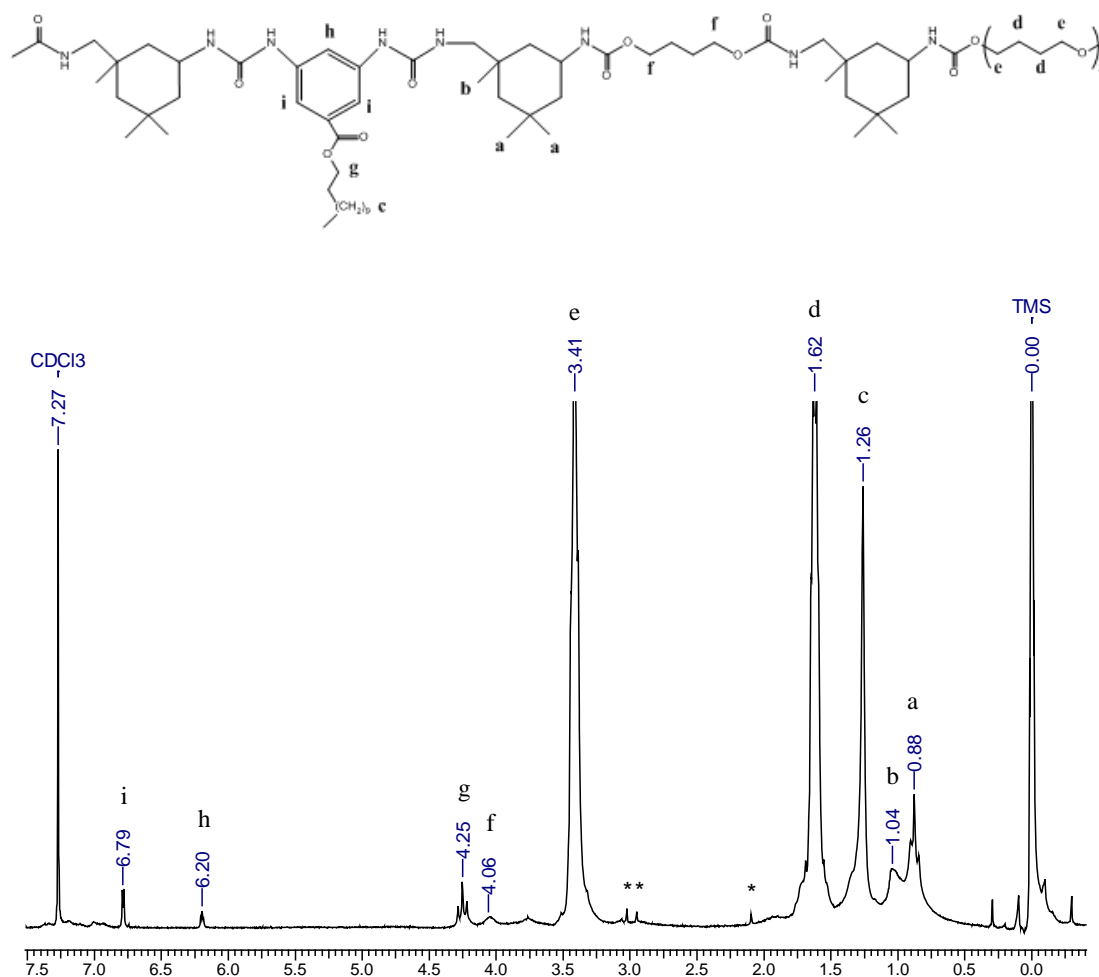
Figure 4.7 ^{1}H-NMR spectrum of B12-PUU100.

4.1.3 B22-PUU Series

The ^{1}H-NMR(200) spectrum of B22-PUU10 is shown in **Figure 4.8**. The major peaks seen in the spectrum are identical to those described in **Figure 4.4** and have the same assignment. Evidence for the reaction of diamine with diisocyanate was provided by the ^{1}H-NMR(500) spectrum as shown later.
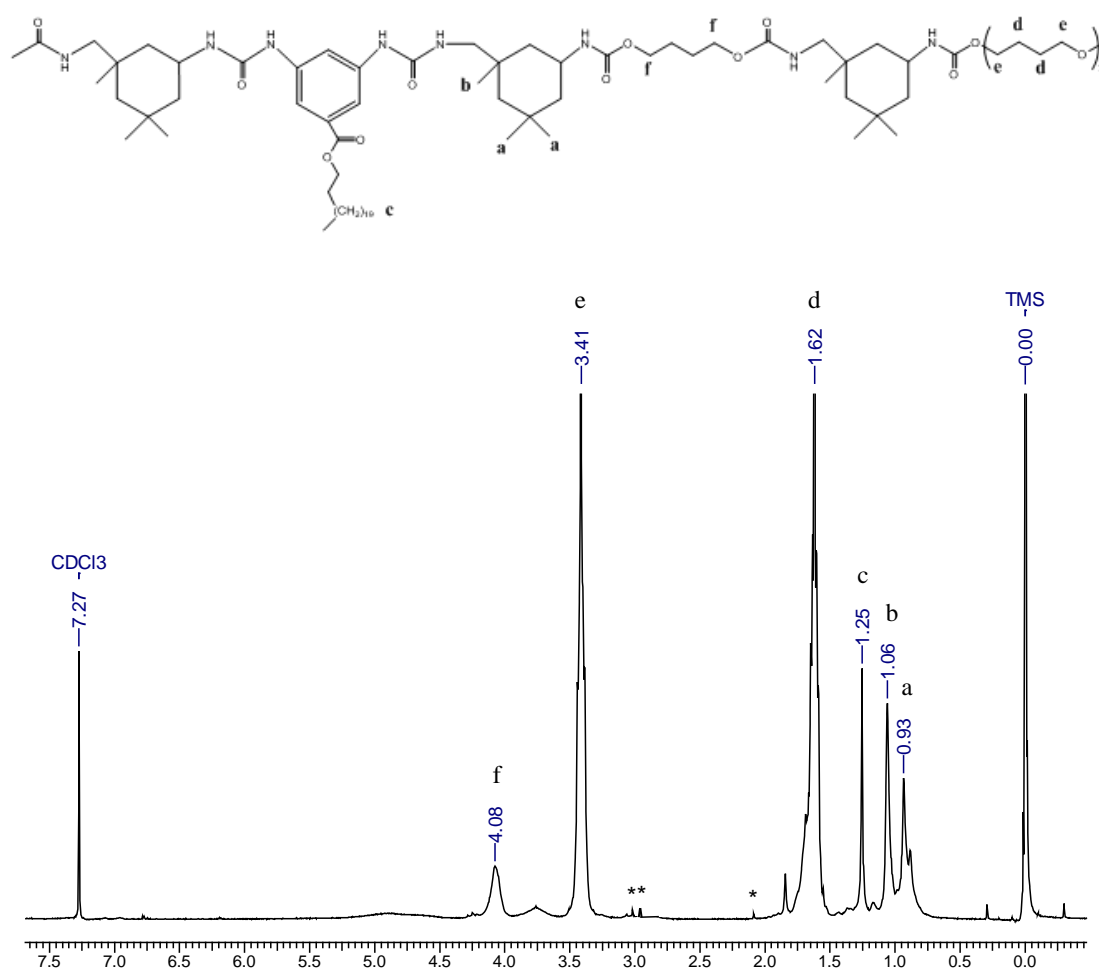
Figure 4.8 ^{1}H-NMR spectrum of B22-PUU10. Peaks marked as * are of DMAc.

Figure 4.9 shows ^{1}H-NMR(200) spectrum of B22-PUU30. It can be seen that the peaks are identical to that observed in **Figure 4.8** and have the same interpretation. Increased strength of the peak at 1.25 δ ppm is in correspondence with the B22 diamine incorporation.
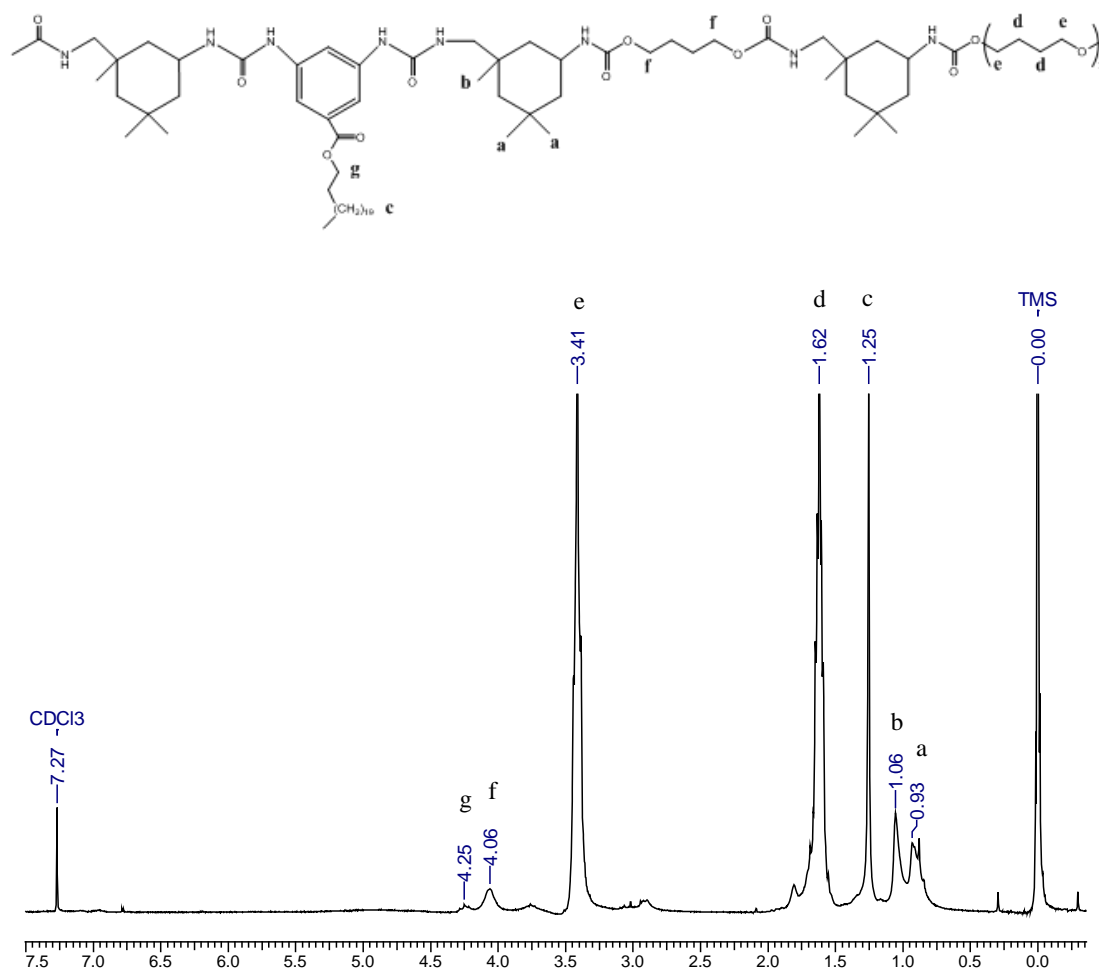
Figure 4.9 ^{1}H-NMR spectrum of B22-PUU30.

The major peaks seen in the ^{1}H-NMR spectrum of B22-PUU50 (see **Figure 4.10**) are identical to those shown in **Figure 4.7** and have the same assignments.
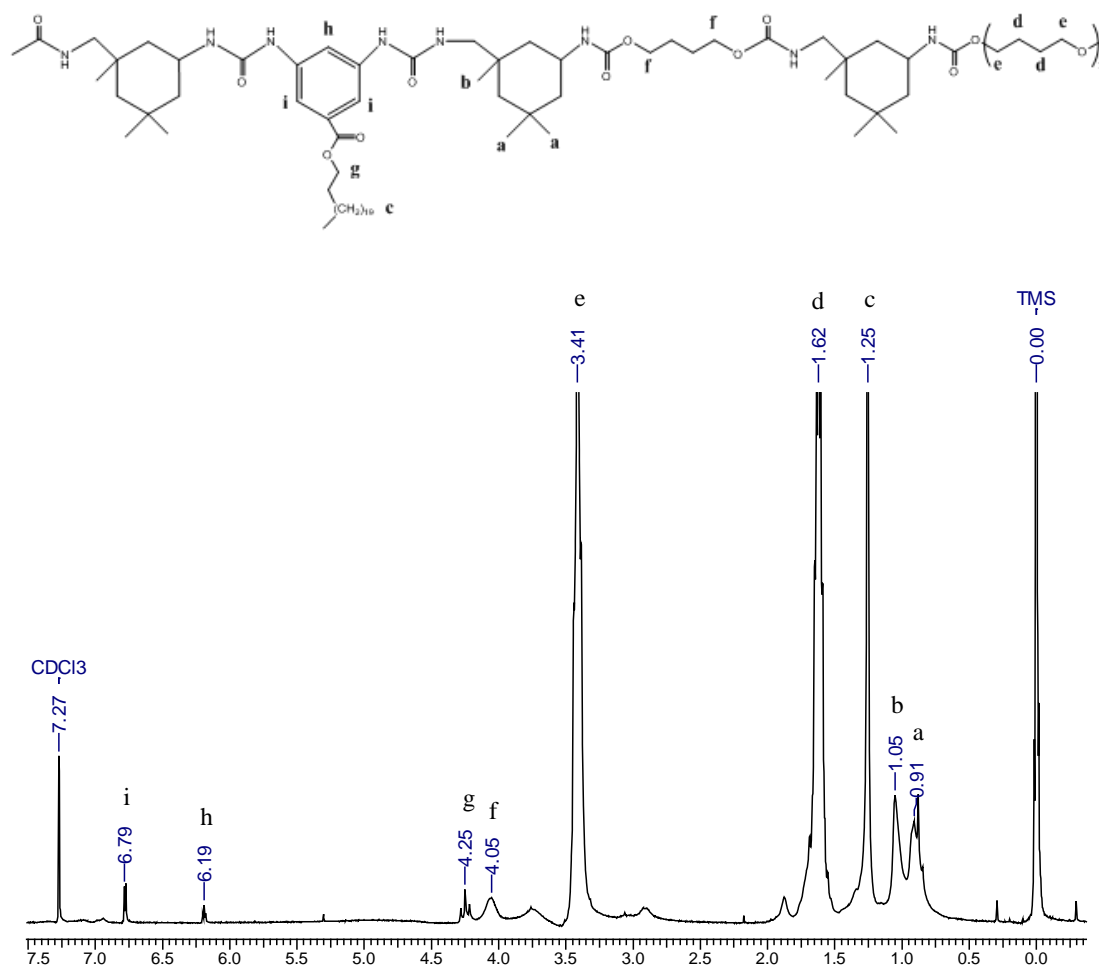
Figure 4.10 ^{1}H-NMR spectrum of B22-PUU50.

The major peaks seen in the ^{1}H-NMR spectrum of B22-PUU100 (**Figure 4.11**) are identical to those seen in **Figure 4.10** and have the same assignments. Like the B12-PUU100, this sample was also readily soluble in *d*-chloroform in contrast to the L-PUU100 sample.
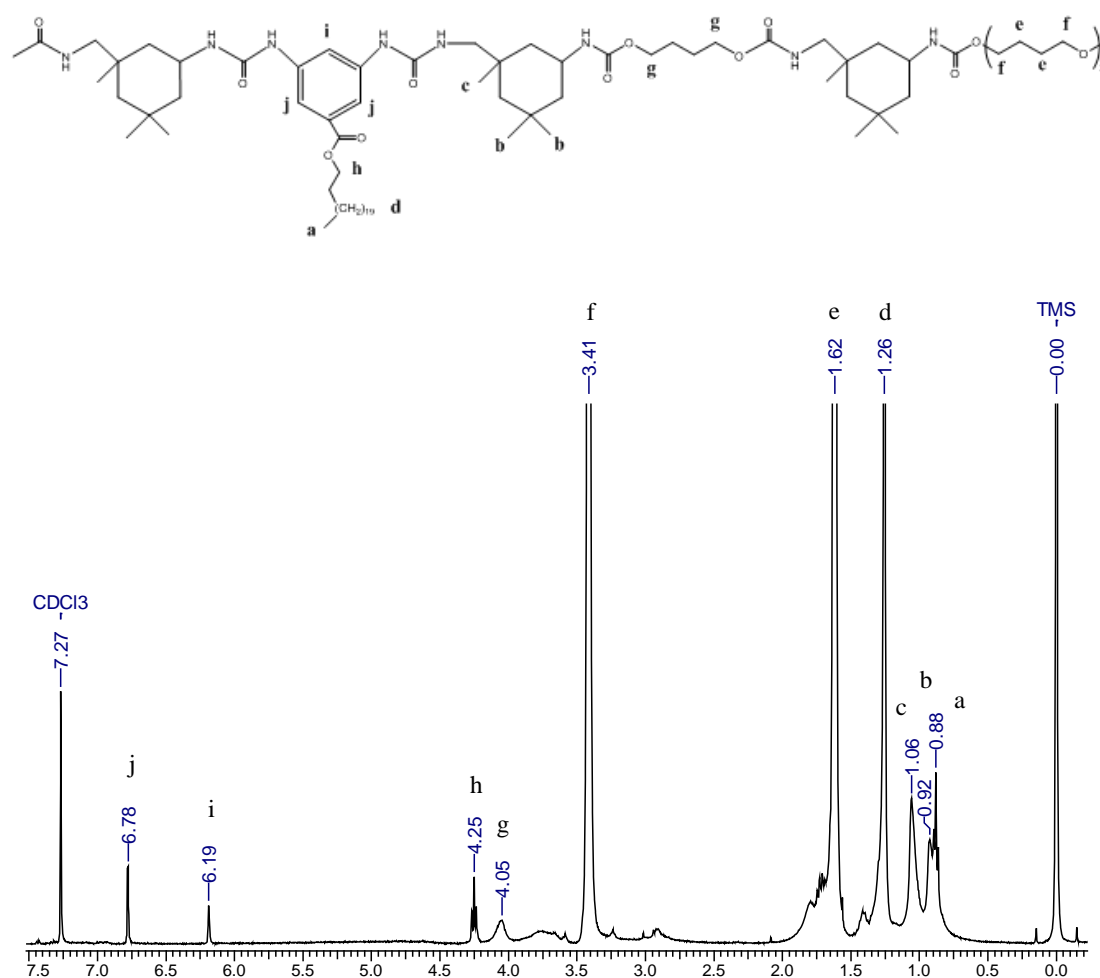
Figure 4.11 ^{1}H-NMR spectrum of B22-PUU100.

4.2 Fourier Transform Infrared Spectroscopy (FTIR)

A Perkin Elmer Spectrum GX spectrometer was used for FTIR measurements. Samples were prepared by drop casting a thin film from dilute chloroform solution onto a piece of silicon wafer. Films were vacuum dried for about two hours, and also under an IR lamp (for 15 minutes) before scanning. An FTIR spectrum of the silicon wafer was recorded as background, and was subtracted appropriately from the sample spectra for analysis. Twenty scans were signal averaged at a resolution of 4 cm^{-1} before Fourier transformation.

Table 4.1 Assignments of important infrared absorption modes.[1,2]

Wavenumber (cm^{-1})	Assignments
~ 3440	v(NH) free
3340	v(NH) H-bonded, urethane
3340 – 3320	v(NH) H-bonded, ordered urea
~ 3340	v(NH) H-bonded, disordered urea
3240	v(N-H) H-bonded to ether –O-
2939	v_a(CH$_2$)
2857	v_s(CH$_2$)
2794	v_s(CH$_2$)
1730	v(C=O) free urethane
1710	v(C=O) H-bonded urethane
1690 – 1700	v(C=O) free urea
1666	v(C=O) H-bonded, disordered urea
1643 – 1628	v(C=O) H-bonded, ordered urea
1600	v(C-C) aromatic
1540	v(C-N) + δ(N-H) amide II
1450	δ_a(C-H) in CH$_3$
1370	ω(C-H) in CH$_2$
1365	δ_s(C-H) in CH$_3$
1240	v(C-N) + δ(N-H) amide III
1110	v(C-O-C)

Vibration mode: v = stretching, δ = bending, ω = wagging;

Subscript: a = asymmetric, s = symmetric;

Intensity: s = strong, m = medium, w = weak.

4.2.1 L-PU and L-PUU Series

The FTIR spectrum of L-PU (**Figure 4.12)** shows characteristic peaks of a strongly hydrogen bonded polyurethane hard segment. These include urethane N-H stretching absorption at 3332 cm^{-1}, C=O stretching absorption at 1701 cm^{-1}, and C-N stretching and N-H bending absorptions at 1536 cm^{-1}. The stretching absorption of ether linkage (C-O-C) corresponding to the soft segment was observed at 1112 cm^{-1}. In addition, absorption bands arising from asymmetric –CH$_2$ stretching centered at 2948 cm^{-1} and symmetric –CH$_2$ stretching at 2859 cm^{-1} were also observed. A list of assignments of typical FTIR absorption modes for polyether urethanes and polyurethane-urea is given in **Table 4.1**.
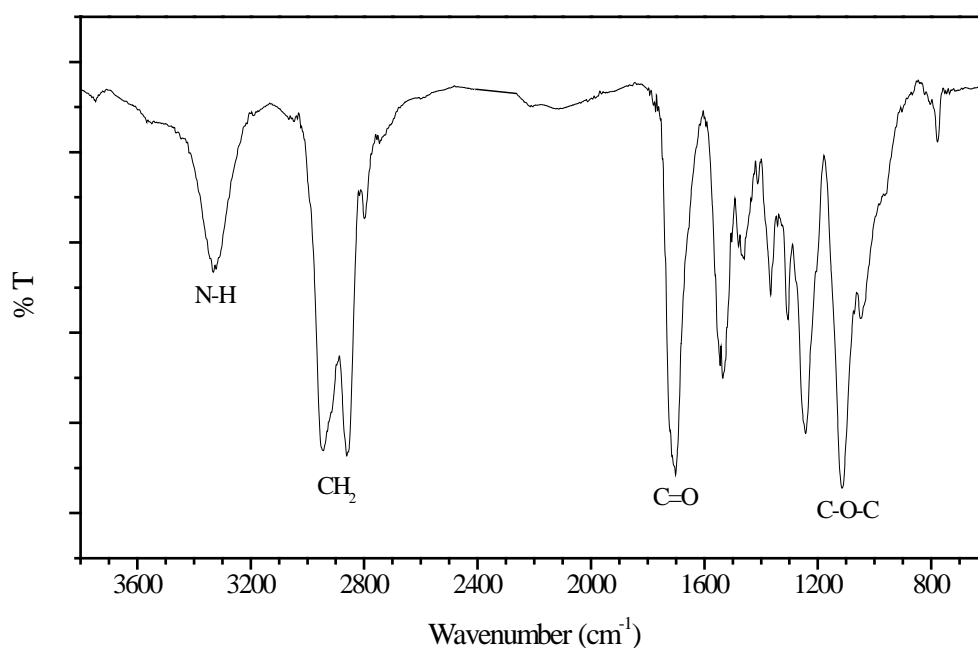
Figure 4.12 FTIR spectrum of L-PU solution cast film.

The FTIR spectrum of L-PUU10 (**Figure 4.13)** shows peaks that are identical to those seen in **Figure 4.12** and have the same assignments. No absorption band corresponding to the presence of urea carbonyl was observed.

National Chemical Laboratory
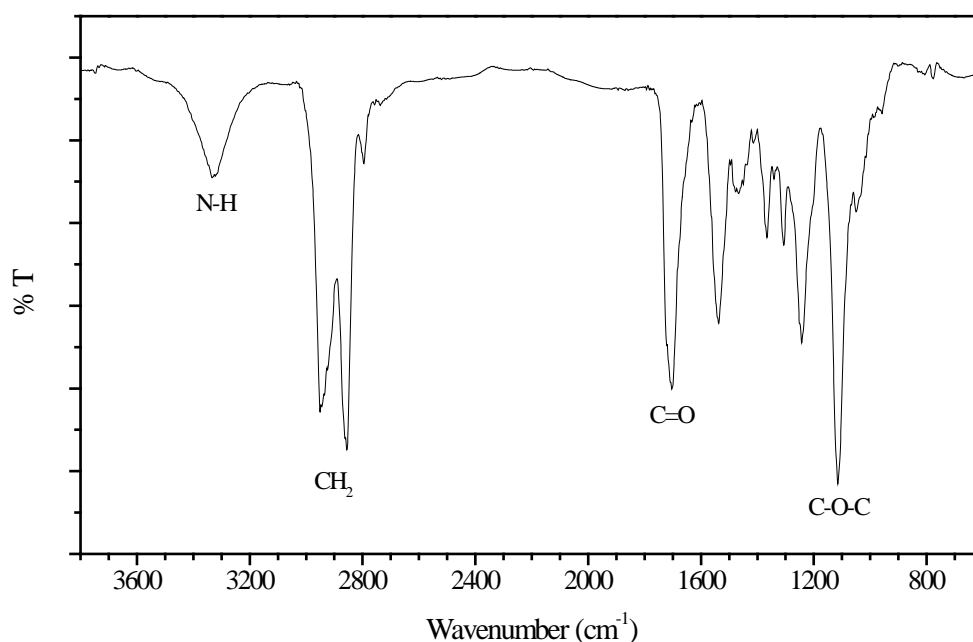
Figure 4.13 FTIR spectrum of L-PUU10 solution cast film.

Figure 4.14(A) shows the FTIR spectrum of L-PUU50. Absorption bands at 3345 cm^{-1} and 1702 cm^{-1} are observed due to bonded N-H, and bonded urethane carbonyl respectively. However, the latter is broadened due to merging of bonded urea carbonyl absorption at 1645 cm^{-1}. A tiny absorption peak at 1608 cm^{-1} for aromatic C-C stretching is also seen. The latter two peaks can be seen more clearly in **Figure 4.14(B)** which shows the expanded carbonyl region. Thus the FTIR spectrum indicates the presence of urea, thereby indicating that the reaction between diisocyanate and m-phenylene diamine chain extender has indeed occurred. The other peaks are identical to those seen in **Figure 4.12**.
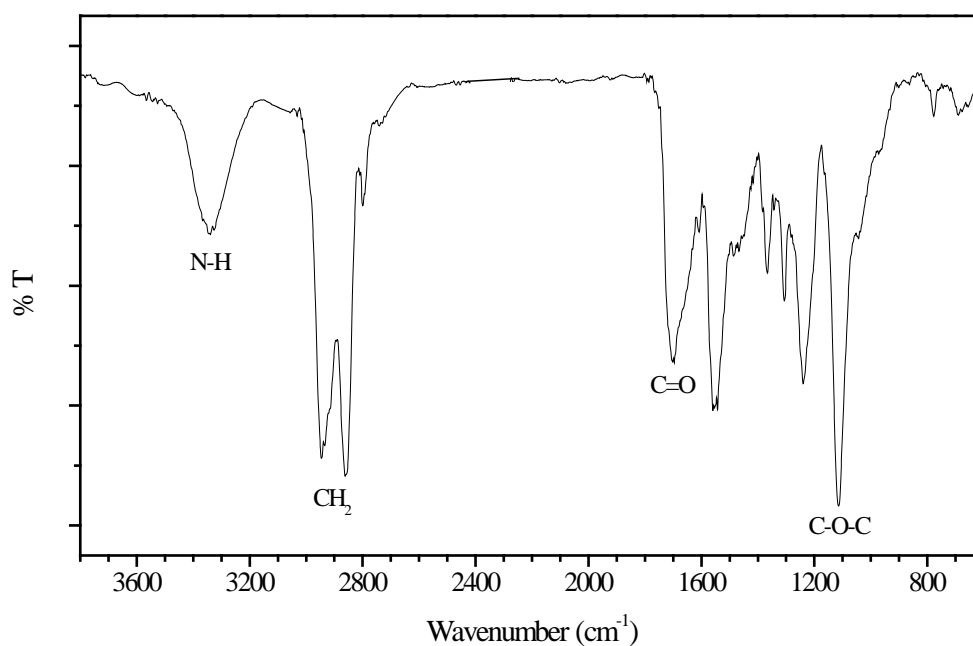
Figure 4.14(A) FTIR spectrum of L-PUU50 solution cast film.
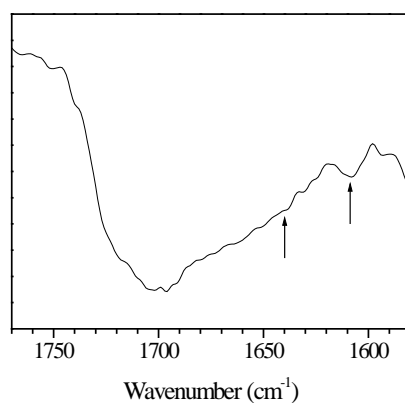
Figure 4.14(B) FTIR spectrum of L-PUU50 showing carbonyl region.

The polymer L-PUU100 was insoluble in common solvents, and thus could not be characterized for FTIR. The insolubility was likely due to its high urea content.

4.2.2 B12-PUU Series

The FTIR spectrum of B12-PUU10 can be seen in **Figure 4.15**. Most of the peaks seen here are similar to those seen in **Figure 4.13** and have identical assignments. Peaks corresponding to hydrogen bonded hard segments include N-H at 3333 cm^{-1}, urethane C=O at 1702 cm^{-1}, C-N stretching and N-H bending (amide II) at 1536 cm^{-1}, and C-N stretching and N-H bending (amide III) at 1244 cm^{-1}. Peaks corresponding primarily to soft segments include CH$_2$ stretching (2939, 2859 cm^{-1}), CH$_2$ wagging (1366 cm^{-1}), and C-O-C stretching (1113 cm^{-1}).Signals that could be attributed to the presence of urea linkages are not very obvious from the spectrum.
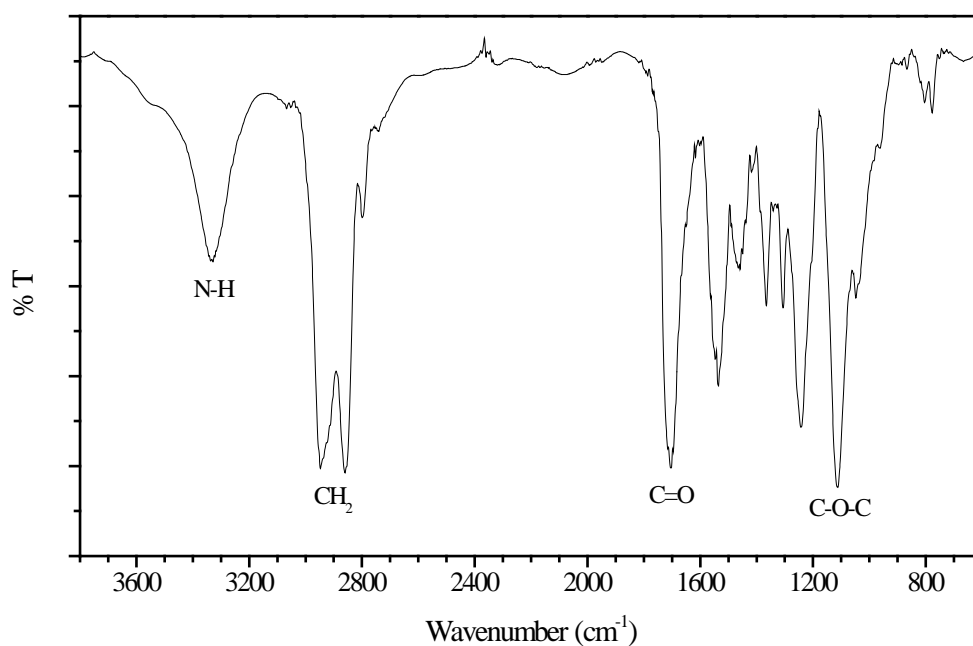
Figure 4.15 FTIR spectrum of B12-PUU10 solution cast film.

Figure 4.16(A) shows FTIR spectrum of a B12-PUU50 solution cast film. The spectrum features a broader absorption band at 3345 cm^{-1} due to bonded N-H, and a broad C=O band due to merging of bonded urethane carbonyl at 1718 cm^{-1} and urea carbonyl at 1638 cm^{-1}. The expanded carbonyl region of this spectrum showing these two peaks is presented in **Figure 4.13(B)**. This provides evidence for the reaction of n-dodecyl 3,5-diaminobenzoate with isocyanate. A small absorption peak of aromatic

C-C stretching at 1608 cm^{-1} is also noticeable. Broad absorption signals can also be seen for C-N stretching and N-H bending (1547, 1236 cm^{-1}) modes due to different environments. Absorption signals corresponding to soft segment are also noticed in the spectrum.
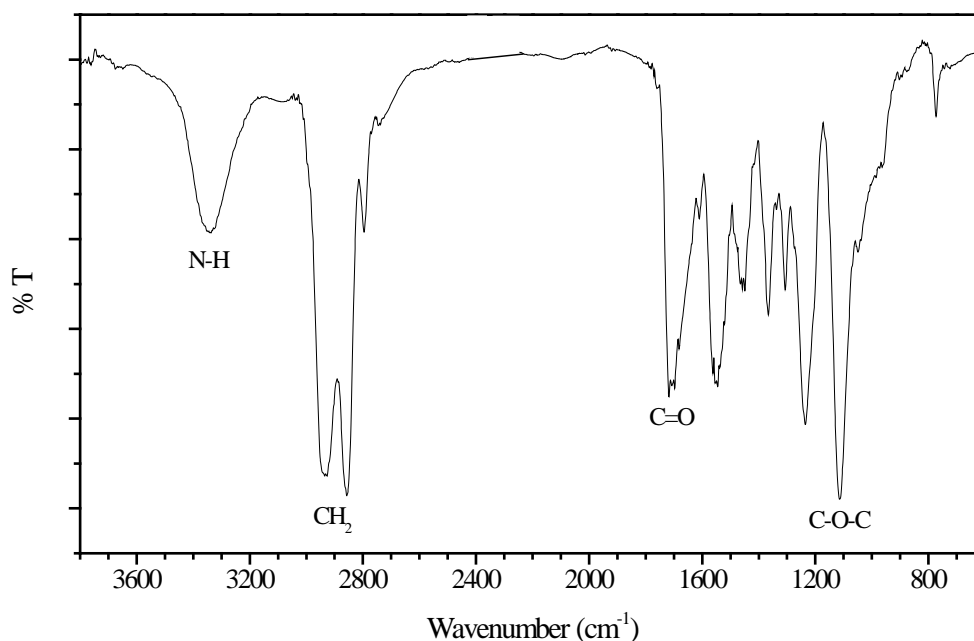
Figure 4.16(A) FTIR spectrum of B12-PUU50 solution cast film.
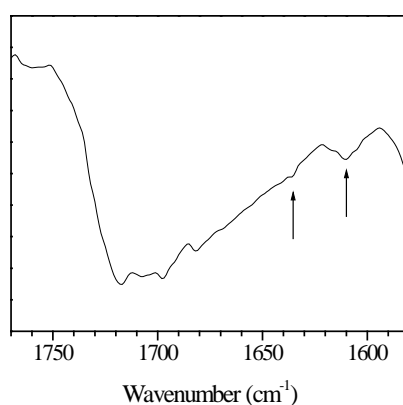
Figure 4.16(B) FTIR spectrum of B12-PUU50 showing carbonyl region.

The FTIR spectrum for B12-PUU70 is given in **Figure 4.17.** A broad absorption band at 3354 cm^{-1} indicates less ordered, weak N-H hydrogen bonding. A

bimodular feature is seen for the carbonyl absorption region with peaks at 1717 cm^{-1} for urethane C=O, and 1646 cm^{-1} due to urea C=O absorption. Comparison of this spectrum with that of B12-PUU10 and B12-PUU50 indicates that the absorption band due to urea linkage becomes increasingly visible with increase in the content of n-dodecyl 3,5-diaminobenzoate. A broader C-N stretching and N-H bending modes are observed at 1558 cm^{-1} (amide II), 1239 cm^{-1} (amide III).

Figure 4.18 shows FTIR spectrum of B12-PUU100. A small, broad band at 3354 cm^{-1} due to bonded N-H is indicative of a weak hydrogen bonding associated with poor structural order. This is also reflected in a weak absorption signal for bonded urethane C=O (1716 cm^{-1}). A relatively stronger signal for bonded urea C=O absorption at 1635 cm^{-1} is due to the presence of higher number of bonded urea carbonyls.
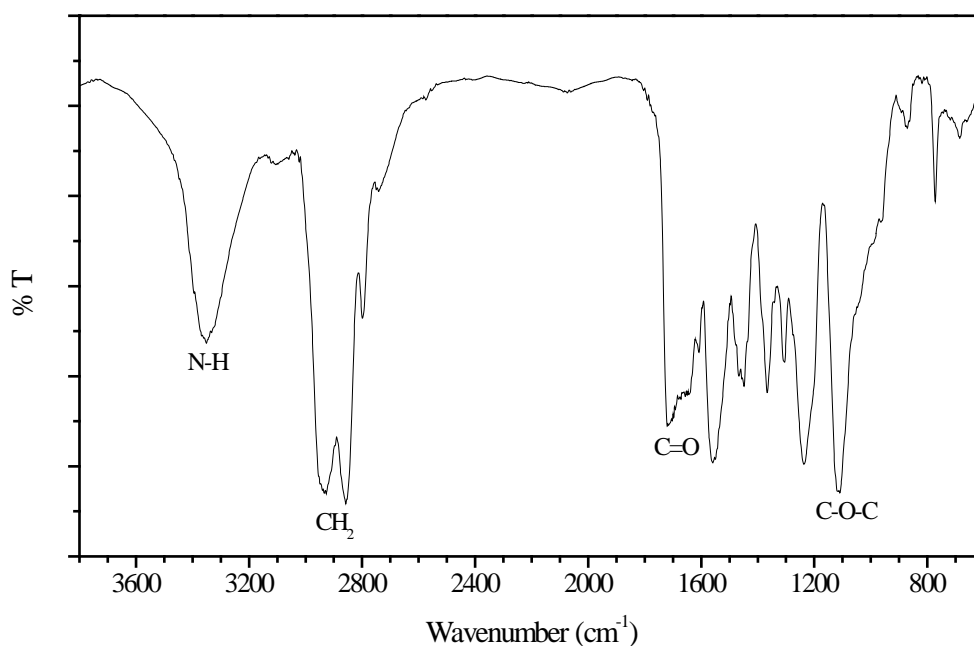
Figure 4.17 FTIR spectrum of B12-PUU70 solution cast film.
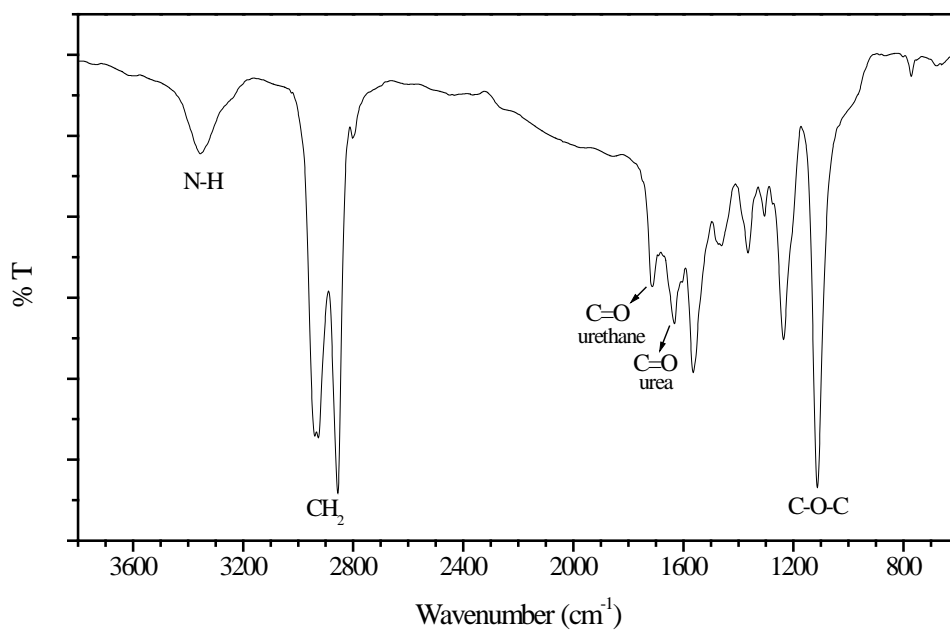
Figure 4.18 FTIR spectrum of B12-PUU100 solution cast film.

4.2.3 B22-PUU Series

The FTIR spectrum for B22-PUU10, as seen in **Figure 4.19,** shows peaks that are similar to those seen in **Figure 4.15** and have the same assignments.
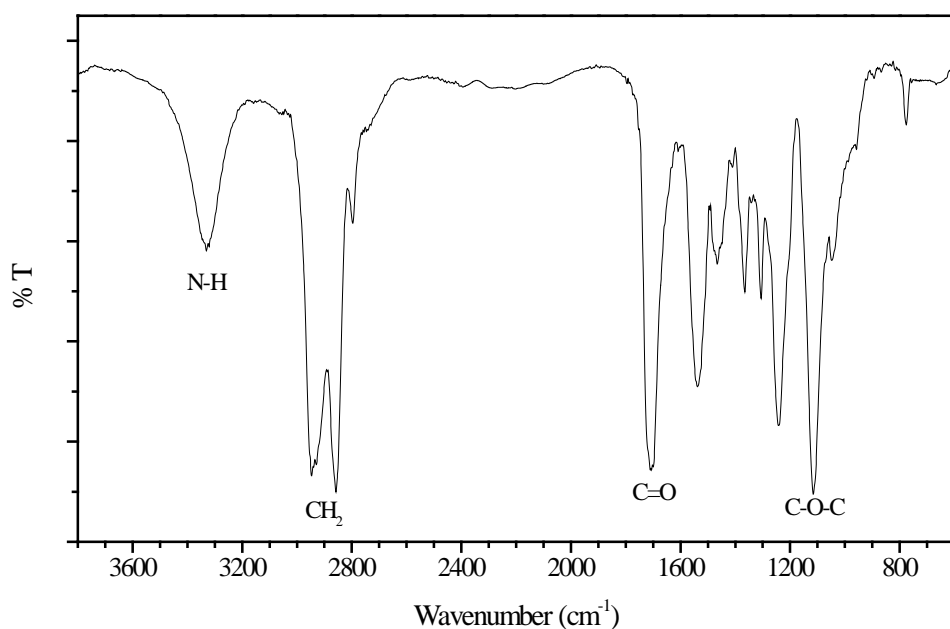
Figure 4.19 FTIR spectrum of B22-PUU10 solution cast film.

The FTIR spectrum of B22-PUU30 (**Figure 4.20)** shows less intense, and slightly broad peaks for bonded N-H absorption at 3344 cm^{-1}, and for bonded urethane carbonyl at 1704 cm^{-1}. A weak shoulder at 1640 cm^{-1}, corresponding to the bonded urea C=O absorption is also seen. This provides qualitative evidence for the reaction of n-docosyl 3,5-diaminobenzoate with isocyanate. Absorption bands due to C-N stretching and N-H bending as well as soft segment absorption peaks are observed as seen in the figure.
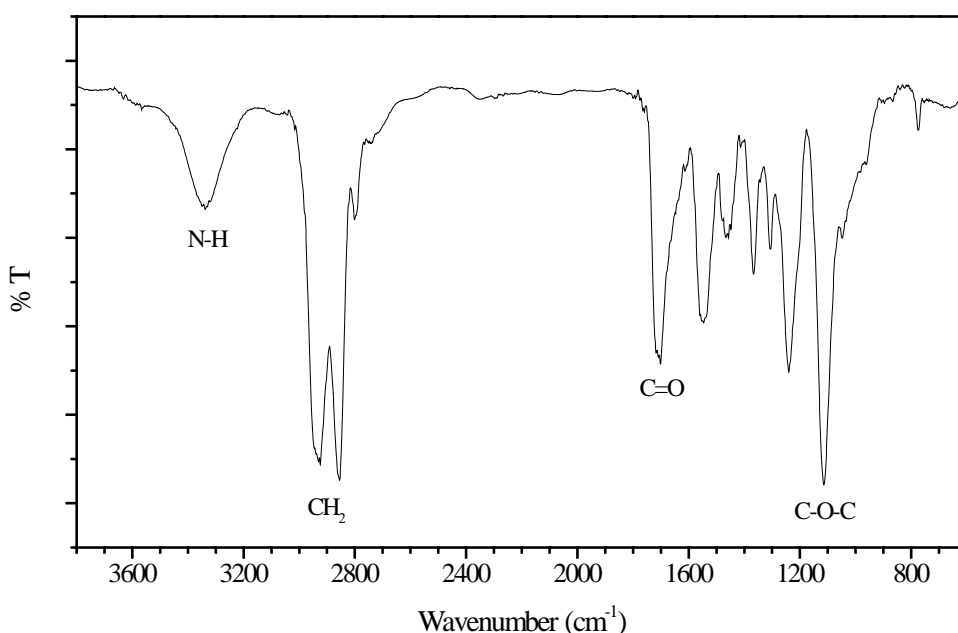
Figure 4.20 FTIR spectrum of B22-PUU30 solution cast film.

The FTIR spectrum of B22-PUU50 is shown in **Figure 4.21**. An absorption band due to bonded N-H in the hard segment was observed at 3358 cm^{-1}. Two peaks observed in the carbonyl region are due to bonded urethane carbonyl at 1711 cm^{-1} and bonded urea carbonyl at 1644 cm^{-1}. The absorption due to C-N stretching and N-H bending (amide II) was seen at 1554 cm^{-1} and 1240 cm^{-1} (amide III). Absorption bands from soft segment were observed at expected wavenumbers.

The FTIR spectrum of B22-PUU100 is presented in **Figure 4.22**. Spectrum features hard segment absorption bands at 3358 cm^{-1} due to bonded N-H, two bonds in the carbonyl region at 1706, 1633 cm^{-1} arising respectively from bonded urethane C=O and bonded urea C=O in the ordered region. Spectrum also shows C-N stretching and N-H bending amide II (1561 cm^{-1}) and amide III (1239 cm^{-1}) absorption bands along with bands from soft segment at expected wavenumbers.
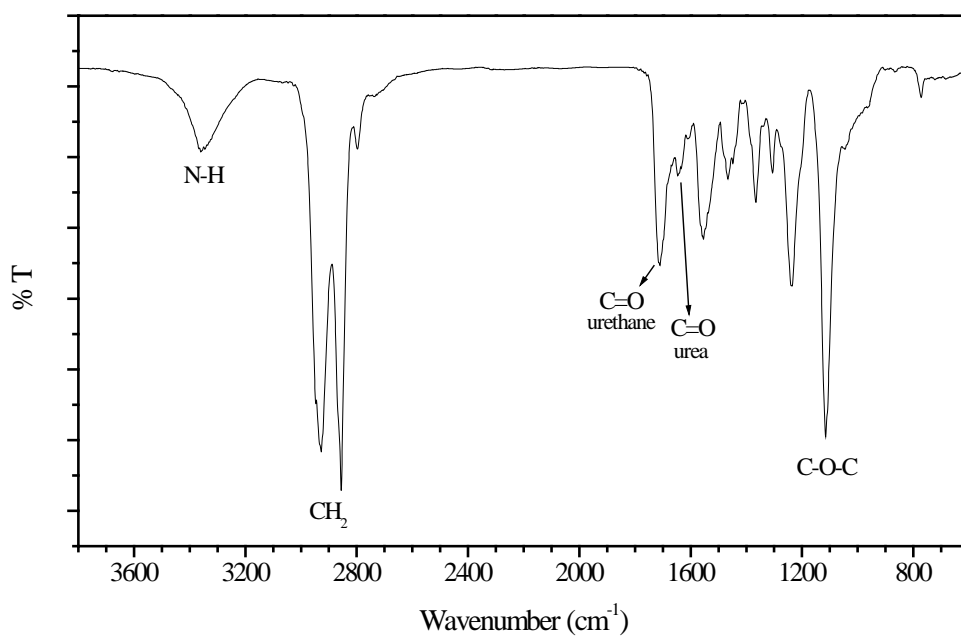
Figure 4.21 FTIR spectrum of B22-PUU50 solution cast film.
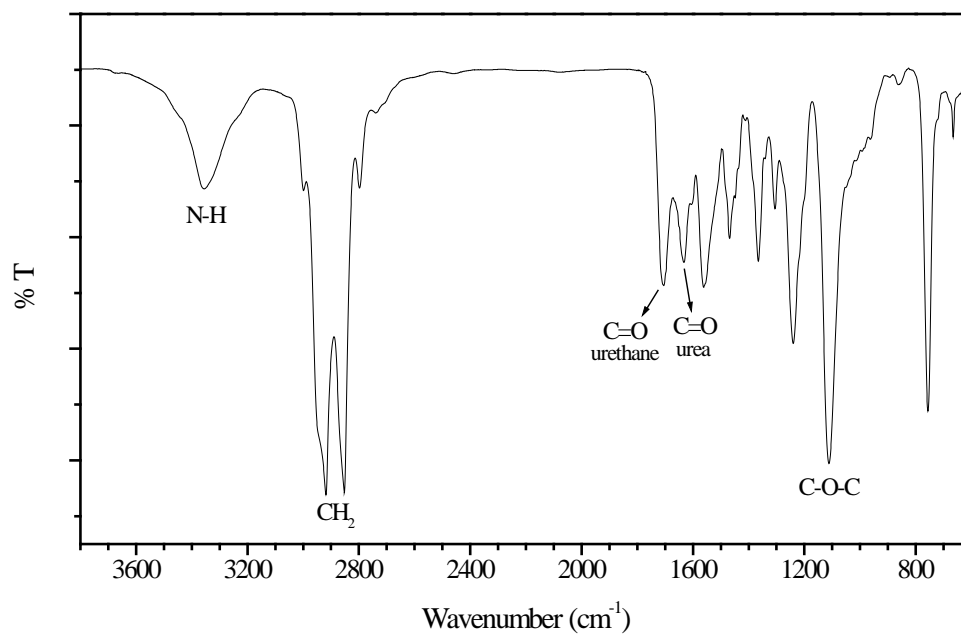
Figure 4.22 FTIR spectrum of B22-PUU100 solution cast film.

4.3   Gel Permeation Chromatography (GPC)

Molecular weight distributions of the polymers were measured using a Thermoqest GPC equipped with an ultraviolet (UV) and a refractive index (RI) detector. Tetrahydrofuran (HPLC grade) filtered through 0.5 mm Teflon filter served as the mobile phase. Polymer samples were dissolved in the mobile phase to prepare solutions of known concentrations (approx. 2 mg/ml). The same were filtered through 0.2 mm PTFE disposable filters. Elution was done through a stainless steel mix bed column (from PSS) packed with Styragel having 5µm particle size and Å100 porosity. The flow rate of the mobile phase was maintained at 1mL/min and the operating temperature was 30°C. A series of narrow molecular weight distribution polystyrene standards (Polymer Laboratory) were employed to generate the universal calibration curve and molecular weight estimation was done using RI detector signal. All molecular weights reported here are in terms of polystyrene standards.

The measured average molecular weights and polydispersity index (PI) of all polymers used in this work are provided in **Table 4.2**. Weight average molecular weights of the polymers varied from ca. 23000 – 74000 g/mol with PI index within 2.0. In case of polyurethanes it is difficult to control molecular weight, and no attempt was made to do so. Instead, polymerization temperature and time were kept constant for all samples synthesized in this study.

Figure 4.3(a-d) shows representative GPC elugrams for L-PU, L-PUU10, B12-PUU10 and B22-PUU10 samples respectively.

(a)

(b)

(c)

(d)
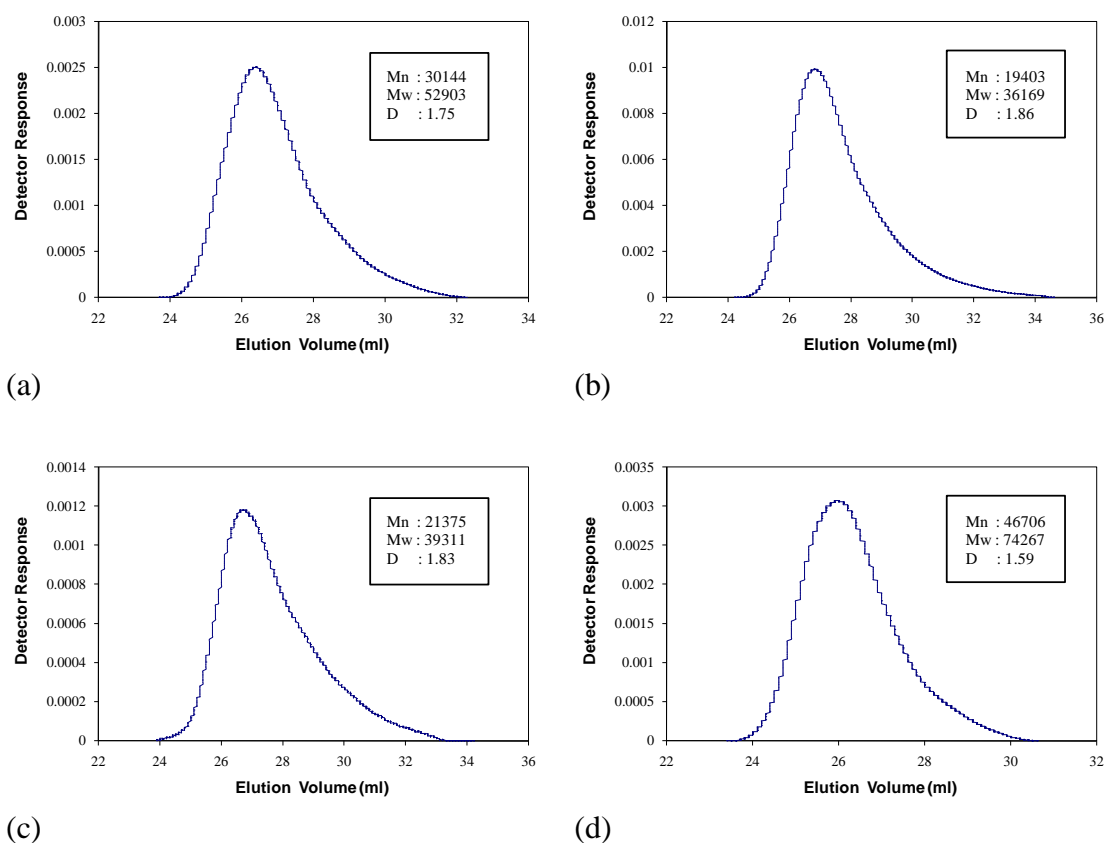
Figure 4.23 Representative GPC elugrams (a): L-PU, (b): L-PUU10, (c): B12-PUU10 and (d): B22-PUU10.

Table 4.2 Details of polymers synthesized in this work.

Polymer	Hard Segment wt. %	Diamine		Molecular Weight		
		wt. %	mol %	M_n (g/mol)	M_w (g/mol)	D
L-PU	51.17	-	-	30144	52903	1.75
L-PUU10	49.95	1.52	4.34	19403	36169	1.86
L-PUU50	50.46	7.56	21.74	11379	23206	2.03
L-PUU100	51.08	14.93	43.48	*	*	*
B12-PUU10	53	5.64	4.75	21375	39311	1.83
B12-PUU50	49.88	16.77	21.03	23596	45359	1.92
B12-PUU70	52.3	22.49	29.51	15911	26521	1.66
B12-PUU100	51.52	27.57	41.02	18745	26741	1.42
B22-PUU10	50.78	5.89	4.25	46706	74267	1.59
B22-PUU30	49.72	14.5	12.55	24268	39444	1.62
B22-PUU50	51.08	21.33	20.64	37026	64050	1.72
B22-PUU100	50.24	30.67	38.80	19641	29853	1.52

* Sample insoluble in solvent used for GPC.

4.4 Estimation of Diamine from ^{1}H-NMR(500)

For the quantification of diamine that was actually incorporated in the branched PUUs, polymer samples of B12 and B22 series were analyzed by ^{1}H-NMR using a Bruker AV500 spectrometer operating at a frequency 500 MHz. Samples were dissolved in an equivalent solvent mixture of $CDCl_3$ and DMSO-d_6, with 1 % (v/v) TMS as internal standard. Peaks were referenced to the TMS peak ($\delta = 0$ ppm). These spectra will be referred to as the ^{1}H-NMR(500) spectra.

Figure 4.24 shows ^{1}H-NMR(500) spectrum of N-Docosyl 3,5-Diaminobenzoate in the mixed solvent. Assignment of important peaks in the spectrum is shown in the adjoining structure. The peaks at 6.13 and 6.61 δ ppm corresponding to the aromatic protons of the diamine are of relevance to the present discussion. **Figure 4.25** illustrates an example of a ^{1}H-NMR spectrum of B22-PUU30 used for the estimation of diamine. Assignment of important peaks observed in the spectrum is shown in the adjoining structure. A slight shift in the peak positions for some peaks is seen the spectrum compared to that seen in **Figure 4.9**. This is

primarily due to the effect of mixed solvents used in this case. The spectrum features a surprisingly large number of peaks in the aromatic region (from 6.0 to 7.7 δ ppm) corresponding to the aromatic protons *para* and *ortho* to the ester linkage of the diamine. These peaks are collectively labeled as 'k' in the spectrum. A plausible explanation for this is the presence of many different environments for these protons. Polydispersity in the length of the hard segment where diamine is incorporated could also be a factor influencing this. The aromatic protons of the diamine appearing at 6.13 and 6.61 δ ppm in **Figure 4.24** are expected to shift downfield upon formation of urea linkage in the polymerization reaction. The absence these two peaks in **Figure 4.25** indicates that there is no free diamine in the polymer to at least within the NMR500 detection limit. Further, the downfield shift for the aromatic protons is a validation of the reaction of diamine with diisocyanate. All B12 and B22 PUUs showed the same trend except B12-PUU100 and B22-PUU100. For these two polymers a small amount of amine protons at their unshifted positions (6.13 and 6.61 δ ppm) were also observed indicating that perhaps not all the amine was reacted.

In order to estimate the amount of diamine incorporated in the polymers we first assume that the absence of unshifted amine protons indicates that there is no free diamine left behind in the polymer. Secondly, we have used the methylene protons α-to ester oxygen in the aliphatic chain (at δ 4.21 ppm) for the estimation of diamine in the polymer. We did not use the amine protons themselves for the purpose of estimation because despite using a 500 MHz machine and collecting a large number of scans, the amine protons unfortunately showed poor signal quality.
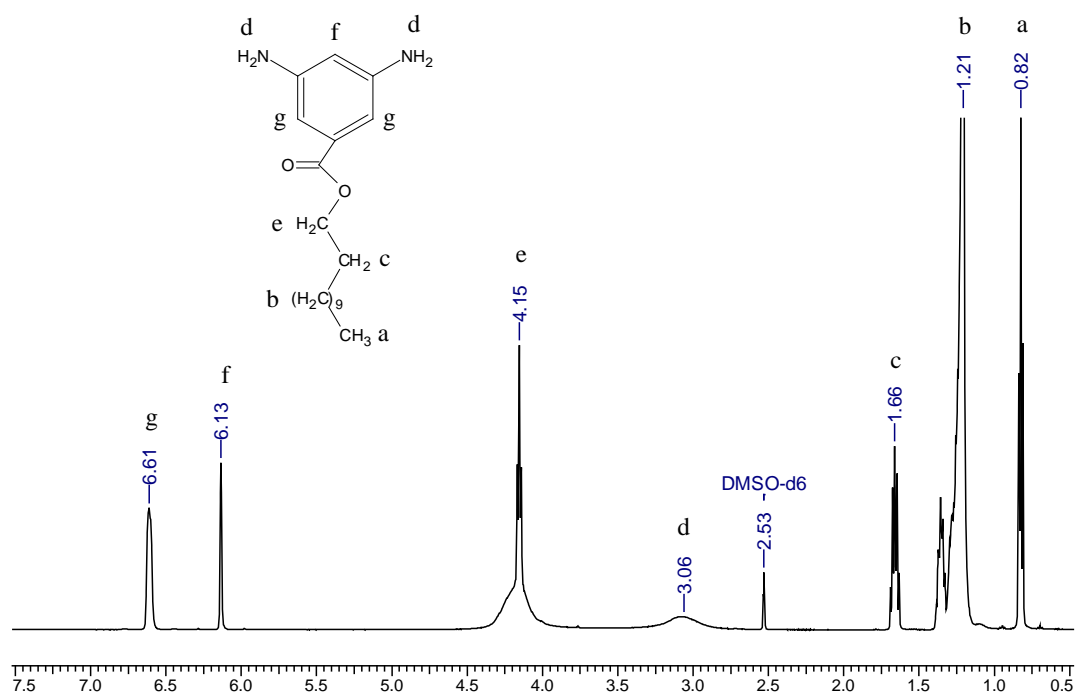
Figure 4.24 ^{1}H-NMR spectrum of n-dodecyl 3,5-diaminobenzoate.
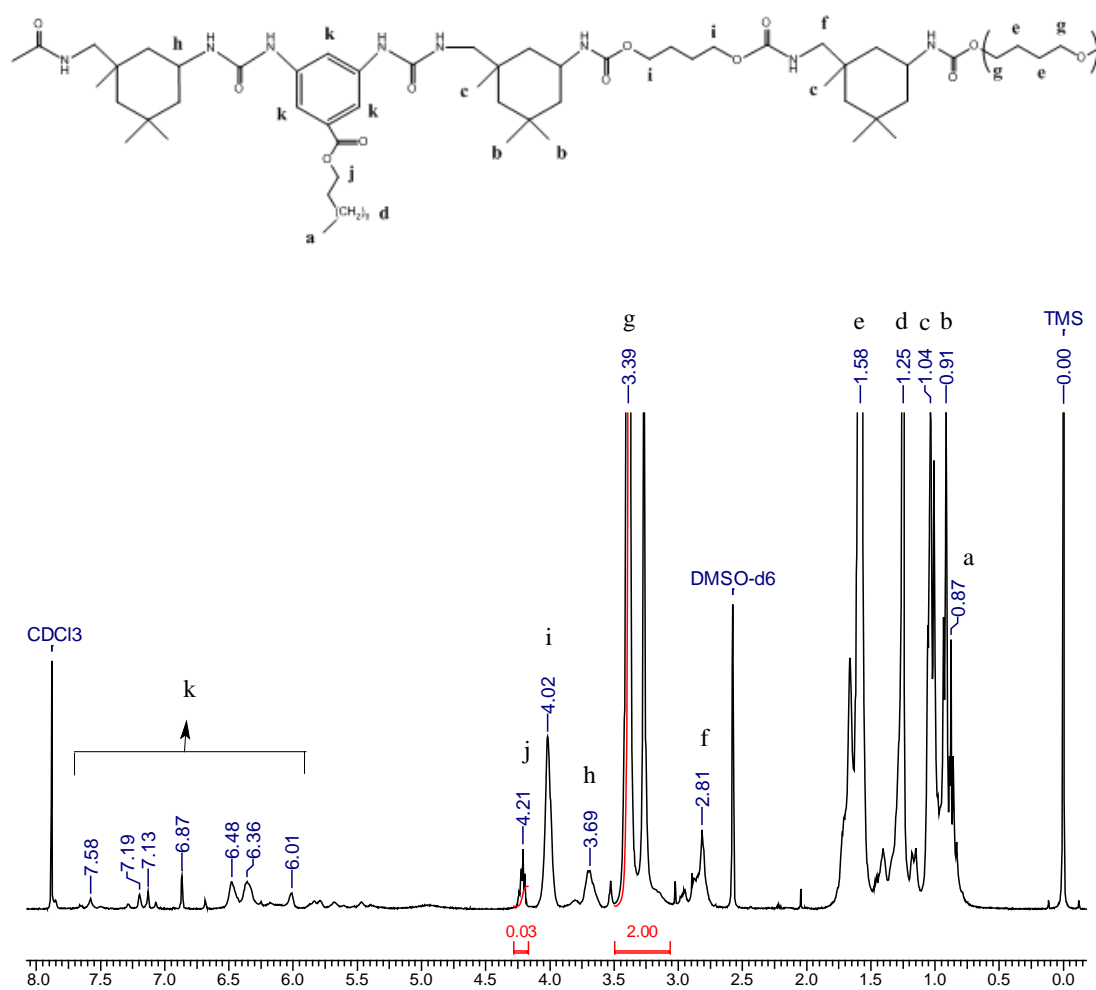
Figure 4.25 ^{1}H-NMR spectrum of B22-PUU30.

Estimation was done by comparing theoretical or feed ratio, and observed ratio of amine:PTMO protons as per calculations given below. Integration of PTMO signal from methylene protons β- or α- to ether oxygen atom (at δ 1.58 ppm or 3.39 ppm), and integration of amine signal from methylene protons α- to ester oxygen in the aliphatic chain (at δ 4.21 ppm) were used for estimation of proton ratio.

Mol. wt. of PTMO = 3000 gm mol

PTMO repeat unit mol. wt. = 72 gm mol

Mol. wt. of B12 diamine = 320 gm mol

Mol. wt. of B22 diamine = 460 gm mol

$$\text{moles of PTMO repeat unit} = \frac{\text{wt. of PTMO in gm}}{\text{mol. wt. of PTMO repeat unit}} \qquad (4.1)$$

$$\text{moles of amine repeat unit} = \frac{\text{wt. of amine in gm}}{\text{mol. wt. of amine repeat unit}} \qquad (4.2)$$

Thus we have,

$$\frac{4 \times \text{moles of PTMO repeat unit}}{2 \times \text{moles of amine repeat unit}} = \frac{\text{integration of PTMO methylene protons } \beta \text{ - to ether oxygen}}{\text{integration of methylene protons of amine } \alpha \text{ - to ester oxygen}}$$

$$(4.3)$$

Where, the numbers '4' and '2' come from the number of methylene protons of PTMO (α- or β- to ether oxygen) and diamine chain extender (α- to ester oxygen atom), whose signals were used for the estimation.

Rearranging equation (4.3),

$$\frac{\text{moles of amine repeat unit}}{\text{moles of PTMO repeat unit}} = \frac{4}{2} \times \frac{\text{integration of methylene protons of amine } \alpha \text{ - to ester oxygen}}{\text{integration of PTMO methylene protons } \beta \text{ - to ether oxygen}}$$
$$(4.4)$$

Equation (4.4) gives the ratio of amine to PTMO as calculated from the ^{1}H-NMR(500) spectrum. The feed ratio of amine to PTMO was calculated from the actual moles of the two reactants used for the synthesis of the respective polymers (see **Table 4.2**).

Table 4.3 shows comparison between the feed ratio (theoretical) and the estimated amine:PTMO ratio calculated using the above procedure. The table also shows % incorporation determined as 100 x (estimated amine:PTMO ratio divided by the theoretical ratio). The calculations show a progressive increase in the estimated amine content with increasing feed ratio for both B12 and B22-PUU series. The calculated diamine content was found to be lower than the theoretical values. This difference may be attributed either to the incomplete reaction of diamine and

diisocyanate followed by removal of the unreacted diamine during purification of the polymer or to the limits of the NMR technique used for the determination of diamine content in the polymer.

Table 4.3 Estimated diamine from ^{1}H-NMR.

Polymer	Feed Ratio Amine / PTMO	Observed Ratio Amine / PTMO	Incorporation %
B12-PUU10	0.0228	0.01	44
B12-PUU50	0.0753	0.05	66
B12-PUU70	0.1061	0.07	66
B12-PUU100	0.128	0.11	86
B22-PUU10	0.0187	0.01	53
B22-PUU30	0.0454	0.03	66
B22-PUU50	0.0683	0.05	73
B22-PUU100	0.0966	0.06	62

4.5   Summary

In summary this chapter described

- Proton NMR and FTIR evidence of the formation of L-PU and three series of PUUs namely L-PUU, B12-PUU and B22-PUUs.

- Polymer molecular weights by gel permeation chromatography.

- Estimation of diamine chain extender from proton NMR.

References:

(1)   Mattia, J.; Painter, P. C. *Macromolecules* **2007**, 40, 1546.

(2)   Yilgor, E.; Burgaz, E.; Yurtsever, E.; Yilgor, I. *Polymer* **2000**, 41, 849.

Morphological Characterization of Polyurethane-ureas

Chapter - 5

5.1 Fourier Transform Infrared Spectroscopy

FTIR experiments were conducted on a Perkin Elmer Spectrum GX spectrometer.

Polymer samples were scanned by drop casting a thin film from dilute chloroform solution onto a piece of silicon wafer. Films were then dried under vacuum for about 1 h and under IR lamp for about 20 min to remove all traces of solvent before scanning. The FTIR spectrum of silicon wafer was collected and subtracted as background from all sample spectra. Twenty five scans were signal averaged at a resolution of 4 cm^{-1} before Fourier transformation. High temperature experiments were carried out by inserting the silicon wafer in a Mettler FP 90 hot stage having a temperature accuracy of $\pm$ 0.1°C. Scans were recorded at 10°C intervals starting from 30°C. Between two consecutive readings the temperature was ramped up at a rate of 5°C/min. Sample was allowed to equilibrate for two minutes after each temperature rise before the FTIR spectra were recorded. The temperature protocol is shown in **Figure 5.1**.
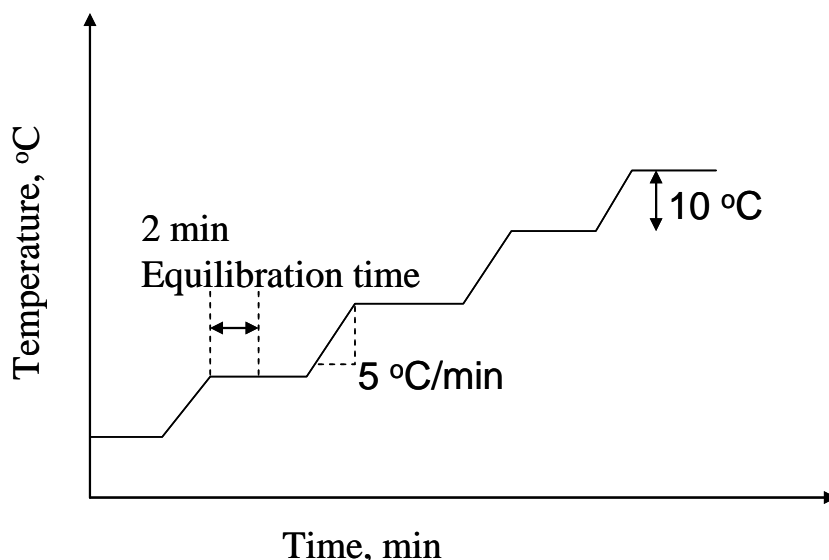
Figure 5.1 Experimental protocol followed for high temperature FTIR experiments.

A brief account on the nature of hydrogen bonding and importance of FTIR in probing hydrogen bonding in polyurethanes was given in Chapter 1 (section 1.5). The two IR sensitive modes N-H and C=O can be utilized to derive essential information

on hydrogen bonding. In both polyurethane and polyurethane-urea the N-H group acts as a proton donor and the C=O group acts as a proton acceptor. A urethane linkage thus has one donor and one acceptor, while a urea linkage has two donors and one acceptor. These groups primarily hydrogen bond with each other forming hard segment domains. In spite of their structural similarity, differences in electron delocalization in the urea and urethane linkages lead to differences in the frequency at which their carbonyl groups absorb in the IR region. The stretching mode of urea carbonyl appears at a lower frequency (free carbonyl = 1691 cm^{-1}) compared to the urethane carbonyl (free carbonyl = 1730 cm^{-1}) due to greater electron delocalization in the π- bonds in the former. In general for PUUs the interpretation of carbonyl region in the FTIR spectra is complicated because of closely located carbonyl absorption modes in urea and urethane linkages and also because of the presence of both urea and urethane groups in the same polymer. In comparison, the N-H stretching modes are not much influenced by the delocalization of electrons making interpretation less difficult. For this reason we have primarily used N-H absorption to understand the hard segment hydrogen bonding. Corresponding changes in the carbonyl absorption have also been detected and will be mentioned briefly.

Before moving to the data analysis let us review important peak positions in the polyurethane FTIR spectrum. Chapter 4, Table 4.1 lists important absorption bands that are observed in polyurethanes and polyurethane-ureas. As hydrogen bonding alters the distribution of electrons, hydrogen bonded groups absorb at lower frequency than the non-bonded groups. Here we use FTIR assignments reported in the literature for the analysis of our data. Painter and coworkers[1-3] and Yilgor and coworkers[4-7] have done extensive studies on the FTIR characterization of model compounds, polyurethanes, polyurethane-ureas, and have assigned C=O and N-H stretching modes in different environments. However, it should be kept in mind that the differences in structural factors (difference in chemistry), and environmental factors (difference in the degree of order) could give rise to minor deviations in the observed absorption frequencies.

Here, we will briefly review important peak assignments required for data analysis. Hydrogen bonded urea N-H groups in 'ordered' environment absorb from 3340-3320 cm^{-1}, while those from 'disordered' environment absorb at about 3340 cm^{-1}. The adjectives disordered and ordered refer respectively to the regions of sample

that are primarily amorphous, and the regions that have some degree of regularity. Similarly, urethane C=O in the ordered region absorb at around 1711 cm^{-1}, whereas C=O absorption at about 1722 cm^{-1} corresponds to the disordered state. Similar assignments for carbonyl region of polyurea are: ordered C=O absorption at about 1630 cm^{-1} and disordered C=O absorption at about 1650 – 1665 cm^{-1}. Thus, absorption wavenumbers serve as an indicator of the strength as well as order of hydrogen bonding.

5.1.1 L-PUU Series

With the help of FTIR we intend to examine qualitatively the effects of incorporation of branched moiety on the hard segment microstructure. **Figure 5.2** illustrates an example of L-PU showing changes in N-H and C=O absorption regions as a function of temperature. Peak positions were obtained by peak deconvolution using the PeakFit^{TM} software. **Figure 5.3** demonstrates an example of decovolution by using Gauss + Lorentz amplitude for N-H absorption band of L-PU at 30°C. The thick solid line in the upper panel displays actual FTIR data, while a thin line shows fit to the data. The lower panel displays result of deconvolution. An r^{2} value of 0.99 shows the accuracy of deconvolution. L-PU spectrum does not show any peak at about 2260 cm^{-1}, corresponding to the presence of free isocyanate groups.

The data in **Figure 5.2 (A)** shows N-H absorption in L-PU at around 3328 cm^{-1} at 30°C indicating an ordered hard segment environment. A shift in the main absorption peak frequency to higher wavenumbers with a concurrent broadening of the peak and reduction in the peak intensity was noted with increasing temperature. Deconvolution of the spectra showed that heating the sample resulted in a gradual appearance of a peak corresponding to the free N-H absorption (3340 cm^{-1}) accompanied with shift in the bonded N-H peak to higher wavenumbers. The temperature induced upward shift in wavenumber for the N-H peak suggests that the bonded N-H gradually changed from an ordered state at lower temperatures to a relatively more disordered state at higher temperatures. This implies a loss of hydrogen bonding strength / association with increase in temperature. However even at the highest temperature studied here the hydrogen bonding between hard segments was intact although increasingly disordered. A similar observation has already been reported in the literature.[8,9]
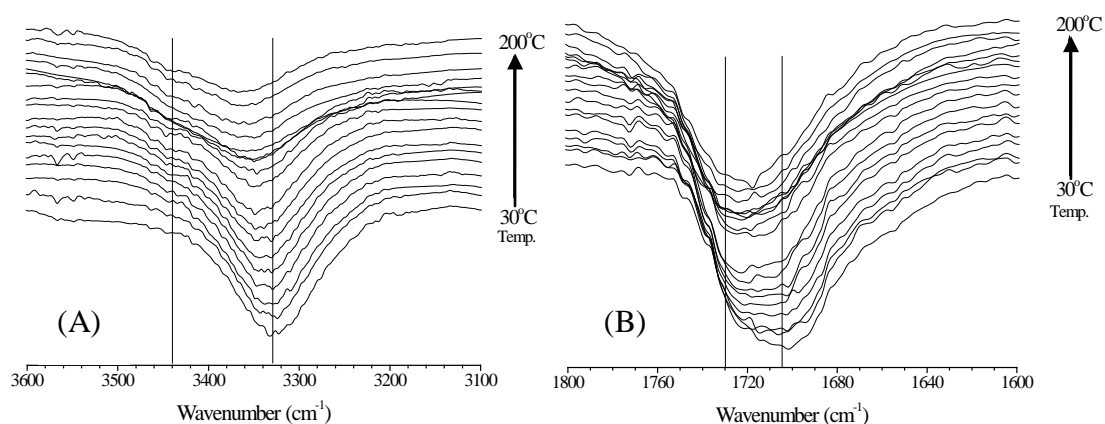
Figure 5.2 FTIR spectra of L-PU (A) N-H absorption region and (B) C=O absorption region with temperature interval of 10°C.
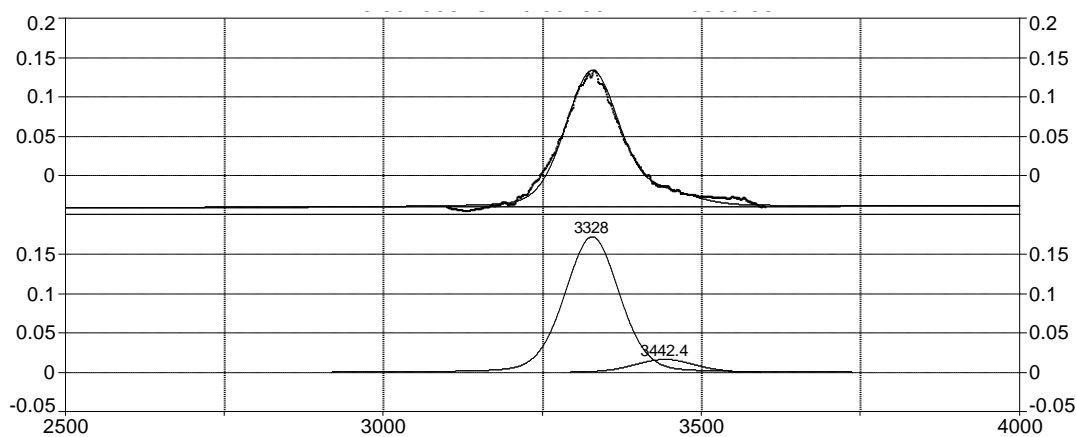
Figure 5.3 Example of Peak fitting for N-H absorption band of L-PU data at 30°C.

A strong carbonyl absorption band at 1705 cm^{-1} as seen in **Figure 5.2 (B)** also corresponds to the ordered hard segment environment. Increasing intensity of the shoulder at 1730 cm^{-1} at higher temperatures can be similarly attributed to the dissociation of bonded carbonyls. Thus changes in the N-H and C=O absorptions with temperature as observed in figures **(A)** and **(B)** are correlated. The shift to higher wavenumers with a simultaneous decrease in intensity at higher temperatures is again related to the decrease in the strength of the bond with increasing thermal motion. We confirmed that except small shifts in amide II (~1540 cm^{-1}) and amide III (~1240 cm^{-1}) absorption modes, other bands in the spectrum did not shift with increase in temperature, although some decrease in the strength of the signal was observed.

All L-PUUs studied here showed similar qualitative behaviour to that shown by L-PU. **Figure 5.4** shows the effect of temperature on the bonded N-H absorption

peak wavenumber for the L-PUU series. Shown here are data for L-PUU10 and L-PUU50 polymers. As mentioned in Chapter 3 the polymer L-PUU100 was insoluble in suitable solvents and hence could not be characterized. At 30°C the N-H absorption maximum for L-PU was observed at lower wavenumbers compared to the L-PUUs. This suggests the presence of a stronger and ordered hydrogen bonding in L-PU originating from better organization (or packing) of hard segments, when compared with L-PUUs. This might be due to the introduction of a defect (or kink) structure in the hard segments of L-PUUs in the form of the aromatic ring of *m-phenylenediamine* chain extender. Indeed for a given temperature, the N-H absorption peak of L-PUU50 containing higher amount of *m-phenylenediamine* chain extender was located at higher wavenumber compared to L-PU. For reasons not understood by us, the behavior of L-PUU10 from 100°C to 170°C was different as seen in **Figure 5.4**. This trend was reconfirmed by repeat scanning of a fresh sample.

5.1.2   B12-PUU and B22-PUU Series

Figure 5.5 shows N-H absorption vs. temperature for B12-PUUs plotted with L-PU. A shift in the peak absorption wavenumber along with declining peak intensity was also seen for B12-PUUs. The Figure shows a diminution of the strength of N-H hydrogen bonding with the incorporation of B12 diamine. For B12-PUU70 and B12-PUU100, the N-H absorption wavenumber indicates the formation of disordered hard segment domains even at the room temperature. This is better seen in **Figure 5.6** which shows N-H and C=O regions of B12-PUU100 at room temperature. An expanded view of the N-H absorption region (**Figure 5.6 (A)**) shows that the bonded N-H absorption is centered at 3354 cm^{-1} corresponding to disordered hard segments, and a shoulder at around 3240 cm^{-1} corresponding most likely to the N-H hydrogen bonded to ether oxygen in the soft segment. The carbonyl region (**Figure 5.5 (B)**) exhibited two broad peaks at 1713 and 1632 cm^{-1}, respectively from the disordered urethane C=O, and ordered urea carbonyl. Also seen in the figure, is a shoulder at 1655 cm^{-1} due to disordered urea carbonyl. As mentioned in Chapter 3, preferential reactivity of amine group with isocyanate could result in the formation of longer sequences or blocks of urea linkages (B12 diamine + IPDI). There is an increasing propensity of formation of such polyurea blocks in PUUs with higher B12 diamine concentration. We propose that such polyurea blocks organize to form ordered

domains, and the carbonyl groups of these urea linkages absorb at 1632 cm^{-1}. Support to this hypothesis came from the fact that the absorption at 1632 cm^{-1} was only seen for B12-PUU70 (as a small peak) and B12-PUU100 (as a well resolved peak).
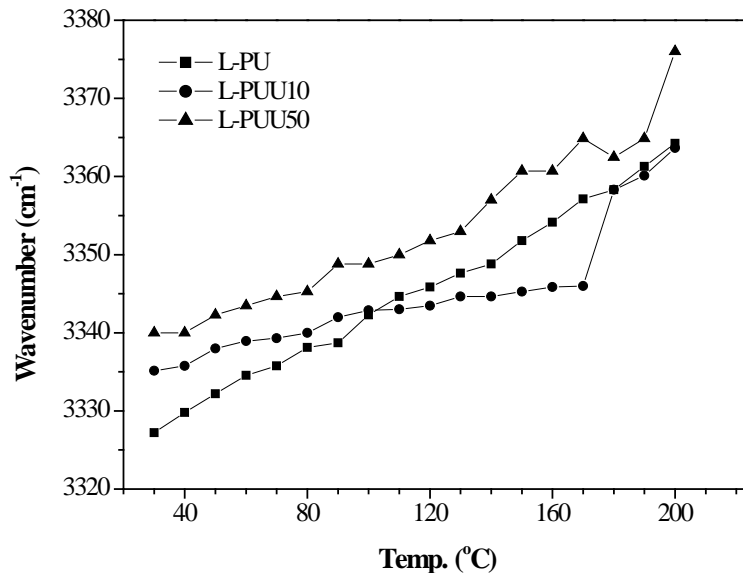
Figure 5.4 Comparison of FTIR N-H absorption peak wavenumber as a function of temperature for L-PUUs in comparison with L-PU.

Figure 5.5 exemplifies the role of defect moiety in hindering hard segment packing leading to more disordered hard segment domains. At any given temperature the bonded N-H absorption of B12-PUUs was found to be shifted to higher wavenumbers with increasing diamine incorporation. Thus the consequence of attaching a 12-carbon pendent chain on the aromatic ring of chain extender and incorporating the same in the polymer is that the ordered hard segment domains became increasingly disordered and the strength of hydrogen bonding decreased with increase in diamine content. Concurrent changes in the carbonyl region have also been observed for all samples.
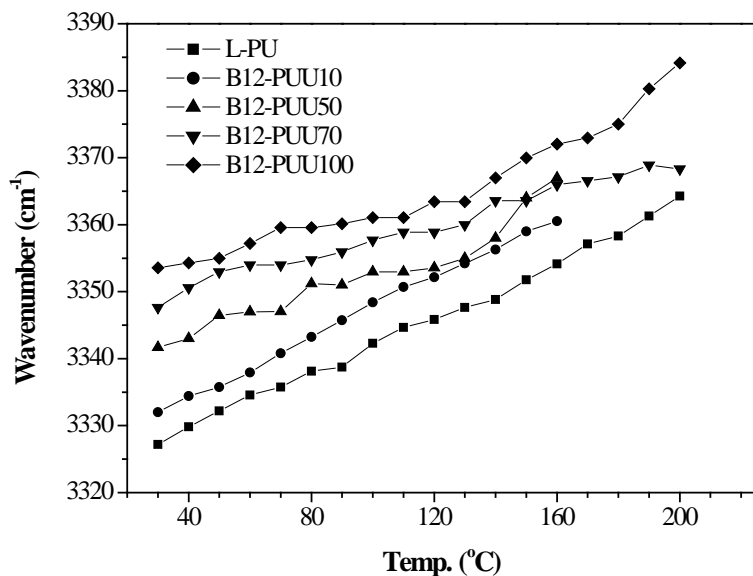
Figure 5.5 Comparison of FTIR N-H absorption peak wavenumber as a function of temperature for B12-PUUs in comparison with L-PU.
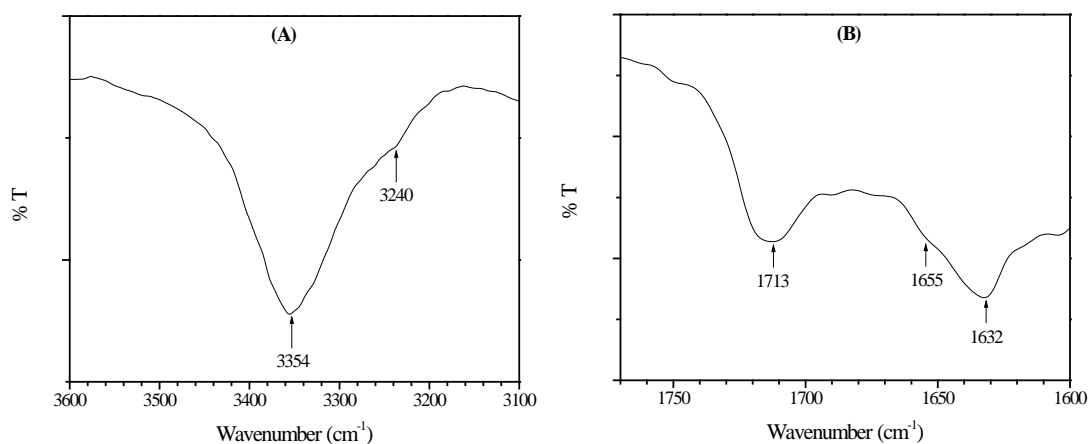
Figure 5.6 (A) N-H absorption and **(B)** carbonyl absorption of B12-PUU100 at 30°C.

Figure 5.7 shows a plot of N-H absorption wavenumber with increasing temperature for B22-PUUs. The Figure shows similar trends of decreased hydrogen bonding strength with higher amine incorporation, as seen for B12-PUUs. The observed peak wavenumbers indicate the formation of disordered hard segments even at 50% incorporation of B22 diamine. Further increase in diamine content to 100% (B22-PUU100) did not seem to change the observed peak wavenumbers. This is seen from the data for N-H and C=O absorption bands for B12-PUU100 at 30°C provided in **Figure 5.8**. As seen in **Figure 5.8(A)**, a broad peak due to bonded N-H is observed at 3356 cm⁻¹, which is very close to the corresponding absorption of B22-PUU50 at 30°C and results from disordered hard segments. The two shoulders, pointed by arrows, at 3443 and 3235 cm⁻¹ correspond respectively to the presence of free N-H,

and N-H hydrogen bonded to ether oxygen in the soft segment. This is indicative of the presence of phase mixed regions. The carbonyl absorption for this sample, as provided in **Figure 5.8(B)**, exhibits a broad peak centered at 1706 cm^{-1}, due to free urea C=O. The increased peak width is due to an overlapping absorption of urethane C=O in the disordered state at about 1720 cm^{-1}. Hydrogen bonded urea C=O absorption in the ordered state gives rise to a second peak at 1632 cm^{-1}. The latter is primarily due to the formation of polyurea blocks, as explained earlier. A shoulder, pointed by an arrow, at about 1645 cm^{-1} can be assigned to the disordered urea C=O absorption. The observation of free urea carbonyl is also indicative of the formation of mixed hard and soft phases at high B22 diamine content.
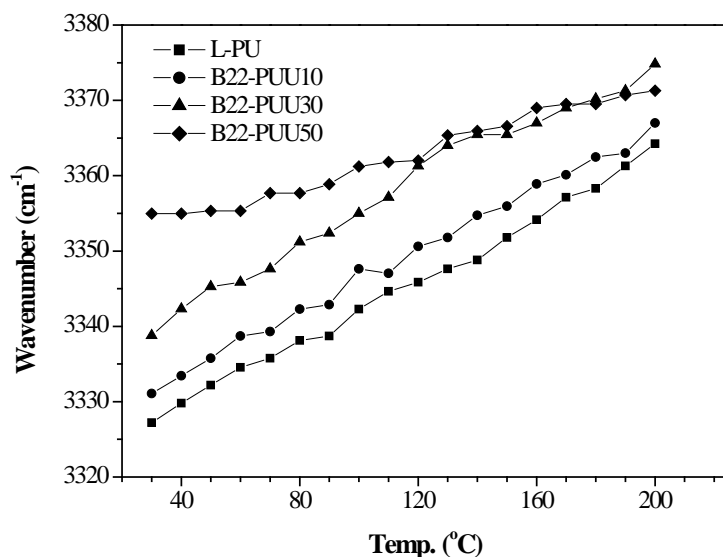
Figure 5.7 Comparison of FTIR N-H absorption peak wavenumber as a function of temperature for B22-PUUs in comparison with L-PU.
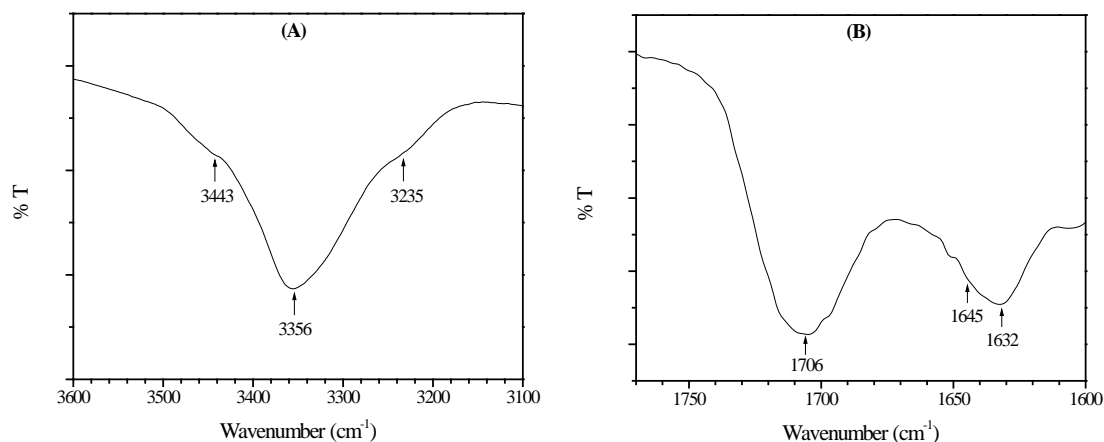
Figure 5.8 (A) N-H absorption and **(B)** carbonyl absorption of B22-PUU100 at 30°C.

Comparison of data in **Figure 5.5** and **Figure 5.7** shows a larger shift of N-H absorption maximum to higher wavenumber for the B22-PUUs compared to their B12 counterparts for a given diamine content and temperature. This reflects the effect of almost doubling the length of the pendent alkyl chain of diamine upon the strength and environment of hard segment hydrogen bonding. **Figure 5.9** shows such a comparison for B12-PUU50 and B22-PUU50. Also shown as reference is the L-PU control sample.
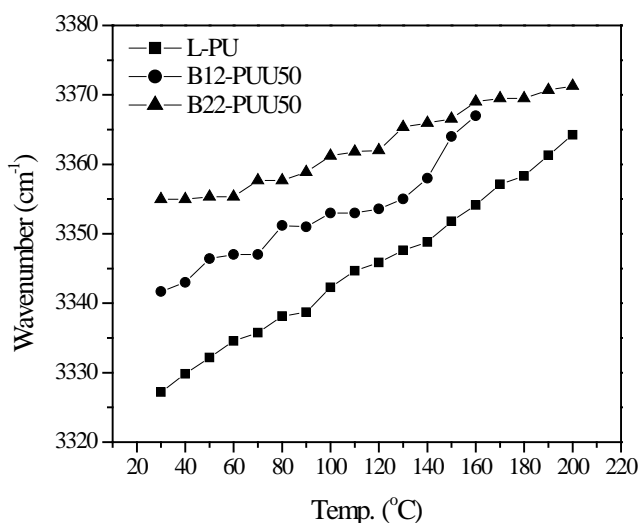
Figure 5.9 Comparison of FTIR N-H absorption peak wavenumber as a function of temperature for B12-PUU50, B22-PUU50 and L-PU.

5.2   Differential Scanning Calorimetry

The thermal response of all polymers in this work was measured using a TA-Q100 DSC instrument. The instrument was calibrated for energy and melting point using an indium metal standard sample. Polymer samples were cut from compression molded sheets. Compression molding was done at $100^{o}C$ and the sheet was allowed to cool to ambient temperature by water circulation in the mould cavity which took about 25 min. It will be shown later in the section describing the temperature response of small angle x-ray scattering from the polymers studied here that the microphase morphology of the polymers remained essentially unchanged till about $100^{o}C$. Thus it

is quite likely that during compression molding the microphase morphology as developed during the precipitation and sample drying process did not change significantly. Compression molded sheets were then stored at room temperature in a desiccator before thermal analysis. About 5 mg of sample was hermatically sealed in aluminum pan and scanned under nitrogen purge at a rate of 20°C/min. The protocol used was as follow. Samples were first cooled to -120°C, heated at a rate of 20°C/min up to 150°C (first heat scan), then cooled at a rate of 50°C/min, and then reheated again to150^{o}C at a heating rate of 20°C/min (second heat scan). The glass transition temperature was measured at the half width of the transition after plotting tangents on the curve, while melting temperature was recorded as the peak temperatures of observed endotherms.

Figure 5.10 displays the second heating DSC thermogram of neat PTMO (2900) polyol. The crystalline, waxy solid (at ambient temperature) exhibited a sharp melting endotherm at about 23°C. Its glass transition was not detectable since the sample crystallized rapidly during the quenching step in between the two heating scans so that the amorphous content in the polymer was very small.
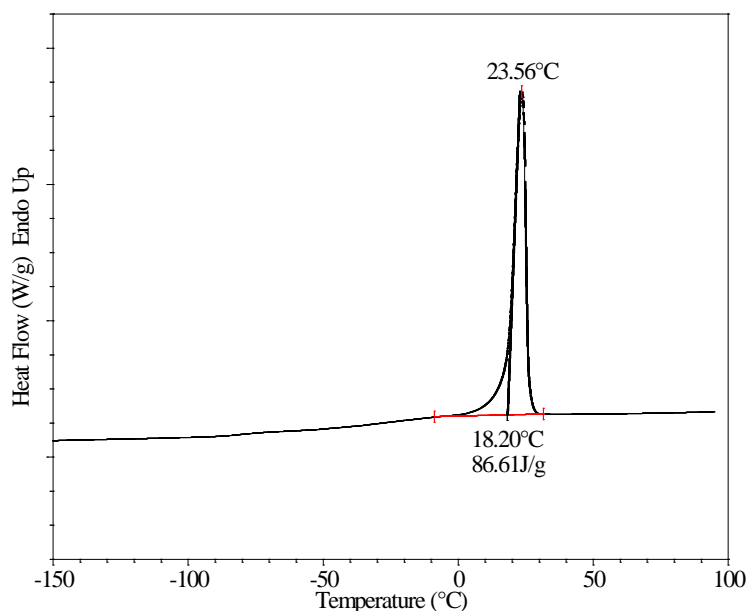
Figure 5.10 DSC thermogram of PTMO soft segment. Conditions: 20°C/min, second heat.

DSC studies on polyurethanes often report the presence of two T_gs, one associated with the amorphous soft phase, and the other with the hard phase. Stronger

segregation of segments can reduce the soft segment T_g, while segmental mixing is expected to lead to an increment in the soft segment T_g. In case of strong segmental mixing, one can expect the copolymer T_g to have a value that is in between the T_gs of the hard and soft segments. Velankar and Cooper have reported similar observations for polyester polyurethanes.[10]

One important feature related to the polyurethane hard segment glass transition deserves mention here. Unlike soft segment, the hard segment glass transition is usually poorly resolved in DSC. This is primarily due to following two reasons: I) The sequence length of the hard segment is often broadly distributed thereby resulting in a broad T_g. The chemistry involved in polyurethane synthesis is such that it is difficult to achieve a control on the hard segment polydispersity. One needs to employ special synthetic protocols to control hard segment length distribution. II) The change in heat capacity of polyurethane hard segments is often small, making them difficult to observe. For the polymers under study here, hard segment glass transitions were smeared out and were difficult to determine unambiguously.

5.2.1 Model Hard Segments

Before presenting DSC data for the polymers studied here, the thermograms of model hard segments are discussed below. **Figure 5.11** shows DSC second heat scan of model hard segment polyurethane recorded at a heating rate of 10°C/min. The T_g for this polymer was observed to be about 35°C. DSC traces of the model B-12 hard segment PUUs obtained at the same heating rate are plotted separately in **Figure 5.12**. The T_gs of the model B-12 hard segment PUUs were found to be substantially higher than that of the model hard segment polyurethane, and were found to increase with the increasing B12 amine content (see **Table 5.1**). Glass transition for model B12-hard segment polyurea was observed to be ca. 180°C. Note that the presence of C12 pendant branches in the polymer can have two effects: internal plasticization of the polymer and disruption of hydrogen bonding between hard segments. Both effects would tend to decrease the T_g of the polymer. Despite this the observed increase in T_gs of model hard segment PUUs relative to the urethane polymer underlines the overwhelming effect which the more strongly (bifurcate) hydrogen bonded urea

linkages have relative to urethane linkages on increasing the rigidity of the model hard segment polymers.
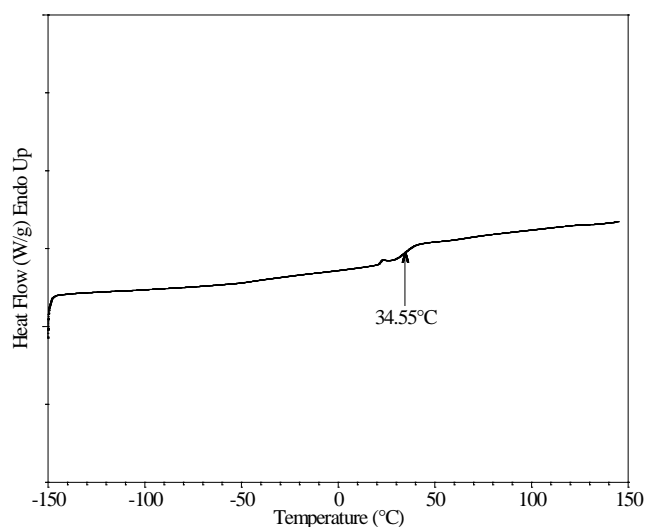
Figure 5.11 Second heating DSC thermogram of model hard segment polyurethane (IPDI + BDO) recorded at 10°C/min.
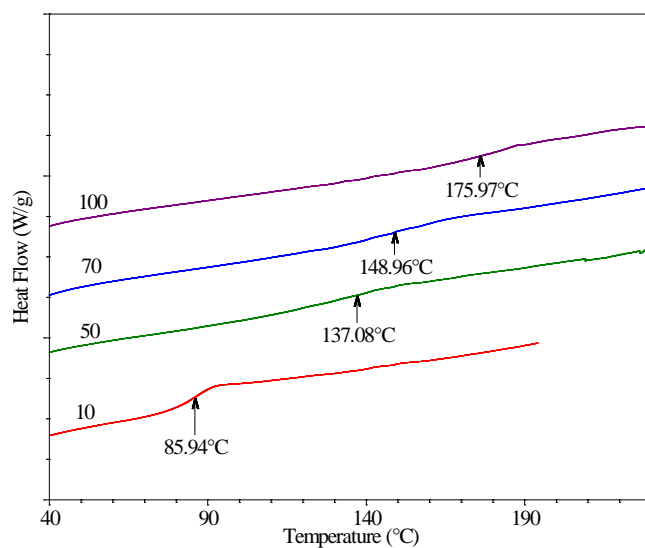
Figure 5.12 Second heating DSC thermogram of Model hard segment PUUs IPDI + BDO + DAB recorded at 10°C/min. Numbers on the curve correspond to the B12 diamine % in the copolymer. Endotherm up.

Table 5.1 Model Hard Segment Polymers.

Sr. No.	Model Polymers		T_g (°C)	Mass Density (g/cc)
	Isocyanate	Chain Extender		
1	IPDI	BDO	35	1.109
2	IPDI	BDO (90 mol%) + DAB (10 mol%)	86	1.137
3	IPDI	BDO (50 mol%) + DAB (50 mol%)	137	1.087
4	IPDI	BDO (30 mol%) + DAB (70 mol%)	149	1.037
5	IPDI	DAB	180	-

* IPDI – Isophorone diisocyanate

* BDO – 1,4-Butanediol

* DAB – N-Dodecyl 3,5-diaminobenzoate

5.2.2 L-PUU Series

The first heating thermograms of L-PU and L-PUU polymers are presented in **Figure 5.13**. We observed that the hard segment T_gs of L-PUUs were better resolved in the first heating scans, therefore, we report here first heating scans of L-PUUs. Samples were scanned twice to confirm their transition temperatures. The Figure shows two T_gs for the control L-PU sample, as marked by dashed lines, suggesting microphase separation in the sample. The lower T_g corresponds to the soft segment, while the higher corresponds to the IPDI-BDO hard segment. **Table 5.2** lists T_g data for all polymers studied here. A slight decrease in the soft segment T_gs for L-PUU10 and L-PUU50 compared to the T_g of L-PU is visible in the figure. This observation supports two well known facts: (1) microphase separation in L-PU is incomplete, i.e, some amount of segmental mixing is observed in L-PU, and (2) L-PUUs show stronger segregation caused by a greater number of strongly hydrogen bonded urea linkages in the hard segments. A corresponding increase in the hard segment T_gs for L-PUU10 and L-PUU50 compared to the hard segment T_g of L-PU was also observed in support of the second conclusion noted above. The increase in hard segment T_gs of L-PUUs resemble the observed increase for the model hard segments discussed earlier although the diamine chain extender used in the case was different. Essentially, the increase in the hard segment T_g arises from stronger hydrogen bonding in urea linkage compared to urethane linkage thereby making the hard segments more rigid.

In case of L-PUU100 a well resolved melting endotherm having a peak temperature at the same location as that for the pure soft segment (**Figure 5.10**) was observed indicating that the soft segment had crystallized. This caused the T_g of the

soft segment to be poorly resolved. Rapid crystallization of almost pure PTMO phase in this sample was also confirmed in the second heating DSC scan, not shown here. Crystallization of the soft segment is perhaps an indicator of an even stronger microphase separation in this polymer.
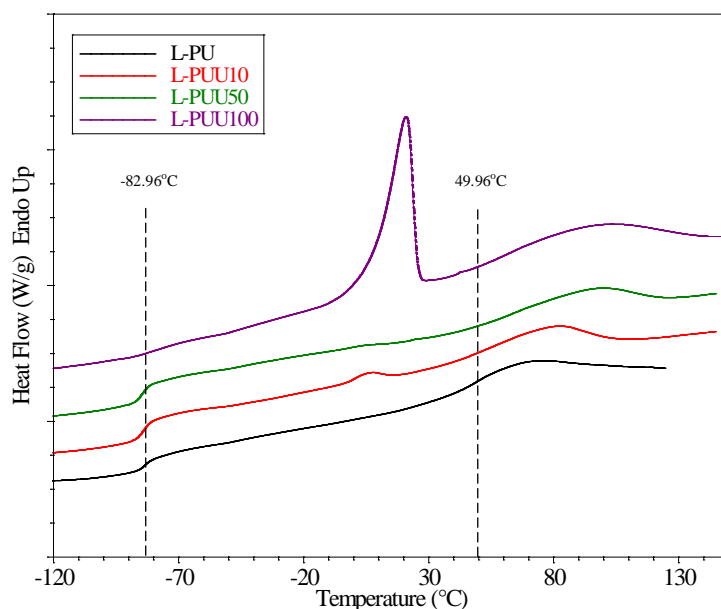
Figure 5.13 DSC traces for L-PUU series. Conditions: 20°C/min, first heat.

5.2.3 B12-PUU Series

Figure 5.14 (A) and **(B)** respectively presents the first and second heating DSC thermograms of B12-PUUs. We observed that the soft segment T_gs were similarly resolved in the first and second heating runs, whereas hard segment T_gs were better resolved in the first run compared to the second. The reason for this is probably related to the fact that the first heating scan was recorded on a sample that was heated to 100°C (in compression molding) followed by slow cooling while the second heating scan was recorded on the sample had been heated to 150°C followed by rapid cooling (see DSC protocol). Heating to a higher temperature can be expected to cause increased phase mixing between the soft and hard segments. FTIR results of the polymers studied here as discussed in the previous section also indicate disordering of hard segments and increased phase mixing upon heating. SAXS data, which will be presented later, also supports increasing mixing upon heating. Rapid cooling of the sample from higher temperature is likely to trap the PUUs into a metastable state with

increased degree of phase mixing, whereas slower cooling from a lower temperature would retain greater degree of phase separation. As will be shown later, phase mixing was found to affect the T_gs of the hard segments. Hence it is likely that the T_gs of the hard segments were better resolved in the first heat than in the second heat.

Figure 5.14 (A) shows a small increase in the soft segment T_g with increasing B12 diamine content, up to B12-PUU70. This may be attributed to smaller extent of mixing of hard segments in the soft segment domains. In comparison B12-PUU100 showed a marked rise in the soft segment T_g, suggesting the inclusion of a large amount of hard segments in the soft segment domains. This behaviour is qualitatively different than that seen for the L-PUUs (**Figure 5.13**, **Table 5.2**) for which the soft segment T_g decreased with increasing diamine content. Observations of the glass transitions of hard segment were not very conclusive because of the difficulty in determining the T_gs. However, it is clear from **Figure 5.14 (A)** that the glass transitions of hard segments of the B12-PUUs were significantly broader than the glass transition seen for L-PU for samples subjected to similar thermal history. This made difficult the detection of their T_g. The data in the Figure suggests that compared to the T_g of L-PU the T_gs of B12-PUUs increased for B12-PUU70 and B12-PUU100. However the observed increase was much lower than that observed for the B12-model hard segments shown in **Figure 5.12** for the same diamine content. Information about hard segment dynamics was better obtained from DMA data as will be shown later.

Figure 5.14 (A) DSC traces for B12-PUU series. Conditions: 20°C/min, first heat.

National Chemical Laboratory
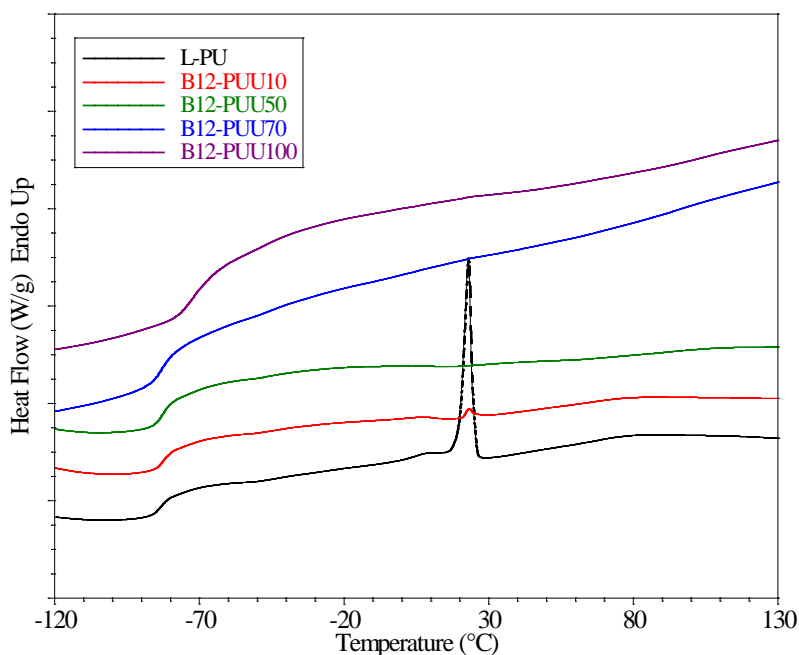
Figure 5.14 (B) DSC traces for B12-PUU series. Conditions: 20°C/min, second heat.

In the temperature range analyzed, absence of any melting peak indicates that the samples are primarily amorphous in nature. A sharp melting peak (at 23°C) observed in **Figure 5.14 (B)** for L-PU is due to the crystallization of PTMO segments. None of the B12-PUUs showed evidence for soft segment crystallinity in the second heat scan. The increase in soft segment T_g and the broadening of hard segment T_g may be attributed to increased phase mixing of the soft and hard domains driven possibly by the presence of defects/kinks in the hard segments due to the C-12 pendant branch. The FTIR results presented earlier had indicated disordering of the hard segment domains due to the presence of the diamine chain extender. The B12-PUU100 polymer showed significant presence of highly disordered N-H and C=O bonding. The corresponding large increase in soft segment T_g for this polymer further supports substantial degree of phase mixing. The lower $\Delta C_{p,hs}$ for hard segment glass transition observed in case of B12-PUUs compared to L-PU (see **Table 5.2**) might also be due to plasticization by pendent aliphatic chain on the diamine. Also, the fact that the increase in hard segment T_g of B12-PUUs with increasing diamine content was much lower than the corresponding increase in T_gs of the B12-model hard segments suggests that there is mixing between the soft and hard segments.

5.2.4 B22-PUU Series

First and second heating DSC thermograms for B22-PUUs are provided in **Figure 5.15 (A)** and **(B)** respectively. Thermograms of B22-PUU100 are plotted separately in Figure **5.15 (C)**. Samples were scanned twice, and their transition temperatures and associated enthalpies are displayed in **Table 5.2**. As observed from Figure **5.15(A)**, B22 diamine incorporation up to 50 mol% marginally increased the soft segment T_gs of B22-PUUs in a manner similar to that observed for the B12-PUU series. Unfortunately it was not possible to record the low temperature DSC data for the B22-PUU100 sample (see **Figure 5.15 (C)**). Small endotherms were observed in the interval 3^oC - 20^oC for B22-PUU10 and B22-PUU30. The presence of the endotherms made it more difficult to assign hard segment T_gs for these polymers. The B22-PUU50 polymer exhibited an interesting DSC thermogram. In addition to a small endotherm at about 7^oC this sample showed a sharp bimodular melting endotherm (combined ΔC_p = 21.95 J/g) with peaks at 57.16 and 81.61^{o}C. The peak temperatures of the two endotherms are significantly different than the peak melting temperature of the soft segment. Thus these melting endotherms cannot be attributed to crystallinity of soft segments. The small endotherms (around 10^oC) observed for three B22-PUUs, are found to be sensitive to the thermal treatment, and are also noticed in the second heating scan in **Figure 5.15(B)**. The bimodular melting endotherms were not visible in the second heating scan, while the endotherm moved to a higher temperature (about 30^oC).

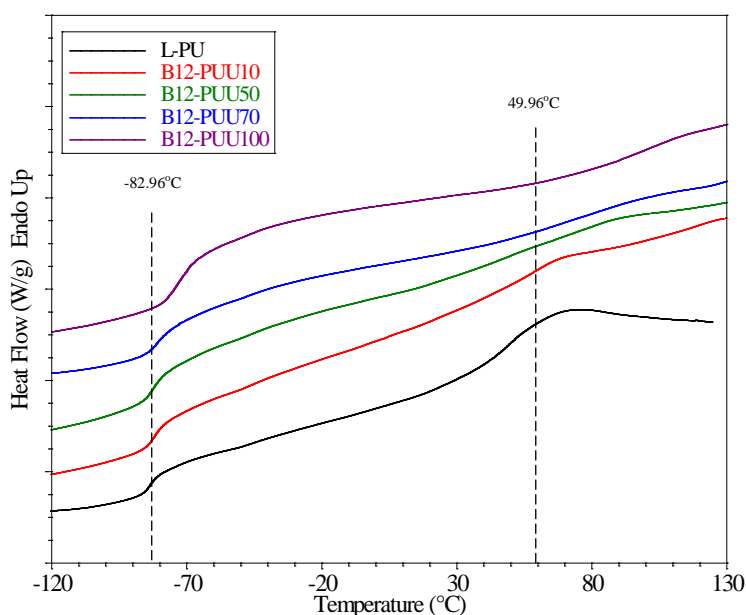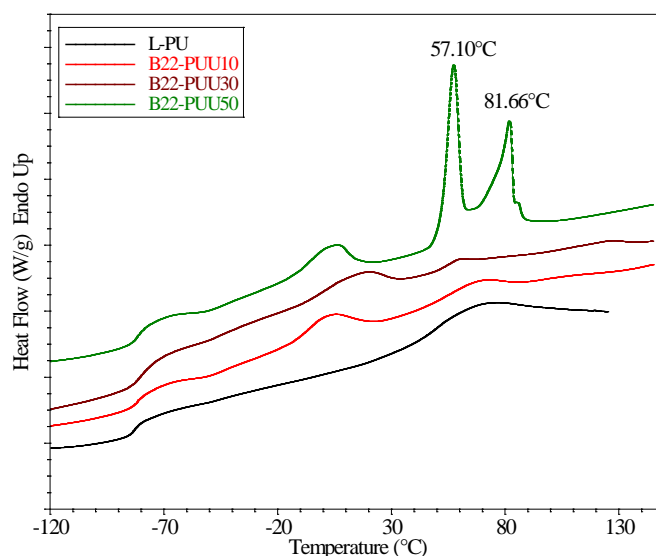**Figure 5.15 (A)** DSC traces for B22-PUU series. Conditions: 20^oC/min, first heat.
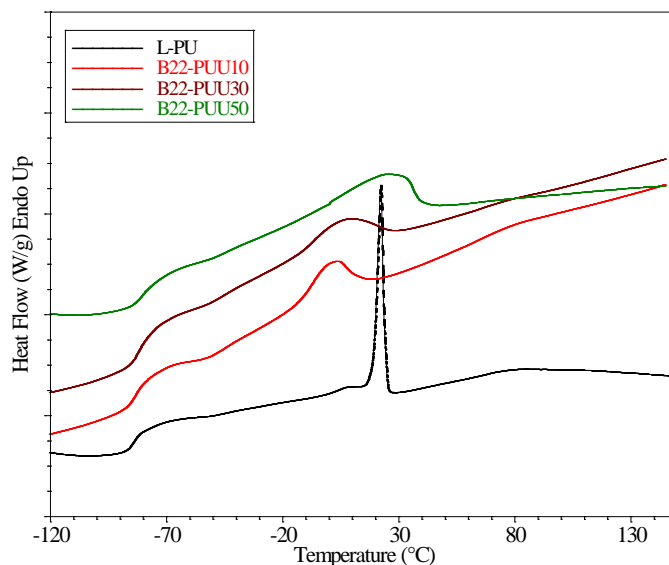
Figure 5.15 (B) DSC traces for B22-PUU series. Conditions: 20°C/min, second heat.

The thermogram of B22-PUU100 was similar to that of B22-PUU50 and is presented in **Figure 5.15 (C)**. The first heating thermogram of this sample features a small endotherm at 8°C and bimodular melting peaks, at temperatures higher than those observed in B22-PUU50. Associated enthalpy of this transition (33.93 J/g) is also found to be higher than for B22-PUU50 (21.95 J/g). The cooling curve (not shown) following the first heating cycle, exhibited a small crystallization exotherm at 27°C, which shows the propensity of crystallization at ambient temperature. The second heating scan, as shown by a dashed line in the figure, again shows appearance of two endothermic transitions although of much lower specific heats, broader and at lower temperatures. These features demonstrate the possibility of formation of a new phase that crystallizes at ambient temperature. Indeed it was observed that upon storing this polymer at ambient temperature it turned opaque accompanied with embrittlement over a period of weeks. Reheating the sample to 100°C resulted in a transparent polymer, which again turned opaque slowly upon storage.

Figure 5.15 (A)-(C) indicates that the thermal response of B22-PUUs is different than that of B12-PUUs. Soft segment T_gs of B22-PUUs remain almost unaffected upon the incorporation of B22 diamine. Although, low temperature data for B22-PUU100 is not available, the DMA response of this sample to be described later does not show a large increase in the segmental loss process, in contrast to what was observed for its B12 counterpart. Though a marginal rise in the soft segment T_gs is observed, the soft segment phase remained segregated and largely unmixed. A

small amount of segmental mixing could be due to short hard segment sequences, and those that are not chain extended by 1,4-butanediol or B22 diamine. Evidence for the latter came from **Figure 5.8 (A)** which shows the presence of hard segment N-H hydrogen bonded to polyether soft segments.
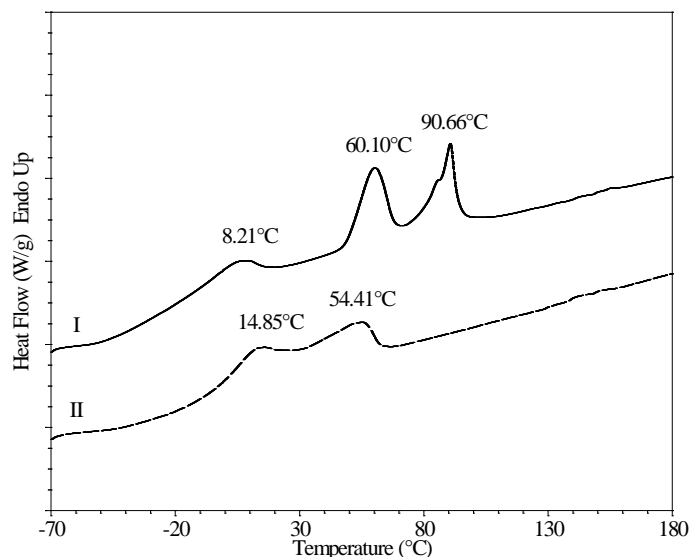
Figure 5.15 (C) First (solid line) and second (dashed line) heating DSC traces of B22-PUU100. Conditions: 20°C/min.

Appearance of small endotherms, in the range 3°C - 20°C in all B22-PUU thermograms is intriguing, and these were found to be temperature sensitive. The small endotherms appear at progressively higher temperature with increasing B22 diamine content. It is difficult to assign these smaller endotherms to specific structures or relaxations. However, the sharper bimodal transitions seen in the first heating scan for B22-PUU100 are clearly related to the melting of some long order microstructure. The crystallization exotherm appearing at 27°C in the cooling curve also supports this conclusion. Since for crystalline PTMO soft segment the melting endotherm occurs at 23°C and the crsyatllization exotherm appears at about 0°C, the phase transitions seen in B22-PUU100 cannot be attributed to the soft segments. Therefore they can arise out of three other possibilities: (1) crystallization of hard segments, (2) crystallization of unreacted diamine, or (3) crystallization of pendent C22 chains. Hard segments made of IPDI are not prone to crystallization easily because of the intrinsic structure of this diisocyanate. Also the presence of a long, plasticizing aliphatic chain on in the hard segment would hinder its crystallizability. This rules out the first possibility. The results from NMR500 spectroscopy discussed

in Chapter 4 (section 4.4) showed that a small part of unreacted diamine chain extender was detected in the B22-PUU100. The melting point of the pure diamine was found to be 91°C (see Chapter 3, section 3.2.4). Thus it is possible that some free unreacted diamine could have crystallized in this polymer and appears as the 90°C endotherm seen in **Figure 5.15 (C)**. However the endotherm appearing at 60°C in the same figure is not explained by this argument. Similarly, no free diamine was detected in the B22-PUU50 polymer and yet it showed an endotherm at about 82°C (see **Figure 5.15 (A)**). Thus, the possibility (2) can also be ruled out. We are then left with the possibility that crystallization of C22 chains has resulted in the formation of a new phase having the unique melting endotherms and crystallization exotherms discussed above. The microstructure of the B22-PUU50 and B22-PUU100 polymers is therefore rather unique. It appears that there are three distinct phases in the polymer: soft segment phase, hard segment phase and a crystalline C22 segment phase. The physical location of the third phase is not known. It is likely to be located within the hard domains.

It is likely that the smaller endotherms located between 3°C - 20°C are also due to dissociation of the C22 chains. In B22-PUU10 the concentration of C22 chains is very low, but it appears that although weakly they associate and give rise to the small endotherm at about 3°C (**Figure 5.15 (A) and (B)**). With the increase in diamine concentration in B22-PUU30 the endotherm moved to 20°C (**Figure 5.15 (A)**), indicating a better C22 association than the previous copolymer composition. In B22-PUU50 a further increase in the C22 chain concentration probably resulted in crystallization of a poorly organized 3-D ordered structure. Whereas, for the highest B22 diamine content (B22-PUU100) the C22 chains are in sufficient concentration to form a well ordered 3-D structure with higher melting points.

Process of paraffin crystallization is complicated and is a subject of academic as well as industrial research. n-Alkanes are known to undergo on heating to a strong first order transition a few degrees below the melting point into the so-called rotator phase.[11-14] Previous work demonstrate that C22 shows a rotator phase on heating and cooling.[15] The B22-PUU100 sample was analyzed by wide angle x-ray diffraction (WAXD) and the result is shown in **Figure 5.16**. Also shown is wide angle diffraction result for the L-PU. Whereas the L-PU showed only an amorphous halo the B22-

PUU100 sample showed the presence of a small peak (2θ= 20.65 deg, q = 4.29 Å^{-1}) and a shoulder (2θ=23.85 deg, q = 3.72 Å^{-1}) over and above the amorphous halo an indication of crystalline order. The *d*-spacings are in close agreement with reported values of triclinic geometry.[15]
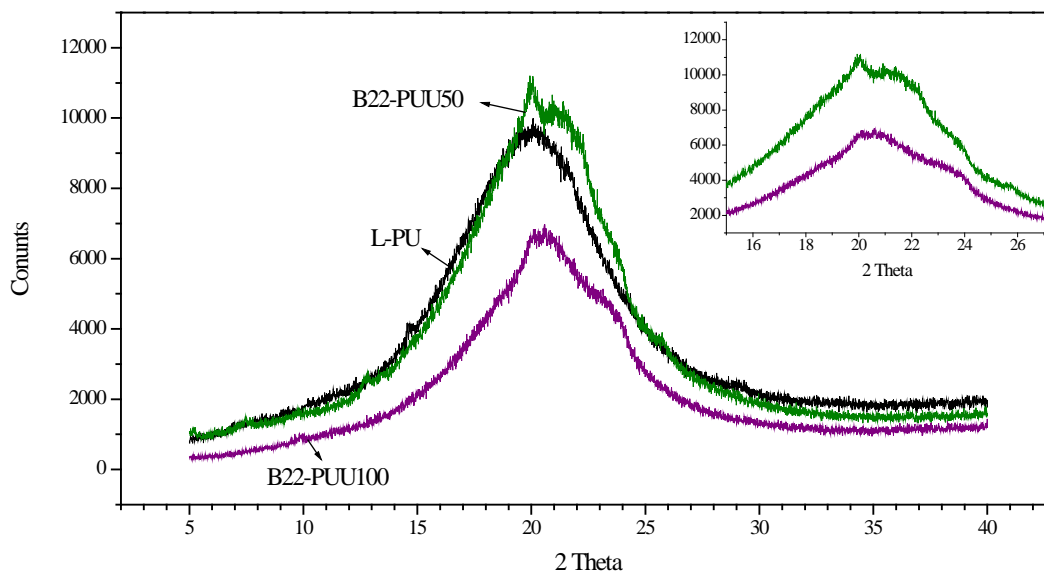
Figure 5.16 WAXD patterns of L-PU, B2-PUU50 and B22-PUU100.

Table 5.2 DSC results of PUUs.

Polymer	T_g ss (°C)	ΔC_p ss (J/g °C)	T_g hs (°C)	ΔC_p hs (J/g °C)
L-PU	-82.96	0.26	49.96	0.54
L-PUU10	-83.61	0.39	56.86	0.38
L-PUU50	-84.57	0.38	69.97	0.55
L-PUU100	-	-	-	-
B12-PUU10	-81.72	0.27	56.89	0.40
B12-PUU50	-82.07	0.29	62.46	0.40
B12-PUU70	-80.40	0.31	80.41	0.29
B12-PUU100	-72.95	0.43	95.60	0.32
B22-PUU10	-80.57	0.34	55.72	0.33
B22-PUU30	-79.27	0.40	52.38	0.17
B22-PUU50	-80.68	0.39	-	-
B22-PUU100	-	-	-	-

5.3   Dynamic Mechanical Analysis

DMA tests were carried out in tensile mode using DMTA 3E instrument from Rheometric Scientific. Rectangular test specimens were cut from compression molded sheets. Measurements were carried out under nitrogen atmosphere at a frequency of 10 rad/s and a temperature ramp rate of 5°C/min. Temperature was ramped from -150°C to a temperature at which the sample became too soft, as evidenced by an increasing gap between sample fixtures. A strain sweep test was carried out for each sample before the temperature ramp measurement to delineate the linear and non-linear viscoelastic regimes. Samples were scanned twice to confirm the transition temperatures.

DMA was used to study the effects of incorporation of diamine on segmental motions in the polymers under study. Multiple segmental relaxations in DMA confirms the presence of heterophase morphology in polyurethanes. Since segmental relaxations are associated with a maximum in energy dissipation, therefore in this work, a peak in loss modulus is used as an indicator of the α relaxation, which is equivalent to the glass transition process in a quiescent system.

5.3.1 L-PUU Series

Figure 5.17 displays dynamic mechanical temperature sweep data for L-PU in terms of storage modulus (E'), loss modulus (E'') and dissipation factor (tan δ). The presence of two mechanical relaxation processes (peaks in E'') indicates microphase separated nature of the sample. The slowly decreasing E' between the two transitions corresponds to the temperature region in which the soft segments are in rubbery state and are attached at either ends to glassy hard domains which serve as crosslink points. The relaxation at lower temperature of about -90°C can be assigned to the α relaxation or the glass transition of PTMO soft segment, while the second relaxation at about 44°C can be assigned to the α relaxation or the glass transition of hard segment sequences. This is immediately followed by sample flow from about 50°C. The behaviour of E' and tanδ was consistent with that of E'' for the soft segment relaxation, although a difference of few degrees was noted between the peak E'' and peak tan δ values. Often peaks in tanδ are used to indicate T_{α}, and this relaxation

temperature is typically found to be greater than the T_g measured by DSC. In the present work peaks in *E"* are used because it is more appropriate to do so and also because in many polymers studied here the peaks in tanδ especially for the hard segment relaxation were not clearly observed.

Dynamic mechanical temperature sweep data of L-PUU10 is provided in **Figure 5.18**. The figure displays two prominent segmental relaxations in *E"* at about -91°C, corresponding to the soft segment T_g and at 68°C corresponding to the hard segment T_g. A reduction in *E'* as the sample passes these two transitions is also seen in the figure. The narrow width of soft segment relaxation and a well separated hard segment relaxation, indicates the presence of a strong microphase separation in the sample. The sample also exhibited a small intermediate relaxation at about 0°C, clearly seen in *E'* and *E"* signals.

Dynamic mechanical temperature sweep data of L-PUU50, provided in **Figure 5.19**, shows two main segmental loss processes at about -91°C and 90°C. The two relaxations respectively correspond to the soft and hard segment T_gs. A small transition at about 0°C is also noticed in this sample. The polymer L-PUU100 was so brittle that it was not possible to perform dynamic mechanical testing of this sample.
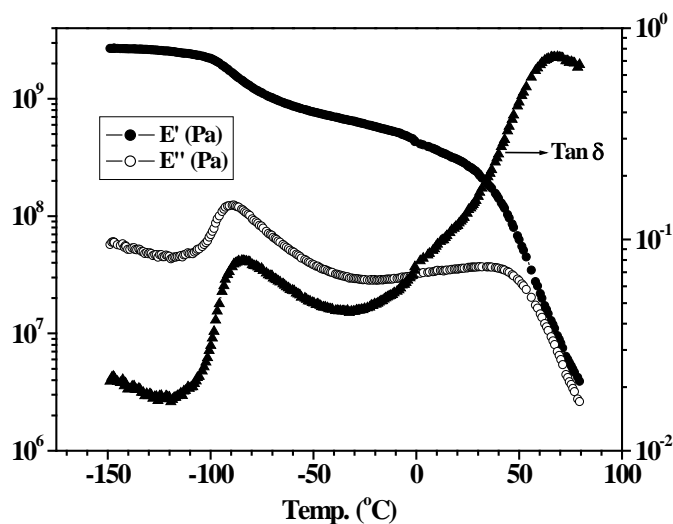
Figure 5.17 DMA curves of L-PU. Conditions: 5°C/min, 1 Hz, film in tensile mode.

Figure 5.18 DMA curves of L-PUU10. Conditions: 5°C/min, 1 Hz, film in tensile mode.

Figure 5.20 displays a plot of loss moduli (*E"*) of L-PUUs in comparison with the control sample L-PU. Soft and hard segmental relaxations are labeled as I and II respectively. Soft segment relaxations of L-PUU10 and L-PUU50 were found to be marginally shifted to lower temperature compared to L-PU (-89.65^{o}C), and were observed at -92°C and -93°C respectively. The loss modulli peak of the two PUUs was observed to have narrowed down. Also when compared with the L-PU sample, the hard segment glass transition of L-PUUs was seen to increase with the amount of aromatic chain extender *m-phenylenediamine*. Additionally, both L-PUUs showed a third segmental relaxation near 0°C which is in between the soft and hard segment relaxations. This transition was observed at a slightly higher temperature for L-PUU10 than for L-PUU50.
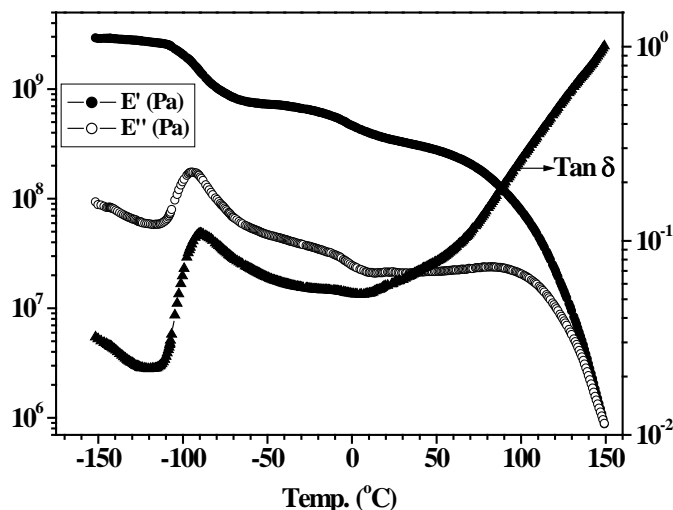
Figure 5.19 DMA curves of L-PUU50. Conditions: 5°C/min, 1 Hz, film in tensile mode.

The shifts in T_gs of soft and hard segments observed in DMA for the L-PUUs are consistent with the previously presented DSC results. It can be concluded that the microstructure of L-PUUs consist of strongly segregated hard and soft segment phases possibly driven by the formation of stronger (bifurcate) hydrogen bonding between the urea functional groups of the hard segments. This also rendered rigidity to the hard segments causing an increase in the hard segment T_gs. In continuation of this trend the possibility of hard segment association is the highest in L-PUU100 (100% *m-phenylenediamine* chain extender) sample of this series, and this sample failed to soften even at 200°C. Brittleness of this sample precluded its mechanical testing. The peaks in *E"* corresponding to the relaxations of hard segments were found to be weaker and broader than those corresponding to soft segment relaxation. This was again consistent with previously presented DSC observations of weaker and broader T_gs of hard segments. However, the DMA data for L-PUUs showed an additional segmental relaxation process at a temperature in between the soft and hard segment relaxation temperatures. This intermediate relaxation may be attributed to the glass transition of the diffuse interface between the hard and soft domains. The presence of such an intermediate phase will be discussed later while presenting the SAXS data analysis of these samples.
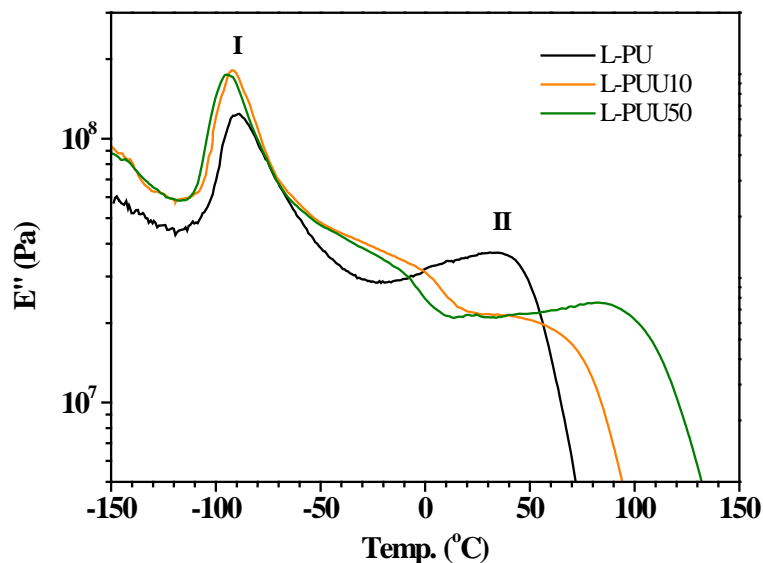
Figure 5.20 DMA loss modulus curves of L-PUUs in comparison with L-PU.

5.3.2 B12-PUU Series

DMA behavior of B12-PUU10 is plotted in **Figure 5.21**. From the two segmental loss processes the existence of two phase morphology in the sample is evident. The lower α relaxation in E'' (-88°C) corresponds to the glass transition of PTMO segment, while second relaxation at 44°C is attributed to the hard segment glass transition. The DMA response of this sample is quite similar to that of L-PU.

Figure 5.21 DMA curves of B12-PUU10. Conditions: 5°C/min, 1 Hz, film in tensile mode.

Dynamic mechanical temperature sweep of B12-PUU50 (**Figure 5.22**), shows presence of a single relaxation in E'' at -84°C corresponding to the PTMO glass

transition. This transition is broadened and observed at a higher temperature compared to B12-PUU10. The presence of a second transition corresponding to hard segments is subtle but still observable.

Figure 5.22 DMA curves of B12-PUU50. Conditions: 5°C/min, 1 Hz, film in tensile mode.

Figure 5.23 presents DMA response of B12-PUU70. The *E'*, *E''*, and tan δ responses exhibited the presence of a broad, single relaxation associated with PTMO glass transition at -80°C. The presence of a second transition corresponding to hard segments is subtle and barely discernable. Similarly, the DMA plot of B12-PUU100 in terms of *E'*, *E''* and tan δ is shown in **Figure 5.24**. Here, the only relaxation seen at -77°C is due to the soft segment glass transition. This transition leads to sample flow without any detectable hard segment transition.
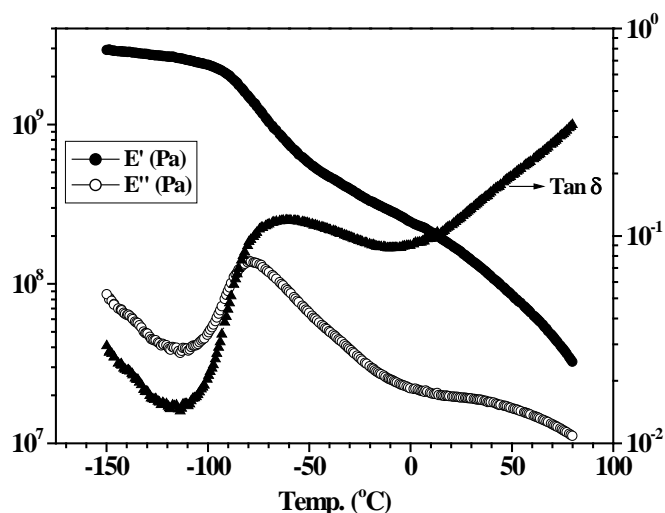
Figure 5.23 DMA curves of B12-PUU70. Conditions: 5°C/min, 1 Hz, film in tensile mode.
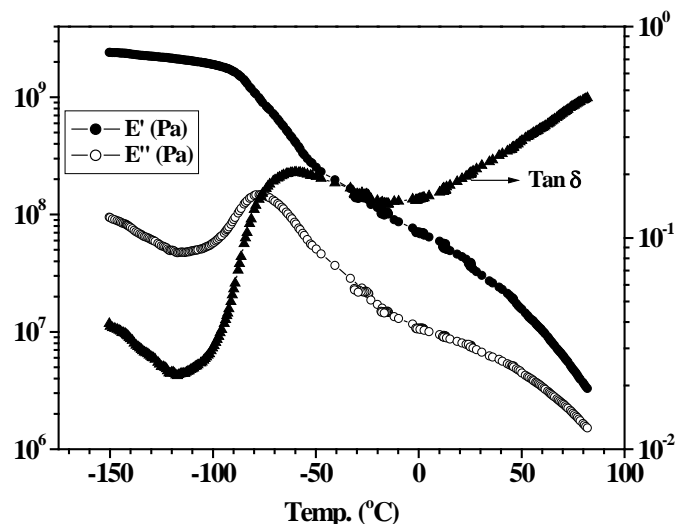
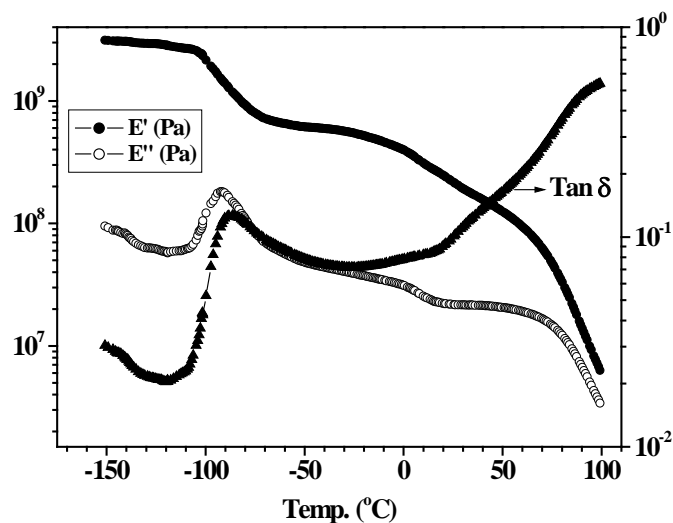**Figure 5.24** DMA curves of B12-PUU100. Conditions: 5°C/min, 1 Hz, film in tensile mode.

Figure 5.25 displays loss moduli of B12-PUUs in comparison with L-PU. A progressive increase in *E"* peak maximum along with an increase in the width of the peak was observed with increasing B12 diamine content. The α relaxation of PTMO segments for B12-PUU70 and B12-PUU100 were observed at about -79°C and -77°C respectively. On the other hand, a gradual disappearance of second relaxation (labeled as II) associated with hard segments is seen after 50 mol% amine incorporation. Unlike L-PUUs the B12-PUUs did not show any additional relaxations at temperature in between those for the soft and hard segment relaxations.
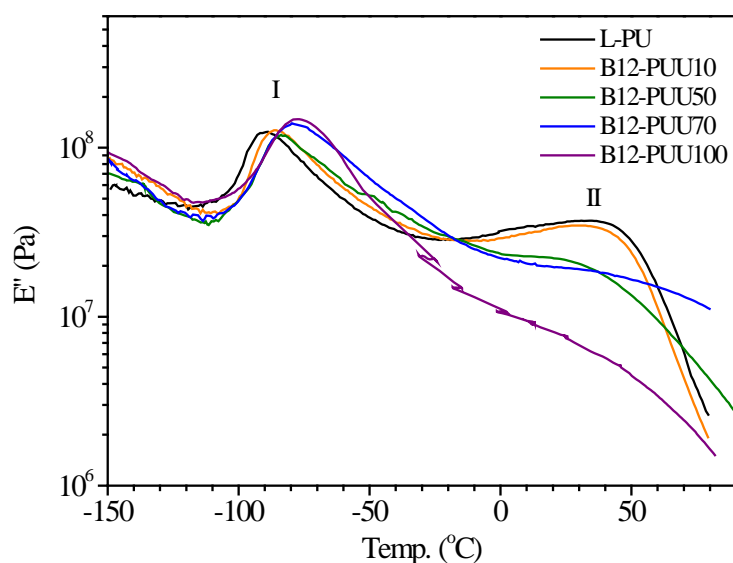
Figure 5.25 DMA loss modulus curves of B12-PUUs in comparison with L-PU.

The effect of diamine incorporation in B12-PUUs is in contrast to that observed in L-PUUs (**Figure 5.20**). Polymers in the B12-PUU series showed a small increase in soft segment glass transition, upto 50 mol% B12 diamine incorporation. With further use of diamine in B12-PUU70 and B12-PUU100 polymers a marked increase in soft segment glass transition as well as in the width of the transition was noticed. This observed increase in soft segment relaxation temperature is again consistent with previously presented DSC data and suggest increased mixing of the soft segments with hard segments. The simultaneous gradual weakening of the hard segment relaxation might be due to two plausible effects operating simultaneously: 1) pendent aliphatic chains on the diamine forbid hard segment packing, thus forcing a large proportion of hard segments to mix with the soft segments, and 2) pendent chains plasticize hard segments so much that B12-PUU70 and B12-PUU100 fail to exhibit a discernable hard segment glass transition. The evidence for effect 1) was seen from FTIR data presented earlier. Evidence for plasticization may be seen from **Figure 5.25** which shows reduction in the E'' in the plateau region between the soft and hard segment relaxations with increasing diamine content. However, it may be noted that the absolute values of moduli in DMA also depend on other factors such as sample geometry and dimensions. Although all samples tested in this work were of roughly similar dimensions, inferences based on comparisons of actual moduli values should be regarded with caution.

5.3.3 B22-PUU Series

Figure 5.26 presents the DMA response of B22-PUU10 in terms of E', E'' and tan δ. The presence of two discernable segmental loss processes is evident in the figure. The main α relaxation of PTMO glass transition at about -88°C is broader compared to its B12 analogue. The presence of a second relaxation due to hard segment glass transition, at about 38°C is subtle but still observable.
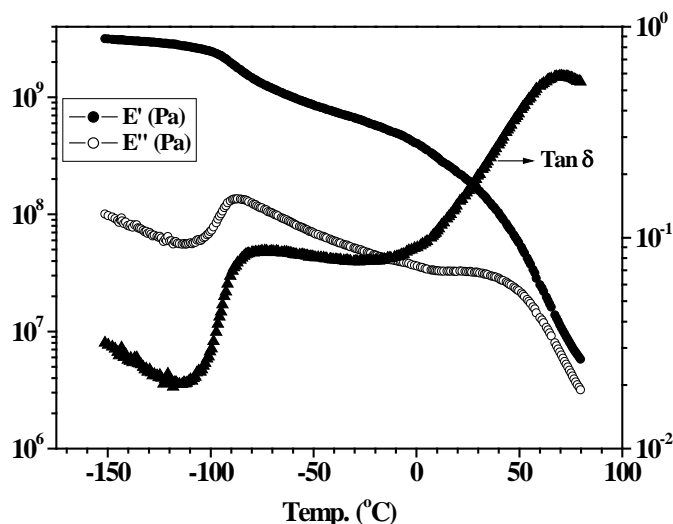
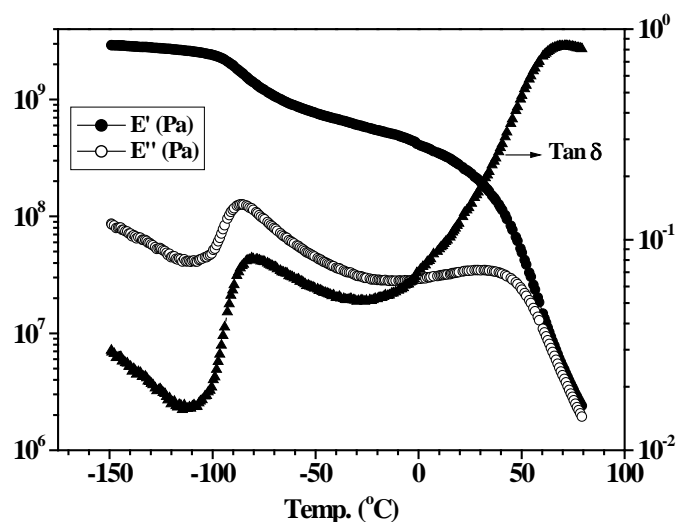**Figure 5.26** DMA curves of B22-PUU10. Conditions: 5°C/min, 1 Hz, film in tensile mode.

Dynamic mechanical temperature sweep of B22-PUU30 is shown in **Figure 5.27**. As compared to B22-PUU10, a slightly higher PTMO glass transition was noted (about -84°C). The segmental relaxation corresponding to the hard segment was not distinctly observed in the temperature window probed, and sample flow can be seen from ambient temperature onwards.
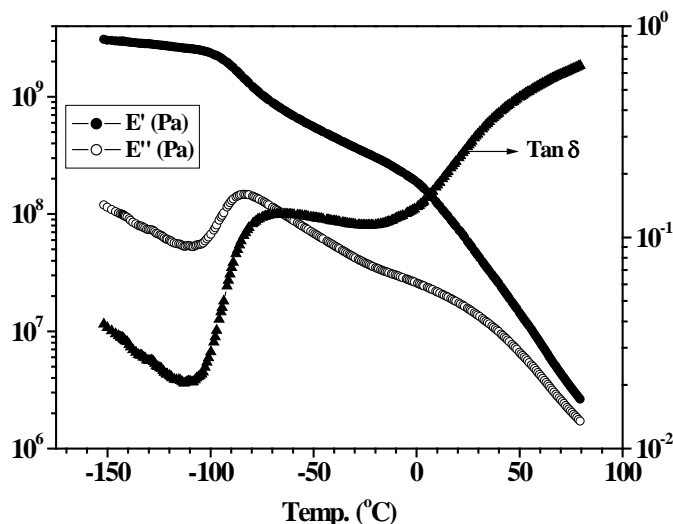
Figure 5.27 DMA curves of B22-PUU30. Conditions: 5°C/min, 1 Hz, film in tensile mode.

DMA data of B22-PUU50, as presented in **Figure 5.28**, shows soft segment relaxation at about -84°C, and another transition at about 50°C. A large drop in the moduli is seen after the latter transition. It is important here to recollect the DSC thermogram seen for this polymer in **Figure 5.15 (A)**. The DSC trace of this sample

showed two melting endotherms, with the first endotherm seen at 56°C. Also note, a very shallow but visible (particularly well in *E'* signal) transition at about 3°C corresponding to a small endotherm observed in the DSC data at nearly the same temperature.
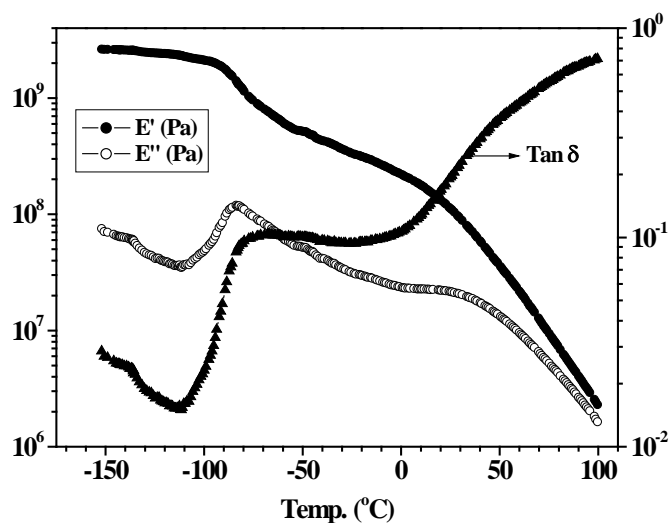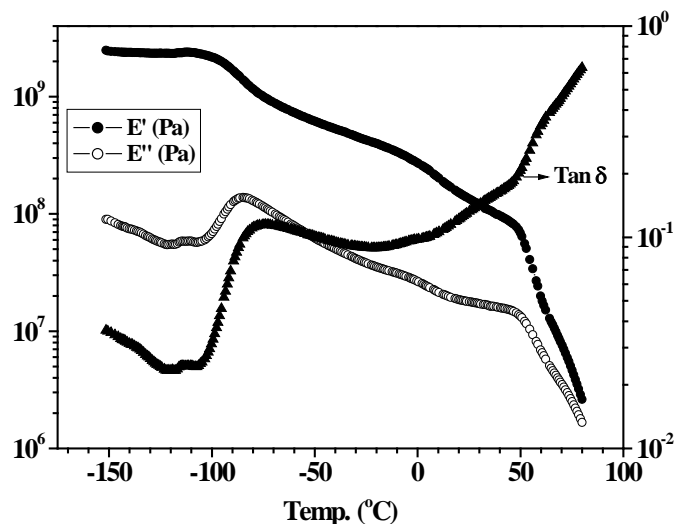

Figure 5.28 DMA curves of B22-PUU50. Conditions: 5°C/min, 1 Hz, film in tensile mode.

Figure 5.29 displays the DMA response of B22-PUU100. The DMA scan for this sample exhibited features that are similar to those observed for B22-PUU70 namely, a soft segment relaxation at about -84°C and a second relaxation at about 50°C. A subtle relaxation at about 10°C is also seen for this sample. Once again these relaxations correspond to thermal transitions observed in the DSC thermogram of this sample.
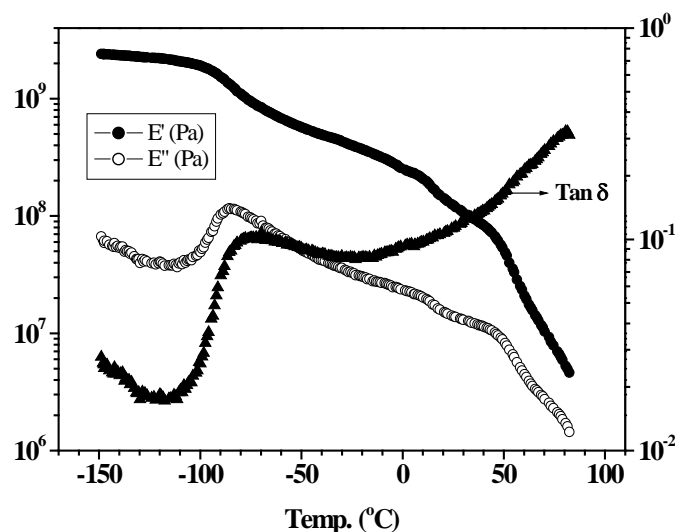
Figure 5.29 DMA curves of B22-PUU100. Conditions: 5°C/min, 1 Hz, film in tensile mode.

Figure 5.30 shows a comparison of loss moduli of B22-PUUs with L-PU. The overlaid data clearly shows an increase in the temperature of soft segment relaxation (labeled as I) as well as an increase in the width of this relaxation with increasing B22 diamine content. The Figure also shows a subtle hard segment relaxation for B22-PUU10 (at about 40°C), absence of second transition for B22-PUU30, and reappearance of a second transition at around 50°C for B22-PUU50 and B22-PUU100.
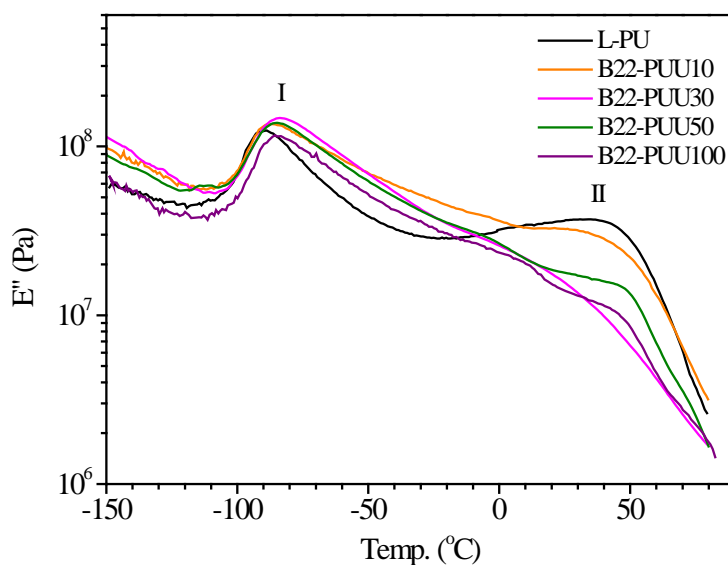
Figure 5.30 DMA loss modulus curves of B22-PUUs in comparison with L-PU.

The C22 pendant branch in B22-PUU series had similar effect on the soft segment relaxation as for the C12 branch. The soft segment relaxation temperature and the width of the relaxation increased in comparison to L-PU for both the B22-PUU and B12-PUUs (see values for full-width-at-half-maximum, FWHM, for the soft segment relaxation peak in **Table 5.3**). However the increase was substantially higher for B12-PUU100 (by ca.13°C) compared to the B22-PUU100 (~ 5°C), while the width of the transition was greater for the B22-PUUs compared to the B12-PUUs. Increasing the length of the pendent branch from C12 to C22 led to a pronounced effect on the hard segment relaxation. For instance, in case of B22-PUU30 no hard segment relaxation was discernable whereas the same was observable, although barely, even for B12-PUU50. A plausible explaination for these observations is that the C22 pendent chains discourage hard segment packing and thereby promote mixing

with the soft segments. The FTIR data presented earlier clearly supports the hypothesis for disordered hard segment phase. Additionally, the C22 chains can plasticize hard segments resulting in decrease in their rigidity. Upon further increase in the diamine concentration (i.e., for B22-PUU50 and B22-PUU100), the C22 pendent chains start to interdegitize/crystallize forming a separate phase. Support for this hypothesis came from the observation of crystalline melting endotherms seen for these samples in DSC run. The first peaks of bimodular endotherms for B22-PUU50 and B22-PUU100 were observed at 56 and $60^{o}C$ respectively. These temperatures roughly correspond to the high temperature transitions observed in DMA response for these copolymer compositions. Thus the reappearance of the second transition in DMA is likely to be due to melting of the crystalline phase comprising C22 segments. The large loss in modulli after this transition also supports the hypothesis that this crystalline phase results from association of C22 segments that are part of the polymer chain rather than any free unreacted diamines.

Table 5.3 DMA data of PUUs.

Polymer	*E''* (SS)	FWHM of SS	*E''* (HS)
L-PU	-89.65	15.59	44.36
L-PUU10	-92.49	15.82	68.7
L-PUU50	-93.98	18.19	91.76
B12-PUU10	-88.16	16.88	44.69
B12-PUU50	-84.29	17.77	39.22
B12-PUU70	-79.62	23.74	34.4
B12-PUU100	-76.93	21.83	*
B22-PUU10	-87.73	18.71	37.85
B22-PUU30	-83.77	20.79	*
B22-PUU50	-84.39	21.13	*
B22-PUU100	-84.71	18.77	*

FWHM − full width at half maximum

* - absence of a discernable transition

DMA tests could not be conducted on the model hard segments because of their highly brittle nature.

5.4   Couchman Analysis

The data obtained from thermal (DSC) and thermo-mechanical (DMA) experiments can be used to extract quantitative information on phase composition. Towards this end the Couchman equations were used in the present study to calculate the compositions of the soft and hard domains, each being assumed to be in a single phase state, from the measured glass transition temperatures of the two domains. The Couchman equation[16] for predicting the glass transition of a single phase is

$$T_g = \frac{w_{ss}T_{g,ss} + \alpha.w_{hs}T_{g,hs}}{w_{ss} + \alpha.w_{hs}} \tag{5.1}$$

Here, w_{ss} is the weight fraction of soft segments, w_{hs} the weight fraction of hard segments, $T_{g,ss}$ the T_g of pure soft segment phase, $T_{g,hs}$ the T_g of pure hard segment phase, and α is the ratio of heat capacity change for pure components:

$$\alpha = \Delta C_{p,hs} / \Delta C_{p,ss} \tag{5.2}$$

where, $\Delta C_{p,hs}$ is the heat capacity change for pure hard segment and $\Delta C_{p,hs}$ is the heat capacity change for pure soft segment.

Equation 5.1 when suitably rearranged can be used for the estimation of composition of a specific phase in a microphase separated sample. Thus, the composition of the soft phase containing dissolved hard segments can be estimated using

$$w_{ss}^s = \frac{\alpha\left(T_{g,hs} - T_g^s\right)}{\left(T_g^s - T_{g,ss}\right) + \alpha\left(T_{g,hs} - T_g^s\right)} \tag{5.3}$$

Here w_{ss}^s is the weight fraction of soft segments in the soft phase and T_g^s is the T_g of the soft phase. Similarly, the composition of the hard phase containing dissolved soft segments can be estimated using

$$w_{hs}^h = \frac{\left(T_g^h - T_{g,ss}\right)}{\left(T_g^h - T_{g,ss}\right) + \alpha\left(T_{g,hs} - T_g^h\right)} \tag{5.4}$$

Here w_{hs}^h is the weight fraction of hard segments in the hard phase and T_g^h is the T_g of the hard phase.

Calculations were done only for the B12-PUU series. The values used for T_g^s and T_g^h were those measured from DMA, i.e., the α relaxations of the soft and hard phases. The DMA data was preferred since hard segment glass transitions were better seen in DMA experiments compared to DSC thermograms. $T_{g,ss}$ was assigned the value of -93.98 ^{o}C (we assume that phase separation is nearly complete in L-PUU50, and therefore used this value of soft segment relaxation as noted in the *E"* DMA response) since it was not possible measure this value in DSC due to rapid crystallization of PTMO even upon quenching from melt state as noted earlier. The values of $T_{g,hs}$ for the B12 hard segments are those given earlier in **Table 5.3**. The phase compositions of soft and hard domains from equations 5.3 and 5.4 are presented in **Table 5.4** below.

Table 5.4 Phase composition from Couchman analysis ($\alpha = 1.43$)

Polymer	Soft Phase		Hard Phase	
	w_{ss}^s	w_{hs}^s	w_{hs}^h	w_{ss}^h
L-PU	0.978	0.022	1.0	0.0
B12-PUU10	0.977	0.023	0.783	0.217
B12-PUU50	0.970	0.030	0.594	0.406
B12-PUU70	0.957	0.043	0.640	0.360
B12-PUU100	0.955	0.045	0.611	0.389

The results shown in **Table 5.4** suggest that the soft segment phase is nearly pure for all compositions of the diamine. In contrast, substantial degree of mixing of soft segments in the hard segment phase with increasing diamine incorporation was predicted by the Couchman equations.

5.5 Small-Angle X-ray Scattering (SAXS)

Small Angle X-ray Scattering (SAXS) experiments were carried out on a rotating anode NanoSTAR machine from Bruker AXS having three pinhole collimation and multiwire 2-D detector. X-ray wavelength used for scanning was 1.542 Å from copper target and sample to detector distance was calibrated to 106.25 cm. A specially designed sample holder with a temperature accuracy of $\pm$ 0.1^{o}C, supplied by Bruker, was used to heat the sample for high temperature scattering

experiments. High temperature experiments were performed on any given sample by heating it at the rate of 5°C/min.

Compression molded film specimens were used for scanning, and it was ensured that all samples had experienced similar thermal history.

5.5.1 Background Information – SAXS Experiment

SAXS is an analytical method used to determine the microstructure of multiphase systems in terms of averaged sizes or shapes and/or their spatial correlations. In a SAXS experiment, the incident beam penetrates the sample and the scattered radiation is recorded by the detector. By measuring the angle dependent distribution of the scattered radiation (intensity) information useful about the microstructure can be extracted. **Figure 5.31** shows a typical X-ray scattering experimental set up.
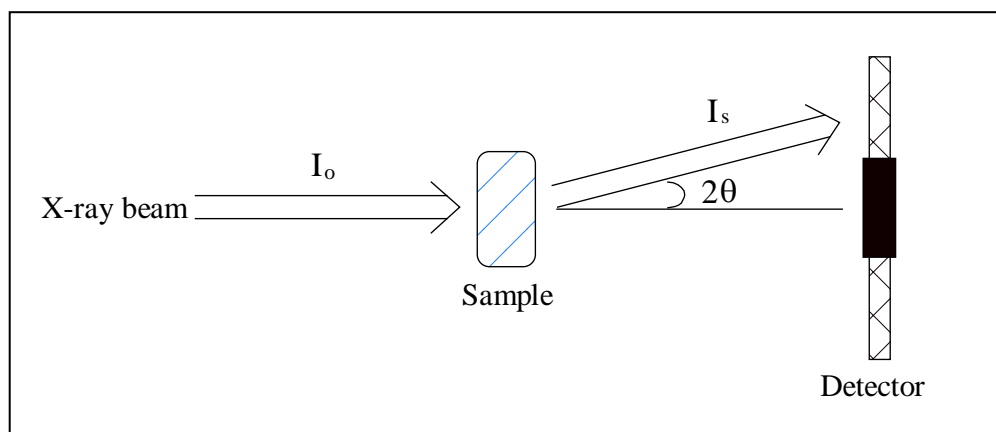
Figure 5.31 X-ray Scattering Experiment.

Most materials not only scatter, they also absorb X-rays. The ratio of the scattered intensity (I_s) and incident intensity (I_o) is called the transmission coefficient (τ) and is defined as

$$\tau = e^{-\mu \cdot d} = \frac{I_s}{I_o} \tag{5.5}$$

Here μ is the linear absorption coefficient and d is the sample thickness.

In order to determine the transmission coefficient for the sample (τ_s), the intensity of the primary beam with and without the sample in the path must be measured. With the present experimental facility used in this work, this is done by an indirect method. This

method uses a glassy carbon sample, with a known transmission coefficient (τ_{gc}), as a secondary standard to measure the transmission coefficient of sample as follows:

$$\tau_s = \frac{I_{s+gc} - \tau_{gc}.I_s}{I_{gc} - \tau_{gc}.I_b} \tag{5.6}$$

where, I_{gc} is the scattered intensity from glassy carbon, I_b is the background (primary beam) intensity, and I_{s+gc} is the scattered intensity from sample and glassy carbon held together in the beam path.

The scattered intensity that is required for SAXS data analysis is obtained after background subtraction ($I_{(sub.)}$). This step is essential as other sources such as thermal density fluctuations, amorphous halo of the WAXS extending to small angles, etc. can also contribute to the measured SAXS signal. In the present study this is done by using the following formula.

$$I_{(sub.)} = I_s - \tau_s \cdot I_b \tag{5.7}$$

The term SAXS signal (i.e, scattered intensity) used hereafter in the present work implies background subtracted intensity. Since a 2D detector was used in the present work the scattered intensity was averaged over the azimuthal angle to give *I(q)* versus *q* data.

5.5.2 Background Information – SAXS Theory

SAXS provides extremely useful qualitative and quantitative information about the morphology of a two phase system when there is sufficient electron density contrast between the phases, and the domain sizes are on the order of nanometers. In case of polyurethanes, SAXS data has been used for the measurements of interdomain spacings, domain boundary diffuseness, and the extent of microphase separation. The latter two measurements require detailed analyses of the data.

The simplest of these data analyses is the estimation of average periodicity or interdomain spacing (*d*) from the observed peak position (q_{max}), by a simple application of the Bragg equation:

$$d = 2\pi / q_{max} \tag{5.8}$$

where *q* is the modulus of the scattering vector defined as:

$$q = \frac{4\pi}{\lambda} \cos\theta \tag{5.9}$$

Here λ is the wavelength of the X-rays and the scattering angle is 2θ.

As noted in Chapter 3 the polymers studied in this work have an equivalent amount of hard and soft segments. Based on studies on microphase morphologies in diblock copolymers[17] it is reasonable to assume that polyurethanes with equivalent hard and soft segments are likely to have lamellar domains of hard segments dispersed in soft segment phase. For such morphology the SAXS intensity is Lorentz corrected to estimate the average periodicity / mean interdomain spacing. In the present work *d* was estimated from the Lorentz corrected scattering intensity (i.e., using q_{max} from the plot of Iq^2 vs *q*). However, the difference between the *d* values calculated with and without Lorentz correction was found to be small.

For isotropic systems, scattering depends on *q* as:

$$I(q) = n.\ P(q).S(q) \tag{5.10}$$

In eq (5.10) *n* is a constant which becomes important when the mass or the surface of the particle is investigated. For this *I(q)* must be in absolute units. The form factor *P(q)* describes the scattering observable from an isolated body in the absence of interference effects and depends on the particle size, shape, and internal structure of the particle. *S(q)* is the structure factor, which represents the effects of interference due to neighboring scatterers and depends on their relative positions. It bears the information about particle interaction, such as inter-particle distances and degree of ordering. *P(q)* and *S(q)* can be studied even when *I(q)* is in arbitrary units, because the information content lies in the *q* dependence only.

For the present purpose, we will regard polyurethane as a two phase system with volume fractions of the two phases denoted by ϕ_1, ϕ_2 and average electron

densities of the two phases denoted by ρ_1 and ρ_2. The invariant for an ideal system with constant phase densities and sharp interfaces is given by

$$Q_{max} = 2\pi^2 \phi_1 \phi_2 (\rho_1 - \rho_2)^2 \tag{5.11}$$

If ρ_1 and ρ_2 are equal, the x-ray beam does not 'see' the heterogeneity. The visibility increases with increasing difference in the electron densities between the two phases. Scattering from a heterogeneous system, such as polyurethane, is given by

$$\frac{I(q)}{VI_e(q)} = 4\pi\overline{\Delta\rho^2} \int_0^\infty r^2 \gamma(r) \frac{\sin(qr)}{qr} dr \tag{5.12}$$

where scattering intensity $I(q)$ is normalized by sample volume V and single electron scattering function $I_e(q)$, $\overline{\Delta\rho^2}$ is the mean square amplitude of electron density fluctuations, and $\gamma(r)$ is the density correlation function which carries information about the spatial extent of the heterogeneity. The invariant Q is the integral of the Lorentz corrected intensity

$$Q = \int_0^\infty q^2 \frac{I(q)}{VI_e(q)} dq = 2\pi^2 \overline{\Delta\rho^2} \tag{5.13}$$

The ratio of invariants Q/Q_{max} has been used as a measure of the extent of microphase separation in polyurethanes. The ratio of invariants close to 1 indicates a good microphase separation, whereas a value much less than 1 is indicative of microphase mixing either at the interface or in the bulk. For polyurethanes the value of this ratio has been reported to be less than 0.5.

SAXS data can also be employed to obtain valuable information about the width of interfaces in biphasic systems. Small-angle X-ray scattering by an ideal two phase system (i.e. system having sharp interfaces, and constant electron density within each phase), as illustrated in **Figure 5.32 (A)**, has been treated by Porod. For such systems Porod's law states that the scattered intensity decreases with the reciprocal fourth power of the scattering vector q:

$$\lim_{q \to \infty} [I(q)] = \frac{K_p}{q^4} \tag{5.14}$$

where K_p is called as Porod constant. In other words, at high angles the product $I(q)q^4$ reaches a constant value, K_p, which is related to the interfacial area in the system.

Real multiphasic polymeric systems contain thermal density fluctuations and diffuse phase boundaries which lead to deviations from the Porod law. The presence of thermal density fluctuations or mixing within the phases, illustrated in **Figure 5.32 (B)**, typically leads to enhanced scattering at high angles that is independent of the scattering vector. Therefore a plot of Iq^4 *vs* q^2 tends to have positive slope. This is called as a positive deviation from Porod's law.

In the case of a diffuse boundary assuming that the boundary is characterized by sigmoidal concentration (density) gradient, the Porod law can be modified as:

$$I(q) = \frac{K_p}{q^4} \exp\left(-4\pi^2\sigma^2 q^2\right) \tag{5.15}$$

For typical values of q the exponential decay can be approximated by retaining only the first term in the series expansion of the exponential. This gives a negative slope to the Iq^4 *vs* q^2 plot, and is known as negative deviation from Porod's law (**Figure 5.32 (C)**). The net scattering from real multiphase systems is given by

$$I(q) = \frac{K_p}{q^4} \exp\left(-4\pi^2\sigma^2 q^2\right) + I_b \tag{5.16}$$

(A)

$\overline{\Delta\rho^2}$

$\rho\,(r)$

$\Delta\rho$

r ⟶

(B)

$\rho\,(r)$

r ⟶

(C)

$\rho\,(r)$

r ⟶
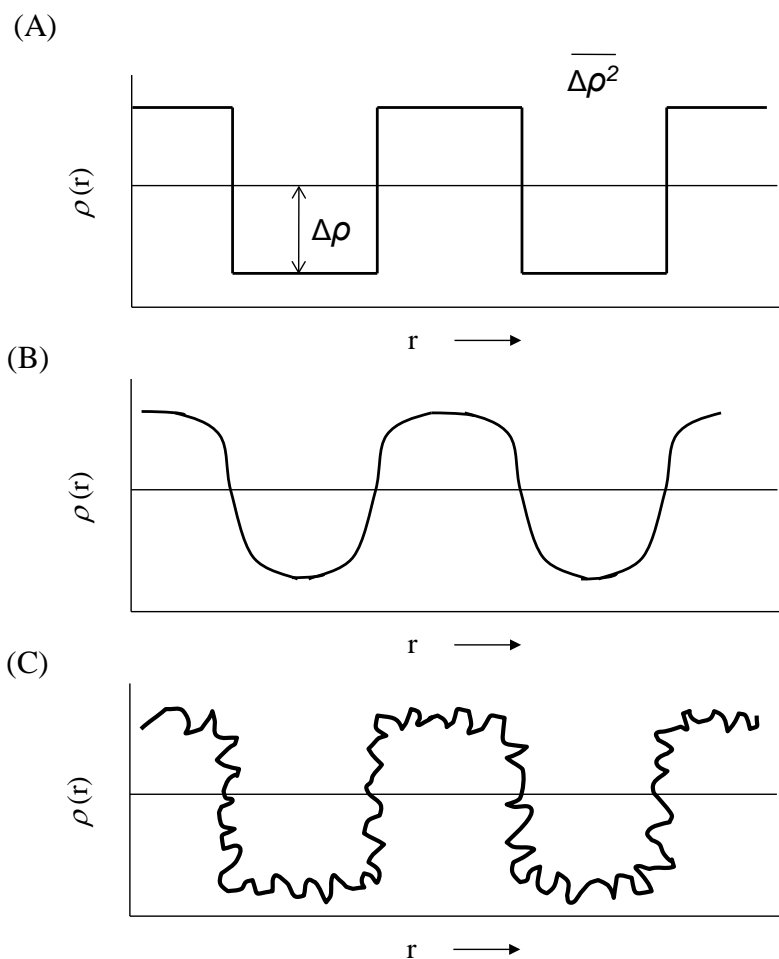
Figure 5.32 Electron density profile for (A) ideal system having sharp phase boundary, (B) system having thermal density fluctuations (C) system having diffuse phase boundary.

5.5.3 L-PUU Series

Figure 5.33 shows background corrected, normalized SAXS intensities for L-PUUs plotted in comparison with L-PU. Normalization here refers to the intensity normalization by sample volume, and is primarily carried out to compare the data for all samples. The sample volume of relevance here is the volume exposed to the x-ray beam. This is equal to the area of a circular disk of diameter equal to the beam diameter multiplied by the thickness of the compression molded sample sheet. Since the beam diameter does not change, normalization by sample volume is equivalent to normalization by the thickness of the sample.

SAXS data for all samples presented here display a peak at $q = 0.011$ Å^{-1} corresponding to the scattering from beam stop. The intensity signal above this value of q is due to scattering from sample. SAXS from polyurethanes typically shows a single peak at low q and is ascribed to the microphase separated morphology. This is an indication of short range order commonly seen in polyurethanes.[18,19] Higher order peaks are not observed because of lack of long range order such as that typically seen in microphase separated monodisperse block copolymers. **Figure 5.33** shows a single SAXS peak for each of the L-PU and L-PUU samples indicating that the microstructure is made of domains of hard and soft segments. The intensity of the peak was found to increase with the introduction of *m-phenylenediamine*, which is an indication of greater extent of phase separation in L-PUUs compared to L-PU. The brittle L-PUU100 sample could not be mounted in the sample holder and was not analyzed by SAXS.

Figure 5.34 (A) and **(B)** displays high angle (q) or Porod behavior of L-PU and L-PUUs respectively. The SAXS scaling in this region carries information about the nature of interface. The plot of $Iq4$ vs $q2$ for L-PU exhibited almost constant slope suggesting the presence of relatively sharp interfaces between the hard and soft domains. However, we see a negative deviation from porod behavior in L-PUUs, which is an indication of diffuse interfaces.

Figure 5.33 Background corrected SAXS intensities as a function of the scattering vector for L-PUUs in comparison with L-PU.
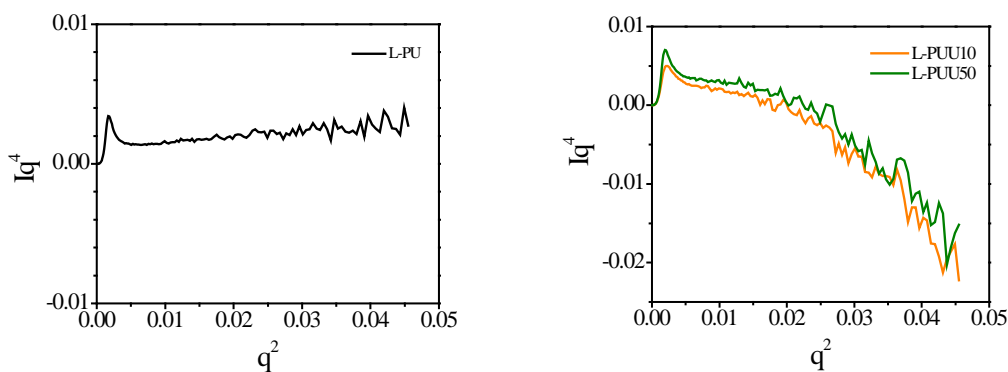
Figure 5.34 Porod behavior of **(A)** L-PU and **(B)** L-PUUs.

The SAXS data presented above when considered together with the FTIR, DSC and DMA data discussed earlier provides more detailed information about the microphase separated structure. The DSC and DMA data for L-PUUs suggested an increased extent of phase separation as indicated by the lowering of soft segment T_g, increased strength of hydrogen bonding due to urea linkages as indicated by increase in the hard segment T_g, and possible presence of a mixed phase having a segmental relaxation temperature in between those of soft and hard segments. The FTIR data suggested increased disorder in hard segment association as indicated by the increase in N-H wavenumber compared to L-PU. The disordered packing was suggested to be caused by the presence of aromatic ring in the diamine. The increase in intensity of the SAXS peak seen for L-PUUs compared to L-PU suggests relatively stronger phase segregation in the former in agreement with the DSC and DMA data. Similarly, the observance of a negative deviation from porod behavior can be ascribed to a diffused interface caused by local mixing of hard and soft segments. It is plausible that the diffused interface consists of disordered polyurea hard segments with some soft segments mixed within.

5.5.4 B12-PUU and B22-PUU Series

The SAXS patterns for B12-PUUs are presented in **Figure 5.35(A)**. Unlike L-PUUs, the B12-PUUs display a decrease in peak intensity and increase in peak width with increasing B12 diamine content. The B12-PUU100 did not show any scattering. The average periodicity (Lorentz corrected) as measured from $q^2I(q)$ vs. q plot also reduced with the increasing B12 diamine concentration. The Porod behavior of B12-PUUs seen in **Figure 5.35 (B)**, show a positive deviation for B12-PUU10 and B12-

PUU50. For B12-PUU70 the deviation is significant and is indicative of strong segmental mixing.
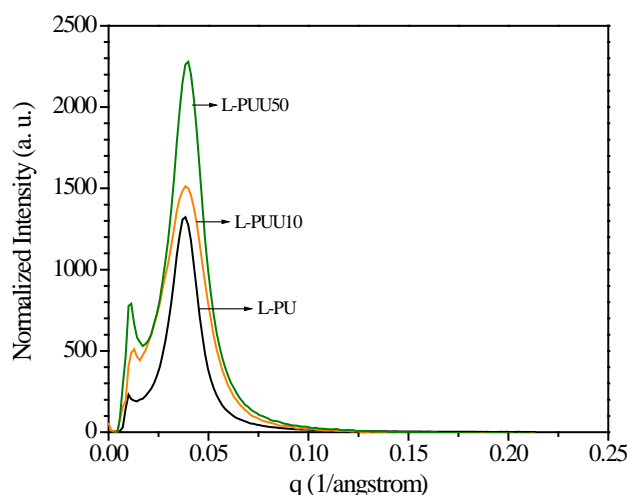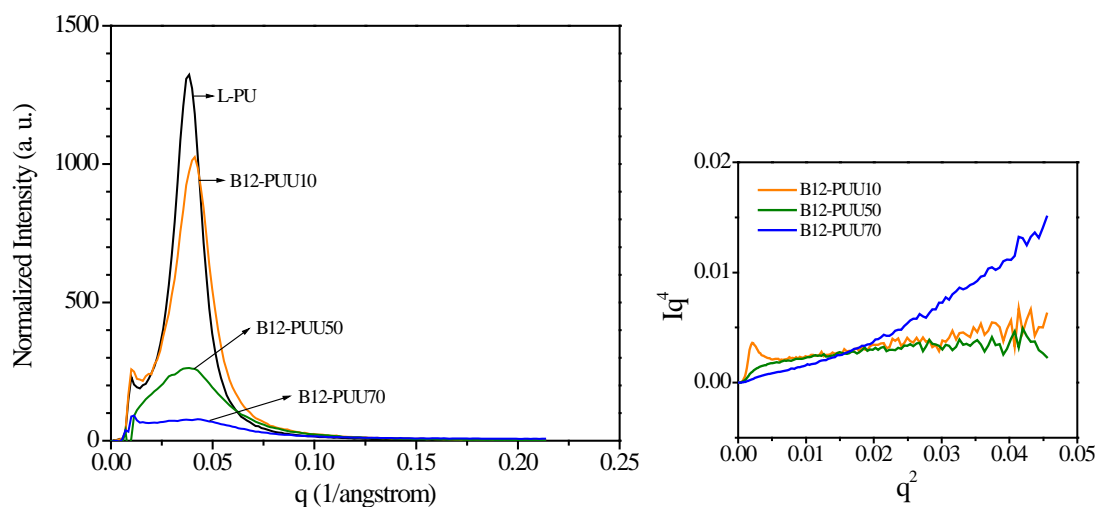

Figure 5.35 (A) Background corrected SAXS intensities as a function of the scattering vector for B12-PUUs in comparison with L-PU and **(B)** Porod behavior of B12-PUUs.

Background corrected SAXS intensities of B22-PUU10 and B22-PUU30 are plotted in **Figure 5.36 (A)** with control L-PU. As seen in the figure, only B22-PUU10 displayed a detectable peak in the small angle region with its intensity considerably reduced compared to L-PU and its q_{max} shifted to higher value. Samples B22-PUU30, B22-PUU50 and B22-PUU100 did not show any evidence of heterogeneity in the small angle region. Analysis of the Porod region of B22-PUUs (**Figure 5.36 (B),** only two polymers of the series are shown here) showed a slight positive deviation resembling that of L-PU.
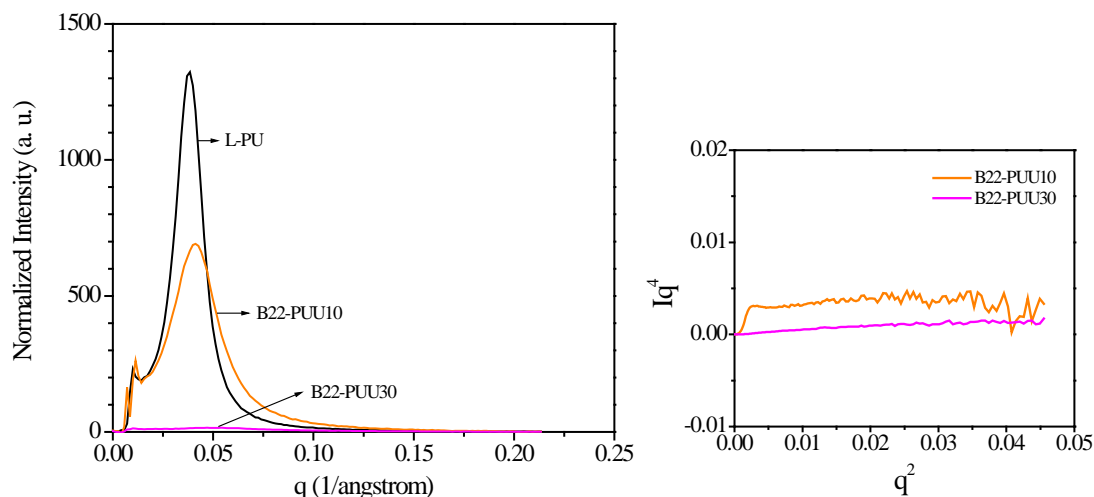
Figure 5.36 (A) Background corrected SAXS intensities as a function of the scattering vector for B22-PUUs in comparison with L-PU and **(B)** Porod behavior of B22-PUUs.

SAXS data of B12-PUUs and B22-PUUs show a common trend of decaying signal strength on incorporation of respective diamine chain extenders in contrast to what was observed for L-PUUs. Also, in the Porod region these PUUs show a positive deviation from Porod law in contrast to the negative deviation observed for the L-PUUs. These observations suggest increased phase mixing between the hard and soft segments, which is in agreement with inferences drawn from other techniques. Both DSC and DMA data had indicated an increase in soft segment T_g, increase in the width of soft segment relaxation and gradual disappearance of hard segment relaxation, all of which indicate phase mixing. The FTIR data had also shown increased disorder in hard segment packing. However, in all cases where the SAXS peak had nearly disappeared such as for B12-PUU50, B12-PUU70 and B22-PUU30 the DSC and DMA had clearly shown the presence of a soft segment T_g. Therefore, the decrease in SAXS peak intensity should be interpreted with caution. The primary reason for exercising caution is to recollect the fact that there has to be sufficient electron density contrast between the domains in order for them to be 'visible' in SAXS.

5.5.5 Electron Density Contrast

As mentioned earlier, small angle X-ray scattering is based on the difference in the electron density contrast between phases ($Q = 2\pi^2 \overline{\Delta\rho^2}$). Thus, a high electron density contrast leads to strong scattering in SAXS and vice versa. Since in the

present work the composition of the hard segment domain and hence its electron density is subjected to change upon incorporation of the diamine comonomer, it is worthwhile to calculate the electron density contrast between hard and soft segment domains with increase in diamine content. These calculations were done for the B12-PUU series only. Following equation was used for calculating the electron density of a phase.

$$\rho_{phase} = \frac{(\text{electrons} / \text{repeat unit}) \times (\text{mass density of phase}) \times N_{AV}}{\text{mol. wt. of repeat unit}} \qquad (5.17)$$

This involves calculation of electrons per repeat unit of a given phase and measurement of mass density of the phase as shown below.

Electrons / repeat unit:

1) Isophoronediisocyanate (Molecular Formula = $C_{12}H_{17}N_2O_2$)

Element	Electrons	Total electrons
C_{12}	6 x 12	72
H_{17}	1 x 17	17
N_2	7 x 2	14
O_2	8 x 2	16
Total		**119**

Electron/repeat unit of IPDI = 119

Molecular weight of IPDI = 222

The electrons/repeat unit of other components was similarly calculated. They are:

2) 1,4-Butanediol (Molecular Formula = $C_4H_{10}O_2$)

Electrons/repeat unit of BDO = 50

Molecular weight of BDO = 90

3) Polytetramethylene oxide $M_n \sim 2900$ (Repeat unit = $[-(-CH_2)_4-O]_n$)

Electrons/repeat unit = 40

Repeat unit molecular weight = 72

4) N-Dodecyl 3,5-diaminobenzoate (B12 diamine, Molecular Formula = $C_{19}H_{32}N_2O_2$)
Electrons/repeat unit of B12 diamine = 176

Molecular weight of B12 diamine = 320

Mass density:

1) Mass density of PTMO = 0.97 g/cm^3 = 0.97 x 10^{-21} g/nm^3

2) Mass density of IPDI-BDO model hard segment = 1.109 g/cm^3 = 1.109 x 10^{-21} g/nm^3 [Velankar & Cooper[10]]

3) Mass densities of B12 diamine containing model hard segments were determined at room temperature as follows. Density of the solid polymer samples was measured at ambient temperature using a density measurement accessory fitted to a sensitive weighing balance. Polymer samples were compression molded to form discs (25 mm diameter, 1.5 mm thickness) for density measurement. Density was determined by first measuring the weight of the sample in air and then in a liquid of known density. The liquid has to be a non-solvent for the polymer, and accordingly hexane was used in the present study. The ratio of weight in air to the loss of weight in liquid was used to calculate the density of the sample.

$$\text{Density} = \frac{\text{Wt. of sample in air} \times \text{Density of liquid}}{\text{Wt. of sample in air} - \text{Wt. of sample in liquid}} \qquad (5.18)$$

The densities of the B12-diamine containing model hard segments so measured were:

a) IPDI-BDO-B12 diamine (10 mol%) = 1.137 g/ml = 1.137 x 10^{-21} g/nm^3

b) IPDI-BDO-B12 diamine (50 mol%) = 1.087 g/ml = 1.087 x 10^{-21} g/nm^3

c) IPDI-BDO-B12 diamine (70 mol%) = 1.037 g/ml = 1.037 x 10^{-21} g/nm^3

The density of IPDI -B12 diamine (100 mol%) could not be determined because of the difficulties in making a sample from this highly brittle polymer.

Calculation of electron density of soft and hard phases:

Avogadro's number NAV = 6.02214x10^{23} mol^{-1}

1) *Soft Segment PTMO*

$$\rho_{phase} = \frac{(\text{electrons / repeat unit}) \times (\text{density of phase}) \times N_{AV}}{\text{mol. wt. of repeat unit}}$$

$$\rho_{ss} = \frac{(40) \times (0.97 \times 10^{-21}) \times 6.023 \times 10^{23}}{72} = 324.6 \ e^{-}/nm^{3}$$

2) *Hard Segment IPDI-BDO*

$$\rho_{hs} = \frac{((119 \times 0.54) + (50 \times 0.46)) \times (1.109) \times 602.3}{((222 \times 0.54) + (90 \times 0.46))} = 361.4 \ e^{-}/nm^{3}$$

3) *IPDI-BDO-B12 diamine (10 mol%)*

$$\rho_{hs} = \frac{((119 \times 0.54) + (50 \times 0.46 \times 0.9) + (176 \times 0.46 \times 0.1)) \times (1.137) \times 602.3}{((222 \times 0.54) + (90 \times 0.46 \times 0.9) + (320 \times 0.46 \times 0.1))} = 370.8$$

4) *IPDI-BDO-B12 diamine (50 mol%)*

$$\rho_{hs} = \frac{((119 \times 0.54) + (50 \times 0.46 \times 0.5) + (176 \times 0.46 \times 0.5)) \times (1.087) \times 602.3}{((222 \times 0.54) + (90 \times 0.46 \times 0.5) + (320 \times 0.46 \times 0.5))} = 355.3$$

5) *IPDI-BDO-B12 diamine (70 mol%)*

$$\rho_{hs} = \frac{((119 \times 0.54) + (50 \times 0.46 \times 0.3) + (176 \times 0.46 \times 0.7)) \times (1.037) \times 602.3}{((222 \times 0.54) + (90 \times 0.46 \times 0.3) + (320 \times 0.46 \times 0.7))} = 339.3$$

The electron densities of the hard segment and soft segment phases, and the electron density contrast between the two phases assuming that they are pure, are listed in **Table 5.5**. Incorporation of 10% B12 diamine increases the electron density of the hard segment phase compared to the hard segment in L-PU. However, further increase of diamine in the hard segment monotonically decreases the electron density contrast between the hard and soft domains.

Table 5.5 Electron Density Contrast for Model Hard Segment Copolymers.

Phase	Electron density of phase ρ_{hs} (e⁻/nm³)	Squared electron density contrast[*] $(\rho_{hs}\text{-}\rho_{ss})^2$ (e⁻/nm³)²
PTMO	324.6	
IPDI-BDO	361.4	1354 (L-PU)
IPDI-BDO-B12 diamine 10%	370.8	2137 (B12-PUU10)
IPDI-BDO-B12 diamine 50%	355.3	945 (B12-PUU50)
IPDI-BDO-B12 diamine 70%	339.3	216 (B12-PUU70)

[*]Assuming pure hard segment phase

Electron density contrast using phase compositions from Couchman analysis:

It has been discussed in previous sections that the presence of B12 diamine in the hard segment induces mixing of soft segments with the hard segments. The extent of phase mixing in the soft segment domain and hard segment domains was estimated from Couchman analysis presented earlier. The electron density contrast between these impure hard and soft segment domains are calculated as follows:

1) **L-PU**

$$\rho_{ss} = 1.0 \times 324.6 = 324.6 \text{ e}^-/\text{nm}^3$$

$$\rho_{hs} = 1.0 \times 361.4 = 361.4 \text{ e}^-/\text{nm}^3$$

$$\left(\rho_{hs} - \rho_{ss}\right)^2 = 1354 \text{ (e}^-/\text{nm}^3)^2$$

2) **B12-PUU10**

$$\rho_{hs} = 0.688 \times 370.8 + 0.312 \times 324.6 = 356.4 \text{ e}^-/\text{nm}^3$$

$$\rho_{ss} = 0.988 \times 324.6 + 0.012 \times 370.8 = 325.2 \text{ e}^-/\text{nm}^3$$

$$\left(\rho_{hs} - \rho_{ss}\right)^2 = 973 \text{ (e}^-/\text{nm}^3)^2$$

3) **B12-PUU50**

$$\rho_{hs} = 0.496 \times 355.3 + 0.504 \times 324.6 = 340 \text{ e}^-/\text{nm}^3$$

$$\rho_{ss} = 0.979 \times 324.6 + 0.021 \times 355.3 = 325.2 \text{ e}^-/\text{nm}^3$$

$$\left(\rho_{hs} - \rho_{ss}\right)^2 = 219 \ (e^-/nm^3)^2$$

4) B12-PUU70

$$\rho_{hs} = 0.465 \times 339.3 + 0.535 \times 324.6 = 331.4 \ e^-/nm^3$$

$$\rho_{ss} = 0.963 \times 324.6 + 0.037 \times 339.3 = 325.1 \ e^-/nm^3$$

$$\left(\rho_{hs} - \rho_{ss}\right)^2 = 40 \ (e^-/nm^3)^2$$

Table 5.6 Electron Density Contrast using Couchman Phase Compositions.

Polymer	$\left(\rho_{hs} - \rho_{ss}\right)^2 \ (e^-/nm^3)^2$
L-PU	1354
B12-PUU10	973
B12-PUU50	219
B12-PUU70	40
B12-PUU100	-
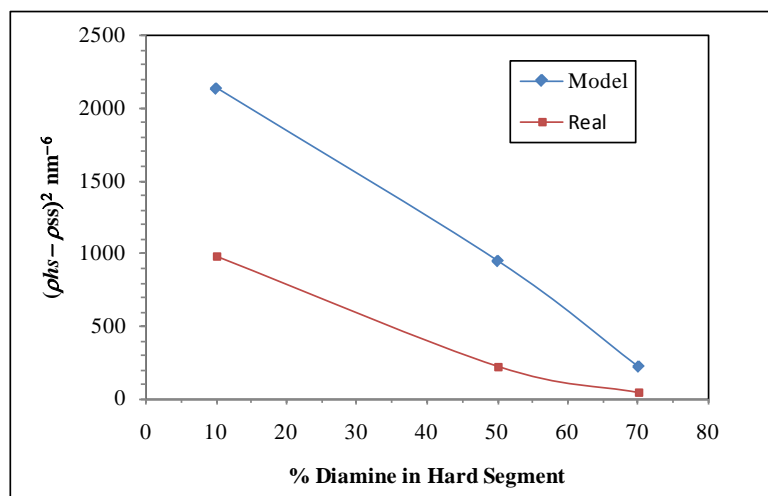
Figure 5.37 Squared electron density contrast vs B12 diamine content for model and real copolymers.

The calculated squared electron density contrast for B12-PUUs is plotted in **Figure 5.37**. Solid lines connecting the points serve merely as a guide for the eye. The first series of data labeled as 'model', is calculated (as shown above in **Table 5.5**) considering an ideal case i.e. pure phases and sharp interfaces. The second series labeled as 'real', is calculated by using phase compositions as determined from the Couchman analysis (**Table 5.6**), and represents a more accurate estimate of the

electron density contrast for B12-PUUs. The figure highlights a very important point namely that a fast decay of electron density contrast with increasing B12 diamine concentration is expected for the 'model' case. The 'real' scenario exhibits an even more pronounced decrease in the electron density contrast between the hard and soft domains of B12-PUUs.

It is evident from these calculations that the C12 pendant chain in the diamine chain extender decreases the electron density contrast in two ways: there is an intrinsic decrease in contrast with increase in diamine content from 10% onwards, and there is a further decrease in the contrast caused by mixing of soft segments in the hard segment domains due to the presence of the C12 pendant chain. The loss in SAXS peak seen in **Figure 5.35 (A)** is thus caused by loss in contrast between the hard and soft domains. It can be said that the C12 pendant chain acts like a masking agent making the microphase separation invisible to SAXS.

The disappearance of SAXS intensity peak for the B22-PUUs can also be explained qualitatively on similar arguments as the B12-PUU series. Like the B12 diamine, it is reasonable to expect attenuation of electron density contrast on insertion of B22 diamine. However, since model hard segment copolymers of B22 series were not synthesized, their mass densities and glass transition temperatures are not known. Hence calculations of electron density contrasts for the corresponding 'model' and 'real' cases are not possible. Presumably the effect of B22 incorporation is substantial as even B22-PUU30 did not show any scattering in SAXS.

It is worthwhile here to put together pieces of information of B22-PUUs, deduced from morphological techniques discussed so far. FTIR analysis tells us that the hard segments do not form ordered domains at high B22 diamine content. Soft segment T_gs from DSC as well as DMA suggests that the soft and hard segment mixing is not significant. DSC also indicates the formation of C22 crystalline domains in 50 and 100 mol% copolymer compositions. SAXS data indicates loss of electron density contrast due to aliphatic chains. On considering these facts, it is fair to speculate that for the B22-PUU50 and B22-PUU100 polymes the pendant C22 chains associate to form crystalline domains while causing disordered packing of hard segments. The enthalpy associated with this crystallization is quite high (B22-PUU= 21.95 J/g, B22-PUU=33.93 J/g), which can compensate for the disordering of the hard segment associations. The Porod behavior of B22-PUUs suggests a sharp interface

between domains. Since DSC and DMA suggest that phase mixing of hard and soft domains is not significant in this series, it is plausible that the C22 chains crystallize near the soft segment interface leaving disordered hard segments in the interior. This gives rise to the possibility of sharp interfaces between PTMO and crystalline C22 domains.

5.5.6 High Temperature Experiments

High temperature SAXS experiments were carried out on all samples to study qualitatively morphological consequences of heat treatment. The experiment was done by increasing the temperature at a rate of 5°C/min to the desired temperature, equilibrating for 2 min, recording the scattered intensity and repeating the sequence. Scans were recorded at 10°C interval, starting from room temperature. Following figures provide high temperature SAXS profiles of several samples. Polymers which did not show a clear SAXS peak were not used for high temperature measurements. For the purpose of clarity, SAXS curves are displayed at temperature intervals of 20°C.
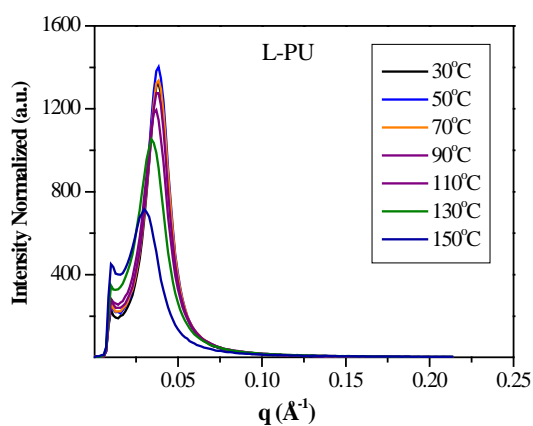
Figure 5.38 SAXS intensity vs *q*.
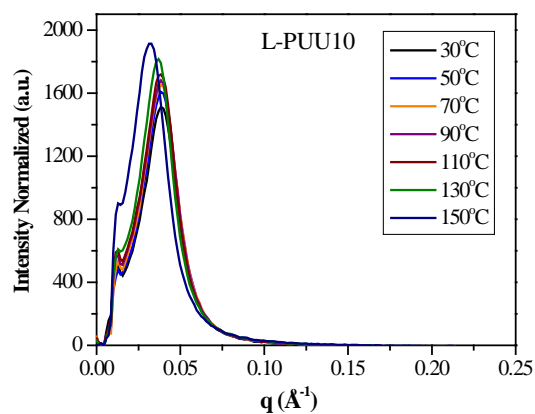
Figure 5.39 SAXS intensity vs *q*.
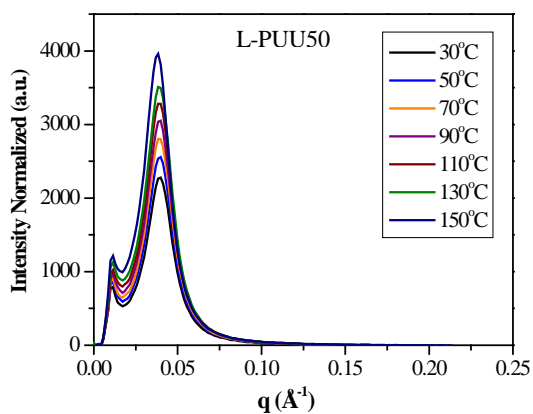
Figure 5.40 SAXS intensity vs *q*.
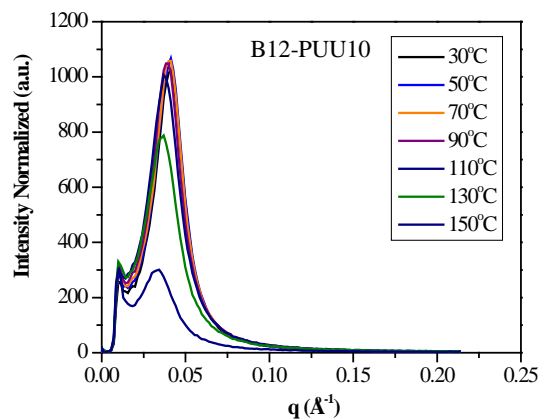
Figure 5.41 SAXS intensity vs *q*.
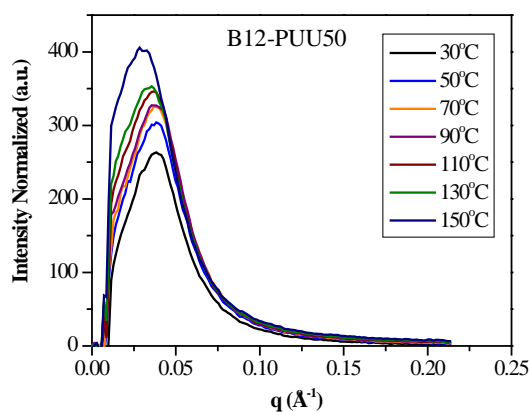
Figure 5.42 SAXS intensity vs *q*.

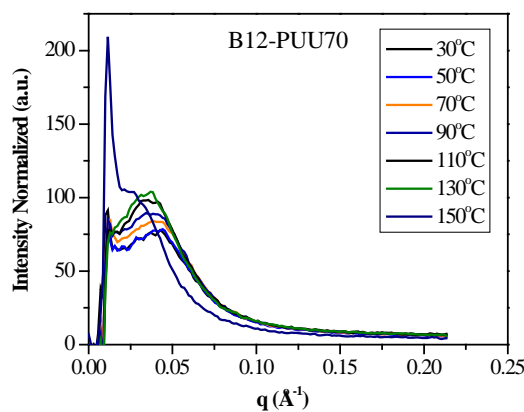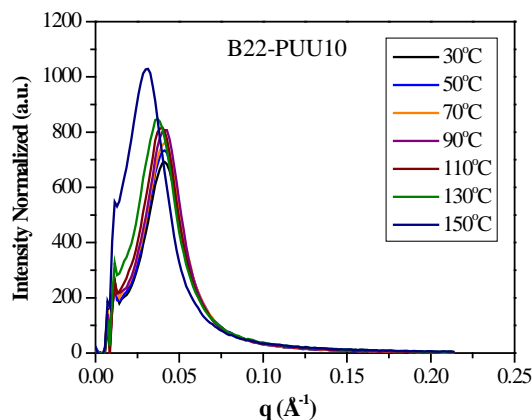**Figure 5.43** SAXS intensity vs *q*.

Figure 5.44 SAXS intensity vs *q*.

From the data presented in the above figures the average periodicity (or mean interdomain spacing) between hard domains ($d = 2\pi/q_{max}$) was calculated after Lorentz correction for every sample at each temperature. L-PU showed the highest interdomain spacing (15.7 nm at ambient temperature) among the samples under

study. The d value remained constant up to about 100°C after which it increased with temperature. The SAXS data in **Figure 5.38** showed that the position and intensity of the peak remained constant until 100°C after which the peak intensity decayed together with shifting of the peak position to lower q values.

The L-PUU10 and L-PUU50 polymers (**Figure 5.39** & **5.40**) exhibited a contrasting trend relative to the L-PU polymer. The SAXS peak intensity for these two polymers increased with temperature while the average periodicity remained more or less constant over the temperature range studied here expect at the highest temperatures (above 110°C) where the periodicity started to increase. This indicates the higher temperature stability of the microphase separated structures in L-PUU polymers.

The temperature responses of B12-PUU10 and B12-PUU50 were intermediate between those of L-PU and L-PUUs. With increasing temperature while the intensity of the SAXS peak increased like that of L-PUU, the position of the peak maximum continuously shifted to lower q values like L-PU. Lesser scattering from B12-PUU70 polymer lowers the confidence in accurate measurement of average periodicity. However it is evident that at any given temperature for the B12-PUU series the average periodicity d exhibited a systematic decrease with increasing diamine content (**Figure 5.45**). This is different from the L-PUU behaviour which showed that at any given temperature the periodicity of L-PUU50 (d = 15.2 nm at ambient temperature) was slightly higher than that of L-PUU10 (d = 14.7 nm at ambient temperature). **Figure 5.45** shows the mean domain spacing for L-PU and B12-PUUs remains almost unchanged till 100°C after which it increases steadily with temperature. Among B22-PUUs, we could only measure peak positions of B22-PUU10 with sufficient confidence. The temperature response of the microstructure in this polymer is similar to that for the B12-PUU polymers.

The decrease in interdomain spacing with B12 diamine content in the B12-PUU series is suggestive of formation of smaller (but larger number of) domains. The relative inability to form bigger domains compared to L-PU is likely due to the difficulty in ordering of the hard segments because of the presence of the C12 pendant branch. The increased packing disorder in these polymers was already suggested by FTIR data. In contrast, the L-PUUs showed slight increase in domain spacings (or formation of slightly larger domains) with increase in diamine content. FTIR

however, had indicated an increased disorder in hydrogen bonding due to the presence of diamine for these polymers.

An increase in the average periodicity with rising temperature as seen in the SAXS profiles of L-PU, B12-PUUs and B22-PUUs could originate from at least two reasons: One possibility is the thermal expansion of phases with increasing temperature thereby increasing the mean domain spacing. The other possibility is that the polymers have a distribution of domain sizes and/or packing order such that smaller or relatively more disordered domains melt (or phase mix) at lower temperatures thereby causing the mean distance between the remaining larger or more ordered domains to increase. The relative insensitivity of mean domain spacing in L-PUUs to the increase in temperature is suggestive of higher T_g or phase mixing temperature of the hard domains probably due to the presence of strongly hydrogen bonded urea linkages. On the other hand, the urea linkages in B12-PUUs and B22-PUUs are not as strongly hydrogen bonded (or are relatively more disordered) and hence have greater temperature sensitivity. The increase in intensity of the SAXS peak with temperature is also suggestive of annealing of domains (possibly larger domains annealing at the expense of smaller). However at some

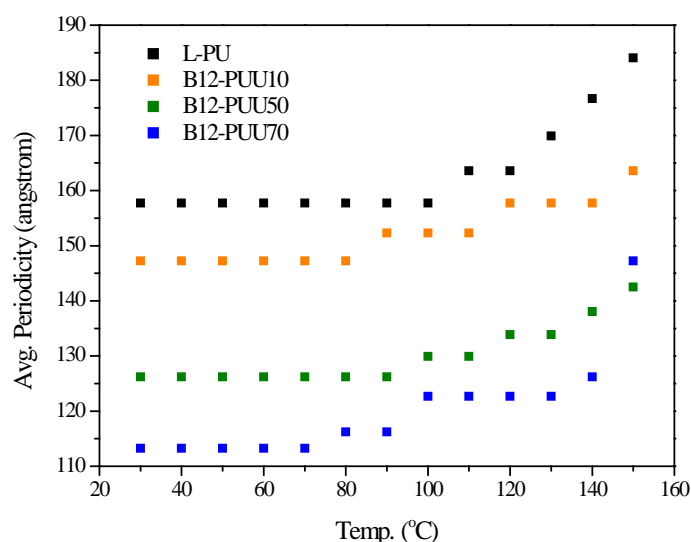high enough temperature phase mixing dominates and the intensity is expected to reduce.

Figure 5.45 Average periodicity as a function of temperature for B12-PUUs in comparison with L-PU.

5.6   Rheology

Rheological tests were performed using parallel plate geometry (8 mm diameter) on a strain controlled ARES rheometer from Rheometric Scientific. Test specimens were cut form a compression molded film and stored in air tight containers until the test. All rheological tests were carried out in the linear viscoelastic regime, which was ensured by first performing a strain sweep test on each sample. Fresh sample specimen was used for every test. Sample temperature was maintained at $\pm$ 1°C by controlled nitrogen gas flow in a forced convection oven.

Viscoelastic properties of polymers were studied by performing a set of three rheological tests on each sample. Isothermal frequency sweep, isochronal temperature sweep and isothermal time sweep. Small amplitude oscillatory frequency sweeps were carried out by shearing the sample at a constant temperature and sweeping the frequency from 0.1 to 100 rad/s. Tests were performed at a temperature interval of 10°C. In an isochronal temperature sweep test, the temperature was ramped at a rate 5°C/min while shearing the sample at a constant frequency of 1 rad/sec and at small strain amplitude (in linear viscoelastic regime). Isothermal time sweep involved shearing the sample at a constant frequency for one hour.

5.6.1   Background: Rheology basics

Among several small strain experiments used in rheological study, dynamic oscillatory tests are commonly used to characterize the frequency dependence of materials. The strain deformations applied in these experiments are sufficiently small, and thus material properties are studied in near equilibrium state. In a typical test, a sinusoidal shear deformation (γ) is applied to the sample when placed in a suitable geometry e.g. parallel plate, and resultant stress response (σ) is measured. The time scale probed is determined by the frequency of oscillation (ω) of the shear deformation. Generally when the sample is deformed sinusoidally, the response stress will also oscillate sinusoidally at the same frequency, but will be shifted by a phase angle (δ) with respect to the strain wave. The phase angle (δ) is dependent on the nature of the material. For elastic solid $\delta = 0$, for viscous fluid $\delta = \pi/2$, and for viscoelastic material $0 < \delta < \pi/2$.

In a typical frequency sweep experiment, the sample is placed between two parallel plates (or in between a cone and a plate) as shown in **Figure 5.46 (A)**. While the top plate remains stationary, a motor rotates the bottom plate, thereby imposing a time dependent strain $\gamma(t) = \gamma_0 \sin(\omega t)$ on the sample. Simultaneously, the time dependent stress $\sigma(t)$ is quantified by measuring the torque that the sample imposes on the top plate. For a sinusoidal strain deformation the stress response of a viscoelastic material is given by

$$\sigma(t) = G'(\omega)\gamma_0 \sin(\omega t) + G''\gamma_0 \cos(\omega t) \qquad (5.19)$$

where the elastic modulus (G'), also called the storage modulus, describes the storage of energy in the structure, and the viscous modulus (G''), also called the loss modulus, describes the part of the energy which is lost as viscous dissipation. Therefore, in an oscillatory experiment, the primary aim is to calculate the two modulli (G' and G'') as a function of frequency and the phase angle given by $\tan \delta = G''/G'$.

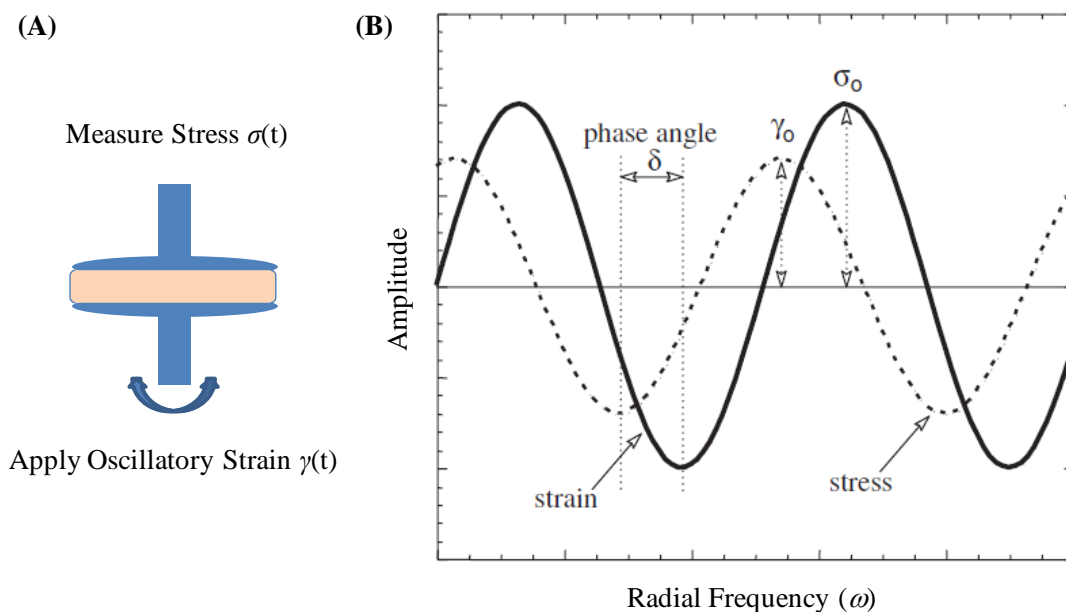**Figure 5.46 (A)** Schematic of a rheometer; **(B)** Oscillating strain and stress response.[25]

Temperature is a measure of molecular motion. The interdependence of time and temperature was explored by M.L. Williams, R.F. Landel, and J.D. Ferry. They provided a theoretical understanding of the temperature dependence of time constants (relaxation times) that bring the material to equilibrium state. The William-Landel-

Ferry (WLF) equation (eq'n 5.21) expresses a logarithmic relationship between time and temperature. The time-temperature superposition (TTS) principle states that for viscoelastic materials, time and temperature are equivalent to the extent that data at one temperature can be superimposed on data at another temperature by shifting the curves along the log time axis. This allows measurements made at different temperatures to be superposed onto a single master curve by multiplying the time or frequency axis by a shift factor (a_T), which represents the temperature sensitivity of relaxation times. Following **Figure 5.47** illustrates the application of TTS to generate master curve.
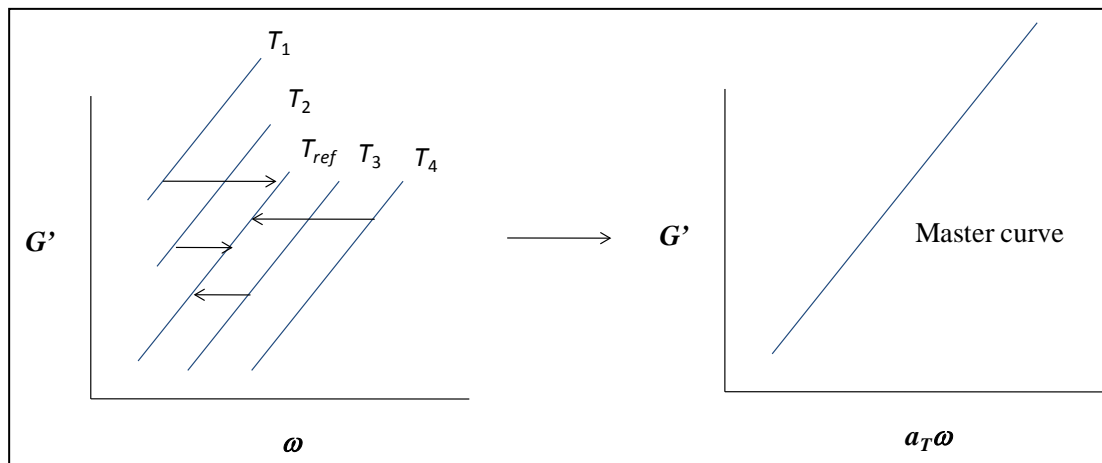
Figure 5.47 Dynamic frequency sweep data generated at different temperatures superposed on a reference temperature T_{ref} by application of TTS to create master curve.

The WLF equation for shift factor a_T is given by

$$\log(a_{T_g}) = \frac{-C_1\left(T - T_g\right)}{C_2 + \left(T - T_g\right)} \tag{5.20}$$

The values of $C_1 = 17.66\,\text{K}$ and $C_2 = 51.6\,\text{K}$ have been known to work well for a large number of polymers. TTS using eq (5.20) has been shown to work well from T_g onwards. Often the temperature dependence of shift factor is also expressed as an Arrhenius law give by

$$\log(a_T) = \frac{E_A}{R}\left(\frac{1}{T} - \frac{1}{T_{ref}}\right) \tag{5.21}$$

However, eq (5.21) works only for temperatures $T_{ref} \gg T_g$.

TTS is extremely useful to experimentalists as it allows for extrapolation of rheological data to frequencies which not easily accessible experimentally. By applying TTS one can predict material response at time scales either much longer or much shorter than measured by conventional rheometry. Fluids for which linear viscoelastic data, such as G' and G'', superimpose at different temperatures are said to be 'thermorheologically simple'. Generally, amorphous, single component polymers obey the principle of TTS. Thus in the case of phase separated systems having multiple T_gs and different temperature dependence of relaxation times for each phase, the methodology of TTS is not expected to work. For the present study, we have used TTS as independent test of phase segregation.

5.6.2   L-PU and B12-PUU Series

Figure 5.48 shows isothermal time sweep experimental data of storage modulus for L-PU as at various temperatures. A decrease in G' upon increasing temperature is quite apparent. The figure shows that the storage modulus gradually increases upon holding the sample at temperatures above the hard segment T_g. The rate of increase in G' is high for temperatures below 100°C and above 160°C. Below 100°C where the polymer is in phase segregated state, annealing of microstructure could be responsible for an increase in the G'. Between 100°C and 140°C annealing is countered by phase mixing as evidenced from DMA, high temperature FTIR and high temperature SAXS measurements. At still higher temperatures of 160°C and 180°C inception of cross linking reactions (allophanate and biuret) could be the reason for the sharp rise observed in the G'. It is known that at temperatures ~150°C these reactions occur at an appreciable rate.

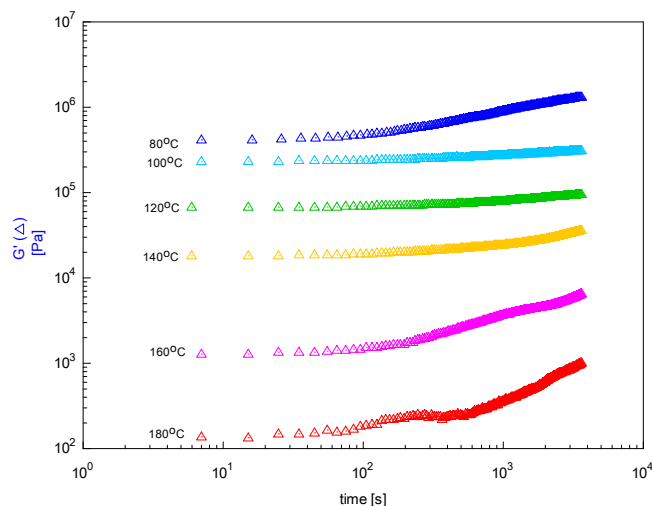An analogous time sweep behavior was noted for B12-PUUs and can be explained by the same reasoning.

Figure 5.48 Time sweep curves of L-PU at different temperatures. Frequency = 1 rad/s.

For the present study, viscoelastic behavior of samples was studied primarily 1) as an independent tool for validation of morphological heterogeneity and 2) to qualitatively monitor phase transition in the samples, if any. Polyurethane literature reports some examples of rheological studies carried out in this direction.[10,18,20] Dynamic storage and loss moduli in a frequency sweep test, particularly the terminal region ($\omega \ll \omega_c$) can yield valuable information about the microstructure. Rheologically simpler fluids are identified by a characteristic scaling response in the terminal region i.e. $G' \sim \omega^2$, $G'' \sim \omega$. Presence of a second phase however is known to lead to a deviation from this behavior and slopes of $G' \sim G'' \sim \omega^{0.5}$ have been observed for $T < T_{MST}$ where T_{MST} is the temperature at which transition from a phase mixed to a microphase separated state occurs (also called as microphase separation transition).[21-23]

Figure 5.49 provides an example of dynamic frequency sweep tests carried out on L-PU samples by keeping constant strain and varying the frequency (0.1-100 rad/s). For all polymers frequency sweep response was studied in a temperature window of 70°C to 150°C and the same data was also used to generate TTS mastercurves. Each frequency sweep measurement took about 12 minutes, i.e., 720 s to complete. Based on the isothermal time sweep data presented above (**Figure 5.48**) it can be said that the rheological properties of the polymer are likely to change during the duration of the frequency sweep test. The change may be considerable below 100°C but almost negligible for temperatures between 100°C and 150°C. This may

have an effect on TTS. However, the same is neglected in the TTS analysis presented later.

Figure 5.49 (a) and **(b)** displays dynamic modulli at lower temperatures and it can be seen that the modulli have almost equal slopes in the terminal region. In contrast, the behavior at higher temperatures **Figure 5.49 (c)** and **(d)** is different with the frequency scaling of *G'* and *G"* approaching the characteristic homogeneous fluid response, as indicated at the bottom of the figures.

(a) 70°C: *G'*~$\omega^{0.38}$, *G"*~$\omega^{0.35}$

(b) 80°C: *G'*~$\omega^{0.35}$, *G"*~$\omega^{0.38}$

(c) 120°C: *G'*~$\omega^{1.10}$, *G"*~$\omega^{0.70}$

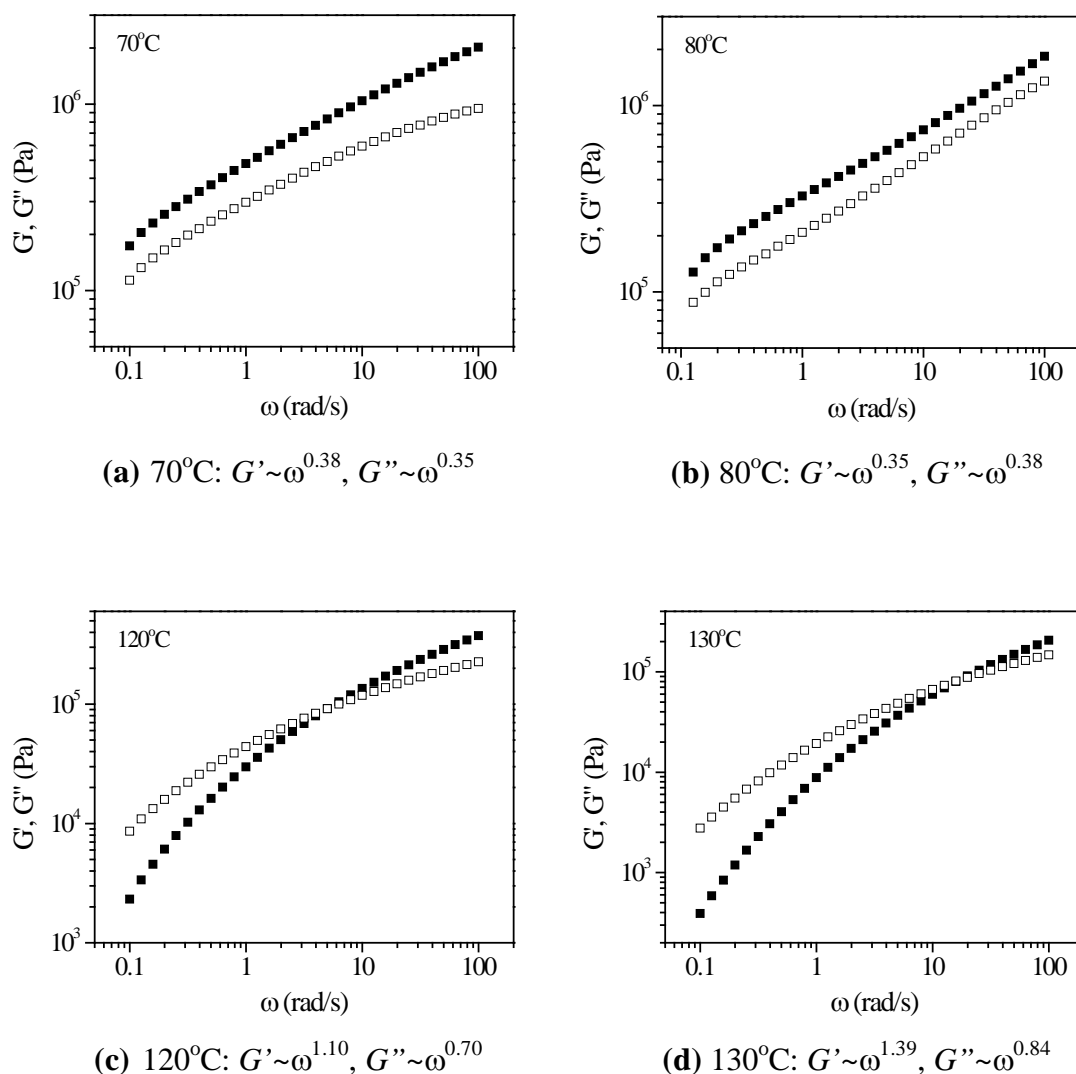**(d)** 130°C: *G'*~$\omega^{1.39}$, *G"*~$\omega^{0.84}$

Figure 5.49 Frequency sweep response of L-PU at different temperatures. *G'* (filled squares) and *G"* (empty squares).

The equal scaling of moduli at 70°C and 80°C can be reasonably ascribed to the phase segregated morphology. Upon increasing the temperature, there is a clear

indication of a transition from ordered state to the disordered one as seen in the moduli scaling. The TTS methodology provides yet another way to investigate the temperature dependence of phase morphology. Following Velankar and Cooper[10] the methodology used for TTS of frequency sweep data on the polymers studied here is as follows. For an arbitrarily chosen reference temperature the shift factor is given by

$$\log(a_T) = \log(a_{T_g}) - \log(a_{T_{ref}})$$
(5.22)

Here, the first term of the right side of eq (5.22) is given by eq (5.20) and the second term is obtained by substituting $T = T_{ref}$ in eq (5.20). In the present work the reference temperature has been chosen to be $T_{ref} = 100\,^{o}C$. The value of T_g is calculated from the Couchman eq(5.1). Thus it is assumed that the polymer has a single, fully mixed phase. The frequency sweep data is horizontally shifted using the shift factors obtained from eq(5.22). Thus it can be expected that TTS will fail for PUs and PUUs in which the hard and soft phases are strongly segregated. Similarly, TTS will improve with increased extent of phase mixing. The following discussions are limited to only L-PU and B12-PPU series for which calculations of single phase T_g were possible since the corresponding model hard segment glass transitions were prepared and characterized.

Figure 5.50 shows TTS for L-PU obtained by using the above procedure. It is clear that the frequency sweep data at various temperatures do not superpose to produce a mastercurve. The loss modulli in the figure are arbitrarily shifted up in order to show the two sets of curve more clearly. The shift factors calculated from eq(5.22) are listed in **Table 5.7**. For B12-PUU10 the superposition of isothermal frequency sweep data is shown in **Figure 5.51** where it can be seen that TTS nearly works to produce a single mastercurve for both modulli. The superposition is complete for B12-PUU50 and B12-PUU70 as seen in **Figures 5.52** and **5.53**. The shift factors for the B12-PUUs are listed in **Table 5.7**.

It is evident that the strongly phase segregated morphology of L-PU as detected by several techniques presented earlier is responsible for the failure of TTS to produce a mastercurve. The data for the lowest three temperatures superpose completely but the data at other temperatures do not superpose, thus indicating the possibility of a separate low-temperature branch as seen for diblock or tri-block copolymers. The failure of superposition at temperatures above $100\,^{o}C$ suggests that

the microphase separated morphology persists at higher temperature. High temperature SAXS data presented earlier however did indicate a gradual disappearance of the short range order above 100°C. This is however not reflected in the TTS. It is worth noting here that instead of calculating T_g of the polymer using eq (5.22), if it were to be used entirely as a fit parameter then a value of $T_g = 42^{o}$C gives rise to the TTS mastercurve shown in **Figure 5.54**. It appears here that the TTS principle indeed works if the glass transition temperature of the polymer were chosen to be nearly equal to that of the hard domain.

In case of B12-PUUs the polymer containing 10 mol% B12 diamine showed failure of TTS although to a considerably lower extent than that observed for L-PU. The corresponding SAXS data had shown a distinct peak indicating substantial extent of short range order. DSC and DMA data had suggested presence of a relatively pure soft phase, while FTIR and Couchman analysis had indicated respectively increased disorder in hard segment packing and some amount (~30%) of mixing of soft segments in the hard domains. The polymers containing 50 mol% and 70 mol% diamine showed complete success of TTS to produce mastercurves. The corresponding SAXS data for these two polymers had shown a significantly subdued signal for short range order. This was however attributed to the loss in electron density contrast. DSC and DMA data, and Couchman analysis of this data, had suggested that there is an increased tendency of mixing between the hard and soft segments, especially in the hard domain phase in these polymers. However all indicators of microphase morphology did suggest the existence of a phase segregated state. Hence the success of TTS for the B12-PUUs is indeed surprising. It seems that mixing of greater than 30% of soft segments in the hard domain phase (as seen from Couchman analysis) was enough to cause TTS to work. The above discussions suggest that the success of TTS is determined by the temperature dependence of hard segment mobility and it is perhaps not always a sensitive indicator of microphase separation in polyurethane polymers.

Table 5.7 Shift factors for L-PU and B12-PUUs.

L-PU		B12-PUU10		B12-PUU50		B12-PUU70	
$T_{g,ss}$ (K)	179	$T_{g,ss}$ (K)	179	$T_{g,ss}$ (K)	179	$T_{g,ss}$ (K)	179
$T_{g,hs}$ (K)	317	$T_{g,hs}$ (K)	359	$T_{g,hs}$ (K)	410	$T_{g,hs}$ (K)	422
T_g (K)*	260	T_g (K)*	285	T_g (K)*	315	T_g (K)*	322
T (^{o}C)	a_T	T (^{o}C)	a_T	T (^{o}C)	a_T	T (^{o}C)	a_T
60		60	415.14	60		60	
70	17.28	70	60.89	70		70	
80	5.86	80	12.31	80	71.38	80	141.42
90	2.28	90	3.19	90	6.82	90	9.10
100	1.00	100	1.00	100	1.00	100	1.00
110	0.48	110	0.37	110	0.20	110	0.16
120	025	120	0.15	120	0.05	120	0.036
130	0.14	130	0.07	130	0.016	130	0.0098
140	0.082	140		140	0.006	140	0.0032
150	0.051	150		150		150	

$$^{*}T_g = \frac{w_{ss}T_{g,ss} + \alpha.w_{hs}T_{g,hs}}{w_{ss} + \alpha.w_{hs}}$$
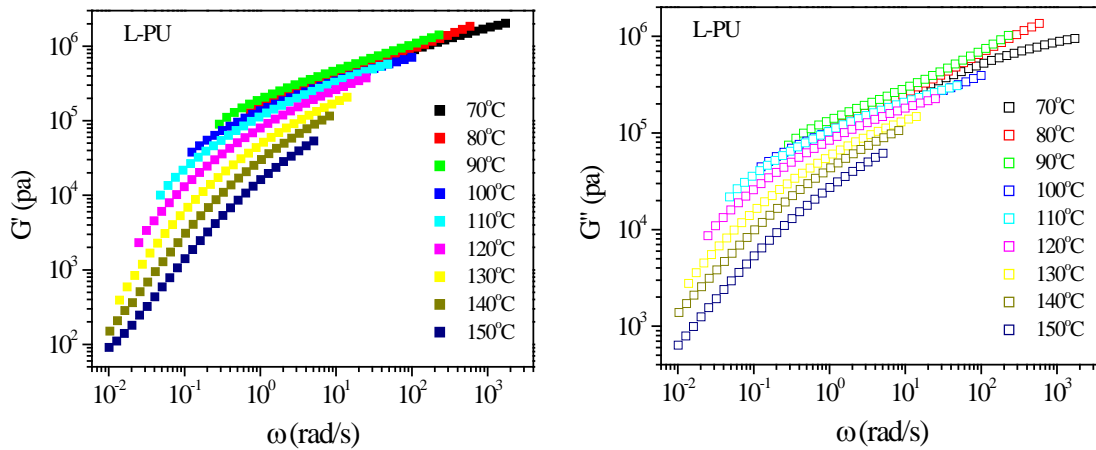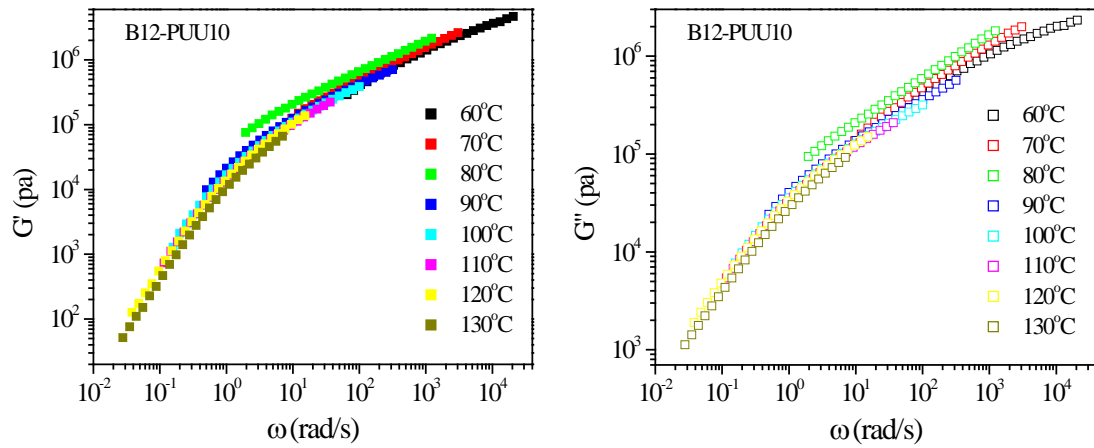

Figure 5.50 TTS for L-PU. $T_{ref} = 100^{o}$C.

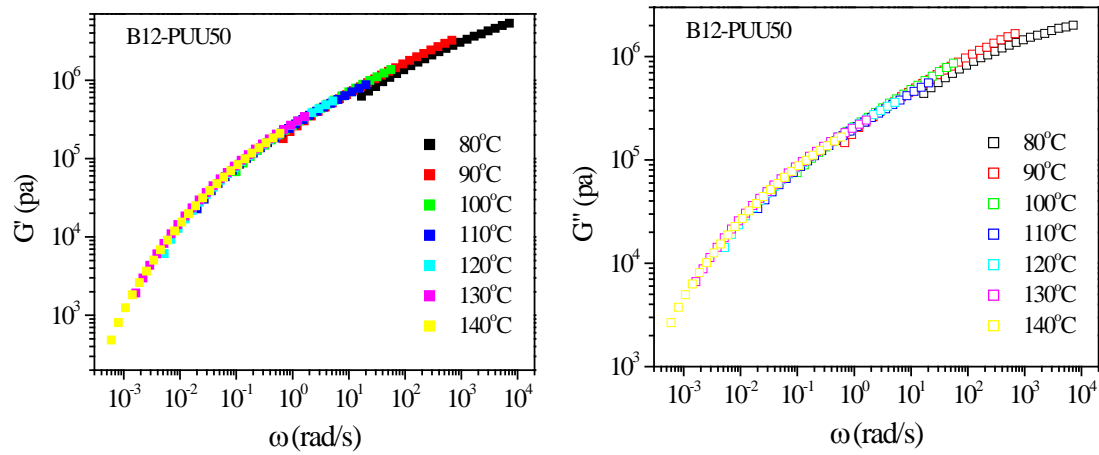**Figure 5.51** TTS for B12-PUU10. $T_{ref} = 100^{\circ}C$.
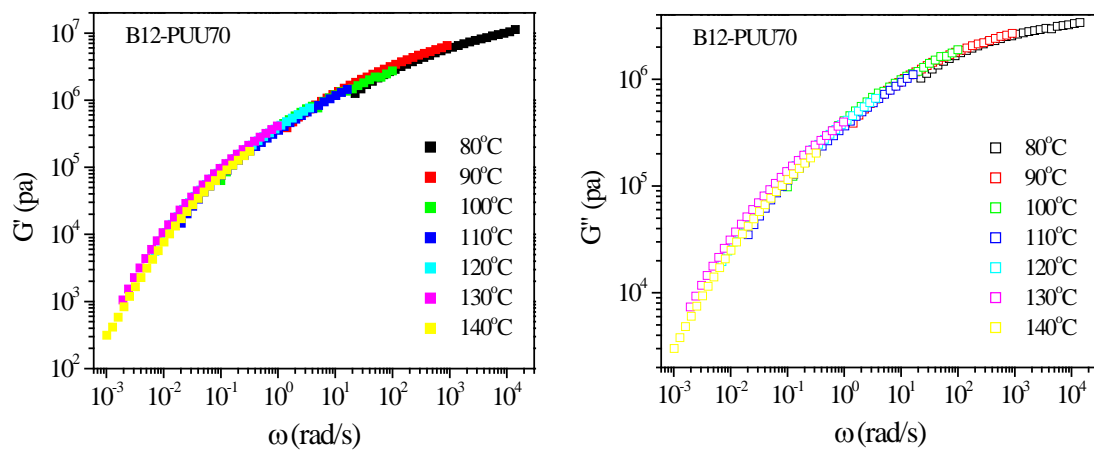

Figure 5.52 TTS for B12-PUU50. $T_{ref} = 100^{\circ}C$.
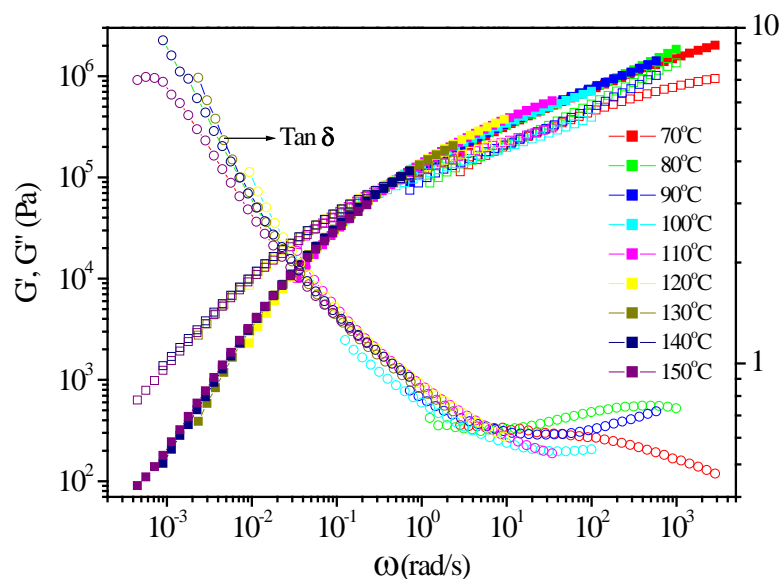

Figure 5.53 TTS for B12-PUU70. $T_{ref} = 100^{\circ}C$.

Figure 5.54 Time-temperature-superposition master curve for L-PU, $T_{ref.}$ = 100°C. *G'* (filled squares), *G"* (open squares), tan *δ* (open circles).

5.7   Tensile Testing

Tensile testing of polymers studied here was performed using a microtensile tester (Linkam Scientific, Model TST350) at ambient temperature. Samples were gripped between two clamping plates which were driven by a stepper motor in opposite directions at equal speed. The distance traveled was measured using a LVT sensor and the force required for pulling on the specimen was measured using a 200 N load cell. The testing speed was set at 500 μm/s. Non standard dog bone shaped film specimens having a central test region 3.0 mm wide and approximately 0.3 mm thick were used for tensile measurements. Specimens were cut from compression molded sheets using a home-made punch cutter consisting of a pair of razor blades formed into the requisite shape. A minimum of five specimens were tested for each polymer. Data is reported in the form of engineering stress versus engineering strain. While data till yield point was reasonably reproducible, the strain hardening region was not highly reproducible. Better reproducibility in the strain hardening regime can be obtained by plotting the true stress versus true strain data. This was however not done in the present work. The ultimate (or break) properties themselves, i.e., strain to break and stress to break could not be measured since most specimens did not break even at the maximum strain that the machine could impose. Also, possibilities of sample

slippage from grips increase at large strains. Hence the large strain data is not considered to be very reliable and is not discussed much here. An example of raw data is shown in **Figure 5.55** for L-PUU10 and B12-PUU10.

Figure 5.56 compares the stress-strain plots for L-PUU polymers. Increase in the content of m-phenylenediamine from 10 mol% to 50 mol% causes an increase in the yield stress and a decrease in the elongation to break. The initial modulus also increased marginally from ca. 0.7 MPa for 10 mol% to ca. 1.2 MPa for 50 mol%. Both polymers showed a diffused yield transition indicating reduced mobility and spatial delocalization of stress. The L-PUU10 showed strain hardening after yield while the L-PUU50 did not show any significant strain hardening.

Figure 5.57 compares the stress-strain plots for the B12-PUU series. The B12-PUU10 polymer showed a clear yield transition with a significant post yield stress drop followed by strain hardening. With increase in the B12 diamine content the yield stress decreased, the initial modulus decreased and the yield transition became diffused. For the B22-PUU series, as seen in **Figure 5.58**, there was a dramatic decrease in yield stress, initial modulus and strain hardening with increase in the B22 diamine content from 10 mol% to 30 mol%. However, further increase in the diamine content increased the yield stress, modulus and tendency to strain harden.

The morphological characterization of the various polymers studied here was discussed in previous sections. It was seen that for L-PUUs the hard domains became stiffer due to increase in urea linkages. Mixing of soft and hard segments occurred to a limited extent and was suggested to be located in the diffuse interface between the domains. It has been suggested that phase mixing tends to decrease energy storage while increasing the viscous or dissipative processes.[24] In case of L-PUUs the decrease in phase mixing compared to L-PU and the increase in hard segment rigidity is likely to have caused the increase in yield stress and initial modulus. B12-PUUs present a contrasting case. With increase in B12 diamine content the hard segments became increasingly disordered and phase mixed with soft segments. Mixing is not restricted to just an interfacial layer but occurs in the bulk. This reduces the energy storage mechanism and increases the viscous dissipative processes. As a result the yield stress, initial modulus and strain hardening tendency decreased with increasing diamine content in these polymers. In case of B22-PUU series the drop in yield stress, initial modulus and magnitude of strain hardening when going from 10 mol% to 30%

in B22 diamine content can be argued on similar lines of increased hard segment disorder and phase mixing as corroborated by FTIR and thermo-mechanical evidence presented earlier. With further increase in the diamine content crystallization of the diamine was noticed. A corresponding increase in yield stress and modulus was observed for the 50 mol% and 100 mol% B22-PUU polymers. **Table 5.8** summarizes the yield stress and initial modulus of all polymers for which tensile measurements were performed.
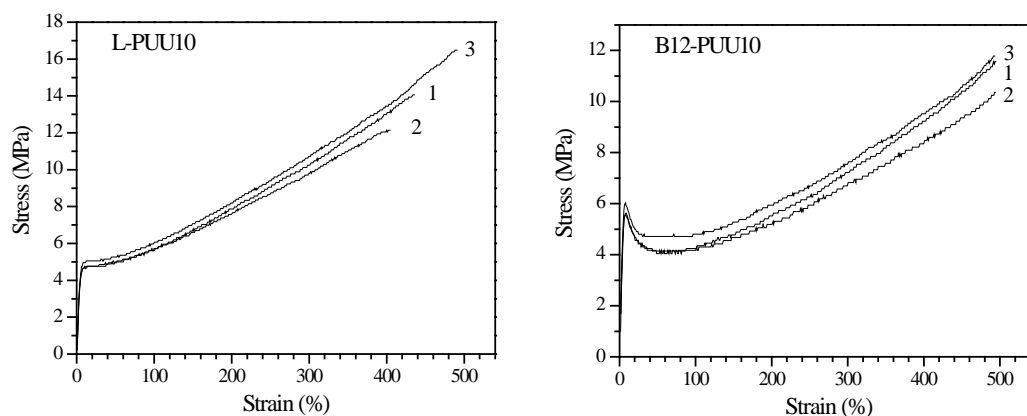

Figure 5.55 Engineering stress-strain data for two representative polymer samples (L-PUU10 and B12-PUU10) studied in this work.
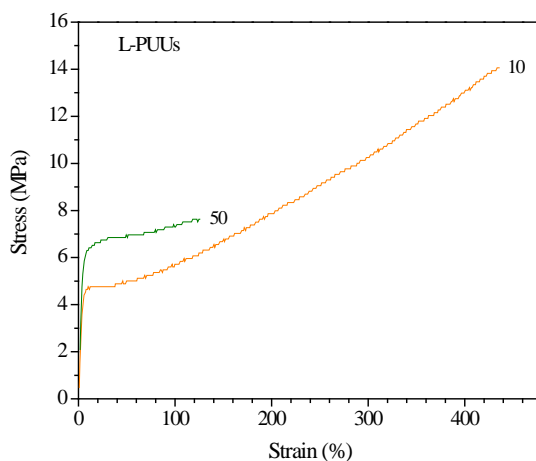

Figure 5.56 Stress-strain behaviour of L-PUUs.
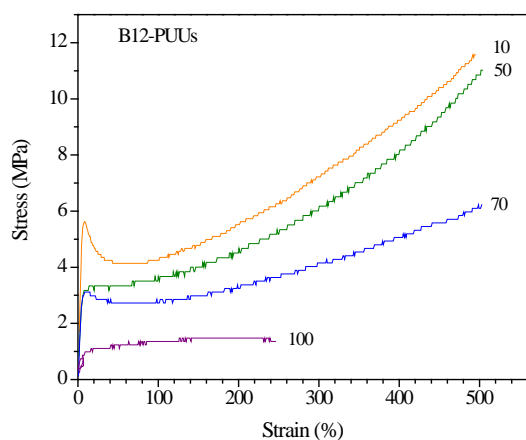
Figure 5.57 Stress-strain behavior of B12-PUUs.
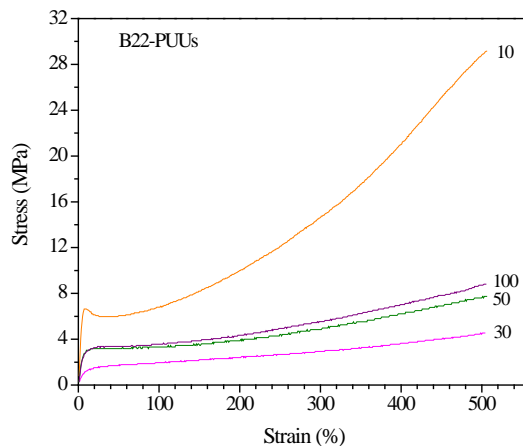
Figure 5.58 Stress-strain behavior of B22-PUUs.

Table 5.8 Tensile testing results of PUU films.

Sample	Tensile strength at yield (MPa)	Initial modulus (MPa)
L-PUU10	4.8	0.7
L-PUU50	6.2	1.2
B12-PUU10	5.4	1.0
B12-PUU50	3.3	0.6
B12-PUU70	3.2	0.7
B12-PUU100	0.67	0.1
B22-PUU10	6.2	1.0
B22-PUU30	1.3	0.2
B22-PUU50	3.4	0.5
B22-PUU100	3.1	0.5

References:

(1)   Coleman, M. M.; Lee, K. L.; Skrovanek, D. J.; Painter, P. C. *Macromolecules* **1986**, 19, 2149.

(2)   Coleman, M. M.; Skrovanek, D. J.; Hu, J.; Painter, P. C. *Macromolecules* **1988**, 21, 59.

(3)   Mattia, J.; Painter, P. C. *Macromolecules* **2007**, 40, 1546.

(4)   Yilgor, I.; Yilgor, E.; Guler, G. I.; Ward, T. C.; Wilkes, G. L. *Polymer* **2006**, 47, 4105.

(5)   Yilgor, I.; Mather, B. D.; Unal, S.; Yilgor, E.; Long, T. E. *Polymer* **2004**, 45, 5829.

(6)   Yilgor, E.; Burgaz, E.; Yurtsever, E.; Yilgor, I. *Polymer* **2000**, 41, 849.

(7)   Yilgor, I.; Yilgor, E. *Polym. Rev.* **2007**, 47, 487.

(8)   Teo, L. S.; Chen, C. Y.; Kuo, J. F. *Macromolecules* **1997**, 30, 1793.

(9)   Yoon, P. J.; Han, C. D. *Macromolecules* **2000**, 33, 2171.

(10)   Velankar, S.; Cooper, S. L. *Macromolecules* **1998**, 31, 9181.

(11)   Ungar, G. *Macromolecules* **1986**, 19, 1317.

(12)   Sirota, E. B. *Langmuir* **1997**, 13, 3849.

(13)   Sirota, E. B.; King Jr., H. E. *Science* **1998**, 281, 143.

(14)   Sirota, E. B.; Singer, D. M. *J. Chem. Phys.* **1994**, 101, 10873.

(15)   Sirota, E. B.; Herhold, A. B. *Science* **1999**, 283, 529.

(16)   Couchman, P. R. *Macromolecules* **1978**, 11, 117.

(17)   Bates, F. S.; Fredrickson, G. H. *Annu. Rev. Phys. Chem.* **1990**, 41, 525.

(18)   Ryan, A. J.; Macosko, C. W.; Bras, W. *Macromolecules* **1992**, 25, 6277.

(19)   Velankar, S.; Cooper, S. L. *Macromolecules* **2000**, 33, 382.

(20)   Nichetti, D.; Grizzuti, N. *Polym. Eng. Sci.* **2004**, 44[8], 1514.

(21)   Widmaier, J. M.; Meyer, G. C. *Polym. Sci. , Polym. Phys. Ed.* **1980**, 18, 2217.

(22)   Bates, F. S. *Macromolecules* **1984**, 17, 2607.

(23)   Adams, J. L.; Graessley, W. W.; Register, R. A. *Macromolecules* **1994**, 27,

6026.

(24)   Sormana, J. L.; Maredith, J. C. *Macromolecules* **2004**, 37, 2186.

(25)   *Rheology for Chemists An Introduction*, 2nd Ed., Jim W Goodwin, Roy W
Hughes, 2008.

Conclusions and Future Work

Chapter - 6

6.1   Conclusions

Design and synthesis of diamine chain extenders *n-dodecyl 3,5-diaminobenzoate* and *n-docosyl 3,5-diaminobenzoate*, having different length of pendent branch, starting from *3,5-dinitrobenzoylchloride* was successfully carried out. The pendent aliphatic branch in the two diamines respectively consisted of linear, saturated hydrocarbon chains of twelve and eighteen carbons. The diamines were obtained in high purity and good yields. The compounds were characterized by elemental analysis and spectroscopic techniques. *n-docosyl 3,5-diaminobenzoate* is a new compound synthesized in this work; the synthesis of this diamine is not yet reported.

Additionally, linear polyurethane and a series of linear polyurethane-ureas (with *m-phenylenediamine* chain extender) were synthesized via conventional two-step solution polymerization scheme. These polymers served as control or benchmark samples in understanding morphological consequences of incorporation of aliphatic pendant branches on the hard segment. Spectroscopic characterization and molecular weight analysis of synthesized polymers revealed respectively the evidence of formation of urea linkages and build up of sufficiently high molecular weight.

Two series of short chain branched polyurethane-ureas namely, B12-PUUs and B22-PUUs were synthesized by incorporation of pendent aliphatic chains on the hard segments. An equivalent hard and soft segment composition was maintained in order to achieve maximum phase separation. Also, a series of model hard segment copolymers was synthesized by using IPDI and a combination of *1,4-butanediol* and *n-dodecyl 3,5-diaminobenzoate* in similar compositions as used in B12-PUUs. Glass transitions of these hard segment copolymers were found to increase with the concentration of diamine. Whereas, a progressive decrease in the mass density of these copolymers was observed.

Morphology of PUUs was investigated to understand the role of systematic variation of the amount and the length of the aliphatic chain in hard segment. The morphologies of three series of PUUs were characterized at molecular, mesoscopic and macroscopic length scales.

On the basis of the detection of the ordered hard segment hydrogen bonding and the observation of two glass transitions in DSC and DMA, we conclude that the

control polyurethane sample L-PU synthesized in this study has a microphase separated hard and soft phase morphology. Signature of soft segment crystallization as seen in 2nd heat DSC scan also suggests purity of PTMO phase in the sample. The presence of microphase separated morphology was validated by SAXS and rheological analysis. L-PU showed a strong scattering in small angle region with average domain periodicity of 15.7 nm and the presence of a sharp phase interface. The sample displayed highest average periodicity possibly resulting from greater hard segment ordering. There is a correlation seen in the high temperature FTIR and the SAXS data of this sample. On heat treatment, hard segment hydrogen bonding changes from a relatively more ordered state to an increasingly disordered state. The average interdomain spacing increases with temperature, especially above 100°C. Both evidences suggest gradual mixing of hard segments with soft segments with increase in temperature. Rheological studies showed failure of time-temperature-superposition (TTS) over the entire range of temperatures thereby independently supporting microphase segregated morphology.

Presence of strong hard segment hydrogen bonding is also observed for L-PUUs. However, the strength of the N-H hydrogen bonds was found to be lower than that of L-PU as suggested by shifting of bonded N-H absorption peak to higher wavenumbers with increasing concentration of *m-phenylenediamine*. This is thought to be due to introduction of a defect or kink in the form of aromatic ring in hard segments resulting in formation weaker hydrogen bonds than L-PU. Experimental findings from DSC, DMA and SAXS indicate enhanced phase separation in this series of PUUs. DSC and DMA provide a clear evidence of a relatively pure soft segment phase as suggested by the reduced soft segment T_gs compared to L-PU. L-PUU50 sample displayed a peak due to soft segment crystallization. Increased hard segment T_gs for these samples were more clearly resolved in DMA. One would expect an increase in hard segment T_gs from a similar trend seen in the model hard segment copolymers synthesized using B12-diamine. Small intermediate transitions around $(0^{o}$C) seen in these polymers, particularly well seen in DMA, can be attributed to the diffuse phase interface. Porod scaling in the SAXS analysis provides a support to this hypothesis. Average periodicities, as obtained from strong scattering of L-PUU10 (14.7 nm) and L-PUU50 (15.2 nm) are not very different from the periodicity of L-PU (15.7 nm). Introduction of *m-phenylenediamine* was thus found to enhance phase separation of hard and soft segments along with the formation of a diffuse interface.

National Chemical Laboratory

B12-PUUs displayed progressively disordered hard segment hydrogen bonding in FTIR. This correlates well with the DSC, DMA and rheology measurements all of which suggest increased phase mixing of hard and soft segments driven by the B12 diamine. Decaying SAXS signal for this series of copolymes could be due to two reasons 1) pendent aliphatic chains favour phase mixing, and 2) presence of aliphatic chains on the hard segment reduces the electron density contrast between the phases and making them invisible in SAXS. SAXS analysis also reveals a systematic decrease in average periodicity values relative to L-PU. Even a small amount of mixing of soft segments in hard segments is found to favour successful superposition of frequency sweep data by TTS. Incorporation of B12 diamine thus leads to decreased hard segment packing as well as plasticization of hard segments and their mixing with the soft segment phase. However, the presence of a discernable soft segment T_g even in B12-PUU100, as seen in DSC and DMA, indicates that the phase mixing is incomplete.

The microstructural organization of B22-PUUs is intriguing. FTIR analysis demonstrates disordered hard segment hydrogen bonding. N-H absorption region in B22-PUU100 also shows presence of free N-H groups as well N-H groups bonded to soft segments. B22 diamine incorporation did not influence soft segment T_gs of B22-PUUs indicating that the phase is relatively unmixed even at the highest diamine content. DSC thermograms of B22-PUU50 and B22-PUU100 displayed endotherms that can be ascribed to the crystalline melting of C22 pendent chains. In B22-PUU100 the endotherms had higher peak temperatures than those in B22-PUU50 and this sample also showed a crystallization exotherm at $27^{o}C$. Presumably the concentration of C22 chains is sufficient to form a 3D ordered crystalline phase. The fairly high enthalpies observed for these melting transitions together with the WAXD evidence supports the proposition of C22 chain crystallization. C22 chains are known to crystallize into triclinic phase through a metastable rotator phase on heating and cooling. The known lattice spacings for the rotator phase matched with those observed in the B22-PUU100 sample. Intermediate endotherms around $10^{o}C$ seen in these samples could be originating from weak associations of C22 chains. The temperature at which the first melting peak was observed in DSC corresponded with the temperature at which segmental relaxation was observed in DMA response of B22-PUU50 and B22-PUU100. Due to the loss of electron density contrast, SAXS failed to give any information on the morphology. Based on FTIR, DSC and DMA

analysis we propose that B22-PUU50 and B22-PUU100 have three-phase morphology: a soft segment phase, a hard segment phase and a crystalline C22 phase. We do not have adequate experimental evidence to ascertain the location of the third phase. But it is more likely to be located near the soft segment phase.

6.2   Future Work

Series of short chain branched polyurethane-ureas synthesized in the present work show interesting effects on the hard segment microstructure. A systematic effect of the length as well as the amount of the aliphatic branch has been observed by employing various morphological techniques. However, a real space morphological analysis such as AFM imaging can provide a direct evidence of the microstructure. AFM has been used widely for imaging polyurethane microstructure.

Following **Figure 6.1** shows a plot of average periodicity values of L-PU, B12-PUU10 and B22-PUU10 while heating and cooling cycles in SAXS scattering experiments. Figure shows an interesting trend of hysteresis observed in the three samples. It would be interesting to study this behavior further. We are not aware of any literature reports on the observation of hysteresis in SAXS experiments on polyurethanes.

Similar hysteresis has also been observed in rheological behavior (dynamic temperature ramp test) of these samples as provided in the following figures **6.1**, **6.2** and **6.3**. These examples indicate the temperature sensitivity of morphology. Yoon and Han[1] report a similar rheological finding. Hysteresis of this kind has also been noticed for microphase separated block copolymers[2] and is an interesting area of further investigations.
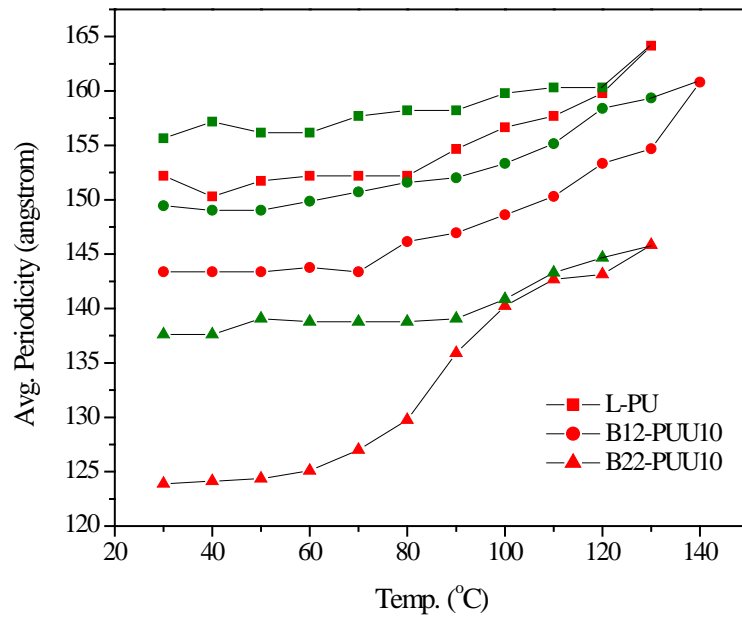
Figure 6.1 Average periodicity after Lorentz correction vs temperature for L-PU (filled squares), B12-PUU10 (filled circles) and B22-PUU10 (filled triangles). Red data points represent heating while green data points represent cooling cycle.
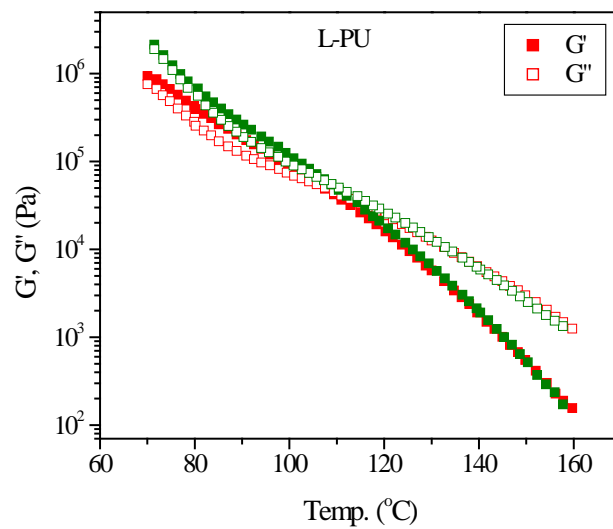

Figure 6.2 Dynamic Temperature Ramp for L-PU while heating (red symbols) and cooling (green symbols) cycle. Conditions: Frequency = 1 rad/s, Temp. ramp rate = 5°C/min.
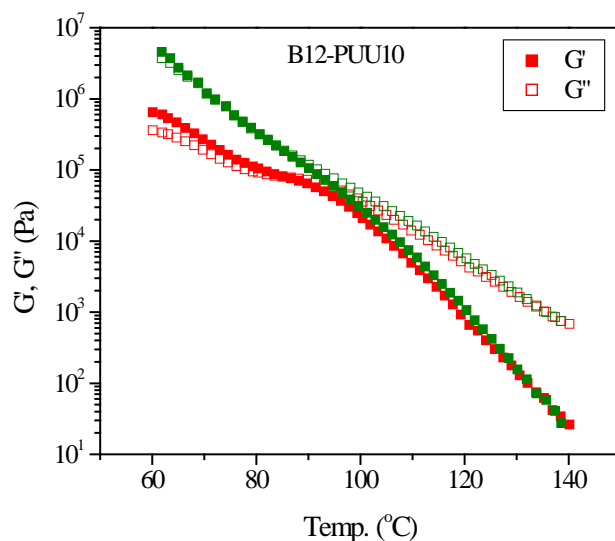
Figure 6.3 Dynamic Temperature Ramp for B12-PUU10 while heating (red symbols) and cooling (green symbols) cycle. Conditions: Frequency = 1 rad/s, Temp. ramp rate = 5°C/min.
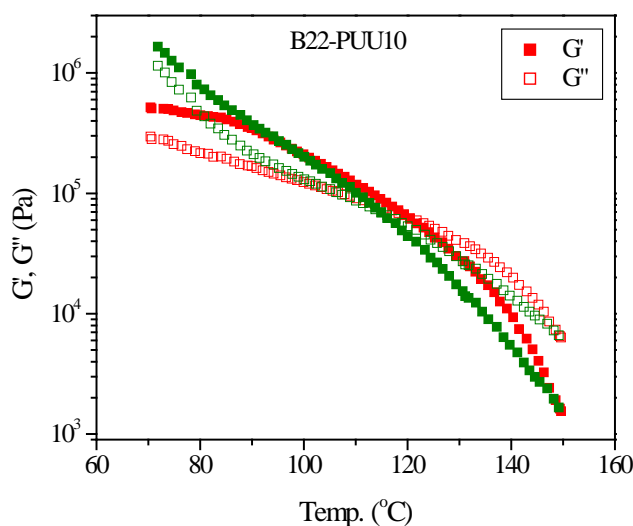

Figure 6.4 Dynamic Temperature Ramp for B22-PUU10 while heating (red symbols) and cooling (green symbols) cycle. Conditions: Frequency = 1 rad/s, Temp. ramp rate = 5°C/min.

This study demonstrates the effect of introducing aliphatic branches on the polyurethane hard segment. Studying the effect of incorporation of branches on the soft segments having different chemical structure can be equally interesting area of research.

References:

(1) Yoon, P. J.; Han, C. D. *Macromolecules* **2000**, 33, 2171.

(2) Sakamoto, N.; Hashimoto, T.; Han, C. D.; Kim, D.; Vaidya, N. Y. *Macromolecules* **1997**, 30, 1621.